Stochastic control, numerical methods, and machine learning in finance and insurance

Xiang Gao

A Thesis
in the Department
of
Mathematics and Statistics

Presented in Partial Fulfillment of the Requirements
for the Degree of
Doctor of Philosophy (Mathematics) at
Concordia University
Montréal, Québec, Canada

May 2021

CONCORDIA UNIVERSITY

SCHOOL OF GRADUATE STUDIES

This is to certify that the thesis prepared

By: Xiang Gao

Entitled: Stochastic control, numerical methods, and machine learning in finance and insurance

and submitted in partial fulfillment of the requirements for the degree of

Doctor Of Philosophy (Mathematics)

complies with the regulations of the University and meets the accepted standards with respect to originality and quality.

Signed by the final examining committee:

_____ Chair
Dr. Alexandre Champagne

_____ External Examiner
Dr. Anatoliy Swishchuk

_____ External to Program
Dr. Lawrence Kryzanowski

_____ Examiner
Dr. Frederic Godin

_____ Examiner
Dr. Wei Sun

_____ Thesis Supervisor
Dr. Cody Hyndman

Approved by _____
Dr. Pawel Gora, Graduate Program Director

5/5/2021 _____
Dr. Pascale Sicotte, Dean
Faculty of Arts and Science

ABSTRACT

Stochastic control, numerical methods, and machine learning in finance and insurance

Xiang Gao, Ph.D.
Concordia University, 2021

We consider three problems motivated by mathematical and computational finance which utilize forward-backward stochastic differential equations (FBSDEs) and other techniques from stochastic control. Firstly, we review the case of post-retirement annuitization with labor income in framework of optimal stochastic control and optimal stopping. We apply the martingale approach to a Cobb–Douglas type utility maximization problem. We have proved the theoretical existence and uniqueness of an optimal solution. Several analyses are made based on the simulations for the optimal stopping choice and strategies. Secondly, We review the convolution method in backward stochastic differential equations (BSDEs) framework and study the application of convolution method to Heston model. We provide an easy representation of the Heston characteristic function that avoids the discontinuities caused by branch rotations in the logarithm of complex functions and is able to be applied in calibration. We proposed two convolution schemes to the Heston model and provide the error analysis that shows the error orders of discretization and truncation. We review two error control methods and improve the accuracy on the boundaries. Numerical results comparing to a Fourier method and an integration method is provided. Thirdly, we review the forecasting problem in bond markets. Our data include both U.S. Treasuries and coupon bonds from twelve corporate issuers. We apply the arbitrage-free model in predicting the yields and the prices of coupon bonds in a sequential model with the Kalman filter, the extended Kalman filter and the particle filter. We implement the arbitrage penalty and obtain the optimal dynamic parameterization using deep neural networks. The purpose of the prediction is to examine the effect of arbitrage penalty and the forecasting performance on different time horizons. Our result shows that the arbitrage-free penalty has improving performance on short time period but downgrading performance on long time period. We provide analysis on the prediction errors, the distribution of errors, and the average excess return. The predicted bond prices shows the prediction errors have non-Gaussian distribution, excess kurtosis, and fat tails. Future works will be from two aspects, refine the importance sampling by non-parametric distribution and refine the term structure model with jump process and credit risk.

Keywords: forward-backward stochastic differential equations, stochastic control optimal stopping, martingale approach, high dimensional option, Heston model, fast Fourier transform, HJM forward rate, dynamic Nelson-Siegel, Kalman filter, particle filter, recurrent neural network.

Acknowledgments

First of all, I would like to express my sincere gratitude to my supervisor Dr. Cody Hyndman for their guidance and support throughout my research and life. I am expressing my gratitude to Dr. Pirvu Traian from McMaster university for his generous help and valuable advice to improve my research project. Their guidance has been extremely helpful through the completion of all my research projects in last five years. I am also thankful to the examining committee members for reading my thesis. This accomplishment would not have been possible without them.

I would like to thank my friends, colleagues, peers, the faculty and staff members of the department of Mathematics and Statistics. Their generous support and kindly care have truly made me feel like being a family in the department. It is my great pleasure to research and work in such a wonderful institute.

Finally, I would like to express my profound gratitude to my parents and my aunt for providing me with unfailing support and continuous encouragement throughout my years of living and studying in Montreal.

Thank you.

Contents

List of Figures

List of Tables

Introduction

This thesis contains three projects: the martingale approach to the optimal annuitization problem with stochastic control and deterministic control, the convolution method in option pricing, and the application of arbitrage-free pricing theory in bond price forecasting. The three topics lead into deep research from pure mathematics to the application of modern tools such as deep neural networks from which we make contribution to both theory and practical methodology. This thesis is organized as follows. In Chapter 1, we present the martingale approach to optimization problem related to retirement planning using stochastic control and deterministic control. In Chapter 2, we demonstrate the convolution method as an extremely fast and accurate approach to pricing options with stochastic volatility and solving BSDEs numerically. In Chapter 3, we show the application of arbitrage-free pricing theory in forecasting bond prices and yields with a dynamic parameterization using deep neural networks.

In Chapter 1, we have studied the optimal annuitization problem with labor constraints. Utility maximization problems using stochastic control and optimal stopping goes back at least to the seminal articles of Merton [99] and has been studied extensively in past decades, for instance Pliska [108] studies its application in optimal trading, Karatzas, Lehoczky, and Shreve [81] study the optimal portfolio and consumption decision in very explicit feedback form and Cox and Huang [27] study the consumption-portfolio problem when asset prices follow a diffusion process. The current papers dealing with financial risk of pre-defined pension schemes in stochastic frameworks is quite rich, for instance Cairns, Blake, and Dowd [17], Gao [62] and Gerrard, Højgaard, and Vigna [63].

Related work by Karatzas and Wang [80] has shown the application of the martingale method together with Lagrange transformations in solving the optimal control problem. Karatzas and Wang [80] introduced the shadow process and the corresponding budget constraint which is applied to relax the control terms from the objective function and obtain a deterministic problem. He and Pages [65] study optimal investment with borrowing constraints. Bodie, Merton, and Samuelson [9] study an optimal problem with flexibility in labor supply and demonstrated the dependence of agent's risk tolerance on flexibility of labor supply. Bodie, Detemple, Otruba, and Walter [10] study the optimal consumption and investment problem in a context of retirement which has a fixed time of retirement rather than an optimal time of retirement. Farhi and Panageas [55] study the binomial choice of leisure with the Cobb-Douglas utility function which is more generally used in measuring labor and capital inputs in economic production and is a special case of the CES utility function. Lim, Shin, and Choi [88] study a similar problem as Farhi and Panageas [55] in optimal consumption-leisure, portfolio, and retirement choice of an infinitely lived investor whose instantaneous utility is given by constant elasticity of substitution (CES) function of consumption and leisure. Lim et al. [88] uses combination of portfolio and consumption-leisure choice and an

optimal stopping time for a retirement problem, in which the investor derives utility from adjusting between consumption and leisure, and also has an option for full retirement from labor. Lim et al. [88] provided a solution to the free boundary problem but without a solid proof of the existence and uniqueness.

We study the properties of the Cobb-Douglas utility function and its application as the objective function in the maximization of the postponed annuitization problem. We fully solve the post-retirement annuity problem with a closed form solution and provide numerical analysis. We review the optimization model in Gerrard et al. [63] and the martingale method in Lim et al. [88] to give some methodological and realistic contribution to finalize the rigorous proof of the closed form that is lacking in most papers. We make contribution to addressing an optimization problem with a stochastic control and a deterministic control in closed-form and provide rigorous proofs to the optimal solutions. In numerical implementations, we investigate the properties of the optimal solution by varying the parameters and analyze the pensioner's behavior in Monte-Carlo simulations. We present the 2-dimensional graph of the utility surface with varying labor rate and wage rate showing that the utility is concave in the labor rate and convex in the wage rate. In the simulation study, we find that the optimal annuitization time is strongly linear with respect to the initial wealth in cases with and without labor income. We also find that there exists a critical wealth level below which the extra labor income decreases the annuitization time, and above which the extra labor income postpones the annuitization time in exchange for higher annuities. With different labor schemes, the pensioners have similar consumption strategies. However, a more interesting finding is that different pension schemes could lead to very differently optimal investment strategies and annuitization times.

In Chapter 2, we study the option pricing problem. Mathematical finance experiences rapid developments since the revolutions made by Markowitz and Black-Scholes in 1970s. Markowitz [96] propose the argument that all rational investors should select mean-variance efficient portfolios either minimizing variance under a given expected return or maximizing expected return under a given variance in Markowitz [95]. Influenced by Markowitz's revolution, Sharpe [112] develop the capital asset pricing model. Black and Scholes [8] bring the second revolution to modern finance by solving the option pricing problem using delta hedging and provided the closed form of solution of option pricing formulas. The theoretical study of option pricing was introduced by Black and Scholes [8] and Merton [99]. Cox and Ross [28] introduce the martingale pricing method based on risk-neutral pricing theory. A simple but efficient binomial tree model is introduced by Cox, Ross, and Rubinstein [29] for solving American style options which allows investors to exercise the option as soon as the payoff is positive. The most adaptable and widely used method in option pricing is Monte-Carlo simulation introduced by Boyle [14]. Monte-Carlo methods are very robust but the cost paid for high accuracy is the increasing computational requirement since the accuracy is highly dependent on the sample size and sample variance. Accelerating techniques were introduced by Boyle, Broadie, and Glasserman [13] in which they compared antithetic variates, control variates, importance sampling and stratified sampling. The theoretical study of backward stochastic differential equations started more recently but has a rapid progress, see El Karoui, Peng, and Quenez [53], Pardoux and Peng [104] and Barles, Buckdahn, and Pardoux [3]. In addition to its excellent mathematical properties, BSDEs have important applications in finance. Many derivatives like options and futures can be theoretically described and priced by BSDEs, see (Duffie and Epstein [48], El Karoui and Quenez [52], El Karoui et al. [53]). For most exotic options without analytic solutions, PDE based numerical methods such as finite difference and finite elements are

developed, see Zvan, Vetzal, and Forsyth [121] and Duffy [50].

We follow another vein that based on Fourier transformations introduced by Carr and Madan [18], and cosine method introduced by [70]. Lord, Fang, Bervoets, and Oosterlee [93] and Hyndman and Oyono Ngou [74] consider transforms for pricing options and demonstrate very fast and efficient results. The convolution method in option pricing is not only new but also has advantages compared to Fourier-based integration method. Our interest is to extend the convolution method to the Heston model. Then we study the feasibility to approach to higher dimensional cases such as basket options. Heston [67] provides semi-closed form solutions to address the volatility smile in pricing vanilla options with the Black-Scholes formula. The traditional approach using the characteristic function given by Heston is problematic since the characteristic function provided by Heston [67] has discontinuities which lead to unreliable integration results. As proposed by many other authors, different schemes are introduced to overcome the discontinuity in the characteristic function such as Kahl and Jäckel [79], Lord and Kahl [92] and Levendorskiĭ [87]. Numerical calibration finds the optimal parameters that best fit the observed data into the Heston model (see Cui, del Baño Rollin, and Germano [32]). Other calibration approach using simulation methods avoid the space complexity in the characteristic function but become time consuming when applied to the BSDEs (see Cohen and Tegnér [24]).

In Chapter 2, we give the explicit solution for the characteristic function of the Heston model in the two-dimensional case from the joint processes. We review the convolution method for numerically solving one-dimensional BSDEs and propose a new method for pricing options with the Heston model. We investigate two boundary control techniques: damping and shifting methods introduced in Carr and Madan [18] and Hyndman and Oyono Ngou [74] and proposing the most efficient way to control the boundary error for the Heston model, which are seldom considered in practice. We will show that the convolution method is faster and more accurate than the direct integration method, especially, in the limiting behavior.

In Chapter 3, we study bond pricing and forecasting with arbitrage-pricing theory. The traditional approach to pricing problems in fixed income markets relies on interpreting the term structure interest rates model or the forward rate model. McCulloch [97] introduced spline methods for measuring the term structure of interest rates and many subsequent work improves the spline method, such as Waggoner [116]. Fama and Bliss [54] applied the bootstrap method to obtain zero-coupon bond prices from coupon bonds, and this method is still used to provide daily and monthly data for research on term structure. In recent years, approaches to term structure modeling are mainly spit in two veins: the no-arbitrage approach following Hull and White [71] and Heath, Jarrow, and Morton [66] or the equilibrium approach following Vasicek [114] and Cox and Huang [27].

Duffie and Kan [49] present a consistent and arbitrage-free multi-factor model of the term structure of interest rates in which yields at selected fixed maturities follow a parametric multivariate Markov diffusion processes with stochastic volatility. Ang and Piazzesi [1] introduce the linearized vector model in which they identify restrictions based on the absence of arbitrage. They conclude that macro factors primarily explain 85% of the movements at the short end and middle of the yield curve while unobservable factors still account for most of the movements at the long end of the yield curve. Diebold and Li [37] describe the evolution of the term structure directly by viewing the factors as time dependent variables. They extended the estimation of yield curves from in-sample fitting to out-of sample forecasting and produced good forecast results. Christensen, Diebold, and Rudebusch [21] assume the dynamic factors in a term structure model evolve as

Vašíček process with latent parameters. Though Christensen et al. [21] claims the factor model with yield adjustment term gives arbitrage-free forward rate curves, it is very hard to provide such evidence. Our proposal follows the regularization method introduced by Kratsios and Hyndman [86] and apply machine learning to minimize the arbitrage opportunity. We theoretically investigate such arbitrage opportunities from a HJM forward rate model and introduce a regularization term which is minimized while solving the optimization problem. Deep feed-forward neural networks, established by Cybenko [33], Hornik, Stinchcombe, White, et al. [69] and Goodfellow, Bengio, and Courville [64], will be applied to dynamically parameterize the yield curves.

In Chapter 3, we first combine the equilibrium model with a no-arbitrage model and introduce an easily implementable method to obtain rigorous arbitrage-free forecasting from both a theoretical and practical perspective. Our arbitrage-free scheme quantifies average excess returns, with minimal arbitrage from the pricing and forecasting process. We also show that the forecasting performance is minimally downgraded by the arbitrage-free regularization scheme in long time predictions, but that it improves the performance in short time predictions. Secondly, we introduce an advanced and efficient framework using dynamic parameterizations in deep neural networks supported by consistent and stable performance in both in-sample and out-of-sample tests. Our method is more flexible in balancing the bias-variance trade-off compared to the classical model using Bayesian inference for the parameters, see Koop [85] and Carriero, Clark, and Marcellino [19]. Thirdly, we investigate bond price differences between the observation and theoretical prices and find that the error distribution possesses large kurtosis and fat tails. We also provide an analysis showing that the error distribution could be fitted into a non-parametric distribution smoothed by a Gaussian density. Finally, we present numerical results that show the performance of machine learning in forecasting yield curves and bond prices on different forecasting time horizons.

In Chapter 4, we conclude our work in the thesis and discuss future work for each of the projects in Chapters 1, 2, and 3. All proofs are provided in the appendix.

Chapter 1

Optimal annuitization with labor constraints

In this chapter, we study the utility maximization problem in a defined contribution scheme where pensioners balance their consumption and investment with a limited capacity to gain extra labor income after retirement until they reach the level of optimal annuity. The benefit of including labor income is to help interpret the value of the solution more realistically when the labor and wage rates can be viewed as a benchmark. One of our purposes is to investigate the effect of labor work and wage rate after retirement to achieve the optimal annuity. The current papers dealing with financial risk of defined contribution schemes in a stochastic framework are quite rich, for instance Cairns et al. [17], Gao [62] and Gerrard et al. [63]. Most of this literature shares the common setting of an agent who receives a deterministic initial capital, which he must then invest in a market (complete or incomplete) so as to maximize the expected utility of his consumption and terminal wealth. Utility maximization problems in the form of stochastic control and stopping problems go back at least to the seminal articles of Merton [99] and have been studied extensively in the past decades.

Karatzas and Wang [80] show the application of martingale methods together with the Lagrange transformation in solving the optimal control problem. They introduced the shadow process and the corresponding budget constraint which is applied to relax the control terms from the objective function and obtain a deterministic problem. He and Pages [65] studied optimal investment with borrowing constraints. Bodie et al. [9] studied an optimal problem with flexibility in labor supply and demonstrated the dependence of an agent's risk tolerance on the flexibility of labor supply. Bodie et al. [10] studied the optimal consumption and investment problem in a context of retirement which has a fixed time of retirement rather than an optimal time of retirement. Lim et al. [88] studied a similar problem as Farhi and Panageas [55] in optimal consumption-leisure portfolio, and retirement choice of an infinitely lived investor whose instantaneous utility is given by a CES function of consumption and leisure. Farhi and Panageas [55] combine investment with borrowing

constraints, consumption-leisure choice and an optimal stopping time for the retirement problem, in which the investor derives utility from adjusting between consumption and leisure, and also has an option for full retirement from labor. Farhi and Panageas [55] choose the Cobb-Douglas utility function with a choice of binomial leisure (l_1 before retirement and $\bar{l}$ after retirement) and solve the free boundary problem but without a proof of the existence and uniqueness of the solution. Inspired by Farhi and Panageas [55], we choose the same utility function and treat the labor-leisure as a deterministic control in our model which is more realistic. By the martingale approach, we derive the closed-form of the value function with optimal strategies and provide a rigorous proof showing they are the optimal solutions.

1.1 Economic background

The classical consumption-investment problem is described by an expectation of the accumulative running profit $f(\cdot)$ plus the terminal value $g(\cdot)$

$$J(c,\tau,x) = \mathbb{E}\left[\int_0^\tau f(t,c_t,X^x) + g(\tau,X_\tau^x)\right], \tag{1.1.1}$$

where the portfolio value X_t^x is a stochastic process with initial value x which is controlled by a deterministic term c_t

$$dX_t^x = b(t,c_t,X_t^x)\,dt + \sigma(t,c_t,X_t^x)\,dW_t. \tag{1.1.2}$$

The goal is to choose a control term and a stopping time (c_t^*,τ^*) such that maximize the objective function

$$(c_t^*,\tau^*) = \arg\sup_{c_t,\tau\in U} J(c_t,\tau,x),$$

where all the available pairs of (c,τ) are from a space of feasible set U which can be generally defined as

$$U = \{(c,\tau)\,|\text{such that } X_t \text{ and } J(c,\tau,x) \text{ are well defined}\},$$

which will be made more precise. Theoretically a unique solution exists if the function f and g are Lipchitz continuous and the process X_t has bounded quadratic variation for all $(c_t,\tau)\in U$.

In our research, we add extra income as the second control term which has a dis-utility effect in the running strategy but will increase the final value by a deterministic amount. Suppose the agent receives a lump sum of size x at retirement when $t=0$. Up until the time of annuitization, the agent can choose to keep working after retirement with labor rate L_t, consume at the rate of c_t and invest some amount of his or her wealth π_t in the financial market. We assume that the remaining lifetime of the agent, T_D, is independent of the financial market and exponentially distributed with force of mortality δ. In defined contribution pension schemes, the agent has the possibility to defer the annuitization of his wealth. The objective function of the agent before annuitization consists of the utility from consumption, dis-utility from labor, and the final utility from annuitization.

The consumption rate c_t is an amount from agent's total wealth that he consumes during one

unit of time. In our model we measure the dis-utility of labor by its utility from leisure $l_t = 1 - L_t$. We assume the labor rate is bounded, $L_t \leq \bar{L} \leq 1$, and so the leisure rate is also bounded $1 - \bar{L} = L \leq l_t \leq 1$. Thus, we set a minimum leisure rate $L = 1 - \bar{L}$ and the leisure rate is bounded, $0 \leq L \leq l_t \leq 1$. In the special case of leisure rate $l_t = 1$, the agent has no extra income except from investment after retirement and the problem becomes a classical consumption-investment problem. If the labor rate L_t is greater than 0 the agent has extra labor income $w_t L_t = w_t (1 - l_t)$ with wage rate w_t but he receives a penalty for his leisure rate l_t which is less than 1. The amount of leisure l_t and the amount of consumption c_t together are measured by a utility function which is introduced in the next section and the annuity is measured by another utility function. Therefore, the objective function is to maximize the agent's total expected utilities from running the consumption and leisure strategies and the choice of final annuity.

For simplicity, we suppose that the wage rate w_t and the annuity scheme k, defined as a portion of the finally wealth, are fixed at the agent's retirement. The financial market consists of a riskless asset and a risky asset. The riskless asset pays interest at fixed rate r which can be the money market account or a locked in retirement account. The risky asset can be a portfolio or funds from a market which evolves as a geometric Brownian motion with mean μ and volatility σ,

$$\frac{dS_t}{S_t} = \mu dt + \sigma dB_t.$$

Here, given the probability space $(\Omega, \mathcal{F}, \mathbb{P})$ and a terminal time $T > 0$, B_t is a standard Brownian motion in $\mathbb{R}^d$ under the probability $\mathbb{P}$ on a finite-time horizon.

Given an initial endowment $x \geq 0$, an income stream from labor work $w(1 - l_t)$, a consumption rate c_t, an investment policy π_t, the remaining wealth stays in a bank account. The agent's total wealth evolves according to the following stochastic process

$$dX_t = (rX_t + \pi_t(\mu - r) - c_t + w(1 - l_t))\, dt + \sigma \pi_t dB_t. \tag{1.1.3}$$

Once the agent annuitizes, he or she receives a fixed periodic payment until death, $t = T_D$. The periodic payment of an annuity purchasable by wealth X is kX, for some constant $k > r$. Thus we define the objective function

$$J(x; \tau) = \mathbb{E}_x \left[\int_0^{\tau \wedge T_D} e^{-rt} U_1(c_t, l_t) dt + \mathbf{1}_{\{\tau < T_D\}} \int_{\tau \wedge T_D}^{T_D} e^{-rt} U_2 \left(k X_\tau^{x,c,l,\pi} \right) dt \right],$$

where

(i) X_t is the pensioner's total wealth at time t with $X_0 = x$;

(ii) c_t is the consumption rate, l_t is the leisure rate, and w_t is the wage rate;

(iii) π_t is the amount invested in the risky asset with price S_t;

(iv) τ is the annuitization time; and

(v) T_D is the pensioner's death time.

We assume the pensioner's force of mortality, δ, is constant and is independent of the Brownian motion. According to the method in Gerrard et al. [63], we can rewrite the the above objective

function as

$$J(x;\tau) = \mathbb{E}^x\left[\int_0^\tau e^{-\rho t}U_1(c_t,l_t)dt + \frac{e^{-\rho\tau}}{\rho}U_2(kX_\tau^x)\right], \tag{1.1.4}$$

where $\rho = r+\delta$. The optimization problem is to determine the four control variables, c_t, l_t, π_t and τ in such a way as to maximize the discounted expected utility in (1.1.4).

Definition 1.1. *(Admissible control): The admissible control set* $\mathbf{U}$ *is the set of all* $\mathcal{F}$*-progressively measurable processes* (c_t,l_t,π_t) *such that*

1) $J(x;\tau) \leq \infty$ *for all* $(c_t,l_t,\pi_t) \in \mathbf{U}$*;*

2) the control terms (c_t,l_t) *satisfy the constraints* $0 \leq c_t$ *and* $L \leq l_t \leq 1$*;*

3) the portfolio strategy π_t *satisfies* $\mathbb{E}|\pi_t|^2 < +\infty$.

The admissible control in Definition 1.1 only ensure the wealth process X_t has bounded quadratic variation. Next, we specify the Lipchitz condition on the utility function to ensure the objective function $J(x;\tau)$ is also bounded.

Remark 1.2. *A sufficient condition for* $J(x;\tau) < \infty$ *in Definition 1.1) is given by*

$$\max\{U_1(x,l),U_2(x)\} \leq k_1 + k_2x^\delta, \qquad \forall x \in (0,\infty) \text{ and } l \in [0,1]$$

for some constant k_1, $k_2 > 0$ *and* $\delta \in (0,1)$*, see Karatzas et al. [81].*

We denote by $\mathbf{S}$ be the class of $\mathcal{F}$-stopping times $\tau : \Omega \to [0,T]$. The value function is defined as the optimal objective function

$$V(x) = \sup_{\substack{(c_t,l_t,\pi_t,\tau)\\ \in \mathbf{U}\times\mathbf{S}}} \mathbb{E}^x\left[\int_0^\tau e^{-\rho t}U_1(c_t,l_t)dt + \frac{e^{-\rho\tau}}{\rho}U_2(kX_\tau^x)\right]. \tag{1.1.5}$$

As is well known from the theory of stochastic control and optimal stopping (see, Øksendal [102] and Pham [107]), the unconstrained value function can be characterized by an HJB equation. Therefore, we now proceed to unconstrain the original problem 1.1.5 to a dual problem using the martingale method. Define the relative risk process

$$\theta = \frac{\mu - r}{\sigma},$$

the exponential martingale

$$Z_t = e^{-\frac{1}{2}\theta^2 t - \theta B_t},$$

and the state-price-density (shadow process)

$$H_t = e^{-rt}Z_t = e^{-\left(r+\frac{1}{2}\theta^2\right)t - \theta B_t}.$$

By Girsanov's theorem, the process

$$d\bar{B}_t = \theta dt + dB_t,$$

defines a standard Brownian motion $\bar{B}_t$ under the equivalent martingale measure $\bar{\mathbb{P}}(A) = \mathbb{E}[Z_T \mathbf{1}_A]$, $0 \leq T$.

Applying Itô's formula to the product of the processes H_t and $X_t + \frac{w}{r}$, we have

$$H_t \left(X_t + \frac{w}{r}\right) + \int_0^t H_s \left(c_s + w l_s\right) ds = x + \frac{w}{r} + \int_0^t H_s \left(\sigma \pi_s - \theta \left(X_s + \frac{w}{r}\right)\right) dB_s. \tag{1.1.6}$$

For any feasible control set (c_t, l_t, π_t), the process

$$H_t \left(X_t + \frac{w}{r}\right) + \int_0^t H_s \left(c_s + w l_s\right) ds, \tag{1.1.7}$$

is a continuous, positive local martingale, hence a supermartingale, under measure $\mathbb{P}$. Therefore, by Fatou's Lemma the stochastic integral of equation (1.1.6) is a $\mathbb{P}$-supermartingale. Thus by the optional sampling theorem, we have the following inequality constraint

$$\mathbb{E}\left[\int_0^\tau H_t \left(c_t + w l_t\right) dt + H_\tau \left(X_\tau + \frac{w}{r}\right)\right] \leq x + \frac{w}{r}, \quad \forall \tau \in \mathbf{S}. \tag{1.1.8}$$

We call the inequality (1.1.8) the budget constraint under which the solvency property $X_t^{c,l,\pi} \geq 0$ over the time interval $[0, \tau]$ is satisfied. In the following sections, we will show that equality can hold for the budget constraint and a martingale approach can relax the control terms from the objective function. Eventually, we can transform the control and stopping problem to a simple stopping problem.

1.2 The optimization problem and dual approach

In the classical Merton problem (Merton [99]), the optimal control terms are derived from the HJB equation in the form of the first order and second order derivatives of the value function. In this approach, we eventually have to solve the HJB equation by a numerical method or by a good ansatz. Jin Choi and Shim [78] and Gerrard et al. [63] give a theoretical representation of the value function and critical wealth level in the form of duality function. However, the exact solution is hard to determine from the dual form and the existence and uniqueness of the solution are not rigorously proved. In this section, we will determine the optimal control term before we reach the HJB equation. Then by the martingale method, we can relax the constraints and transform the optimal control and stopping problem to a dual problem. Finally, we give the mathematical form of the solution and prove the existence and uniqueness of the optimal stopping time.

1.2.1 Utility and conjugate form

The Cobb-Douglas utility function was introduced in Cobb and Douglas [23] and is often used in economics for analyzing supply-side production in the relationship between capital and labor inputs. This utility function has a decreasing marginal rate of substitution and a constant utility elasticity. We choose the utility presented in Barucci and Marazzina [4] with a small adjustment for the elasticities of leisure and consumption. We assume the utility function $U_1(c_t, l_t)$ to be isoelastic (with constant elasticity coefficient) and the relationship between leisure l_t and consumption c_t is similar to the labor and capital in the original Cobb-Douglas utility function:

$$U_1(c,l) = \frac{l^{\beta(1-p_1)} c^{\alpha(1-p_1)}}{1-p_1}. \tag{1.2.1}$$

After annuitization the leisure rate is $l = 1$, so $U_1(\cdot)$ becomes a power utility

$$U_2(x) = \frac{x^{1-p_2}}{1-p_2}, \tag{1.2.2}$$

where $p_1, p_2 > 1$ are the coefficients of relative risk aversion and $\alpha,\ \beta > 0$ are elasticities of consumption and leisure.

We can easily check that U_1 and U_2 satisfy elasticity requirement for utility functions, and existence of the value function. Therefore, the instantaneous utility function $U(c_t, l_t)$ at time t is a concave function for consumption and leisure

$$\frac{\partial U_1}{\partial c_t} > 0,\ \frac{\partial U_1}{\partial l_t} > 0.$$

Since l_t represents leisure, the fact that $\frac{\partial U_1}{\partial \beta} = \left(l^\beta c^\alpha\right)^{-p_1} l^\beta \ln l < 0$ shows that as the value of β increases, the pensioner's utility from the same amount of leisure decreases which means he prefers to work less. Therefore, we say β is the pensioner's preference to labor. We also define α as the pensioner's preference to consume. As the value of α increases, the pensioner prefers to consume more.

We define the conjugate function $\bar{U}_1$ and $\bar{U}_2$ for U_1 and U_2 as

$$\bar{U}_1(y) = \sup_{\substack{0 \le c_t \\ L \le l_t \le 1}} \left[U_1(c,l) - (c + wl)y\right], \tag{1.2.3}$$

and

$$\bar{U}_2(y) = \sup_{x \ge 0} \left[U_2(kx) - xy\right]. \tag{1.2.4}$$

which is the Legendre-Fenchel transform for a concave function.

To optimize $[U_1(c,l) - (c+wl)y]$ over positive c and l, first order conditions will give the optimizer since the function is concave in both c and l. For optimization of $[U_1(c,l) - (c+wl)y]$ over the constraint $l \in [L, 1]$, we consider the following two cases

Definition 1.3. *Optimization rules and conditions for the utility function:*

(i) the optimizer of equation (1.2.3) is unconstrained if the variables belong to some constraint set, or

(ii) the optimizer of equation (1.2.3) is on the boundary of the constraint set.

If case (i) holds, it means that $l \in [L,1]$ but in terms of y this condition is equivalent to $y \in [\tilde{y},\bar{y}]$. We can derive the unconstrained optimizer of c and l from first order condition

$$\frac{1}{w}\frac{\partial \bar{U}_1}{\partial l} = \frac{\partial \bar{U}_1}{\partial c} = y, \tag{1.2.5}$$

from equation (1.2.5) we get the unconstrained relationship between c and l when l is unconstrained

$$c = \frac{\alpha w}{\beta} l, \text{ for } l \in [L,1]. \tag{1.2.6}$$

Replacing c in the first order equation (1.2.5) using the unconstrained relationship (1.2.6), we obtain the following optimal condition for unconstrained l

$$y = \alpha \left(\frac{\alpha w}{\beta}\right)^{\alpha(1-p_1)-1} l^{(\alpha+\beta)(1-p_1)-1}, \text{ for } l \in [L,1]. \tag{1.2.7}$$

Equivalently, we define the unconstrained region for y as $[\tilde{y},\bar{y}]$

$$\tilde{y} = \alpha \left(\frac{\alpha w}{\beta}\right)^{\alpha(1-p_1)-1} \leq y \leq \alpha \left(\frac{\alpha w}{\beta}\right)^{\alpha(1-p_1)-1} L^{(\alpha+\beta)(1-p_1)-1} = \bar{y},$$

and the unconstrained region for c as $[\bar{c},\tilde{c}]$

$$\bar{c} = \frac{\alpha w}{\beta} L \leq c \leq \frac{\alpha w}{\beta} = \tilde{c}.$$

If case (i) fails, i.e., when $y \notin [\tilde{y},\bar{y}]$ then according to case (ii) the boundary condition gives $y < \tilde{y}$ and $c > \tilde{c}$ or $y > \bar{y}$ and $c < \bar{c}$. Denote by $l^*(c) = \frac{\beta c}{\alpha w}$ and according to the optimization rules, we rewrite (1.2.3) as

$$\begin{aligned}\bar{U}_1(y) = &\{U_1(c,L) - (c+wL)y\}\,\mathbf{1}_{y>\bar{y}} \\ &+ \{U_1(c,l^*(c)) - (c+wl^*(c))y\}\,\mathbf{1}_{\tilde{y}\leq y\leq \bar{y}} + \{U_1(c,1) - (c+w)y\}\,\mathbf{1}_{y<\tilde{y}}.\end{aligned} \tag{1.2.8}$$

If we take the partial derivative with respect to c in equation (1.2.8), we get the following system

$$\begin{cases} \dfrac{\partial}{\partial c}U_1(c,L)-y=0, & y>\bar{y} \\ \dfrac{\partial}{\partial c}U_1(c,l^*(c))-(1+\dfrac{\alpha}{\beta})y=0, & \tilde{y}\le y\le\bar{y} \\ \dfrac{\partial}{\partial c}U_1(c,1)-y=0, & y<\tilde{y}, \end{cases} \tag{1.2.9}$$

which solves the optimal consumption on three regions: the full labor region $(0,\tilde{y})$ for $c>\tilde{c}$, the full leisure region $(\bar{y},\infty)$ for $0<c<\bar{c}$, and the flexible labor region $[\tilde{y},\bar{y}]$ for $c\in[\bar{c},\tilde{c}]$.

Solving each equation for c in equation (1.2.9), we get the optimal value of c

$$\begin{cases} c=(y/\alpha)^{p_1'-1}L^{-\frac{\beta}{\alpha}p_1'}, & y>\bar{y} \\ c=(y/\alpha)^{p-1}(\alpha w/\beta)^{\frac{\beta}{(\alpha+\beta)}p}, & \tilde{y}\le y\le\bar{y} \\ c=\left(\dfrac{y}{\alpha}\right)^{p_1'-1}, & y<\tilde{y}, \end{cases} \tag{1.2.10}$$

where

$$p=\frac{(\alpha+\beta)(1-p_1)}{(\alpha+\beta)(1-p_1)-1}\in(0,1), \tag{1.2.11}$$

$$p_1'=\frac{\alpha(1-p_1)}{\alpha(1-p_1)-1}\in(0,1). \tag{1.2.12}$$

Therefore, equation (1.2.8) is reduced to

$$\bar{U}_1(y)=\left[\tilde{A}y^{p_1'}-wy\right]\mathbf{1}_{\{0<y\le\tilde{y}\}}+Ay^p\mathbf{1}_{\{\tilde{y}<y<\bar{y}\}}+\left[\bar{A}y^{p_1'}-wLy\right]\mathbf{1}_{\{\bar{y}\le y\}}, \tag{1.2.13}$$

where $A=-\frac{\alpha+\beta}{p}\alpha^{-\frac{\alpha}{\alpha+\beta}}\beta^{-\frac{\beta}{\alpha+\beta}}w^{\frac{\beta}{\alpha+\beta}p}<0$, $\tilde{A}=-\frac{\alpha^{1-p_1'}}{p_1'}<0$ and $\bar{A}=-\frac{\alpha^{1-p_1'}}{p_1'}L^{-\frac{\beta}{\alpha}p_1'}<0$.

The optimal value of c and l are given by $c^*=I_c(y)$ and $l^*=I_l(y)$

$$\begin{aligned} I_c(y)=&\left(\frac{y}{\alpha}\right)^{p_1'-1}\mathbf{1}_{\{0<y\le\tilde{y}\}}+\left(\frac{y}{\alpha}\right)^{p-1}\left(\frac{\alpha w}{\beta}\right)^{\frac{\beta}{(\alpha+\beta)}p}\mathbf{1}_{\{\tilde{y}<y<\bar{y}\}} \\ &+\left(\frac{y}{\alpha}\right)^{p_1'-1}L^{-\frac{\beta}{\alpha}p_1'}\mathbf{1}_{\{\bar{y}\le y\}}, \end{aligned} \tag{1.2.14}$$

$$I_l(y)=\mathbf{1}_{\{0<y\le\tilde{y}\}}+\left(\frac{y}{\alpha}\right)^{p-1}\left(\frac{\alpha w}{\beta}\right)^{\frac{\beta}{(\alpha+\beta)}p-1}\mathbf{1}_{\{\tilde{y}<y<\bar{y}\}}+L\mathbf{1}_{\{\bar{y}\le y\}}, \tag{1.2.15}$$

where $I_c(\cdot)$ is the inverse of the marginal utility of consumption $\frac{\partial U_1}{\partial c}$ and $I_l(\cdot)$ is the inverse of the marginal utility of labor $\frac{\partial U_1}{\partial l}$. We can easily show that I_c and I_l are decreasing functions; the function I_c maps $(0,\infty)$ onto itself and satisfies $I_c(0^+)=+\infty$ and $I_c(+\infty)=0$; the function I_l

satisfies $I_l(0^+) = 1$ and $I_l(+\infty) = L$.

The conjugate function $\bar{U}_2(y)$ is given by

$$\bar{U}_2(y) = U_2(kx^*) - x^* y = -\frac{1}{p_2'}\left(\frac{y}{k}\right)^{p_2'},$$

where

$$p_2' = \frac{p_2 - 1}{p_2} \in (0,1). \tag{1.2.16}$$

The optimal values x^* and he marginal utility $I(y)$ are given by

$$x^* = I(y) = \frac{1}{k}\left(\frac{y}{k}\right)^{p_2'-1}. \tag{1.2.17}$$

Through the Legendre-Fenchel transform for concave functions (1.2.3) and (1.2.4) and inverse marginal functions $I_c(\cdot)$, $I_l(\cdot)$ and $I(\cdot)$, we have

$$\begin{aligned}
&\bar{U}_1'(y) = -\left(I_c(y) + wI_l(y)\right), \\
&\bar{U}_2'(y) = -I(y),
\end{aligned}$$

and

$$U_2(kx) = \min_{y>0}\left[\bar{U}_2(y) + xy\right] = \bar{U}_2\left(I'(x)\right) + xI'(x).$$

It can be shown that $\bar{U}_1(\cdot)$ and $\bar{U}_2(\cdot)$ are strictly decreasing and convex. We derive the duality form of the utility function and give the optimal controls c_t, l_t and π_t depending on the dual process y. Thus the original optimal problem could be free from the control terms and be simplified by solving the relationship between X_t and the dual process y.

1.2.2 Martingale and convex duality methods

In solving the optimization problem by dynamic programming or the martingale approach, the control process that influences the state process plays an essential role in carrying out the optimization. However, through the duality form of the utility function we find the optimal controls can be obtained from the dual process y. Now we look into the duality of the wealth process X_t by means of a series of super-martingales satisfying the budget constant (1.1.8) at the same time.

We define the dual of X_t as the shadow process Y_t^y

$$Y_t^y = ye^{\rho t}H_t. \tag{1.2.18}$$

with the stochastic dynamics

$$\frac{dY_t}{Y_t} = (\rho - r)dt - \theta dB_t. \tag{1.2.19}$$

For a Lagrange multiplier $y > 0$, we give the dual objective function as the Lagrange function of (1.1.4) and its budget constraint (1.1.8)

$$\bar{J}(x,y;\tau) = J(x;\tau) + y\left(\left(x+\frac{w}{r}\right) - \mathbb{E}\left[\int_0^\tau H_t(c_t+wl_t)dt + H_\tau\left(X_\tau+\frac{w}{r}\right)\right]\right). \tag{1.2.20}$$

By the inequality of budget constraint (1.1.8), it is obvious that

$$\bar{J}(x,y;\tau) \geq J(x;\tau). \tag{1.2.21}$$

Applying the conjugate utilities (1.2.3) to equation (1.2.20)), we move the supremum into the expectation and obtain the following inequality

$$\begin{aligned}
\sup_{c_t,l_t}\bar{J}(x,y;\tau) =& \sup_{c_t,l_t}\mathbb{E}\left[\int_0^\tau e^{-\rho t}\left(U_1\left(c_t,l_t\right) - H_t\left(c_t+wl_t\right)\right)dt\right. \\
&\left. + \left(\frac{e^{-\rho\tau}}{\rho}U_2(kX_\tau^x) - H_\tau\left(X_\tau+\frac{w}{r}\right)\right)\right] + y\left(x+\frac{w}{r}\right) \\
\leq& \mathbb{E}\left[\int_0^\tau e^{-\rho t}\sup_{c_t,l_t}\left(U_1\left(c_t,l_t\right) - H_t\left(c_t+wl_t\right)\right)dt\right. \\
&\left. + \sup_{c_t,l_t}\left(\frac{e^{-\rho\tau}}{\rho}U_2(kX_\tau^x) - H_\tau\left(X_\tau+\frac{w}{r}\right)\right)\right] + y\left(x+\frac{w}{r}\right) \\
=& \mathbb{E}\left[\int_0^\tau e^{-\rho t}\bar{U}_1(Y_t^y)dt + e^{-\rho\tau}\left(\frac{1}{\rho}\bar{U}_2(\rho Y_\tau^y) - \frac{w}{r}Y_\tau^y\right)\right] + y\left(x+\frac{w}{r}\right).
\end{aligned} \tag{1.2.22}$$

We define the equation at the right side of (1.2.22) as the dual value function

$$\bar{V}(x,y;\tau) = \mathbb{E}\left[\int_0^\tau e^{-\rho t}\bar{U}_1(Y_t^y)dt + e^{-\rho\tau}\left(\frac{1}{\rho}\bar{U}_2(\rho Y_\tau^y) - \frac{w}{r}Y_\tau^y\right)\right] + y\left(x+\frac{w}{r}\right). \tag{1.2.23}$$

Actually equality can be obtained with the optimal control given in (1.2.10), we have the equality

$$\bar{V}(x,y;\tau) = \sup_{c_t,l_t}\bar{J}(x,y;\tau). \tag{1.2.24}$$

Therefore, the dual problem is reduced to an optimal stopping problem

$$\begin{aligned}
\bar{V}(x,y) &= \sup_{\tau\in\mathbf{S}}\bar{V}(x,y;\tau) \\
&= \sup_{\tau\in\mathbf{S}}\mathbb{E}\left[\int_0^\tau e^{-\rho t}\bar{U}_1(Y_t^y)dt + e^{-\rho\tau}\left(\frac{1}{\rho}\bar{U}_2(\rho Y_\tau^y) - \frac{w}{r}Y_\tau^y\right)\right] + y\left(x+\frac{w}{r}\right).
\end{aligned} \tag{1.2.25}$$

By equation (1.2.21) we obtain the following inequality between the original and dual objective

functions

$$V(x;\tau)=\sup_{(c_t,l_t,\pi_t)} J(x;\tau)\leq \sup_{(c_t,l_t,\pi_t)} \bar{J}(x,y;\tau)=\bar{V}(x,y;\tau)\leq \sup_{\tau}\bar{V}(x,y;\tau)=\bar{V}(x,y). \quad (1.2.26)$$

The two inequalities in (1.2.26) give us the following important information:

1. As long as the first inequality in (1.2.26) is obtainable, the control terms c_t, l_t and π_t given from the dual value function (1.2.25) is the optimal controls to the original problem

$$c_t^*=I_c\left(Y_t^y\right),\ l_t^*=I_l\left(Y_t^y\right)\ \text{ and }\ X_\tau^*=I\left(\rho Y_\tau^y\right),\ \ \forall 0\leq t\leq\tau\ \ a.s.$$

2. If the second inequality in (1.2.26) holds, then we can obtain the relationship between the optimal wealth process X_t and the shadow process Y_t.

The first inequality in (1.2.26) is obtainable as long as there exists an π_t that satisfies the budget constraint

$$x+\frac{w}{r}=\mathbb{E}\left[\int_0^\tau H_t\left(I_c(Y_t^y)+wI_l(Y_t^y)\right)dt+H_\tau\left(I(\rho Y_\tau^y)+\frac{w}{r}\right)\right], \quad (1.2.27)$$

The second inequality in (1.2.26) holds for all $x>-\frac{w}{r}$ and $y>0$, we obtain the following inequalities

$$V(x;\tau)\leq\inf_{y>0}\bar{V}(x,y;\tau)\leq\inf_{y>0}\bar{V}(x,y). \quad (1.2.28)$$

as well as for the original and the dual problems

$$V(x)=\sup_\tau V(x;\tau)\leq\sup_\tau\inf_{y>0}\bar{V}(x,y;\tau)=\inf_{y>0}\bar{V}(x,y). \quad (1.2.29)$$

Next, we present the main results in this paper and show the optimal solution obtained through the dual problem is the optimal solution to the original problem. Firstly, we show that the equality of the budget constraint (1.2.27) is obtainable.

Lemma 1.4 (Obtainable budget constraint)**.** *For any τ, any $\mathcal{F}_\tau$-measurable B with $\mathbb{P}[B>0]=1$, any progressively measurable process $c_t\geq 0$ and $l_t\in[0,1]$that satisfy, for all $t\leq\tau$*

$$\mathbb{E}\left[\int_0^\tau H_t\left(c_t+wl_t\right)dt+H_\tau\left(B+\frac{w}{r}\right)\right]=x+\frac{w}{r}$$

there exists a portfolio process π_t such that, a.e.

$$X_t^{(c_t,l_t,\pi_t)}>-\frac{w}{r},\ \textit{for all}\ 0\leq t<\tau,\ \textit{and}\ \ X_\tau^{(c_t,l_t,\pi_t)}=B.$$

Proof: see Appendix 5.1.

Note that if $L\leq l_t\leq 1$, we will have the following inequality giving the lower bound for X_t

$$X_t\geq-\frac{w}{r}(1-L).$$

Before we obtain the optimal dual function, we need to show that all x and y that satisfies (1.2.27) cover $(-\frac{w}{r},\infty)$ and $(0,\infty)$. To see this, we define the following map on $(0,\infty)$,

$$\mathbb{X}_\tau(y)=\mathbb{E}\left[\int_0^\tau H_t\left(I_c(Y_t^y)+wI_l(Y_t^y)\right)dt+H_\tau\left(I(\rho Y_\tau^y)+\frac{w}{r}\right)\right]-\frac{w}{r},\ \text{for } \tau\in\mathbf{S}, \tag{1.2.30}$$

Recall from equations (1.2.14), (1.2.15) and (1.2.17) that $I_c(\cdot)$, $I_l(\cdot)$ and $I(\cdot)$ are continuous, strictly decreasing functions satisfy $I_c(0^+)=I(0^+)=+\infty$ and $I_c(+\infty)=I(+\infty)=0$. We can verify that $\mathbb{X}(y)$ is a continuous, strict decreasing function with $\mathbb{X}(0^+)=\infty$ and $\mathbb{X}(\infty)>-\frac{w}{r}$. Therefore, $\mathbb{X}_\tau(y)$ is a map from $(0,\infty)$ onto $(-\frac{w}{r},\infty)$ for all $\tau\in\mathbf{S}$. Thus $\mathbb{X}_\tau$ has an one-to-one inverse function $\mathbb{Y}_\tau(\cdot)$ from $(-\frac{w}{r},\infty)$ onto $(0,\infty)$ with $\mathbb{Y}_\tau(0)=\infty$ and $\mathbb{Y}_\tau(0)=-\frac{w}{r}$. For any $\tau\in\mathbf{S}$, and all $y\in(0,\infty)$

$$\bigcup_{\tau\in\mathbf{S},y\in(0,\infty)}\mathbb{X}_\tau(y), \tag{1.2.31}$$

covers $(0,\infty)$. For any $\tau\in\mathbf{S}$, and all $x\in(-\frac{w}{r},\infty)$

$$\bigcup_{\tau\in\mathbf{S},x\in(-\frac{w}{r},\infty)}\mathbb{Y}_\tau(x), \tag{1.2.32}$$

covers $(-\frac{w}{r},\infty)$. Therefore, the two sets (1.2.31) and (1.2.32) have no gap between initial x in original problem and initial y in dual problem. Therefore, we can conclude the second inequality in (1.2.29) holds and we can obtain the following result given the smoothness of the dual function

Lemma 1.5 (Optimal dual function)**.** *If $\bar{V}(x,y)$ of (1.2.25) is differentiable at $y>0$, then*

$$\frac{\partial\bar{V}}{\partial y}(x,y)=0. \tag{1.2.33}$$

Proof: see Appendix 5.2.

By Lemma 1.5 and the inequality in (1.2.26), we can obtain the optimal solution from the following theorem.

Theorem 1.6 (Attainable dual problem)**.** *Suppose the value function $V(x)$ defined in (1.1.5) is attainable. For any $x>0$, we have*

$$V(x)=\inf_{y>0}\bar{V}(x,y). \tag{1.2.34}$$

Conversely, if $c_t=I_c\left(Y_t^y\right)$ and $l_t=I_l\left(Y_t^y\right)$ are optimal then equation (1.2.34) hold and the optimal stopping rule is $\tau_y^*=\inf\left\{t\,\middle|\,Y_t^y\le y^*\right\}$.

Proof: see Appendix 5.3.

It remains to solve the dual problem (1.2.25) and then we can find the solution to the original problem (1.1.5) by Lemma 1.5 and Theorem 1.6. Following the dynamic programming principle,

we consider the stopping problem on a small interval $[t,\tau]$

$$\psi(t,y)=\sup_{\tau>t}\mathbb{E}\left[\int_t^\tau e^{-\rho s}\bar{U}_1(Y_s)ds+e^{-\rho\tau}\left(\frac{1}{\rho}\bar{U}_2(\rho Y_\tau)-\frac{w}{r}Y_\tau\right)\Big|Y_t=y\right]. \tag{1.2.35}$$

Define the differential operator $\mathcal{L}=(\rho-r)y\frac{\partial}{\partial y}+\frac{1}{2}\theta^2y^2\frac{\partial^2}{\partial y^2}$, then we obtain the following HJB equation (see Fleming and Rishel [59])

$$\max\left\{e^{-\rho t}\left(\frac{1}{\rho}\bar{U}_2(\rho y)-\frac{w}{r}y\right)-\psi(t,y),\ \ \frac{\partial\psi}{\partial t}+\mathcal{L}\psi+e^{-\rho t}\bar{U}_1(y)\right\}=0. \tag{1.2.36}$$

We use the ansatz $\psi(t,y)=e^{-\rho t}\phi(y)$ to separate the time term from the objective function, so that the HJB equation (1.2.36) can be written as

$$\max\left\{\frac{1}{\rho}\bar{U}_2(\rho y)-\frac{w}{r}y-\phi(y),\ \ -\rho\phi(y)+\mathcal{L}\phi(y)+\bar{U}_1(y)\right\}=0. \tag{1.2.37}$$

By analogy of Section 2.7 in Karatzas, Shreve, Karatzas, and Shreve [82], the solution to the stopping problem (1.2.35) satisfies the following variational inequalities. We determine the boundary y^* and a continuous function $\phi\in C^1(\mathbb{R}^+)\cap C^2(\mathbb{R}^+\setminus\{y^*\})$ satisfying

Definition 1.7. *(Variational inequality) Find a free boundary y^* and a non-increasing convex function $\phi\in C^1(\mathbb{R}^+)\cap C^2(\mathbb{R}^+\setminus\{y^*\})$ satisfying*

$$\begin{cases}-\rho\phi+\mathcal{L}\phi+\bar{U}_1(y)=0,\ \ y^*<y\\ -\rho\phi+\mathcal{L}\phi+\bar{U}_1(y)\le 0,\ \ 0<y\le y^*\\ \phi(y)\ge\dfrac{1}{\rho}\bar{U}_2(\rho y)-\dfrac{w}{r}y,\quad y^*<y\\ \phi(y)=\dfrac{1}{\rho}\bar{U}_2(\rho y)-\dfrac{w}{r}y,\quad 0<y\le y^*.\end{cases} \tag{1.2.38}$$

If $\phi(y)$ solves the variational inequalities (1.2.38) then according to the definition of the dual problem (1.2.25) the solution to the dual problem is given by

$$\bar{V}(x,y)=\psi(0,y)+y\left(x+\frac{w}{r}\right)=\phi(y)+y\left(x+\frac{w}{r}\right), \tag{1.2.39}$$

thus we have the following verification theorem as a result of (1.2.25) and (1.2.38).

Theorem 1.8 (Verification theorem)**.** *Suppose $\phi(y)$ is a solution to (1.2.38) and there exists a y^* such that $\phi'(y)$ is absolutely continuous at y^*. Then $\bar{V}(x,y)=\phi(y)+y\left(x+\frac{w}{r}\right)$ and $\tau_y^*=\inf\{t\ge 0:Y_t^y\le y^*\}$ are the unique solution of the problem (1.2.25).*

Proof: see Appendix 5.4.

The following two lemmas give the unique solution to the variational inequalities.

Lemma 1.9 (Existence and uniqueness)**.** *If $p_1' < p_2'$ then there exists an unique $y^* > 0$ such that*

$$\int_{+\infty}^{y^*} \frac{\bar{U}_1(z) + \frac{n(p_2')}{\rho}\bar{U}_2(\rho z) + wz}{z^{n_1+1}} dz = 0, \tag{1.2.40}$$

where $n(x) = \frac{1}{2}\theta^2 x^2 + (\rho - r - \frac{1}{2}\theta^2)x - \rho$.

Proof: see Appendix 5.5.

Lemma 1.10 (Optimal solution)**.** *If $p_1' < p_2'$ then there exists an unique free boundary $y^* > 0$ and a unique function ϕ that solves the free boundary ODE in (1.2.38).*

$$\phi(y) = \begin{cases} Cy^{n_2} + \dfrac{2y^{n_1}}{\theta^2(n_1-n_2)} \displaystyle\int_{+\infty}^{y} \frac{-\bar{U}_1(z)}{z^{n_1+1}} dz - \frac{2y^{n_2}}{\theta^2(n_1-n_2)} \int_{y^*}^{y} \frac{-\bar{U}_1(z)}{z^{n_2+1}} dz, & y^* < y \\ \dfrac{1}{\rho}\bar{U}_2(\rho y) - \dfrac{w}{r} y, & 0 < y \le y^*, \end{cases} \tag{1.2.41}$$

where

$$C = \frac{y^{*-n_2}}{n_1 - n_2}\left((n_1 - p_2')\frac{1}{\rho}\bar{U}_2(\rho y^*) - (n_1 - 1)\frac{w}{r}y^*\right),$$

and n_1 and n_2 are the two roots of

$$n(x) = \frac{1}{2}\theta^2 x^2 + (\rho - r - \frac{1}{2}\theta^2)x - \rho,$$

with $n_1 > 1$, $n_2 \le -\frac{2(\rho - r)}{\theta^2}$.

Proof: see Appendix 5.6.

Consider the case of no labor income ($L = 1$). By Lemma 1.10 we have

$$\frac{2\bar{A}y^{*p_1'}}{\theta^2(p_1' - n_1)} = \frac{(p_2' - n_2)y^{*p_2'}}{\rho p_2'}\left(\frac{\rho}{k}\right)^{p_2'}.$$

The value $p_1' = \frac{\alpha(1-p_1)}{\alpha(1-p_1)-1}$ and $p_2' = \frac{p_2 - 1}{p_2}$ given in (1.2.12) and (1.2.12) are the same in the models with labor income or without labor income. The optimal solution to the model without labor exists if and only if $p_1' \neq p_2'$ and the unique solution to the dual value function is given by

$$y^* = \left(-\frac{p_1'}{p_2'}\frac{\theta^2}{2\rho}(p_1' - n_1)(p_2' - n_2)\alpha^{p_1'-1}\left(\frac{\rho}{k}\right)^{p_2'}\right)^{\frac{1}{p_1' - p_2'}}.$$

According to the Lemma 1.10, we define the critical wealth level

$$x^* = I(\rho y^*).$$

By Lemma 1.5 and Lemma 1.10, we obtain

$$\begin{aligned} x &= -\phi'(y) - \frac{w}{r} \\ &= -Cn_2 y^{n_2-1} - \frac{2n_1 y^{n_1-1}}{\theta^2(n_1-n_2)} \int_{+\infty}^{y} \frac{-\bar{U}_1(z)}{z^{n_1+1}} dz + \frac{2n_2 y^{n_2-1}}{\theta^2(n_1-n_2)} \int_{y^*}^{y} \frac{-\bar{U}_1(z)}{z^{n_2+1}} dz - \frac{w}{r}, \end{aligned}$$

From Theorem 1.6, Theorem 1.8 and Lemma 1.10, we have the following theorem which gives the main results of the original value function.

Theorem 1.11 (Optimal value function)**.** *If $\alpha(1-p_1) > 1-p_2$, then there exists an unique free boundary x^* that solves the optimal stopping problem (1.1.5) and the value function $V(x)$ is given by*

$$V(x) = \begin{cases} y\left(x + \dfrac{w}{r}\right) + Cy^{n_2} + \dfrac{2y^{n_1}}{\theta^2(n_1-n_2)} \displaystyle\int_{+\infty}^{y} \frac{-\bar{U}_1(z)}{z^{n_1+1}} dz \\ \qquad\qquad - \dfrac{2y^{n_2}}{\theta^2(n_1-n_2)} \displaystyle\int_{y^*}^{y} \frac{-\bar{U}_1(z)}{z^{n_2+1}} dz, & x < x^* \\ \dfrac{1}{\rho} U_2(x), & x^* \le x, \end{cases} \tag{1.2.42}$$

and the value of x^* is given by

$$x^* = I(\rho y^*),$$

where y^* is determined by the following equation

$$\frac{2y^{*n_1}}{\theta^2} \int_{+\infty}^{y^*} \frac{\bar{U}_1(z) + wz}{z^{n_1+1}} dz = -(p_2' - n_2) \frac{1}{\rho} \bar{U}_2(\rho y^*), \tag{1.2.43}$$

and y is the solutions to the equation

$$x = -Cn_2 y^{n_2-1} - \frac{2n_1 y^{n_1-1}}{\theta^2(n_1-n_2)} \int_{+\infty}^{y} \frac{-\bar{U}_1(z)}{z^{n_1+1}} dz + \frac{2n_2 y^{n_2-1}}{\theta^2(n_1-n_2)} \int_{y^*}^{y} \frac{-\bar{U}_1(z)}{z^{n_2+1}} dz - \frac{w}{r}. \tag{1.2.44}$$

Equation (1.2.44) in Theorem 1.11 shows the map between wealth level x in the original problem (1.1.5) and the shadow price y in dual problem (1.2.25). To obtain the optimal wealth process and optimal strategy, we let Y_t be the stochastic process defined in equation (1.2.18) and y is the solution from the Theorem 1.11. We substitute Y_t for y and X_t for x into equation (1.2.44), then we get the optimal wealth process

$$\begin{aligned} X_t = -Cn_2 (Y_t)^{n_2-1} &- \frac{2n_1 (Y_t)^{n_1-1}}{\theta^2(n_1-n_2)} \int_{+\infty}^{Y_t} \frac{-\bar{U}_1(z)}{z^{n_1+1}} dz \\ &+ \frac{2n_2 (Y_t)^{n_2-1}}{\theta^2(n_1-n_2)} \int_{y^*}^{Y_t} \frac{-\bar{U}_1(z)}{z^{n_2+1}} dz - \frac{w}{r}. \end{aligned} \tag{1.2.45}$$

The optimal stopping time to both the original problem (1.1.5) and the dual problem (1.2.25) is

given by

$$\tau^* = \bar{\tau}_y^* = \inf\left\{t : Y_t^y \le y^*\right\}.$$

Theorem 1.12 (Optimal controls)**.** *The optimal strategies* $(c_t^*, l_t^*, \pi_t^*, \tau^*)$ *are given by*

$$c_t^* = \begin{cases} \left(\dfrac{Y_t}{\alpha}\right)^{p_1'-1}, & \text{if } Y_t < \tilde{y} \\ \left(\dfrac{Y_t}{\alpha}\right)^{p-1}\left(\dfrac{\alpha w}{\beta}\right)^{\frac{\beta}{(\alpha+\beta)}p}, & \text{if } \tilde{y} \le Y_t \le \bar{y} \\ \left(\dfrac{Y_t}{\alpha}\right)^{p_1'-1} L^{-\frac{\beta}{\alpha}p_1'}, & \text{if } \bar{y} < Y_t, \end{cases}$$

$$l_t^* = \begin{cases} 1, & \text{if } Y_t < \tilde{y} \\ \left(\dfrac{Y_t}{\alpha}\right)^{p-1}\left(\dfrac{\alpha w}{\beta}\right)^{\frac{\beta}{(\alpha+\beta)}p-1}, & \text{if } \tilde{y} \le Y_t \le \bar{y} \\ L, & \text{if } \bar{y} < Y_t, \end{cases}$$

$$\begin{aligned} \pi_t^* = & \frac{\mu - r}{\sigma^2}\Bigg(Cn_2(n_2-1)Y_t^{n_2-1} - \frac{2\bar{U}_1(Y_t)}{\theta^2 Y_t} \\ & + \frac{2n_1(n_1-1)Y_t^{n_1-1}}{\theta^2(n_1-n_2)}\int_{+\infty}^{Y_t}\frac{-\bar{U}_1(z)}{z^{n_1+1}}dz - \frac{2n_2(n_2-1)Y_t^{n_2-1}}{\theta^2(n_1-n_2)}\int_{y^*}^{Y_t}\frac{-\bar{U}_1(z)}{z^{n_2+1}}dz\Bigg), \end{aligned}$$

and

$$\tau^* = \inf\left\{t > 0 :\ X_t \ge x^*\right\}.$$

Proof: see Appendix 5.7.

We obtain the explicit solutions for the optimal control terms (c_t^*, l_t^*, π_t^*) in terms of the dual process. As for the optimal stopping time τ^*, it can be solved by numerical methods, which we will present in the next section.

1.3 Numerical Results

In this section, we present the analytic results and simulation results. In the first part, the analytic results show the connection between the amount of the annuity, labor rate and wage rate under different annuity schemes. In the second part, we investigate the optimal annuity time that is not revealed from the analytic solution. We choose a typical market scenario for investment and simulate the behavior of retirees by Monte-Carlo methods. Throughout the applications we analyze the optimal consumption, labor and investment strategies under the same market scenario with

different labor constraints. Some comparisons are made between retirees with labor income and without labor income after retirement. We show statistical results including the distribution of the optimal annuitization time τ and the size of the annuity upon annuitization.

1.3.1 Analytic results

Recall the optimal solution x^* which is the critical wealth level that once reached triggers annuitization. We are interested in the dependency of the optimal solution x^* on the parameters of the problem. In our model, we have introduced the wage rate w and labor rate $L = 1 - l$ as new factors in addition to the consumption rate c_t. We can also extend the solutions from Lemma 1.10 and Theorem 1.11 to the model without labor by simply letting $w = 0$ and $L = 1$. We include the weights given to the penalty for running consumption v_1 and the penalty for final annuitization, v_2. The ratio of these rates v_1/v_2 is the relevant quantity and it gives us the following objective function.

$$V(x) = \max_{c_t, l_t, \pi_t, \tau} \mathbb{E}^x \left[v_1 \int_0^\tau e^{-\rho t} U_1(c_t, l_t) dt + v_2 \frac{e^{-\rho \tau}}{\rho} U_2(k X_\tau^{0,x}) \right].$$

We choose the death rate of a male retiree at age 60 to be $\delta = 0.00887$ with the same risk aversion between consumption and annuity $p_1 = p_2$. Financial profiles and utility schemes are given by the parameters

$$r = 0.03; \quad \mu = 0.08; \quad \sigma = 0.2; \quad \rho = 0.03887; \quad k = 0.095;$$
$$p_1 = 2; \quad p_2 = 2; \quad \alpha = 0.5; \quad \beta = 1; \quad v_1 = 0.01; \quad v_2 = 0.1;$$

The optimal solution x^* and value functions are given in Figure (1.1) from which we see that the extra labor income after retirement has a significant impact on increasing the critical wealth level. If the retiree does not work after retirement, then his critical wealth level is $x^*(w) = 1028.05$. Otherwise, his critical wealth level are $x^*(w) = 1179.42$ for wage rate $w = 50$ and $x^*(w) = 1413.38$ for wage rate $w = 100$.

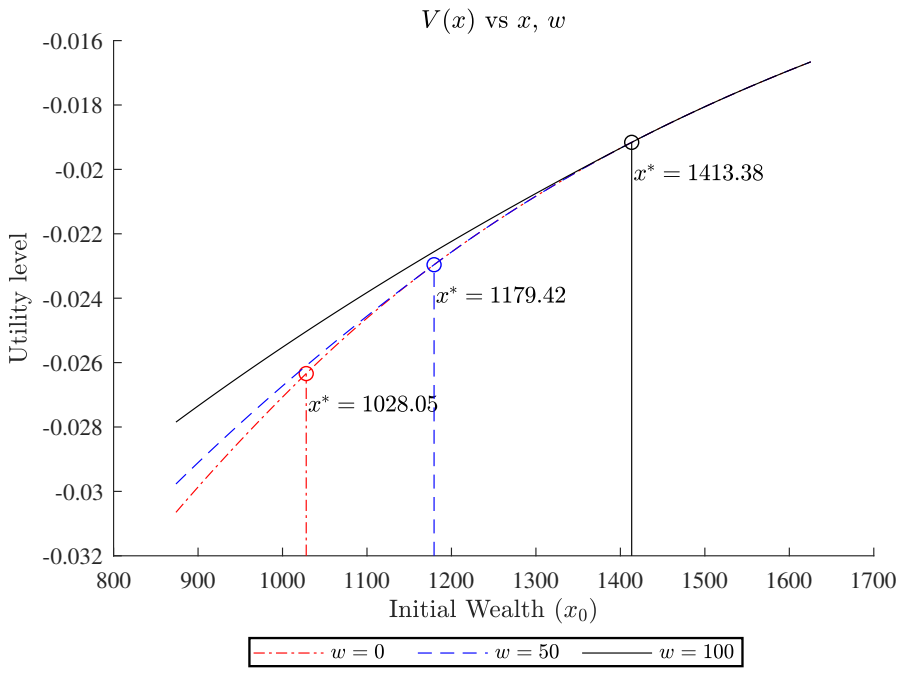

Figure 1.1: Value Function with different wage rates and labor rates

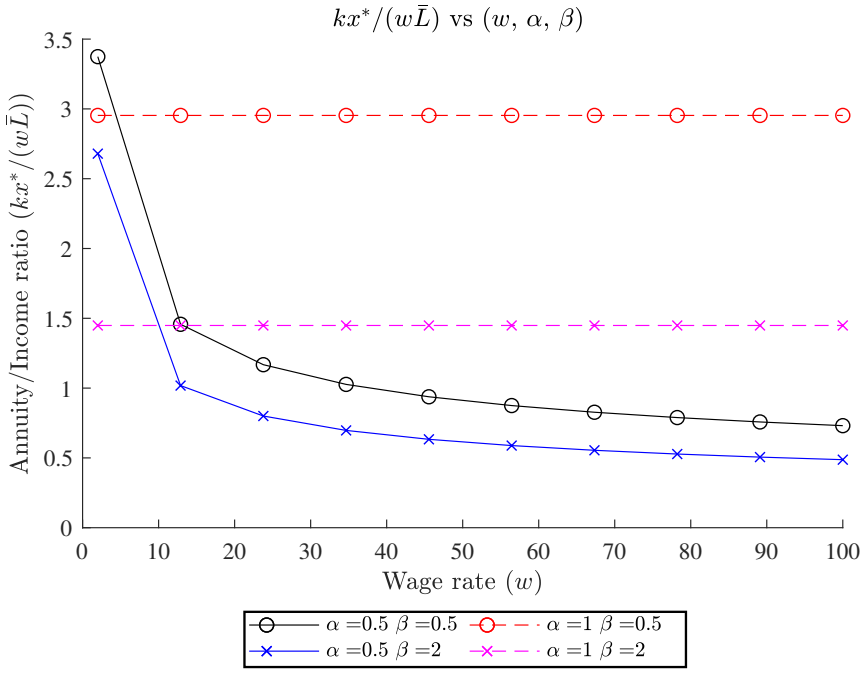

Figure 1.2: Optimal solution ($p_1 = p_2 = 2,\ v_1 = v_2 = 0.01$).

Recall that the value β is the retiree's preference to labor. Since $\partial U_1/\partial\beta < 0$, a retiree with a

higher β prefers to work less. Figure 1.2 shows the dependence of critical wealth level x^* on the choice of labor and consumption. We obtain the following results

1) If $\alpha(1-p_1) = 1-p_2$, the wage rate does not affect the annuity which is shown in the case $\alpha = 1$ in Figure 1.2.

2) If $\alpha(1-p_1) > 1-p_2$, the wage rate has decreasing marginal effect on annuity which is shown in the case $\alpha = 0.5$ in Figure 1.2.

3) Everything else equal, the critical wealth level x^* increases as β decreases. In other words, a labor tolerant retiree receives a higher annuity than a labor averse retiree.

4) Everything else equal, the critical wealth level x^* increases as α increases. In other words, the retiree consumes less before annuitization will receive a higher annuity than the one who consumes more.

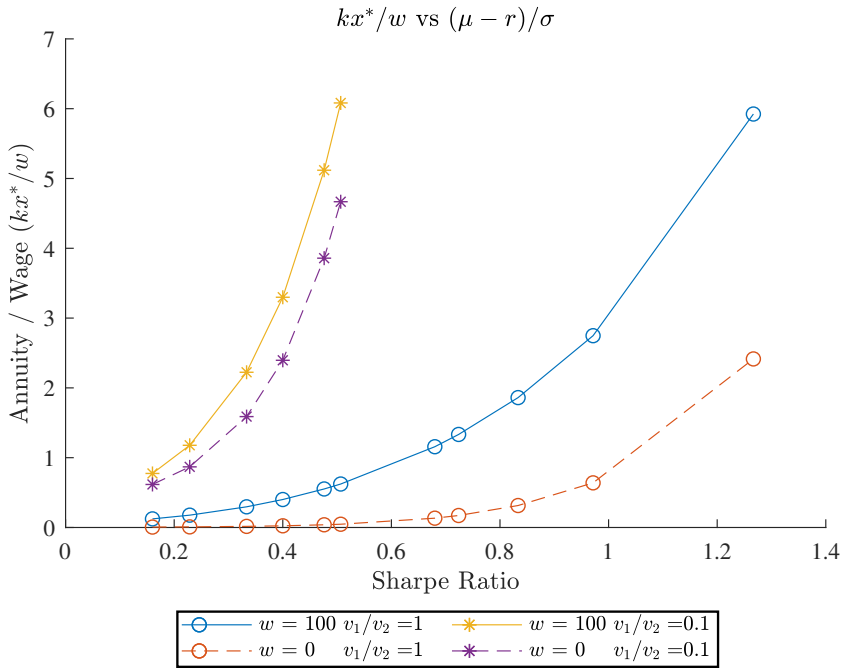

Figure 1.3: Annuity/wage ratio as function of Sharpe ratio

Figure 1.3 shows the dependence of annuity/wage ratio on the Sharpe ratio and (v_1/v_2). The value of the Sharpe ratio is changed by varying the value of $\mu \in (0.07, 0.15)$, $\sigma \in (0.1, 0.25)$. The weight v_1 is fixed at 0.01 and the weight v_2 is chosen between 0.01 and 0.1. The relevant quantity v_1/v_2 shows the retiree's preference between consumption and annuitization. As shown in Figure 1.3, the retiree with high ratio of $v_1/v_2 = 1$ has a lower annuity than the retiree with low ratio of $v_1/v_2 = 0.1$. This can be explained from the weights of utility functions. The retiree with low ratio of v_1/v_2 gets less utility from consumption and gets a higher utility from the annuity as compensation. On the contrary, the pensioner with high ratio of v_1/v_2 receives higher utility from consumption and receives less utility from the annuity.

1) The optimal value with labor is higher than the optimal value without labor in any scenario. The effect of labor on the optimal solution x^* becomes more obviously as the Sharpe ratio increases.

2) Everything else equal, increasing the ratio of v_1/v_2, increases the critical level and it becomes harder to reach x^* when the Sharpe ratio is also high. This can be explained easily. For a higher ratio of v_1/v_2, the retiree puts higher weight on the stopping utility and makes the running utility less important in the objective function, so a higher value is formed.

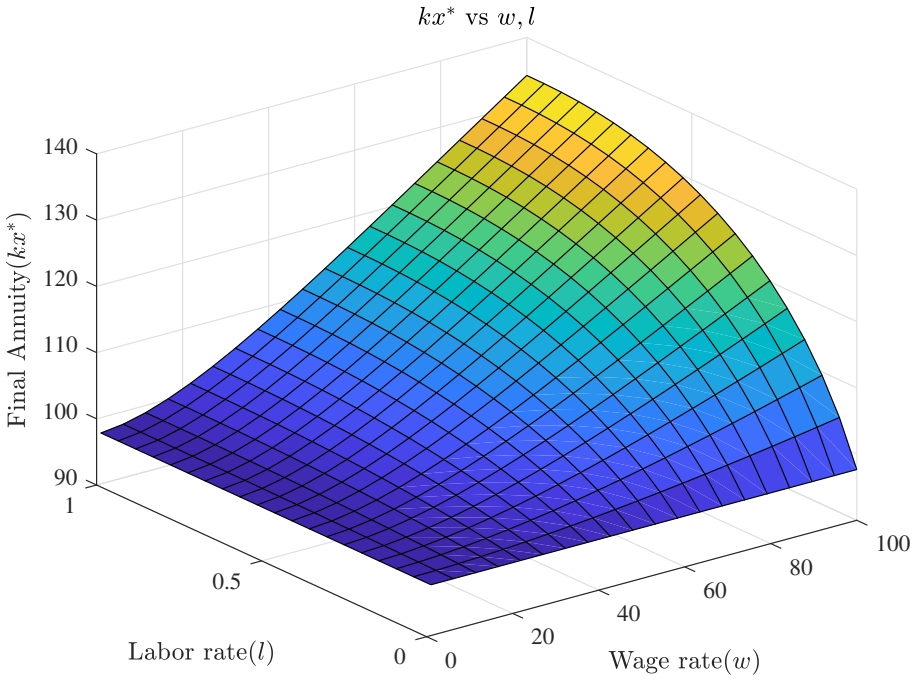

Figure 1.4: Optimal annuity as a function of wage rate and labor rate

Figure 1.4 shows the optimal annuity as a function of wage rate w and maximum labor rate L. Through these results, we can conclude that the labor income is a crucial factor to increase the critical wealth level and the relevant quantity v_1/v_2 has a large impact on balancing consumption and the final annuity. In next section, we assume the retiree wants a higher target value of the annuity, therefore, a low ratio of v_1/v_2 will be chosen in the following simulations.

1.3.2 Simulation results

In this section, we apply the numerical results of our model to analyze the behavior of retirees with different labor schemes. The following scenarios have been implemented by Monte-Carlo simulation for $n = 1000$ financial scenarios and in each scenario the retiree has adopted the optimal investment, labor, and consumption strategies. We also set 15 years as the deadline for annuitization whether the retiree reaches the critical wealth level or not. We study the behavior of a age 60

male pensioner ($\delta = 0.00875$) with labor income ($w = 100$) or no labor income ($w = 0$). We vary the initial lump sum from $x_0 = 300$ to $x_0 = 1500$ and choose other parameters as following

$$r = 0.03; \quad \mu = 0.08; \quad \sigma = 0.20; \quad k = 0.095; \quad L = 0.5867$$

$$p_1 = 2; \quad p_2 = 2; \quad \alpha = 0.5; \quad \beta = 0.65; \quad v_1 = 0.01; \quad v_2 = 0.1.$$

In this case the critical wealth level is

$$x^*(w = 0) = 1028.05, \text{ and } x^*(w = 100) = 1413.38.$$

We investigate how labor income affects annuitization. Firstly, we compare two models one with labor income ($w = 100$) and the other one without labor income ($w = 0$) by fixing the other parameters.

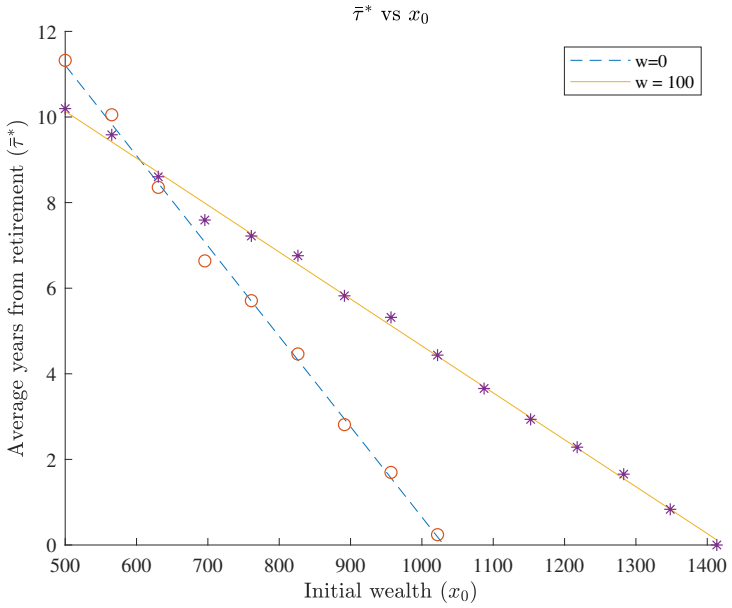

Figure 1.5: Average years to annuitization as a function of initial wealth

Figure 1.5 shows the simulation results of the optimal annuitization (τ^*) time shown as scatter points with fitted straight lines where we start the simulations with different initial wealth (x_0) and different labor schemes (w). As the optimal annuitization times are linear to the initial wealth, we can see that the labor income increases optimal annuitization time as the critical wealth is increased from from $x^*(w = 0) = 1028.05$ to $x^*(w = 100) = 1413.38$. Only when the initial wealth $x_0 < 600$, does the labor income decrease the optimal annuitization time.

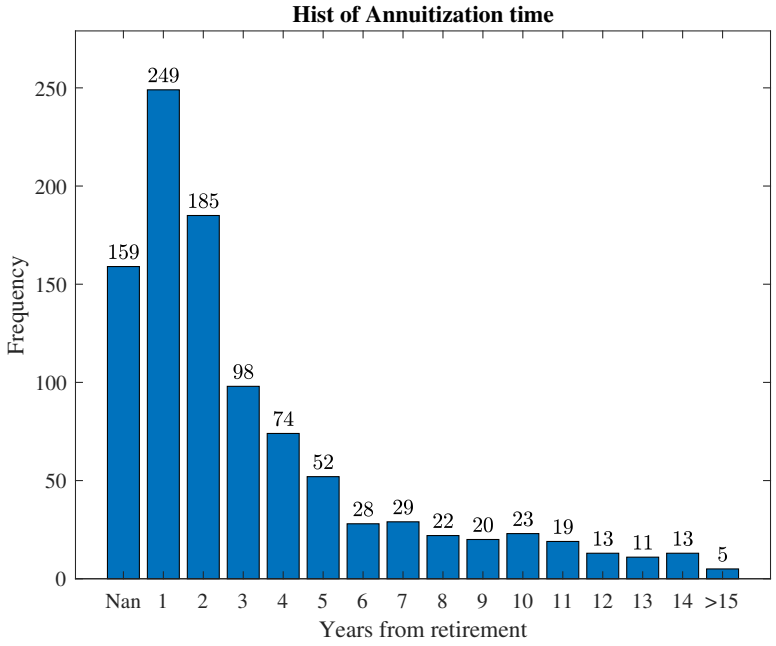

Figure 1.6: Histogram: The distribution of the optimal annuitization time

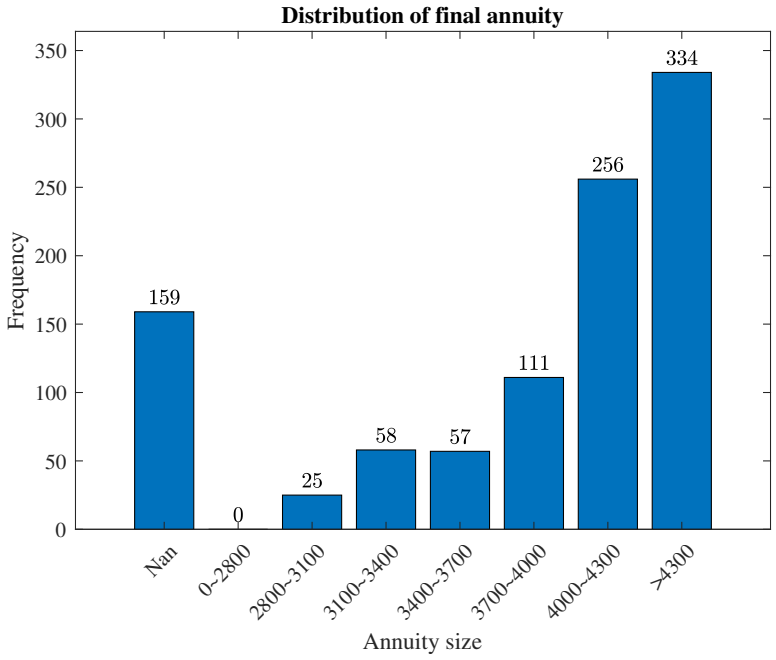

Figure 1.7: Distribution of the present value of total annuity of the pensioner

Figure 1.6 and Figure 1.7 shows the distribution of annuitization time and the present value of the final annuity of the retiree with labor income ($w = 100$). In both figures, the first columns labeled 'Nan' shows 159 cases out of 1000, in which the retiree has failed to reach the critical wealth level within 15 years and thus no optimal annuitization occurred. In other words, the

probability of annuitization within 15 years is 84.10% and the average annuitization time is 5.57 years after retirement. In 59% of the cases, the annuity amount is greater than 4000 and in 25.1% of the cases the annuity amount is less than 4000. The average annuity amount is 3682.60.

Secondly, we compare the two retirees with the same critical level but different labor scheme. The first retiree has labor scheme ($L = 0.5867$, $\beta = 0.65$) and second one has labor scheme ($L = 1$, $\beta = 1$) such that they have the same critical level $x^* = 1413.38$. Figure 1.8 shows their optimal strategies when they face the same market case. The graphs on left side of Figure 1.8 report the strategies of the first retiree who is willing to work more after retirement. The first retiree's investment strategy is to hold stocks in a long position until his total wealth hits the critical level.

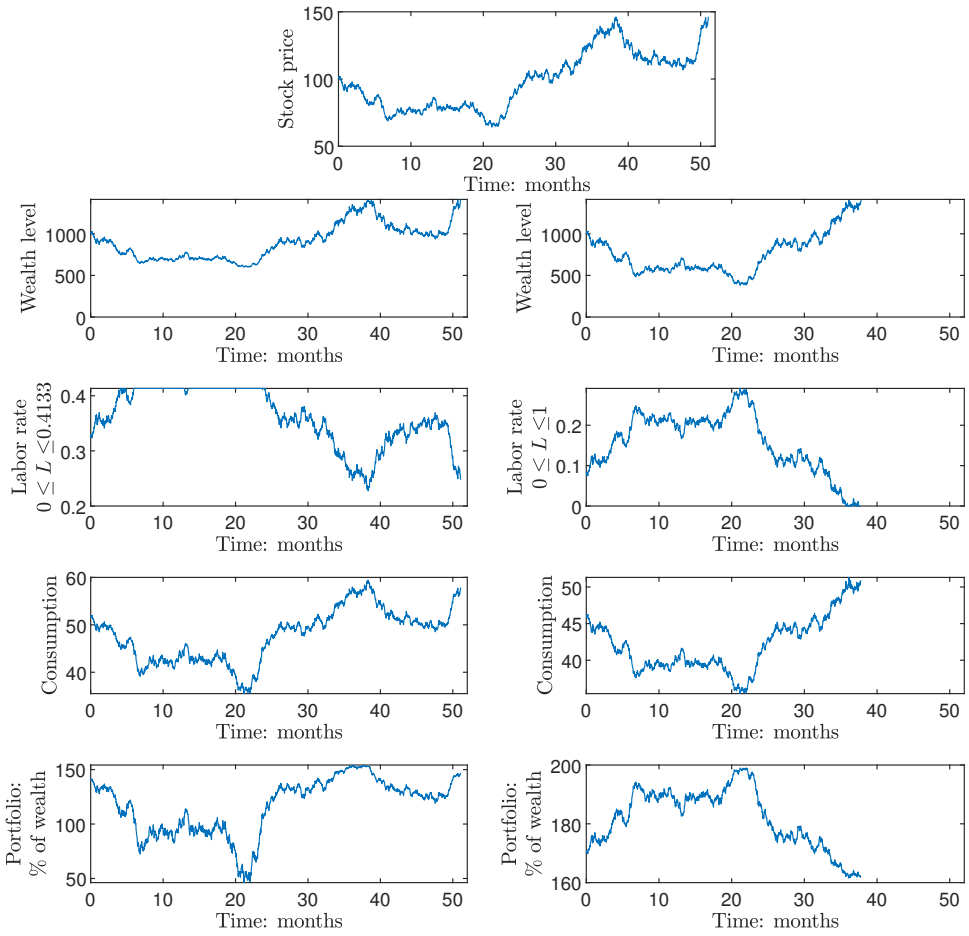

Figure 1.8: Optimal strategies: portfolio, consumption and labor

The graphs on the left side in Figure 1.8 report the strategies of the first retiree and the graphs on right side in Figure 1.8 report the strategies of the second retiree. From the portfolio amount we see they implemented the opposite investment strategies. The first retiree invests more when the stock price is increasing while the second retiree intends to buy low and sell high. We can notice

that the first retiree takes longer to annuitize than the second one because his wealth accumulation speed is lower than the second retiree. However, from the comparison of consumption and labor, the first retiree both consumes and works more than the second retiree. We also find the interesting relationship between the optimal strategies. The consumption rate is exactly positively proportional to total wealth. The labor rate is opposite to the tendency of stock price. Both retirees tend to work more when the stock price is declining and work less when the stock price is increasing. Therefore, we can conclude that the labor income is a hedging tool for the portfolio and the total wealth is sustained with high stability with the help of labor income.

Table 1.1: Comparison of the expected present value of labor income, consumption, annuity and annuitization time

	Labor		Consumption		Annuity		Total EPV		Years	
	model 1	model 2	model 1	model 2	model 1	model 2	model 1	model 2	model 1	model 2
min	3.02	0.37	5.81	4.52	1096.30	302.49	1647.20	735.98	1	1
5th	10.55	1.22	19.59	13.64	1357.30	563.53	1834.90	992.24	1	1
25th	19.90	3.63	29.98	26.57	3507.10	3672.60	3859.60	3942.70	1	1
50th	27.30	6.71	36.92	32.87	4156.20	4220.30	4285.90	4318.10	3	3
75th	30.93	11.77	41.67	36.94	4367.30	4403.30	4417.80	4438.10	9	7
95th	32.89	23.39	47.50	42.20	4444.40	4479.30	4466.10	4498.30	15	15
max	34.91	40.44	52.90	46.95	4516.30	4581.40	4536.30	4597.70	15	15
mean	25.01	8.69	35.59	31.18	3682.60	3676.60	3877.80	3839.40	5.57	5.08

Finally, we summarize the statistical difference between 'model 1' with labor scheme ($L = 0.5867$, $\beta = 0.65$) and 'model 2' with labor scheme ($L = 1$, $\beta = 1$), which is shown in Figure 1.1. For the retirees who do not reach the critical wealth level within 15 years, we force them to annuitize at the end of 15 years. All the streams of labor income, consumption and annuity are discounted to retirement with the interest rate r. The labor column reports the expected present value (EPV) of yearly labor income before annuitization. The consumption column reports the EPV of yearly consumption before annuitization. The annuity column reports EPV of total annuity from annuitization to death. Total EPV reports the EPV of all consumption and annuity since retirement. On average, the optimal annuitization, annuity and total EPV occurs in both models are almost the same. However, the consumption in model 1 is higher than that in model 2 in all cases and the minimums of annuity and total EPV in model 1 are almost double the amounts in model 2. Therefore, the comparison indicates model 1 is more stable in the final results and thus more appealing to risk-averse pensioners.

1.4 Conclusion

In this chapter, we fully solved the maximization of the Cobb-Douglas utility with stochastic control and deterministic control, and derived a closed-form solution to the value function. We give a rigorous proof that shows our solution is the optimal one to the post-retirement annuitization problem with extra labor income. We studied the explicit solution and the property of adding the extra labor income to the system showing that the utility is concave in labor rate and convex in wage rate. In the simulation, we find the optimal annuitization time is strongly linear to the initial wealth in both cases with and without labor income. We also find there exits a critical wealth level

below which the extra labor income shrinks the annuitization time and above which the extra labor income postpone the annuitization time in exchange for higher annuities. We also find that with different labor schemes, the pensioners could have similar consumption strategies. However, they would work and invest in the opposite way and achieve to very different annuitization times.

Chapter 2

Convolution methods in option pricing

In this chapter, we review option pricing problems with a convolution approach. Basket options and spread options with multiple underlying assets are examples of options which depend on multiple assets and risk-factors. The difficulty of pricing high-dimensional options is mainly from two aspects. Classical numerical approaches suffer from the curse of dimensionality. Another important reason is lacking of efficient tools to handle computation under high-dimensional environments. Monte-Carlo simulation is applicable to high-dimensional problems but as the dimension of underlying assets grows, simulation methods require sampling of increasing number of paths. That is computational complexity grows exponentially as the dimension increases, while the accuracy declines sharply. Recently, deep-learning method has have achieved great success in many application areas, such as computer vision, natural language processing, gaming, and other including finance.

2.1 Option pricing background

Black and Scholes [8] proposed what is now called the Black-Scholes formula to price options. The Black-Scholes model gives a theoretical calculation of European-style option price given the following assumptions:

1. The stochastic process of stock price follows a geometric Brownian motion.
2. The stock has no dividends or other cash gains during the life of the option.
3. The financial market is frictionless and complete. There are no taxes, transaction costs or risk-free arbitrage opportunities. Together with the second point, the investors' income comes only from price changes, and there are no other influencing factors.

4. The risk-free rate is constant. Investors can borrow funds at this rate

Mathematically, the above assumptions give the following formulation of the market model. The stock price S_t is geometric Brownian motion

$$dS_t = \mu S_t dt + \sigma S_t dW_t, \tag{2.1.1}$$

where W_t is standard Brownian motion.

Black and Scholes [8] introduced the hedging argument that we can setup a self-financing portfolio using a certain amount of a risky asset and the corresponding option at a specific investing/borrowing rate. Under the hedging argument, Black and Scholes [8] find the option $V(t,S)$ with European-style boundary conditions in a complete market satisfies the PDE given by

$$\begin{aligned} \frac{\partial V}{\partial t} + rS\frac{\partial V}{\partial S} + \frac{1}{2}\sigma^2 S^2 \frac{\partial^2 V}{\partial S^2} &= rV, \\ V(T,S) &= g(S), \end{aligned}$$

where $g(S) = (S-K)^+$ or $(K-S)^-$ is the boundary condition for call or put options with strike K, respectively. The Black-Scholes model model leads to a semi-explicit solution for the price of the option:

$$\begin{aligned} V_c &= S_0 N(d_1) - Ke^{-rT} N(d_2), \text{ for a call option} \\ V_p &= Ke^{-rT} N(-d_2) - S_0 N(-d_1), \text{ for a put option} \end{aligned}$$

where $N(x)$ is the cumulative function of Gaussian distribution

$$\begin{aligned} d_1 &= \frac{\ln\left(\frac{S_0}{K}\right) + \left(r + \frac{1}{2}\sigma^2\right)T}{\sigma sqrtT}, \\ d_2 &= \frac{\ln\left(\frac{S_0}{K}\right) + \left(r - \frac{1}{2}\sigma^2\right)T}{\sigma sqrtT} = d_1 - \sigma\sqrt{T}. \end{aligned}$$

We use the Black-Scholes model model as a benchmark to compare the performance of different models.

A basket option is an exotic option whose underlying asset is composed of a portfolio of different assets. For a d-dimensional basket option with the underlying assets $S_t \in \mathbb{R}^d$ and a strike price K, we define the price as a conditional expected form

$$BC(S,K) = \mathbb{E}\left[e^{-rT} g(S_T) \middle| S_0 = S\cdot\right].$$

where $g(\cdot)$ is the payoff function at terminal time T,

$$g(X) = \max\left\{w^T X - K, 0\right\},$$

$w^T X$ is sum of weighted asset prices, and w represents the percentage investment in each asset.

2.2 BSDE characterization of option prices

Suppose the stock prices S_t are defined with d-underlying assets in $\mathbb{R}^d$

$$S_t = S_0 \exp\left\{\left(\mu - d - \frac{1}{2}\mathrm{tr}\left(\sigma\sigma^T\right)\right)t + \sigma W_t\right\}, \tag{2.2.1}$$

and the logarithm of the stock prices $S_t = S_0 e^{X_t}$ is given by

$$X_t = X_0 + \int_0^t \mu\left(s, X_s\right) - d\left(s, X_s\right) - \frac{1}{2}\mathrm{tr}\left(\sigma\sigma^T\right)\left(s, X_s\right) ds + \int_0^t \sigma\left(s, X_s\right) dW_s, \tag{2.2.2}$$

where d is dividend, the d-dimensional standard Brownian motion W_t is subject to d-dimensional Gaussian density $\mathcal{N}^d(0,t)$ with the density function

$$\phi\left(X\right) = \left(2\pi t\right)^{-\frac{d}{2}} e^{\frac{X^T X}{2t^d}}. \tag{2.2.3}$$

Denote the contingent claim Y_t with payoffs $g(X_T)$ at time T by a backward stochastic process with a control term Z (see Pardoux and Peng [103])

$$Y_t = g(X_T) + \int_t^T f\left(s, X_s, Y_s, Z_s\right) ds - \int_t^T Z_s dW_s \tag{2.2.4}$$

with respect a driver function f which ensures the contingent claim is arbitrage-free under the risk neutral measure and the strategy Z. In the market with borrowing rate R_t, the driver function for basket options of European or American type is given by

$$f(t,x,y,z) = -r_t y - \left(\mu^T - d_t - r\right)\sigma^{-1} z + \left(R_t - r_t\right)\left(y - \mathrm{tr}\left(\sigma^{-1} z\right)\right)^{-}. \tag{2.2.5}$$

Equation (2.2.2) and equation (2.2.4) define a forward-backward stochastic differential equations (FBSDE)

$$\begin{cases} X_t = X_0 + \int_0^t \mu\left(s, X_s\right) ds + \int_0^t \sigma\left(s, X_s\right) dW_s, \\ Y_t = g(X_T) + \int_t^T f\left(s, X_s, Y_s, Z_s\right) ds - \int_t^T Z_s dW_s. \end{cases} \tag{2.2.6}$$

The problem is to find a pair of adapted processes (Y_t, Z_t), which satisfy (2.2.6), given the dynamics of X_t and the terminal condition of Y_T. To ensure the existence and uniqueness of an adapted solution to (2.2.6), we define the following Lipschitz conditions and bounded variation conditions (see e.g. Ma, Morel, and Yong [94]).

Assumption 2.1. *For the existence of a solution of the FBSDE, we assume the following conditions are satisfied:*

(i) The functions $\mu : [0,T] \times \mathbb{R}^d \to \mathbb{R}^d$, $\sigma : [0,T] \times \mathbb{R}^d \to \mathbb{R}^{d\times d}$, $f : [0,T] \times \mathbb{R}^d \times \mathbb{R} \times \mathbb{R}^d \to \mathbb{R}$ and $g : \mathbb{R}^d \to \mathbb{R}$ are uniformly Lipchitz continuous with bounded first order derivatives in the

space variables, for all $t \in [0,T]$,

$$\begin{aligned}
|\mu(t,u)-\mu(t,v)| &\leq K(|u-v|),\\
|\sigma(t,u)-\sigma(t,v)| &\leq K(|u-v|),\\
|g(u)-g(v)| &\leq K(|u-v|),\\
|f(t,\xi)-f(t,\zeta)| &\leq K(|\xi-\zeta|_\infty),
\end{aligned}$$

for some constant K *independent of* $u,v \in \mathbb{R}^d$ *and* $\xi,\zeta \in \mathbb{R}^d \times \mathbb{R} \times \mathbb{R}^d$.

(ii) The volatility $\Sigma = \sigma\sigma^T$ *is continuous and bounded in* L^2 *space*

$$\|\Sigma\|_2 \leq C, \tag{2.2.7}$$

for some positive constant C.

Under the Assumption 1, the FBSDE (2.2.6) has an unique solution and the adapted process in (2.2.4) is given by (see Duffie [47])

$$Y_t^{t,x} = \mathbb{E}\left[g(X_T) + \int_t^T f(s,X_s,Y_s,Z_s)\,ds \middle| X_t = x \right], \tag{2.2.8}$$

Given a deterministic function $u(t,x)$ such that $Y_t^{t,x} = u(t,x)$, by the Markov property of the diffusion process, we have

$$Y_t^{s,x} = u(t, X_t^{s,x}),$$

and $X_t^{s,x}$ satisfies

$$X_t^{s,x} = x + \int_s^t \alpha(u,X_u)\,du + \int_s^t \sigma(u,X_u)\,dW_u.$$

By Itô's formula, we have, for $0 \leq s \leq t \leq 1$

$$\begin{aligned}
Y_t^{s,x} - Y_s^{s,x} &= u\left(t, X_t^{s,x}\right) - u(s,x), &(2.2.9)\\
&= \int_s^t \left(\frac{\partial u}{\partial t} + \mathcal{L}u\right)(r, X_r^{s,x})\,dr + \int_s^t \sigma^T \nabla u(r, X_r^{s,x})\,dW_r. &(2.2.10)
\end{aligned}$$

From the the dynamics of Y_t defined in (2.2.6), we have

$$Y_t^{s,x} - Y_s^{s,x} = -\int_s^t f(r, X_r^{s,x}, Y_r^{s,x}, Z_r)\,dr + \int_s^t Z_r dW_r. \tag{2.2.11}$$

where $\mathcal{L}$ is the infinitesimal generator of the diffusion X. By equating (2.2.9) and (2.2.11), we obtain

$$Z_t(X_t) = \sigma^T(t,X_t)\nabla u(t,X_t). \tag{2.2.12}$$

Applying $\nabla_x Y_t^{s,x} = \nabla_x u\left(t, X_t^{s,x}\right) = \nabla u\left(t, X_t^{s,x}\right) \partial_x X_t^{s,x}$ to equation (2.2.12), we have

$$Z_t^{s,x} = \sigma^T\left(X_t^{s,x}\right) \partial_x Y_t^{s,x} \left(\partial_x X_t^{s,x}\right)^{-1}.$$

The following Feynman-Kac formula for coupled BSDE summarizes the connection between partial differential equations (PDEs), like the heat equation, and expectation of stochastic processes with controls (see Pham [107]).

Theorem 2.2 (Feynman-Kac Theorem)**.** *If the following PDE has a solution $u(t,x) \in \mathcal{C}^{1,2}$,*

$$\frac{\partial u}{\partial t}(t,x) + \sum_{i=1}^{d} \mu_i \frac{\partial u}{\partial x_i}(t,x) + \frac{1}{2} \sum_{i,j=1}^{d} \Sigma_{i,j} \frac{\partial^2 u}{\partial x_i \partial x_j}(t,x) + f\left(t,x,u,\sigma^T \nabla_x u\right) = 0, \tag{2.2.13}$$

$$u(T,x) = g(x), \tag{2.2.14}$$

then the solution $u(t,x)$ can be written as a conditional expectation

$$u(t,x) = \mathbb{E}_{\mathbb{P}}\left[g(X_T) + \int_t^T f(s, X_s, Y_s, Z_s)\, ds | X_t = x\right],$$

where X_t is an Itô process under the probability measure $\mathbb{P}$

$$dX_t = \mu(t, X_t)\, dt + \sigma(t, X_t)\, dW_t,$$

and Y and Z are given by

$$Y_s = u\left(s, X_s^{t,x}\right),$$
$$Z_s = \nabla_x u\left(s, X_s^{t,x}\right) \sigma(s, X_s^{t,x}).$$

for all $s \in [t,T]$.

The PDE problem can be converted to a BSDE problem which can be solved by Monte-Carlo method. Conversely, the BSDE problem can be converted to a PDE problem (see Pardoux and Tang [105]), which can be solved by finite difference method. Since we are aiming at solving a high-dimensional problem, which is restricted by finite difference or finite elements, we will give a method under the BSDE framework. Probabilistic approaches include approximating the conditional expectation with a numerical scheme and simulating the forward process by Monte-Carlo methods (see Bouchard and Touzi [11]).

Next, we look into the discrete form of (2.2.6). Partition the time interval on $[0,T]$ as $0 = t_0 < t_1 < t_2 < ... < t_{N-1} < t_N = T$. We define $\Delta t_i = t_{i+1} - t_i$ and $\Delta W_{t_i} = W_{t_{i+1}} - W_{t_i}$, where $W_{t_i} \sim N^d(0, \Delta t_i)$, for $i = 0, 1, 2, ..., N-1$. Thus we rewrite (2.2.6) as the following Euler discretization

$$X_{t_{i+1}} = X_{t_i} + \mu(t_i, X_{t_i})\, \Delta t_i + \sigma(t_i, X_{t_i})\, \Delta W_i, \tag{2.2.15}$$

$$Y_{t_{i+1}} = Y_{t_i} - f(t_i, X_{t_i}, Y_{t_i}, Z_{t_i})\, \Delta t + Z_{t_i} \Delta W_{t_i}. \tag{2.2.16}$$

By taking the conditional expectation of (2.2.16) with respect to the underlying filtration $\mathcal{F}_t$ we

obtain the following approximation, (see Bouchard and Touzi [11] and Zhang [120])

$$Y_{t_i} = \mathbb{E}_{t_i}\left[Y_{t_{i+1}}\right] + \Delta t_i f\left(t_i, X_{t_i}, Y_{t_i}, Z_{t_i}\right), \tag{2.2.17}$$

Similarly, by multiplying equation (2.2.16) with ΔW_t then taking conditional expectation we have

$$Z_{t_i} = \frac{1}{\Delta t_i}\mathbb{E}_{t_i}\left[Y_{t_{i+1}}\Delta W_t\right], \tag{2.2.18}$$

Under Assumption 2.1, for discretization $\{0 = t_0 < t_1 < ... < t_n = T\}$ and sufficiently small $|\Delta t_i|_\infty = \max_{0\le i<n}|t_{i+1} - t_i|$, Bouchard, Elie, and Touzi [12] show that the following system with $\mathbb{E}_{t_i} = \mathbb{E}\left[\cdot\,|X_{t_i} = x\right]$

$$Y_T = g(X_T), \tag{2.2.19}$$

$$Z_{t_i} = \frac{1}{\Delta t}\mathbb{E}_{t_i}\left[Y_{t_{i+1}}\Delta W_{t_i}\right], \tag{2.2.20}$$

$$Y_{t_i} = \mathbb{E}_{t_i}\left[Y_{t_{i+1}}\right] + f\left(t_i, X_{t_i}, \mathbb{E}_{t_i}\left[Y_{t_{i+1}}\right], Z_{t_i}\right)\Delta t_i, \tag{2.2.21}$$

has a solution (X^π, Y^π, Z^π) and a first order quadratic error

$$\max_{0\le i<n-1}\mathbb{E}\left[\sup_{t\in[t_i,t_{i+1})}|Y_t - Y_{t_i}|^2\right] + \sum_{i=0}^{n-1}\mathbb{E}\left[\int_{t_i}^{t_{i+1}}|Z_s - Z_{t_i}|^2 ds\right] = \mathrm{O}(|\Delta t_i|_\infty).$$

In Bouchard et al. [12], the above result is proved for the explicit scheme and the same techniques can be applied to prove the implicit scheme with $f\left(t_i, X_{t_i}, Y_{t_i}, Z_{t_i}\right)$. From the relationship between the solutions of PDEs and BSDEs, we have that the first order derivative ∂u can be estimated through equation (2.2.18) by a fast Fourier transform (FFT) (see Hyndman and Oyono Ngou [74]). Following the same idea, we develop an estimation for the second order derivatives $\partial^2 u$. When applying the Fourier transform, the Nyquist relation, giving the minimal sampling frequency that is free of aliasing in the discrete time sequence, is required in the Discrete Fast Fourier Transform (DFT) while it is not required in the Fractional FFT algorithm (FrFT). In next section, we review the Discrete Fourier transform and convolution method in solving the BSDE.

2.3 Convolution method for BSDEs

The fast Fourier transform (FFT) algorithm introduced by Cooley and Tukey [25] is a milestone in signal processing which reduces the computation time of discrete Fourier transform (DFT) from $O(N^2)$ to $O(N\log N)$. The DFT algorithm is widely used in all areas of science and technology. Inspired by the convolution approach introduced by Hyndman and Oyono Ngou [74] which shows fast and accurate numerical solutions of the BSDEs associated with European option pricing under the Black-Scholes model, we aim to extend this method to higher-dimensional models such as the Heston model (Heston [67]) or basket options. First, we define the Fourier transform and its inverse as

$$\mathfrak{F}\left[f(x)\right](u) = \int_{\mathbb{R}^d} e^{-\mathrm{i}u^T x} f(x)dx, \tag{2.3.1}$$

and

$$\mathfrak{F}^{-1}\left[F(u)\right](x) = \frac{1}{(2\pi)^d}\int_{\mathbb{R}^d} e^{\mathrm{i}x^T u}F(u)du, \tag{2.3.2}$$

where i is the complex unit. The Discrete Fourier transform and its inverse are defined in a 2-dimensional case as

$$\mathfrak{D}\left[f(x,y)\right](u_i,v_j) = \sum_{k=0}^{N-1}\sum_{l=0}^{M-1} e^{-\mathrm{i}\left(\frac{ki}{N}+\frac{lj}{M}\right)}f(x_k,y_l), \tag{2.3.3}$$

and

$$\mathfrak{D}^{-1}\left[F(u,v)\right](x_k,y_l) = \frac{1}{NM}\sum_{i=0}^{N-1}\sum_{j=0}^{M-1} e^{-\mathrm{i}\left(\frac{ki}{N}+\frac{lj}{M}\right)}F(u_i,v_j), \tag{2.3.4}$$

where u_i, v_j, x_k, and y_l are the $(i,j,k,l)^{th}$ component in the discretization.

When FFT transforms the information from the real space to frequency, inappropriate or adequate sampling frequency may lead to aliasing. When the signal is under sampled, its spectrum has non-zeros overlapping tails and the tail spectrum is folded back onto other spectrum. This inversion phenomenon in spectrum is called aliasing. The aliasing makes the signal indistinguishable in both real and frequency and not recoverable since the Fourier transform carries incomplete information from the sampled signals. For example, when the sampling rate is $T = 1$, the signals at the frequencies 1 and $2\pi - 1$ are indistinguishable. The Nyquist equation gives the highest frequency in the frequency space such that no aliasing occurs (see Lord et al. [93])

$$\Delta x\Delta u = \frac{2\pi}{N}. \tag{2.3.5}$$

Suppose we sample N and M points on each dimension, the discretization in real space and frequency space are performed by

$$x_n = \left(n-\frac{N}{2}\right)\Delta x,\ \ u_n = \left(n-\frac{N}{2}\right)\Delta u,\ \text{for } n = 0,\cdots,N-1, \tag{2.3.6}$$

and

$$y_m = \left(m-\frac{M}{2}\right)\Delta y,\ \ v_m = \left(m-\frac{M}{2}\right)\Delta v,\ \text{for } m = 0,\cdots,M-1. \tag{2.3.7}$$

By the Nyquist equation (2.3.5), the relation between Δx and Δu must satisfy

$$\Delta x\Delta u = \frac{2\pi}{N}, \tag{2.3.8}$$

and

$$\Delta y\Delta v = \frac{2\pi}{M}. \tag{2.3.9}$$

On the truncation region $[x_0,x_N]\times[y_0,y_M]$ in real space, we obtain the following transform of DFT for any objective function $f(x,y)$ to the frequency space $[u_0,u_N]\times[v_0,v_M]$

$$
\begin{aligned}
&\mathfrak{F}\left[f(x,y)\right](u_i,v_j)\\
\approx&\sum_{k=0}^{N-1}\sum_{l=0}^{M-1} w_{k,l}e^{-\mathrm{i}\left(u_ix_k+v_jy_l\right)}f(x_k,y_l)\Delta x\Delta v\\
=&\sum_{k=0}^{N-1}\sum_{l=0}^{M-1} w_{k,l}f(x_k,y_l)\Delta x\Delta y\exp\left(-\mathrm{i}\left(i-\frac{N}{2}\right)\Delta u\left(k-\frac{N}{2}\right)\Delta x-\mathrm{i}\left(j-\frac{M}{2}\right)\Delta v\left(l-\frac{M}{2}\right)\Delta y\right)\\
=&\sum_{k=0}^{N-1}\sum_{l=0}^{M-1} w_{k,l}f(x_k,y_l)\Delta x\Delta y\exp\left(-\frac{2\pi\mathrm{i}}{N}\left(i-\frac{N}{2}\right)\left(k-\frac{N}{2}\right)-\frac{2\pi\mathrm{i}}{M}\left(j-\frac{M}{2}\right)\left(l-\frac{M}{2}\right)\right)\\
=&\Delta x\Delta y e^{-2\pi\mathrm{i}\left(\frac{N}{4}+\frac{M}{4}\right)}e^{(i+j)\pi\mathrm{i}}\sum_{k=0}^{N-1}\sum_{l=0}^{M-1} w_{k,l}e^{-2\pi\mathrm{i}\left(\frac{ki}{N}+\frac{lj}{M}\right)}e^{(k+l)\pi\mathrm{i}}f(x_k,y_l)\\
=&(-1)^{i+j}\Delta x\Delta y\sum_{k=0}^{N-1}\sum_{l=0}^{M-1} w_{k,l}e^{-2\pi\mathrm{i}\left(\frac{ki}{N}+\frac{lj}{M}\right)}(-1)^{k+l}f(x_k,y_l)\\
=&(-1)^{i+j}\Delta x\Delta y\mathfrak{D}\left[\left\{w_{k,l}(-1)^{k+l}f(x_k,y_l)\right\}_{k=0,l=0}^{N-1,M-1}\right]_{i,j}.
\end{aligned}
$$

Similarly, the inverse DFT transform from frequency $[u_0,u_N]\times[v_0,v_M]$ to real space $[x_0,x_N]\times[y_0,y_M]$ is given by

$$
\begin{aligned}
&\mathfrak{F}^{-1}\left[F(u,v)\right](x_k,y_l)\\
=&\frac{1}{(2\pi)^2}\sum_{i=0}^{N-1}\sum_{j=0}^{M-1} w_{k,l}e^{2\pi\mathrm{i}\left(u_ix_k+v_jy_l\right)}F(u_i,v_i)\Delta u\Delta v\\
=&\frac{1}{(2\pi)^2}\sum_{i=0}^{N-1}\sum_{i=0}^{M-1} w_{i,i}F(u_i,v_i)\Delta u\Delta v\exp\left(\mathrm{i}\left(i-\frac{N}{2}\right)\Delta u\left(k-\frac{N}{2}\right)\Delta x+\mathrm{i}\left(j-\frac{M}{2}\right)\Delta v\left(l-\frac{M}{2}\right)\Delta y\right)\\
=&\frac{1}{(2\pi)^2}\sum_{i=0}^{N-1}\sum_{i=0}^{M-1} w_{i,i}F(u_i,v_i)\Delta u\Delta v\exp\left(\frac{2\pi\mathrm{i}}{N}\left(i-\frac{N}{2}\right)\left(k-\frac{N}{2}\right)+\frac{2\pi\mathrm{i}}{M}\left(j-\frac{M}{2}\right)\left(l-\frac{M}{2}\right)\right)\\
=&\frac{1}{(2\pi)^2}\Delta u\Delta v e^{2\pi\mathrm{i}\left(\frac{N}{4}+\frac{M}{4}\right)}e^{-(k+l)\pi\mathrm{i}}\sum_{i=0}^{N-1}\sum_{j=0}^{M-1} w_{i,j}e^{2\pi\mathrm{i}\left(\frac{ki}{N}+\frac{lj}{M}\right)}e^{-(i+j)\pi\mathrm{i}}F(u_i,v_j)\\
=&\frac{(-1)^{k+l}}{\Delta x\Delta y}\frac{1}{NM}\sum_{i=0}^{N-1}\sum_{j=0}^{M-1} w_{i,j}e^{2\pi\mathrm{i}\left(\frac{ki}{N}+\frac{lj}{M}\right)}(-1)^{i+j}F(u_i,v_j)\\
=&\frac{(-1)^{k+l}}{\Delta x\Delta y}\mathfrak{D}^{-1}\left[\left\{w_{i,j}(-1)^{i+j}F(u_i,v_j)\right\}_{i=0,j=0}^{N-1,M-1}\right]_{k,l}.
\end{aligned}
$$

We define the density function of X_t as

$$
\phi(x)=(2\pi\Delta t)^{-\frac{k}{2}}|\Sigma|^{-\frac{1}{2}}\exp\left(-\frac{(x-\alpha\Delta t)^T\Sigma^{-1}(x-\alpha\Delta t)}{2\Delta t}\right), \tag{2.3.10}
$$

We define $\dot{Y}_t$ as the expectation term in equation (2.2.21). The convolution approach to $\mathbb{E}\left[\cdot \Delta W_t | X_t = x\right]$ and $\mathbb{E}\left[\cdot | X_t = x\right]$ in equation (2.2.20) and (2.2.21) are given by

$$\begin{aligned}
\dot{Y}_t(x) =& \mathbb{E}_t\left[Y_{t+1}\middle| X_t = x\right] \\
=& \int_{-\infty}^{\infty}\int_{-\infty}^{\infty} Y_{t+1}(s_1,s_2)\,\phi(s_1-x_1,s_2-x_2)ds_1ds_2 \\
=& \left(Y_{t+1}(s) * \phi(-s)\right)(x) \\
=& \mathfrak{F}^{-1}\left[\mathfrak{F}\left[Y_{t+1}\right](v)\Psi_y(v)\right](x),
\end{aligned} \tag{2.3.11}$$

and

$$\begin{aligned}
Z_t(x) =& \frac{1}{\Delta t}\mathbb{E}_t\left[Y_{t+1}\Delta W_t\middle| X_t = x\right] \\
=& \frac{1}{\Delta t}\int_{-\infty}^{\infty}\int_{-\infty}^{\infty} Y_{t+1}(s_1,s_2)\left(\Delta W_{1,t},\Delta W_{2,t}\right)^T\phi(s_1-x_1,s_2-x_2)ds_1ds_2 \\
=& \frac{1}{\Delta t}\int_{-\infty}^{\infty}\int_{-\infty}^{\infty} Y_{t+1}(s_1,s_2)\,\sigma^{-1}\left(s_1-x_1-\mu_1\Delta t, s_2-x_2-\mu_2\Delta t\right)^T \\
& \phi(s_1-x_1,s_2-x_2)ds_1ds_2 \\
=& \frac{1}{\Delta t}\left(Y_{t+1}(s) * \sigma^{-1}(-s-\Delta t\alpha)\phi(-s)\right)(x) \\
=& \frac{1}{\Delta t}\mathfrak{F}^{-1}\left[\mathfrak{F}\left[Y_{t+1}\right](v)\Psi_z(v)\right](x),
\end{aligned} \tag{2.3.12}$$

where $\Psi_y = \mathfrak{F}[\phi]$ and $\Psi_z = \mathfrak{F}[\sigma^{-1}(-x-\Delta t\alpha)\phi]$ are the kernels, and $*$ denotes the convolution operator

$$(f*g)(x) = \int_{-\infty}^{\infty} f(y)g(x-y)dy. \tag{2.3.13}$$

The DFT approximation of $\dot{Y}_t(x)$ and Z_t is given by

$$\dot{Y}_t(x_k,v_l) = (-1)^{k+l}\mathfrak{D}^{-1}\left[\left\{\psi\left(p_i,q_j\right)W_{i,j}\mathfrak{D}\left[\left\{(-1)^{k+l}Y_{t+1}\right\}_{k,l}\right]\right\}_{i,j}\right]_{k,l}, \tag{2.3.14}$$

$$Z_t = (-1)^{k+l}\mathfrak{D}^{-1}\left[\left\{\mathrm{i}v\sigma^T\psi\left(p_i,q_j\right)W_{i,j}\mathfrak{D}\left[\left\{(-1)^{k+l}Y_{t+1}\right\}_{k,l}\right]\right\}_{i,j}\right]_{k,l}. \tag{2.3.15}$$

The following algorithm summarizes the FFT method to numerically solve the BSDEs. We create a discretized $N_1 \times N_2$ real space with a corresponding $N_1 \times N_2$ frequency space and a equally discretized timeline $0 = t_1 \le t_2 \le \cdots \le t_n = T$.

Algorithm 2.3. *FFT approach to BSDEs problem (2.2.19) to (2.2.21) on $N_1 \times N_2$ two-dimensional grid*

1. *Initialize boundary conditions,* $\forall(i,j) \in \{1,2,\ldots,N_1\} \times \{1,2,\ldots,N_2\}$

$$Z_n^{i,j} = 0,$$
$$Y_n^{i,j} = g(x_{i,j}),$$

2. *for* $k = n-1, n-2, \ldots, 1$, *calculate*

$$\dot{Y}_k^{i,j} = (-1)^{i+j} \mathfrak{D}^{-1} \left[\left(\Psi_y \left(v_{s,l} \right) w_{s,l} \mathfrak{D} \left[\bar{Y}_{k+1} \right] \left(v_{s,l} \right) \right)_{s=1,l=1}^{N_1,N_2} \right] \left(v_{i,j} \right),$$
$$Z_k^{i,j} = (-1)^{i+j} \mathfrak{D}^{-1} \left[\mathrm{i} v \sigma^T \left(\Psi_z \left(v_{s,l} \right) w_{s,l} \mathfrak{D} \left[\bar{Y}_{k+1} \right] \left(v_{s,l} \right) \right)_{s=1,l=1}^{N_1,N_2} \right]_{i,j}.$$

$$Y_k = \dot{Y}_k + \Delta t f \left(t_k, X, \dot{Y}_k, Z_k \right)$$

where $v = \left(v_{i,j} \right)$ *is* $N_1 \times N_2$ *matrix formed by all frequency basis* $v_{i,j}$ *and* $\bar{Y}_k = (Y_k^{i,j})$ *is the matrix form by the value of* Y_k *at point* $x_{i,j}$.

Figure 2.1: European call: Convolution result of Black-Scholes model with BSDE approach

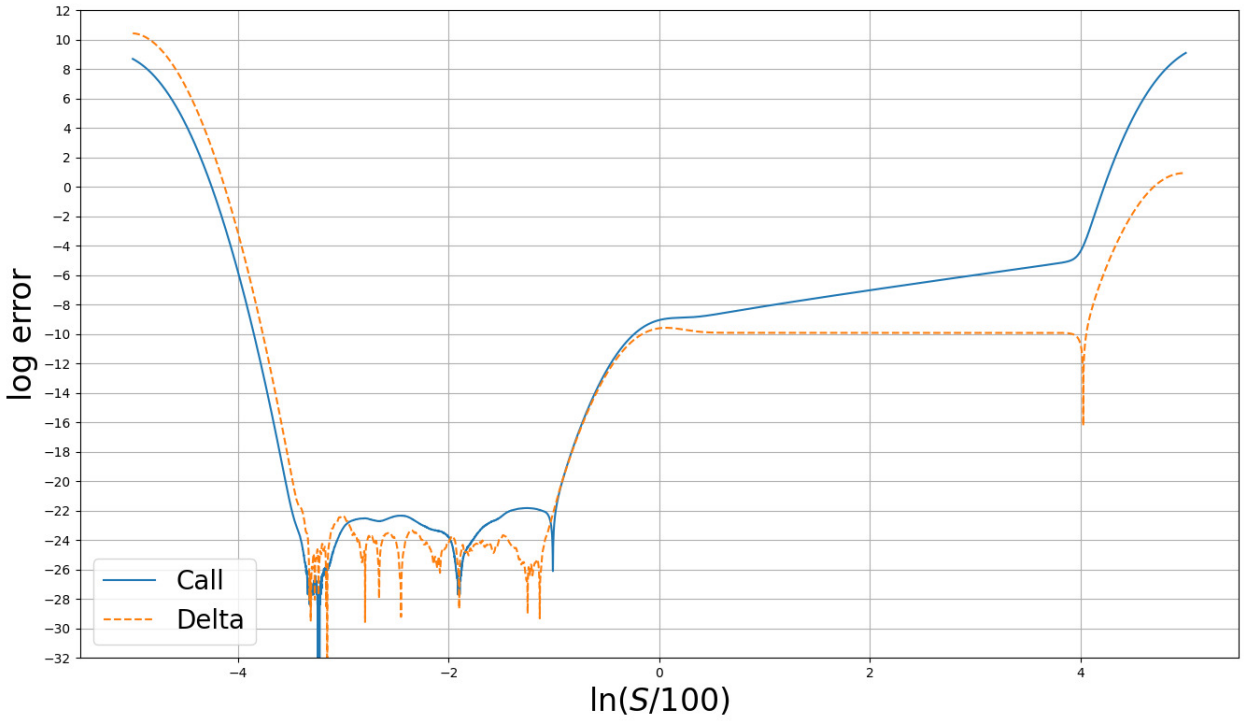

$K = 100$, $r = R = 0.03$, $\mu = 0.05$, $\sigma = 0.2$, $L = 10$, $T = 1$, $N = 8000$, $n = 1000$

In Figure 2.1, we implement the Algorithm 2.3 in 1-dimensional case for a European call option and compare the convolution result to the Black-Scholes model. The real space $X_t = \ln S_t/K$ is truncated on $[-5,5]$ with $N = 8000$ and the time space is discretized with $n = 100$ steps with $\Delta t = 0.01$. As we can see there exist a huge boundary errors and we will discuss and improve the boundary problem in late sections.

2.4 Convolution method for Heston model

The Black-Scholes-Merton model assumes that volatility is constant over time. However, the volatility smile occurs when plotting the stock price and implied volatility calculated from the Black-Scholes model. The volatility smile demonstrates that implied volatility actually varies with strike price. Restricted by the assumptions, the Black-Scholes model is unrealistic in capturing the properties of the underlying assets since it generates the smile phenomenon in the volatility and skewness distribution in the return. Many facts indicate that the volatility, instead of being a constant parameter, is driven by a mean-reverting stochastic process, (see Fouque, Papanicolaou, and Sircar [60]). Therefore, various models are suggested to capture the such properties in stock. A popular model assuming stochastic volatility is proposed by Heston [67] which is a semi-closed form solution for pricing vanilla options.

2.4.1 Heston's stochastic volatility model

We assume the stock price S_t obeys a diffusion process on a filtered probability space $(\Omega, \mathcal{F}, \mathbb{P})$. The filtration $\{\mathcal{F}_t\}_{t\geq 0}$ is generated by two independent Wiener processes satisfying the usual conditions of completeness and right continuity. The stock price is given as

$$dS_t = \mu S_t dt + \sigma_t S_t dW_t, \tag{2.4.1}$$

where W_t is a standard Brownian motion and σ_t is time dependent process which is given by an Ornstein-Uhlenbeck process

$$d\sigma_t = -\beta \sigma_t dt + \delta dW_{1t}, \tag{2.4.2}$$

Consider $\sigma_t = \sqrt{v_t}$, where v_t is the volatility. By Itô's formula, v_t follows a mean reverting process also known as a Cox, Ingersoll, and Ross [30] (CIR) model

$$dv_t = \left(\delta^2 - 2\beta v_t\right) dt + 2\delta\sqrt{v_t} dW_{1t}. \tag{2.4.3}$$

Equation (2.4.3) can be written as square-root process

$$dv_t = \kappa(\theta - v_t)\, dt + \sigma\sqrt{v_t} dW_{1t}, \tag{2.4.4}$$

The coefficient κ represents the speed that pulls the volatility towards its long-term mean θ. The Wiener process W_t is correlated with the Wiener process W_{1t} by

$$dW_t = \rho dW_{1t} + \sqrt{1-\rho^2} dW_{2t}, \tag{2.4.5}$$

where $\rho \in [-1, +1]$ is the correlation coefficient between W_{1t} and W_{2t} the two independent Wiener process.

The Heston model under probability measure $\mathbb{P}$ can be written as

$$dS_t = \mu S_t dt + \sqrt{v_t} S_t \left(\rho dW_{1t} + \sqrt{1-\rho^2} dW_{2t}\right),$$

$$dv_t = \kappa(\theta - v_t)\,dt + \sigma\sqrt{v_t}dW_{1t}. \tag{2.4.6}$$

Feller [56] classifies the boundaries for a one-dimensional parabolic heat equation implies the stochastic volatility process (2.4.4) has the following properties

(i) if $2\kappa\theta \geq \sigma^2$, then zero is unattainable for v_t and $v_t > 0$,

(ii) if $2\kappa\theta < \sigma^2$, then zero is a regular, attainable and reflecting boundary, which means that v_t can touch 0, but does not spend time there.

We assume the market price of risk scheme $\tilde{\Lambda} = (\Lambda_1, \Lambda_2)$ associated with (W_1, W_2) satisfy the following condition

$$\frac{\mu - r}{\sqrt{v_t}} = \rho\Lambda_1 + \sqrt{1-\rho^2}\Lambda_2. \tag{2.4.7}$$

By the Cox and Ross [28] risk-neutral valuation model, we define an equivalent measure $\mathbb{Q}^\Lambda$ on $\mathcal{F}_t$ by

$$\left.\frac{d\mathbb{Q}^\Lambda}{d\mathbb{P}}\right|_{\mathcal{F}_t} = \exp\left(-\frac{1}{2}\int_0^t (\Lambda_1^2 + \Lambda_2^2)ds + \int_0^t \Lambda_1 dW_1(s) + \int_0^t \Lambda_2 dW_2(s)\right). \tag{2.4.8}$$

We have that $\mathbb{Q}^\Lambda$ is equivalent to $\mathbb{P}$ provided that $\mathbb{E}\left[\frac{d\mathbb{Q}^\Lambda}{d\mathbb{P}}|_{\mathcal{F}_t}\right] = 1$ for all $t \in [0,T]$. Though the risk scheme $\tilde{\Lambda}$ can be chosen arbitrarily, to obtain a complete Heston model we follow Heston's suggestion and let $\Lambda_1(v_t) = \Lambda\sqrt{v_t}$ for some positive constant Λ such that Λ_2 is uniquely determined by equation (2.4.7). Further, by Girsanov's theorem, we define two independent Wiener processes under $\mathbb{Q}^\Lambda$

$$dW_1^\Lambda(t) = dW_1(t) + \Lambda\sqrt{v_t}dt, \tag{2.4.9}$$

$$dW_2^\Lambda(t) = dW_2(t) + \frac{\mu - r - \Lambda\rho v_t}{\sqrt{(1-\rho^2)v_t}}dt, \tag{2.4.10}$$

which gives the risk-neutral dynamics

$$dS_t = rS_t dt + \sqrt{v_t}S_t\left(\rho dW_{1t}^\Lambda + \sqrt{1-\rho^2}dW_{2t}^\Lambda\right), \tag{2.4.11}$$

$$dv_t = \bar{\kappa}\left(\bar{\theta} - v_t\right)dt + \sigma\sqrt{v_t}dW_{1t}^\Lambda, \tag{2.4.12}$$

where $\bar{\kappa} = \kappa + \sigma\Lambda$, $\bar{\theta} = \kappa\theta/(\kappa + \sigma\Lambda)$, provided that $\kappa + \sigma\Lambda \neq 0$.

Using the transform from $\mathbb{P}$ to $\mathbb{Q}^\Lambda$, We define the driver function for Heston model without borrowing rate $f : \mathbb{R}^2 \times \mathbb{R} \times \mathbb{R}^2 \to \mathbb{R}$ as

$$f(X,Y,Z) = -rY - Z\rho, \tag{2.4.13}$$

where

$$\rho = \begin{bmatrix} \Lambda\sqrt{v_t} \\ \frac{\mu - r - \Lambda\rho v_t}{\sqrt{(1-\rho^2)v_t}} \end{bmatrix}.$$

We consider the European call option price in the Heston model where the backward stochastic process Y_t is given by

$$\begin{aligned} dY_t &= -f(x_t, v_t, Y_t, Z_t)\,dt + Z_t dW_t^{\Lambda}, \qquad (2.4.14) \\ Y_T &= g(x_T). \\ g(x) &= \max(S_0 e^x - K, 0). \qquad (2.4.15) \end{aligned}$$

Next, we investigate the conditional density of the Heston model under the Feller condition $2\kappa\theta \geq \sigma^2$. Firstly, we review the distribution behavior of the volatility. As indicated in Cox, Ingersoll Jr, and Ross [31], with

$$q = \frac{2\bar{\kappa}\bar{\theta}}{\sigma^2} - 1, \text{ and } c = \frac{2\bar{\kappa}}{\sigma^2\left(1 - e^{-\bar{\kappa}(t-s)}\right)}, \qquad (2.4.16)$$

for $0 < s < t$, the process $2cv_t$ has the non-central Chi-square distribution

$$2cv_t \sim \chi^2\left(q, 2cv_s e^{\bar{\kappa}(t-s)}\right), \qquad (2.4.17)$$

with degree q and non-centrality parameter $2cv_s e^{-\kappa(t-s)}$. The probability density of v_t conditional on its value v_s is given by

$$P(v_t|v_s) = ce^{-u-v}\left(\frac{v}{u}\right)^{\frac{q}{2}} I_q\left(2(uv)^{\frac{1}{2}}\right), \qquad (2.4.18)$$

where

$$\begin{aligned} u &= cv_s e^{-\bar{\kappa}(t-s)}, \\ v &= cv_t, \end{aligned}$$

and $I_q(\cdot)$ is the modified Bessel function of the first kind with order q

$$I_q(z) = \frac{1}{2\pi \mathrm{i}} \oint e^{(z/2)(t+1/t)} t^{-q-1} dt. \qquad (2.4.19)$$

The Feller condition $2\bar{\kappa}\bar{\theta} \geq \sigma^2$ is equivalent to $q \geq 0$ in the conditional density (2.4.18). However, we often observe $2\bar{\kappa}\bar{\theta} \ll \sigma^2$ from market data. When it is the case of $2\bar{\kappa}\bar{\theta} \ll \sigma^2$, the cumulative distribution of the volatility density is singular at the origin. The phenomenon of the fast growing of left tail may lead to significant errors when the integration range is truncated. So we will assume $Y_t = 0$ when the value of v_t falls below 0.

We define the log-stock process, with initial value $X_0 = 0$ by

$$X_t = \log\left(\frac{S_t}{S_0}\right). \tag{2.4.20}$$

By introducing parameter $\tilde{\rho} = \left(\rho, \sqrt{1-\rho^2}\right)$ and the joint process $dW_t^{\Lambda} = \left(dW_1^{\Lambda}(t), dW_2^{\Lambda}(t)\right)^T$, the dynamics of x_t are given by

$$dX_t = \left(r - \frac{1}{2}v_t\right)dt + \sqrt{v_t}\tilde{\rho}dW_t^{\Lambda}. \tag{2.4.21}$$

The joint process $X_t = (x_t, v_t)^T$ is given by

$$dX_t = \eta(v_t, t)dt + \sqrt{v_t}\xi dW_t^{\Lambda}, \tag{2.4.22}$$

where

$$\eta(v_t, t) = \begin{pmatrix} r - \frac{1}{2}v_t \\ \bar{\kappa}(\bar{\theta} - v_t) \end{pmatrix}, \text{ and } \xi = \begin{pmatrix} \rho & \sqrt{1-\rho^2} \\ \sigma & 0 \end{pmatrix}. \tag{2.4.23}$$

Given the value of the v_t, the conditional density of the log-stock price can be studied using the Fokker-Planck equation (see Risken [109]). Drăgulescu and Yakovenko [42] also showed that given a short time period t, the probability distribution of x_t evolves in Gaussian manner in discrete time with the given variance v_i

$$\mathbb{P}(x_{i+1}|x_i, v_i) = \frac{1}{\sqrt{2\pi v_i \Delta t_i}} \exp\left(-\frac{\left(x_{i+1} - x_i - (r - \frac{1}{2}v_i)\Delta t_i\right)^2}{2v_i \Delta t_i}\right). \tag{2.4.24}$$

The following theorem gives the asymptotic behavior of the conditional probability of X_t in a short time period $\Delta t = t - t_i$.

Theorem 2.4. *(Short period asymptotic density function) Given the value of joint process X_s and the filtration $\mathcal{F}_s = \mathcal{F}\{\tau : \tau \leq s\}$, then the increment $\Delta X_t = X_t - X_s$ evolves as bi-variate Gaussian manner in a short time period $\Delta t = t - s$*

$$\Delta X_t \sim \mathcal{N}\left(\eta(v_s)\Delta t_s, \Sigma(v_s)\Delta t_s\right), \tag{2.4.25}$$

the conditional density function is thus given by

$$\phi(\Delta X_t|X_s) = \frac{|\Sigma(v_s)|^{-\frac{1}{2}}}{2\pi\sqrt{\Delta t}} \exp\left(-\frac{(\Delta X_t - \eta(v_s)\Delta t)^T \Sigma^{-1}(v_s)(\Delta X_t - \eta(v_s)\Delta t)}{2\Delta t}\right), \tag{2.4.26}$$

where

$$\Delta X_t = X_t - X_s,\ \eta(v) = \begin{pmatrix} r - \frac{1}{2}v, \\ \kappa(\theta - v) \end{pmatrix},\ \textit{and}\ \Sigma(v) = \xi\xi^T v = \begin{pmatrix} 1 & \sigma\rho \\ \sigma\rho & \sigma^2 \end{pmatrix} v. \tag{2.4.27}$$

Proof: see Appendix 5.8.

The characteristic function of the Heston model has closed form solution and is the key to solving the pricing problem. The original characteristic function given by Heston has a discontinuity problem and the discontinuity problem has been solved by other authors such as Kahl and Jäckel [79] where they count the phase rotation and Cui et al. [32] where they split the term that causes the phase shift. In our approach, we need the characteristic function that applies to two frequency variables thus we consider the boundary function $\mathbb{E}\left[e^{\mathrm{i}px+\mathrm{i}qv}\right]$ including the effect from v.

Definition 2.5. *The characteristic function of the joint variable $X_t = (x_t, v_t)^T$ under measure $\mathbb{P}$ with corresponding characteristic parameter $U = (p,q)^T$ given the current state $X = (x,v)^T$ is defined by*

$$\varphi(U,X,t) = \mathbb{E}^{\mathbb{P}}\left[e^{\mathrm{i}U^T X_T}|X_t = (x,v)^T\right], \tag{2.4.28}$$

with boundary value $\varphi(U,X,T) = e^{\mathrm{i}U^T X}$.

Under a different measure, the form of the characteristic function (2.4.28) would be different. Similar to the Black-Scholes model, the original Heston model contains two measures and we can see this from the pricing formula of European call option

$$\begin{aligned}
C_t =& e^{-r\tau}\mathbb{E}^{\mathbb{Q}}\left[(S_T-K)^+|S_t,v_t\right] && (2.4.29)\\
=& e^{-r\tau}\left(\mathbb{E}^{\mathbb{Q}}\left[S_T\mathbf{1}_{S_T>K}|S_t,v_t\right] - K\mathbb{E}^{\mathbb{Q}}\left[\mathbf{1}_{S_T>K}|S_t,v_t\right]\right) && (2.4.30)\\
=& S_t\mathbb{E}^{\mathbb{Q}}\left[\frac{S_T}{F(t,T)}\mathbf{1}_{S_T>K}|S_t,v_t\right] - Ke^{-r\tau}\mathbb{E}^{\mathbb{Q}}\left[\mathbf{1}_{S_T>K}|S_t,v_t\right] && (2.4.31)\\
=& S_t\mathbb{E}^{\mathbb{S}}\left[\mathbf{1}_{S_T>K}|S_t,v_t\right] - Ke^{-r\tau}\mathbb{E}^{\mathbb{Q}}\left[\mathbf{1}_{S_T>K}|S_t,v_t\right], && (2.4.32)
\end{aligned}$$

where $F(t,T) = e^{r\tau}S_t$ is the forward price, as seen from t. We define the measure change from the risk neutral measure $\mathbb{Q}$ to the equivalent martingale measure $\mathbb{S}$ which can be seen as an invariant measurement

$$\frac{d\mathbb{S}}{d\mathbb{Q}} = \frac{S_T}{F(t,T)}. \tag{2.4.33}$$

For simplicity, we denote $\mathbb{P}_1 = \mathbb{S}$ and $\mathbb{P}_2 = \mathbb{Q}$, under which

$$\begin{aligned}
P_1(S_T,K) =& \mathbb{P}_1(S_T \geq K), && (2.4.34)\\
P_2(S_T,K) =& \mathbb{P}_2(S_T \geq K), && (2.4.35)
\end{aligned}$$

and the pricing formula becomes

$$C_t = S_t P_1\left(S_T,K\right) - Ke^{-r\tau}P_2\left(S_T,K\right). \tag{2.4.36}$$

According to arbitrage pricing theory, the Heston call option $C(S,v,t)$ satisfies the following PDE

(see Heston [67] and Black and Scholes [8]):

$$\frac{1}{2}vS^2\frac{\partial^2 C}{\partial S^2}+\rho\sigma vS\frac{\partial^2 C}{\partial S\partial v}+\frac{1}{2}\sigma^2 v\frac{\partial^2 C}{\partial v^2}+rS\frac{\partial C}{\partial S}+\left[\bar{\kappa}\left(\bar{\theta}-v\right)-\sigma\Lambda v\right]\frac{\partial C}{\partial v}+\frac{\partial C}{\partial t}-rC=0. \tag{2.4.37}$$

Due to the similar structure to the Black-Scholes model, P_1 and P_2 must satisfy the following PDE in terms of $X=\ln\frac{S}{K}$

$$\frac{1}{2}v\frac{\partial^2 P_i}{\partial X^2}+\rho\sigma v\frac{\partial^2 P_i}{\partial X\partial v}+\frac{1}{2}\sigma^2 v\frac{\partial^2 P_i}{\partial v^2}+(r+c_i v)\frac{\partial P_i}{\partial X}+(a-b_i v)\frac{\partial P_i}{\partial v}+\frac{\partial P_i}{\partial t}=0, \tag{2.4.38}$$

where $c_1=\frac{1}{2}$,$c_2=-\frac{1}{2}$, $a=\bar{\kappa}\bar{\theta}$, $b_1=\bar{\kappa}+\Lambda\sigma-\rho\sigma$, $b_2=\bar{\kappa}+\Lambda\sigma$ for $i=1,2$.

By the Feynman-Kac representation theorem, the characteristic functions φ_i defined by (2.4.28) under measures P_i satisfying (2.4.38) are the unique bounded solutions to the following PDEs

$$\frac{\partial\varphi_i}{\partial t}+(r+c_i v)\frac{\partial\varphi_i}{\partial x}+(a-b_i v)\frac{\partial\varphi_i}{\partial v}+\frac{1}{2}v\frac{\partial^2\varphi_i}{\partial x^2}+\frac{\sigma^2}{2}v\frac{\partial^2\varphi_i}{\partial v^2}+\rho\sigma v\frac{\partial^2\varphi_i}{\partial x\partial v}=0, \tag{2.4.39}$$

with boundary condition where $U=(p,q)^T$ and $X=(x,v)^T$

$$\varphi(U,X,T)=e^{\mathrm{i}U^TX}=e^{\mathrm{i}(px+qv)}. \tag{2.4.40}$$

Theorem 2.6. *(Characteristic function) The characteristic functions of the joint variable $X_t=(x_t,v_t)^T$ under measurements P_i with real initials $X=(x,v)^T$ and frequency components $U=(p,q)$ are given by*

$$\varphi_i(U,X)=\exp\left(\mathrm{i}p(x+r\tau)+\mathrm{i}q(v+a\tau)+\frac{\gamma_i+\lambda_i}{\sigma^2}(1-\zeta)v-\frac{\gamma_i-\lambda_i}{\sigma^2}a\tau+\frac{2a}{\sigma^2}\ln\zeta\right), \tag{2.4.41}$$

where

$$\gamma=\sqrt{\sigma^2(p^2-2\mathrm{i}c_i p)+(b_i-\mathrm{i}\sigma\rho p)^2}, \tag{2.4.42}$$

$$\lambda=b_i-\mathrm{i}\sigma\rho p-\mathrm{i}\sigma^2 q, \tag{2.4.43}$$

$$\zeta=\frac{2\gamma}{\gamma+\lambda+(\gamma-\lambda)e^{-\gamma\tau}}. \tag{2.4.44}$$

Proof: see Appendix 5.9.

In the estimation, we will use the characteristic function of the incremental variable X_T-X_t which can be obtained from Theorem 2.6

$$\begin{aligned}\psi(U,X)=&\mathbb{E}\left[e^{\mathrm{i}U^T(X_T-X_t)}\middle|X_t=X\right]\\=&e^{-\mathrm{i}U^TX}\varphi(U,X)\\=&\exp\left(\mathrm{i}pr\tau+\mathrm{i}qa\tau+\frac{\gamma+\lambda}{\sigma^2}(1-\zeta)v-\frac{\gamma-\lambda}{\sigma^2}a\tau+\frac{2a}{\sigma^2}\ln\zeta\right).\end{aligned} \tag{2.4.45}$$

The characteristic function is used to calculate the values of P_i given by Heston [67]

$$P_1 = \frac{1}{2} + \frac{1}{\pi}\int_0^\infty \mathrm{Re}\frac{\varphi_1(u-\mathrm{i},x,v)}{\mathrm{i}u}du, \tag{2.4.46}$$

$$P_2 = \frac{1}{2} + \frac{1}{\pi}\int_0^\infty \mathrm{Re}\frac{\varphi_2(u,x,v)}{\mathrm{i}u}du. \tag{2.4.47}$$

However, in the original characteristic function given by Heston [67], the logarithm term given by

$$\ln\frac{1-\frac{\lambda+\gamma}{\lambda-\gamma}e^{\gamma\tau}}{1-\frac{\lambda+\gamma}{\lambda-\gamma}}, \tag{2.4.48}$$

has two problems: the term $\frac{\lambda+\gamma}{\lambda-\gamma}$ may encounter zero denominator, and discontinuity may occur from the logarithm. The discontinuity is usually caused by the term $e^{\gamma\tau}$ when the ranges of τ and p are large. We see it from the limiting behavior

$$e^{\gamma\tau} \to e^{\sigma\sqrt{1-\rho^2}|p|\tau}, \text{ as } p \to \infty. \tag{2.4.49}$$

which leads to the phase shifting from the logarithm as it goes to infinity. The logarithm term in our characteristic function (2.4.41) will not approach to infinity. Therefore, our version of the characteristic function does not have the discontinuity problem. Other solutions to the discontinuity can be found in Kahl and Jäckel [79] where they use rotation counts and in Cui et al. [32] where they use hyperbolic functions. In Figure 2.2, we present the original characteristic function given by Heston [67] and in Figure 2.3, we present the characteristic function given by (2.4.41). The integrand shown in Figure 2.2 and 2.3 shows the values of $\phi_i/u\mathrm{i}$ in the integral of (2.4.46) and (2.4.47).

Figure 2.2: Heston's characteristic function

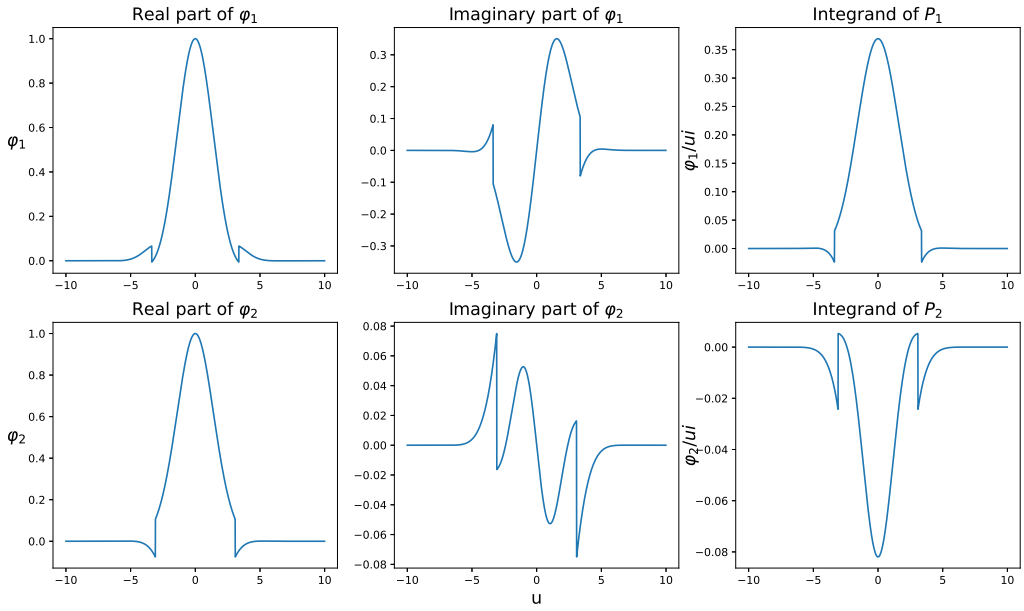

$\Lambda = 1$, $r = 0.03$, $\rho = -0.8$, $\kappa = 3$, $\theta = 0.1$, $\sigma = 0.25$, $\tau = 5$

Figure 2.3: Our characteristic function

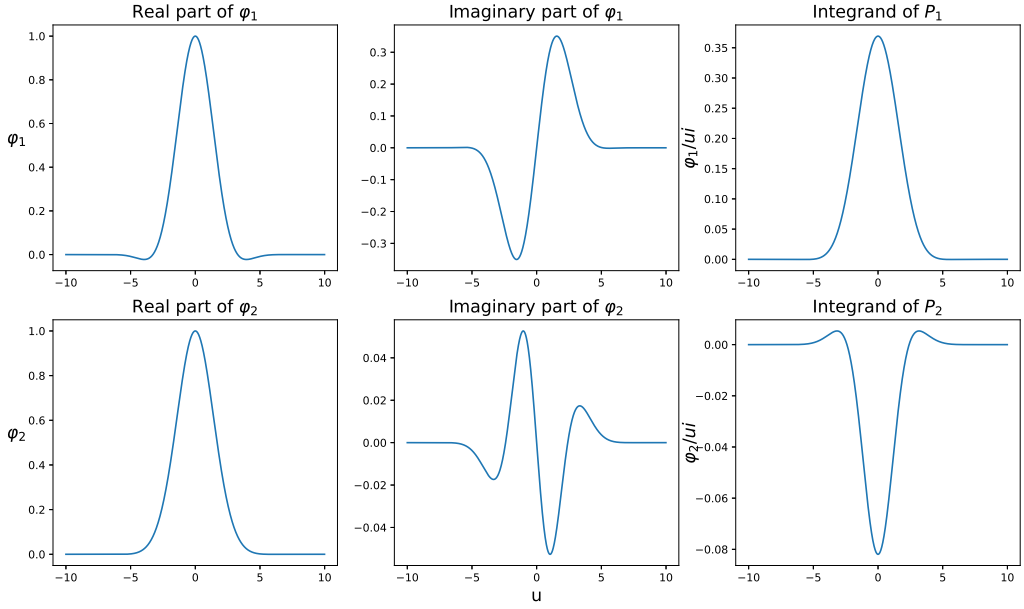

$\Lambda = 1$, $r = 0.03$, $\rho = -0.8$, $\kappa = 3$, $\theta = 0.1$, $\sigma = 0.25$, $\tau = 5$

We introduce the following notation

$$\alpha = \frac{\gamma+\lambda}{\sigma^2},$$
$$\beta = \frac{\gamma-\lambda}{\sigma^2},$$
$$\zeta = \frac{\alpha+\beta}{\alpha+\beta e^{-\gamma\tau}},$$

and simplify equation (2.4.45) as

$$\psi(U,X) = \exp\left(\mathrm{i}pr\tau + \mathrm{i}qa\tau + \alpha(1-\zeta)v - \beta a\tau + \frac{2a}{\sigma^2}\ln\zeta\right). \tag{2.4.50}$$

We obtain the first order derivative from (2.4.50) as

$$\frac{\partial\psi}{\partial p} = \varphi\left(\mathrm{i}r\tau + (\alpha_p(1-\zeta) - \alpha\zeta_p)v - \beta_p a\tau + \frac{2a}{\sigma^2}\zeta_1\right), \tag{2.4.51}$$
$$\frac{\partial\psi}{\partial q} = \varphi\left(\left(\alpha_q(1-\zeta) - \alpha\zeta_q\right)v + \frac{2a}{\sigma^2}\zeta_2\right), \tag{2.4.52}$$

where

$$\gamma_p = \frac{\sigma^2(1-\rho^2)p - \mathrm{i}(\sigma^2 c_i + \sigma\rho b_i)}{\gamma},$$
$$\alpha_p = \frac{\gamma_p - \mathrm{i}\sigma\rho}{\sigma^2},$$
$$\beta_p = \frac{\gamma_p + \mathrm{i}\sigma\rho}{\sigma^2},$$
$$\zeta_p = \frac{\alpha_p+\beta_p}{\alpha+\beta}\zeta - \frac{\alpha_p+\beta_p e^{-\gamma\tau}}{\alpha+\beta}\zeta^2 + \gamma_p\tau\left(1-\frac{\alpha\zeta}{\alpha+\beta}\right)\zeta,$$
$$\zeta_q = \frac{1-e^{-\gamma\tau}}{\alpha+\beta}\zeta^2\mathrm{i},$$
$$\zeta_1 = \frac{\alpha_p+\beta_p}{\alpha+\beta} - \frac{\alpha_p+\beta_p e^{-\gamma\tau}}{\alpha+\beta}\zeta + \gamma_p\tau\left(1-\frac{\alpha\zeta}{\alpha+\beta}\right),$$
$$\zeta_2 = \frac{1-e^{-\gamma\tau}}{\alpha+\beta}\zeta\mathrm{i}.$$

2.4.2 Convolution method for Heston model

The PDE (2.4.38) with boundary conditions $P_1(T,S,v) = P_2(T,S,v) = \mathbf{1}_{S>K}$ cannot lead to a closed form solution, Heston [67] suggests obtaining the analytic solution for the probabilities by inverting their characteristic functions. By comparing equation (2.4.39) to equation (2.4.38), we obtain the

characteristic functions ϕ_1 for P_1 and ϕ_2 for P_2 from Theorem 2.6 by letting $p = u$ and $q = 0$

$$\varphi_1(u;x,v) = \varphi(u;x,v,\gamma_1,\lambda_1), \tag{2.4.53}$$
$$\varphi_2(u;x,v) = \varphi(u;x,v,\gamma_2,\lambda_2), \tag{2.4.54}$$

where for $i = 1,2$

$$\gamma_i = \sqrt{\sigma^2\left(u^2 - 2\mathrm{i}c_i u\right) + \left(b_i - \mathrm{i}\sigma\rho u\right)^2}, \tag{2.4.55}$$
$$\lambda_i = b_i - \mathrm{i}\sigma\rho u. \tag{2.4.56}$$

The solutions given in Heston [67] are

$$P_1 = \frac{1}{2} + \frac{1}{\pi}\int_0^\infty \mathrm{Re}\frac{\varphi_1\left(u - \mathrm{i}, x, v\right)}{\mathrm{i}u} du, \tag{2.4.57}$$
$$P_2 = \frac{1}{2} + \frac{1}{\pi}\int_0^\infty \mathrm{Re}\frac{\varphi_2\left(u, x, v\right)}{\mathrm{i}u} du, \tag{2.4.58}$$

with $x = \ln(S/K)$.

Remark 2.7. *We refer to the numerical evaluation of (2.4.57) and (2.4.58) as the integral method. We shall compare our proposed methods to the integral method in later sections.*

Next, we introduce the convolution approach to estimate the value of P_i. The premise of the convolution method is that the conditional probability density $\phi(y|x,v)$ depends only on the difference of x and y

$$\phi(y|x) = \phi(y - x). \tag{2.4.59}$$

Applying the Fourier transform to P_1 and P_2, we have

$$\begin{aligned}
\mathfrak{F}\left[P_i(x)\right](u) =& \mathfrak{F}\left[\mathbb{E}_i\left[\mathbf{1}_{S_T \geq K}\middle| x = \ln\frac{S}{K}\right]\right](u) \\
=& \mathfrak{F}\left[\int_{\mathbb{R}} \delta(y)\phi_i(y|x)dy\right](u) \\
=& \mathfrak{F}\left[\left(\delta(y) * \phi_i(y - x)\right)(x)\right](u) \\
=& \mathfrak{F}\left[\left(\delta(y) * \phi_i(-y)\right)(x)\right](u) \\
=& \mathfrak{F}\left[\delta(y)\right](u)\mathfrak{F}\left[\phi_i(-y)\right](u),
\end{aligned} \tag{2.4.60}$$

where the delta function $\delta(\cdot)$ is

$$\delta(x) = \begin{cases} 1, & \text{if } x \geq 0 \\ 0, & \text{otherwise.} \end{cases}$$

The Fourier transform of the density function gives us

$$\mathfrak{F}\left[\phi_i(-y)\right](u) = \int_{\mathbb{R}} e^{-\mathrm{i}uy}\phi(-y)dy$$

$$
\begin{aligned}
&= \int_{\mathbb{R}} e^{\mathrm{i}uy} \phi_i(y) dy \\
&= \int_{\mathbb{R}} e^{\mathrm{i}u(y-x)} \phi_i(y-x) dy \\
&= e^{-\mathrm{i}ux} \int_{\mathbb{R}} e^{\mathrm{i}uy} \phi_i(y|x) dy \\
&= e^{-\mathrm{i}ux} \mathbb{E}_i \left[e^{\mathrm{i}ux_T} | x \right] \\
&= e^{-\mathrm{i}ux} \varphi_i(u,x,v) \\
&= \psi_i(u,v). \qquad (2.4.61)
\end{aligned}
$$

We denote (2.4.61) as the kernel for the convolution method which is equivalent to the characteristic function (2.4.45) without the effect of x

$$
\psi_i(u,v) = \exp\left(\mathrm{i}ur\tau + \frac{\gamma+\lambda}{\sigma^2}(1-\zeta)v - \frac{\gamma-\lambda}{\sigma^2}a\tau + \frac{2a}{\sigma^2}\ln\zeta \right), \qquad (2.4.62)
$$

where

$$
\gamma = \sqrt{\sigma^2(u^2 - 2\mathrm{i}c_i u) + (b_i - \mathrm{i}u\rho\sigma)^2},\ \lambda = b_i - \mathrm{i}u\rho\sigma, \text{ and } \zeta = \frac{2\gamma}{\gamma+\lambda+(\gamma-\lambda)e^{-\gamma\tau}}.
$$

We simplify (2.4.60) as

$$
\mathfrak{F}[P_i(x)](u) = \mathfrak{F}[\delta(x)](u)\psi_i(u,v), \qquad (2.4.63)
$$

and recover P_i by

$$
P_i(x) = \mathfrak{F}^{-1}\left[\mathfrak{F}[\delta(x)](u)\psi_i(u,v)\right]. \qquad (2.4.64)
$$

We apply the change of variables to $x = \ln\frac{S}{K}$ with varying S and obtain the pricing formula to (2.4.36) by DFT

$$
\begin{aligned}
C(S,K,v,t) =& SP_1(S,K) - Ke^{-r\tau}P_2(S,K) \\
=& S\mathfrak{F}^{-1}\left[\mathfrak{F}[\delta(x)](u)\psi_1(u,v)\right](x) - Ke^{-r\tau}\mathfrak{F}^{-1}\left[\mathfrak{F}[\delta(x)](u)\psi_2(u,v)\right](x) \\
\approx& S\tilde{P}_1 - Ke^{-r\tau}\tilde{P}_2, \qquad (2.4.65)
\end{aligned}
$$

where the truncation of the real space is

$$
x_n = \left(n - \frac{N}{2}\right)\Delta x, \text{ for } n = 0,1,\cdots,N-1, \text{ and } \Delta x = \frac{L}{N}, \qquad (2.4.66)
$$

the truncation of the frequency space is

$$
u_n = \left(n - \frac{N}{2}\right)\Delta u, \text{ for } n = 0,1,\cdots,N-1, \text{ and } \Delta u = \frac{2\pi}{L}, \qquad (2.4.67)
$$

and the calculations of $\tilde{P}_i$ are

$$\tilde{P}_i = (-1)^n \mathfrak{D}^{-1} \left[\left\{ w_k \mathfrak{D} \left[\{ w_n (-1)^n \delta(x_n) \}_{n=0}^{N-1} \right] (u_k) \psi_i(u_k) \right\}_{k=0}^{N-1} \right]_n . \tag{2.4.68}$$

for some weight scheme w_n.

Remark 2.8. *The pricing formula in (2.4.65) is similar to the Black-Scholes model instead of having the explicit formulas we using (2.4.68) to estimate the probabilities. We call this approach Scheme I.*

Next, we introduce an alternative approach to the pricing formula, which is popular in BSDEs framework as applied by Huijskens et al. [70] and Hyndman and Oyono Ngou [74]. The BSDE based convolution method was introduced in the Section 2.3. Here we introduce an simple version to the option pricing using convolution without BSDEs which we call Scheme II. Scheme II approaches the pricing formula of the option is similar to Carr and Madan [18]'s approach but we apply the Fourier transform on the log-price region. Involving a damping parameter which will be discussed in later section, we obtain the following Fourier transform

$$\begin{aligned} \mathfrak{F}\left[e^{\alpha x} C(x)\right] =& e^{-r\tau} \int_{\mathbb{R}} \mathrm{Re}\left(e^{-\mathrm{i}ux} e^{\alpha x} \mathbb{E}^{\mathbb{Q}} \left[\left(K e^{x_T} - K\right)^+ | x = \ln(S/K) \right] \right) dx \\ =& e^{-r\tau} \mathrm{Re}\left(\int_{\mathbb{R}} e^{-\mathrm{i}ux} e^{\alpha x} \int_{\mathbb{R}} g(y) \tilde{\phi}_2(x-y) dy dx \right) \\ =& e^{-r\tau} \mathfrak{F}\left[e^{\alpha x} g(x)\right] \psi_2(u + \alpha \mathrm{i}), \end{aligned} \tag{2.4.69}$$

where

$$g(x) = \left(K e^x - K\right)^+ \text{ and } \tilde{\phi}(x) = \phi(-x).$$

The call option can be recovered from reverting and undamping (2.4.69)

$$C(x) = e^{(-r\tau - \alpha x)} \mathfrak{F}^{-1}\left[\mathfrak{F}\left[e^{\alpha x} g(x)\right] \psi_2(u + \alpha \mathrm{i}) \right](x). \tag{2.4.70}$$

We denote (2.4.70) as Scheme II which have similar discretization as Scheme I. In next sections, we present the error analysis first then we introduce two method to improve the boundary error.

2.4.3 Error analysis

We denote the convolution result in (2.4.65) as $\tilde{C} = S\tilde{P}_1 - Ke^{-r\tau}\tilde{P}_2$. To analyze the error from truncation and discretization in the calculation, we need knowledge of the bound of the Fourier series and the decay behavior of the characteristic function. Firstly, we investigate the Fourier expansion of a piece-wise smooth function f with finite limiting point on $[-\frac{L}{2}, \frac{L}{2}]$

$$f(x) = \sum_{j=-\infty}^{\infty} F_j e^{-\mathrm{i}j\frac{2\pi x}{L}}, \tag{2.4.71}$$

with the coefficients F_j

$$F_j = \frac{1}{L}\int_{-\frac{L}{2}}^{\frac{L}{2}} f(x)e^{\mathrm{i}j\frac{2\pi x}{L}}dx. \tag{2.4.72}$$

It is well known that the Fourier coefficients F_j tend to 0 as $j \to \pm\infty$ and the modulus of F_j can not exceed $||f||_\infty$ if f is bounded on $[-\frac{L}{2}, \frac{L}{2}]$. Thus we can bound the modulus of F_j by

$$\left|F_j\right| \leq \min\left(||f||_\infty, \frac{\varepsilon(L)}{|j|}\right), \tag{2.4.73}$$

for a positive bounding constant $\varepsilon(L)$ depending only on L.

Secondly, we investigate the limiting behavior of the characteristic function. Usually, the characteristic function of the Black-Scholes model decays as $\exp\left(-cx^2\right)$ and that of the Heston model has exponential decay $\exp(-c|x|)$ for some constant value of c such discussions can be found in Lord and Kahl [91]. More precisely, we summarize the asymptotic behavior of the characteristic function by the following proposition.

Proposition 2.9 (Asymptotic characteristic function)**.** *Assuming that κ, θ, σ, v, $\tau > 0$ and $\rho \in (-1,1)$, we have the following limit for the kernel function (2.4.61)*

$$\lim_{u\to\infty} \psi_i(u) \approx A_\infty e^{\mathrm{i}B_\infty}\exp\left(-D\left|u\right|\right), \tag{2.4.74}$$

where

$$\begin{aligned}
A_\infty &= \left(4\left(1-\rho^2\right)\right)^{\frac{a}{\sigma^2}},\\
B_\infty &= \frac{2a}{\sigma^2}\arcsin\left(\frac{|u|}{u}\rho\right) - \frac{\rho}{\sigma}\left(v + \frac{|u|}{u}a\tau\right)u,\\
D &= \frac{\sqrt{1-\rho^2}}{\sigma}\left(v + a\tau\right) > 0.
\end{aligned}$$

Proof: see Appendix 5.10.

By Proposition 2.9 we could bound the modulus of the characteristic function with a positive constant ε

$$|\psi_i(u)| \leq \varepsilon A_\infty e^{-D|u|}. \tag{2.4.75}$$

Finally, we can give the both truncation and discretization errors using (2.4.75) and (2.4.73). The following theorem gives an error bound for $\left|C - \tilde{C}\right|$.

Theorem 2.10 (Error of convolution method)**.** *Assuming an integrable function f is bounded on $[-\frac{L}{2}, \frac{L}{2}]$, then under measurement P_i, the error between the true value*

$$E(x) = \mathbb{E}^{\mathbb{P}_i}\left[f(x_T)\left|x_0 = x\right.\right],$$

and the estimation using convolution method

$$\tilde{E}(x_n) = (-1)^n \mathfrak{D}^{-1}\left[\left\{w_k \mathfrak{D}\left[\{w_n(-1)^n f(x_n)\}_{n=0}^{N-1}\right](u_k)\psi_i(u_k)\right\}_{k=0}^{N-1}\right]_n,$$

on the truncation regions $[-\frac{L}{2}, \frac{L}{2}]$ *with discretization* $(\Delta x, \Delta u)$

$$x_n = \left(n - \frac{N}{2}\right)\Delta x, \text{ for } n = 0,1,\cdots,N-1, \text{ and } \Delta x = \frac{L}{N},$$
$$u_n = \left(n - \frac{N}{2}\right)\Delta u, \text{ for } n = 0,1,\cdots,N-1, \text{ and } \Delta u = \frac{2\pi}{L},$$

is bounded by

$$\left|E - \tilde{E}\right| \leq \varepsilon_1 e^{-\frac{\pi D}{L}N} + \varepsilon_2 N^{-m},$$

where

$$\varepsilon_1 = \frac{LA_\infty ||f||_\infty e^{\frac{2\pi D}{L}}}{\pi D}\varepsilon_{v,\tau}, \text{ and } \varepsilon_2 = \frac{LA_\infty}{\pi D}\varepsilon_L \varepsilon_{v,\tau},$$

for some positive constants $\varepsilon_{v,\tau}$ *and* ε_L.

Proof: see Appendix 5.11.

Applying Theorem 2.10, we obtain the error estimation for $\left|P_i - \tilde{P}_i\right|$ as

$$|e_i| = \left|P_i - \tilde{P}_i\right| \leq \frac{LA_\infty ||f||_\infty e^{\frac{2\pi D}{L}}}{\pi D}\varepsilon_{v,\tau} e^{-\frac{\pi D}{L}N} + \frac{LA_\infty}{\pi D}\varepsilon_L \varepsilon_{v,\tau} N^{-m}. \tag{2.4.76}$$

We obtain the error estimation for the Heston call option by Scheme I

$$\begin{aligned}
|e(x)| &= \left|C(x) - \tilde{C}(x)\right| \\
&= \left|Ke^x\left(P_1(x) - \tilde{P}_1(x)\right) - Ke^{-r\tau}\left(P_2(x) - \tilde{P}_2(x)\right)\right| \\
&\leq Ke^x |e_1| + Ke^{-r\tau}|e_2| \\
&\leq K\left(e^x + e^{-r\tau}\right)\left(\frac{LA_\infty ||f||_\infty e^{\frac{2\pi D}{L}}}{\pi D}\varepsilon_{v,\tau} e^{-\frac{\pi D}{L}N} + \frac{LA_\infty}{\pi D}\varepsilon_L \varepsilon_{v,\tau} N^{-m}\right).
\end{aligned} \tag{2.4.77}$$

We summarize the error bound of $|e|$ by the following corollary.

Corollary 2.11. *The convolution method to the Heston call option by Scheme I and Scheme II has the following error bound*

$$|e| \leq \mathcal{O}\left(e^{-\frac{\pi D}{L}N}\right) + \mathcal{O}\left(N^{-m}\right), \tag{2.4.78}$$

for $m \geq 2$.

Note 2.12. *We can see from (2.4.77), as we vary the values of $x \in [-\frac{L}{2}, \frac{L}{2}]$, the error would increase when x approaches the boundary. Therefore, as long as the boundary error is bounded the interior error is also bounded. In the next section, we introduce some method that could control and improve the boundary error.*

2.4.4 Boundary control schemes

Sufficient conditions of successfully applying Fourier transform requires the target function to be L_1-integrable. However, we note that the call option itself is not L_1-integrable with respect to either the log-price or the log-strike. Nevertheless we can still apply the Fourier transform to the target function on a truncated region regardless of the non-integrable sides out of the region. As a consequence, the approximation result may suffer large boundary errors and lead to unstable result. Introducing a damping parameter $e^{\alpha x}$ that could dampen the value of non-integral side approaching zero which ensures the Fourier transform can be applied successfully. As suggested by Carr and Madan [18], a positive damping parameter is applied to the target function on the grid of log-strike

$$\begin{aligned}\mathfrak{F}\left[e^{\alpha k}C(k)\right] =& e^{-r\tau}\int_{-\infty}^{\infty} \mathrm{Re}\left(e^{\mathrm{i}uk}e^{\alpha k}\mathbb{E}\left[\left(S-e^{k}\right)^{+}\right]\right)dk \\ =& \frac{e^{-r\tau}\varphi(u-(\alpha+1)\mathrm{i})}{-(u-\alpha\mathrm{i})(u-(\alpha+1)\mathrm{i})}, \\ =& e^{-r\tau}\psi(u,\alpha), \end{aligned} \tag{2.4.79}$$

where

$$\begin{aligned}\varphi(u) =& \mathbb{E}^{\mathbb{Q}}\left[e^{\mathrm{i}u\ln(S_T)}\right] = \varphi_2(u), \\ \psi(u,\alpha) =& \frac{\varphi(u-(\alpha+1)\mathrm{i})}{-(u-\alpha\mathrm{i})(u-(\alpha+1)\mathrm{i})}.\end{aligned}$$

Directly inverting (2.4.79) gives us Fourier pricing formula on the discretization of log-strike

$$C(t,k) = \frac{e^{-r\tau-\alpha k}}{2\pi}\int_{-\infty}^{\infty}\mathrm{Re}\left(e^{-\mathrm{i}uk}\psi(u,\alpha)\right)du. \tag{2.4.80}$$

By the same argument, a negative damping parameter is applied to the Scheme II (2.4.69) method on the grid of log-price.

The advantage of including the damping parameter in (2.4.79) is to increase the numerical stability whereas the equation (2.4.36) could suffer from the cancellation error when the values of P_1 and P_2 get too close. The necessary and sufficient condition that (2.4.80) exists is satisfied as long as the $(\alpha+1)^{\text{th}}$ moment of the asset price exists, as pointed out by Lord and Kahl [91]

$$|\varphi(u-(\alpha+1)\mathrm{i})| \leq \varphi(-(\alpha+1)\mathrm{i}) = \mathbb{E}\left[S_T^{(\alpha+1)}\right] \leq \infty. \tag{2.4.81}$$

A sufficient condition that the Fourier transform could successfully applied in (2.4.79) requires the target function to be integrable. The call option valued on the discretization of the log-strike is bounded between 0 and S. However, as $k \to -\infty$ the call option approaches S that makes the

target function non-integrable with respect to the log-strike. Introducing the damping parameter α could solve the problem as we can see that for some positive value of α the target function would approach zero as $k \to -\infty$. Our method is applied on the discretization of the log-price which has unbounded value of call option as the log-price approaches to infinity. Therefore, the damping method could also applied in our method and we need α to be negative with large absolute value.

Adding a damping parameter $\alpha \leq -1$ to equation (2.2.20) and (2.2.21) would also affect the kernel Ψ

$$\mathfrak{F}\left[e^{\alpha x} f(x)\right](u) = \mathfrak{F}\left[e^{\alpha x} Y(x)\right] \Psi(u + \alpha \mathrm{i}), \tag{2.4.82}$$

and the inverse transform to recover the target function

$$f(x) = e^{-\alpha x} \mathfrak{F}^{-1}\left[\mathfrak{F}\left[e^{\alpha x} Y(x)\right] \Psi(u + \alpha \mathrm{i})\right]. \tag{2.4.83}$$

Comparing the truncation on logarithms of the strike price in Lord and Kahl [91], our truncation on the logarithm of the stock price could lead to large boundary errors when the option is exponentially increasing as the underlying asset moves to deep in-the-money. Such problems can be found in Hyndman and Oyono Ngou [74], however, they introduced a shifting method on the target function to address the boundary error. The basic idea of shifting the target function is to map it from non-periodic to a periodic function which would be considered as a real signal. The shifting method requires a shifting function $h(x)$ with explicit expectation $\mathbb{E}\left[h(x_t)\,|x\right]$. Thus the candidate for shifting function $h(x)$ is usually the polynomial and the exponential functions. Hyndman and Oyono Ngou [74] suggests the first order polynomial as the shifting function $h(x) = Ax + B$ such that the damping of the shifted target function $\tilde{f}^{\alpha}(x) = e^{\alpha x}\left(f(x) - h(x)\right)$ is smooth connected at the boundary

$$\tilde{f}^{\alpha}(x_0) = \tilde{f}^{\alpha}(x_n), \tag{2.4.84}$$

$$\frac{d\tilde{f}^{\alpha}}{dx}(x_0) = \frac{d\tilde{f}^{\alpha}}{dx}(x_n). \tag{2.4.85}$$

In our implemention, we find that shifting the call option by a linear function will generate kinked point at-the-money and does not perform very well. Therefore, we suggest using a similar function to shift the target function. In Scheme I we choose a linear function $h_1 = Ax + B$ to shift the delta function and in Scheme II we choose an exponential function $h_2 = Ae^x + B$ to shift the call option which can also applied in BSDEs based method. We summarize the shifting results to Scheme I

$$\alpha = 0, \tag{2.4.86}$$

$$A = \frac{f(x_N) - f(x_0)}{x_N - x_0}, \tag{2.4.87}$$

$$B = \frac{x_N f(x_0) - x_0 f(x_N)}{x_N - x_0}, \tag{2.4.88}$$

$$h(x) = Ax + B, \tag{2.4.89}$$

$$\tilde{f}^{\alpha}(x) = f(x) - h(x), \tag{2.4.90}$$

$$\tag{2.4.91}$$

and to Scheme II

$$\alpha < -1, \tag{2.4.92}$$
$$h(x) = Ae^x + B, \tag{2.4.93}$$
$$f_0' = \frac{-3f(x_0) + 4f(x_1) - f(x_2)}{2\Delta x}, \tag{2.4.94}$$
$$f_N' = \frac{3f(x_N) - 4f(x_{N-1}) + f(x_{N-2})}{2\Delta x}, \tag{2.4.95}$$
$$A = \frac{e^{\alpha x_N} f_N' - e^{\alpha x_0} f_0'}{e^{(\alpha+1)x_N} - e^{(\alpha+1)x_0}}, \tag{2.4.96}$$
$$B = \frac{x_N f(x_0) - x_0 f(x_N)}{x_N - x_0}, \tag{2.4.97}$$
$$\tilde{f}^{\alpha}(x) = e^{\alpha x}\left(f(x) - h(x)\right). \tag{2.4.98}$$

We can recover Scheme I by reversing the shifting

$$\begin{aligned}
\mathbb{E}^{\mathbb{P}_i}\left[f(x_T)\,|x\right] =& \mathbb{E}^{\mathbb{P}_i}\left[\tilde{f}(x_T)\,|x\right] + \mathbb{E}^{\mathbb{P}_i}\left[h(x_T)\,|x\right] \\
=& \mathfrak{F}^{-1}\left[\mathfrak{F}\left[\tilde{f}(x)\right](u)\psi_i(u)\right](x) + A\mathbb{E}\left[x_T\,|x\right] + B \\
=& \mathfrak{F}^{-1}\left[\mathfrak{F}\left[\tilde{f}(x)\right](u)\psi_i(u)\right](x) - \mathrm{i}A\frac{\partial \varphi_i}{\partial u}(x,0) + B,
\end{aligned}$$

and recover Scheme II by reversing the shifting and the damping

$$\begin{aligned}
\mathbb{E}^{\mathbb{P}_2}\left[f(x_T)\,|x\right] =& \mathbb{E}^{\mathbb{P}_2}\left[\tilde{f}(x_T)\,|x\right] + \mathbb{E}^{\mathbb{P}_2}\left[h(x_T)\,|x\right] \\
=& e^{-\alpha x}\mathfrak{F}^{-1}\left[\mathfrak{F}\left[e^{\alpha x}\tilde{f}(x)\right](u)\psi_2(u)\right](x) + A\mathbb{E}\left[e^{x_T}\,|x\right] + B \\
=& e^{-\alpha x}\mathfrak{F}^{-1}\left[\mathfrak{F}\left[e^{\alpha x}\tilde{f}(x)\right](u)\psi_2(u)\right](x) + A\varphi_2(x,-\mathrm{i}) + B.
\end{aligned}$$

In BSDEs, for the calculation of (2.3.12), we can recover Z from the following transform

$$\begin{aligned}
\mathbb{E}^{\mathbb{P}_2}\left[f(x_T)\Delta W_T\,|x\right] =& \mathbb{E}^{\mathbb{P}_2}\left[\tilde{f}(x_T)\,|x\right] + \mathbb{E}^{\mathbb{P}_2}\left[h(x_T)\Delta W_T\,|x\right] \\
=& e^{-\alpha x}\mathfrak{F}^{-1}\left[\mathfrak{F}\left[e^{\alpha x}\tilde{f}(x)\right](u)\psi_Z(u)\right](x) + A\mathbb{E}\left[e^{x_T}\Delta W_T\,|x\right] \\
=& e^{-\alpha x}\mathfrak{F}^{-1}\left[\mathfrak{F}\left[e^{\alpha x}\tilde{f}(x)\right](u)\psi_Z(u)\right](x) + Ae^x\psi_Z(u) \\
=& e^{-\alpha x}\mathfrak{F}^{-1}\left[\mathfrak{F}\left[e^{\alpha x}\tilde{f}(x)\right](u)\psi_Z(u)\right](x) \\
& + A\sigma^{-1}\left(-\mu\Delta t e^x\psi_Z(-\mathrm{i}) - \mathrm{i}e^x\frac{d\psi_Z}{du}(-\mathrm{i})\right),
\end{aligned}$$

where we assume that $\Delta W_T = \sigma^{-1}\left(x_T - x - \mu T\right)$.

In next section, we present the result of the convolution method for Heston call option and compare our result to the integration method and the Fourier method (2.4.79).

2.4.5 Application and conclusion

We apply the convolution method to the European call with Heston model on the log-price region $x = \log(S/100) \in [-5,5]$ and the log-strike region $k = \log K \in [-10,10]$, $K = 100$. We make the comparison to the Fourier method on the log-strike region. The convolution method and the Fourier method are implemented with different grid points and are compared at $S = 100$.

Figure 2.4: P_1 and P_2 by convolution method

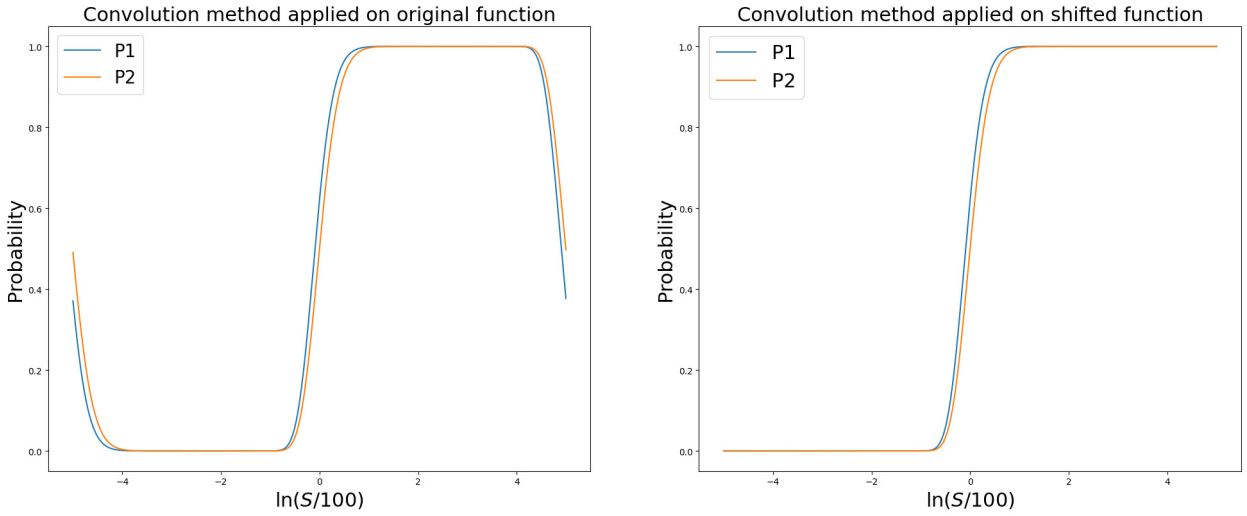

$r = 0.03$, $v = 0.1$, $\Lambda = 1$, $\rho = -0.8$, $\kappa = 3$, $\theta = 0.1$, $\sigma = 0.25$, $L = 10$, $N = 2000$, $T = 1$

In Figure 2.4, we present the value of P_i obtained from the Scheme I convolution method. The left panel of Figure 2.4 shows the original transform without using damping and shifting method. The right panel of Figure 2.4 shows the modified transform without using the shifting. By looking into the values shown in Figure 2.4

$$P_1(x_N) = 0.99999844,$$
$$P_2(x_N) = 0.99999839,$$

we find that adding the shifting scheme in the convolution method could improve accuracy at the boundaries and performs stably even without the damping scheme.

Figure 2.5: Heston call option by convolution method

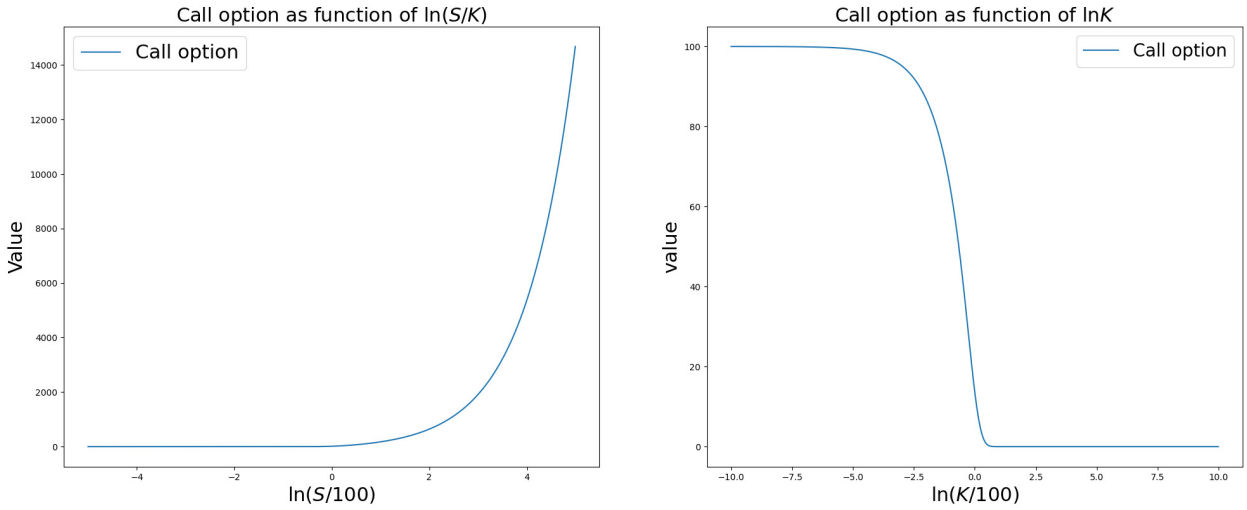

$r = 0.03$, $v = 0.1$, $\Lambda = 1$, $\rho = -0.8$, $\kappa = 3$, $\theta = 0.1$, $\sigma = 0.25$, $L = 10$, $N = 2000$, $T = 1$

Figure 2.5 shows the Heston call option priced using Scheme I method in log-price grid and log-strike grid with $N = 2000$ grid points. The results are smooth everywhere in Figure2.5 and the error is presented in Figure 2.6.

Figure 2.6: Convolution vs Fourier method

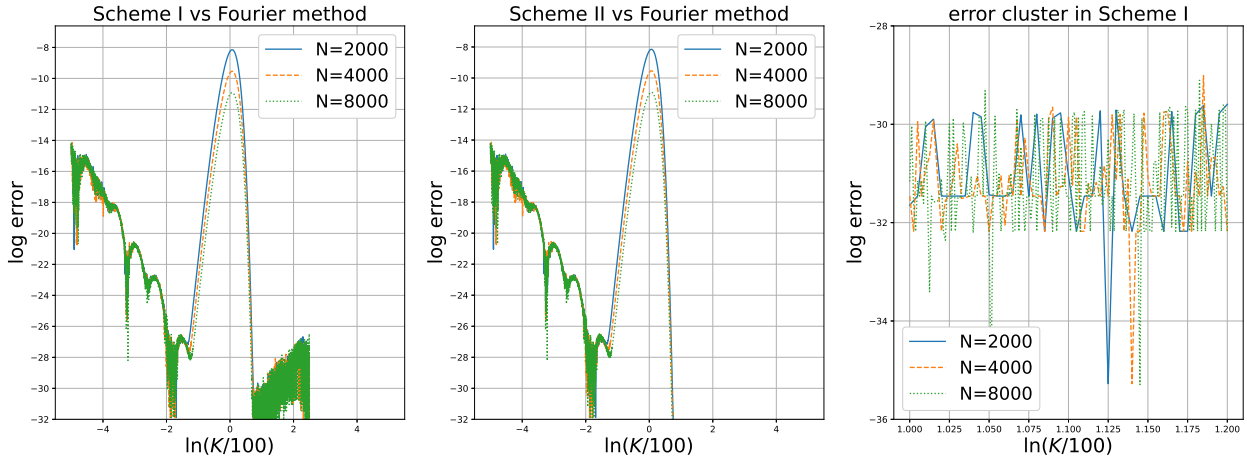

$r = 0.03$, $v = 0.1$, $\Lambda = 1$, $\rho = -0.8$, $\kappa = 3$, $\theta = 0.1$, $\sigma = 0.25$, $L = 10$, $T = 1$, $\alpha = -2$

We implement Scheme I, Scheme II and Carr and Madan [18]'s Fourier method for $N = 2000$, $N = 4000$ and $N = 8000$ grids. The error are taken logarithms and cut when the value is less than 25. The left panel in Figure 2.6 shows the log error of Scheme I method compared to the Fourier method and the right panel in Figure 2.6 shows the log error of Scheme II method compared to the Fourier method. As we can see the error converges as N increases and some oscillation occurs when K near in-the-money side.

Figure 2.7: Comparison with different damping parameters

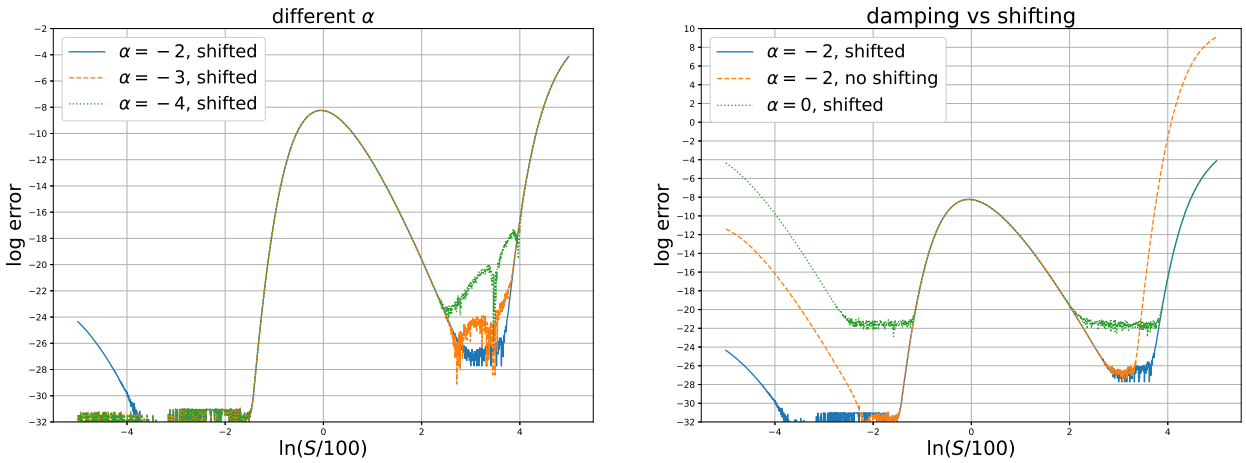

$r = 0.03$, $v = 0.1$, $\Lambda = 1$, $\rho = -0.8$, $\kappa = 3$, $\theta = 0.1$, $\sigma = 0.25$, $L = 10$, $T = 1$, $N = 2000$

Figure 2.8: Convolution method in BSDE with Black-Scholes model

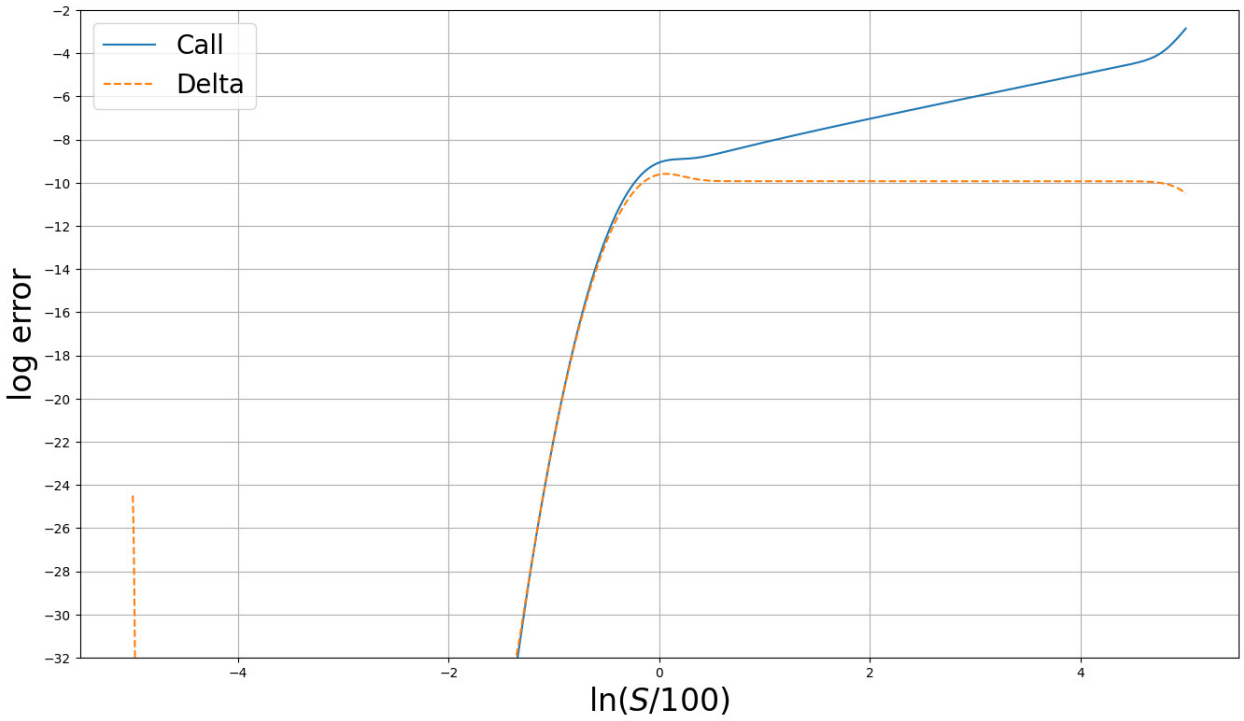

$r = R = 0.03$, $\mu = 0.05$, $\sigma = 0.2$, $L = 10$, $T = 1$, $N = 8000$, $n = 1000$, $\alpha = -2$

When we implement the convolution method in BSDEs structure, the error at deep in-the-money side would accumulate through time iterations and the result is shown in Figure 2.8. In Figure 2.8, we present the improved result of Figure 2.1 for a European call option in the Black-Scholes model with consistent damping scheme and exponential shifting scheme. Comparing to

Hyndman and Oyono Ngou [74]'s result shown in Figure 2.1, our method greatly improve the boundary errors and increases the stability of the convolution method.

Table 2.1: Heston model: CPU time, European Call price and error of Scheme II

	CPU time (s)		S=80,K=100		S=100,K=100		S=120,K=100	
	Convolution	Fourier	Call	Error	Call	Error	Call	Error
N=2000	1.80E-04	2.25E-04	3.80787	8.84E-05	13.45867	2.60E-04	28.06620	9.96E-05
N=4000	2.81E-04	3.96E-04	3.80779	8.04E-06	13.45887	6.50E-05	28.06607	3.05E-05
N=8000	4.50E-04	7.44E-04	3.80779	6.86E-06	13.45892	1.63E-05	28.06609	3.36E-06

2.5 Conclusion

The main advantages of the convolution method are its flexibility and computational speed. Like other FFT-based methods, we achieve a complexity of $\mathcal{O}(N \log_2 N)$, where N is the number of grid points. We provide a new scheme in formulating the characteristic function of the Heston model. Our formula has no-discontinuity and is easy to take derivatives which gives us the flexibility for applications to calibration. We have studied the application of the convolution method in a direct approach and in a BSDE approach for pricing options. In the direct approach, we propose a new method to accurately estimate the probabilities under the martingale measures with risk neutral measures. In the BSDE approach, we have improved performance with consistent damping parameter and exponential shifting function which shows large decreases in boundary errors. We also show that the convolution method in BSDEs framework has a error problem in-the-money which is accumulated from the boundary error during time iterations. We make comparisons between the convolution method, Fourier method and the integration method on grid of log-strike and log-price. Our comparison shows that convolution method possess good convergence on the whole grid and very fast computational speed and the Scheme II convolution method is even faster than the Fourier method. Our methods have advantages in a wide range of accuracy, fast computation and stable boundary control, which could be applied in calibration in the future studies. Future research will focus on reducing the accumulated boundary error in the BSDE approach and to extend the convolution method to high-dimensional applications.

Chapter 3

Arbitrage-free pricing and forecasting of coupon bonds with dynamic parameterization with deep neural networks

In this chapter, we propose the deep-learning based neural network structure to model the time-varying factors of term-structure and filter-based methods to capture the information from time evolution. We test our model by forecasting yield curves and prices of coupon bond. In practice, our forecast shows accurate forecasting of yields at both short and long horizons and accurate forecasting of bond prices with short-term of tenors.

3.1 Introduction

No-arbitrage modeling has many applications in economic and financial markets: from studying term structure of interest model, pricing bonds and its derivatives to risk management. The no-arbitrage tradition follows from the theoretical structure introduced by Heath et al. [66] which allows for infinite-dimensional risk factors in the dynamics of forward rate curve. Ang and Piazzesi [1] implemented the no-arbitrage restriction in affine term structure model which precludes the arbitrage opportunity between the dynamic evolution of the yield curve factors. The interest rate point forecasting introduced by Diebold and Li [37] shows good out-of-sample forecasting performance using no-arbitrage approach. Christensen et al. [21] demonstrates that the no-arbitrage approach the downgrades in the forecasting performance when the model is restricted to preclude the arbitrage opportunity. However, it is still hard to draw the conclusion that the no-arbitrage model is not important in forecasting especially when achieving a no-arbitrage model is compli-

cated using statistic models.

The no-arbitrage approach using HJM-type models are popular for pricing bonds and term-structure derivatives where interest rate forecasting becomes crucial for the risk management. The most widely used no-arbitrage models are Hull-White model introduced by Hull and White [71] and HJM model introduced by Heath et al. [66]. The HJM model allows the infinite dimensional expansion of the risk factors which is considered to be problematic but is also fitting very well in long time. The Hull-White model is a single-factor short rate model which can be seen as a simplified version of Vasicek [114]. Both Hull-White and Vašíček assume that the short rates have a normal distribution and that the short rates are subject to mean reversion. Cox et al. [31] introduces the CIR model to overcome the negative interest problem in both Hull-White and Vašíček models. However, the recent economic environment shows that negative interest rates are not impossible. These short rate models all demonstrate accurate valuation of interest rate related derivatives in a short time period. Motivated by their work, we choose the Vašíček model for the short-time period factor selection.

The fitting of the yield curve has a long history and dates back to McCulloch [97], which applies cubic splines in fitting yield curve. Fama and Bliss [54] firstly proposed discounting method also known as smooth bootstrap method to extract zero-coupon bonds from market data. However, the discounted bonds have only one to five years to maturity and are available by monthly due to the lack of enough long-term bonds in market. The limitation of Fama-Bliss method is obviously: one is that it is not possible to study the excess returns for longer holding periods and the other one is that it contains only a short period for the term structure.

The earliest bond price forecasting starts since 1980s, such literature is given by Brennan and Schwartz [15]. The most widely used model is Nelson-Siegel term structure introduced by Nelson and Siegel [101] due to the simple interpretation from economics perspective and the applicable of forecasting. Recent literature that involves forecasting includes Duffee [44] and Diebold and Li [37] where they extended the estimation work of yield curve from in-sample fitting to out-of sample forecasting. Their prominent contribution in predicting the yield curves mainly depends on the dynamic affine structure and the linearity between observations and models. Christensen et al. [21] advanced the prediction work by implementing Kalman filter on sequential observations and proceed to maximize the log-likelihood. Later Duffee [45] shows how important the no-arbitrage restriction is when using the term structure to forecast future bond yields. The arbitrage-free condition is claimed from the theoretical perspective, however, there is little practical evidence layer that shows that the models are actually arbitrage-free. In our approach, we will quantify the arbitrage opportunity in the dynamic Nelson-Siegel model and use it as the regularization term.

The application of machine learning in finance, appears earlier in equity markets and especially focuses on forecasting methods with deep neural network such as Ding, Zhang, Liu, and Duan [40], Selvin, Vinayakumar, Gopalakrishnan, Menon, and Soman [111] and Chong, Han, and Park [20]. Recent work by Ganguli and Dunnmon [61] extend machine learning to bond price forecasting where they evaluated the performance of various supervised learning algorithms and presented results by the weighted error in prediction per sample. Bianchi, Büchner, and Tamoni [5] applied machine learning in bond return forecasting and studied the risk factors between macroeconomic and yield information. Their research are based upon pure machine learning technique to analyze the dependence layer between the observation and input variable. In our model, we will deploy several deep neural networks such as Long Short-term memory (LSTM), Recurrent Neural Networks (RNN) and Convolutional Neural Network (CNN) that serves as the parameter selection.

Our research in bond price forecasting includes three parts: arbitrage-free pricing theory, deep neural networks, and a filter-based sequential method using the Kalman filter, extended Kalman filter, or particle filter. For the filtering theory we refer to Musoff and Zarchan [100], Del Moral [36], and Wan and Van Der Merwe [117]. A good summary of the particle filter can be found in Doucet and Johansen [41] and the application of filtering in finance can be found in Javaheri, Lautier, and Galli [76].

We organize the following sections by such an order. First, we review HJM forward rate model and derive the arbitrage-free condition under risk neutral measure. We assume the yield curve can be explained by a Nelson-Siegel term structure with three state variables that evolve dynamically and are modeled by a Vašíček process. Second, we review filter based method in finance and introduce the Kalman filter based method for updating and forecasting the linear model of yield curve. Then we extended the updating framework in the Kalman filter to the extended Kalman and which is applied for bond price forecasting. In the particle filter we consider using the updating process in the extended Kalman filter for importance sampling and systematic resampling. Instead of maximizing the log-likelihood, we choose our objective function to minimize the mean square error of the target values (yields or prices). Third, we introduce the parameter selection method by deep neural networks. We use convolution neural networks as a dimension reduction tool to process the multiple observations each of which contains multiple features. We use recurrent neural networks to capture temporal information from sequential observations. We train our model by minimizing the mean square prediction error and minimizing the arbitrage penalty at the same time. Finally, we present forecasting results when the methodology is applied to Treasury bonds and corporate bonds. We provide the error analysis of predicted yields and prices of coupon bond for different time horizons and maturity horizons. We present the average excess return (AER) as the quantified arbitrage opportunity for different time horizons. The effect of arbitrage-free regularization will be viewed through the comparison between the performance of non-arbitrage forecasting and arbitrage-penalized forecasting. In addition, we also investigate arbitrage regularization and show their effect on the filters.

3.2 Background

The term structure of interest rate has been widely studied since McCulloch [97] introduced spline method, McCulloch [98] introduced second-order and third-order spline method, Vasicek and Fong [115] introduced exponential spline, Fisher, Nychka, and Zervos [58] and Waggoner [116] improved the cubic spline with smooth penalty. The cubic spline

$$y(x) = \sum_{i=1}^{K} \left(a_i + b_i(x-\tau_i) + c_i(x-\tau_i)^2 + d_i(x-\tau_i)^3\right) \mathbf{1}_{\{\tau_i \le t < \tau_{i+1}\}}$$

is constructed using polynomials smoothly connected at the knots τ_i for $i = 1, \cdots, K$, which are selected in a way such that the observations are spread equally between adjacent knots. The approach to cubic spline using basis spline is given by

$$y(x) = \sum_{i=1}^{K} \beta_i \phi_i^p(x),$$

where the p denotes the degree of the basis $\phi_i^p(x)$, $p = 3$ for a cubic spline. The basis $\phi^p(x)$ is defined by Cox-de Boor recursion

$$\phi_n^p(x) = \frac{x - \tau_n}{\tau_{n+p-1} - \tau_n}\phi_n^{p-1}(x) + \frac{\tau_{n+p} - x}{\tau_{n+p} - \tau_{n+1}}\phi_{n+1}^{p-1}(x),$$

with

$$\phi_n^0(x) = \begin{cases} 1, & \text{if } \tau_n \leq x < \tau_{n+1} \\ 0, & \text{otherwise.} \end{cases}$$

Denote the cubic spline basis by a row vector

$$\phi(x) = (\phi_1(x), \cdots, \phi_K(x)).$$

Then for any $x \in [\tau_i, \tau_{i+1})$, there are four adjacent non-zero basis at ϕ_{i-1}, ϕ_i, ϕ_{i+1} and ϕ_{i+2}, with adjacent intervals sharing three basis. Thus the augmented basis matrix

$$\Phi = (\phi(x_1), \cdots, \phi(x_N))^T,$$

for N observations x_n, $n = 1, \cdots, N$, gives a semi-orthogonal structure which provides numerical stability. The parameter $\beta = (\beta_1, \beta_2, \cdots, \beta_K)^T$ can be obtained using ordinary least square estimation or regression estimation with an extra linear penalty that controls the smoothness of the tail of the yield curve.

These models provide good fits for the data and controlling for the tail smoothness. However, the cubic spline models are lack of sufficient support from economic theoretical perspective. Nelson and Siegel [101] propose flexible parametric curves and Svensson [113] introduced an additional term in the Nelson-Siegel term structure to compensate the hump in the term structures. Filipovic et al. [57] extend Nelson-Siegel term structure to exponential polynomial model. Comparing to cubic spline models, the Nelson-Siegel model is a parsimonious term structure with only four parameters: level (L), slope (S), curvature (C) and decay (λ) (or shape) :

$$y(\tau) = L + S\left(\frac{1 - e^{-\lambda\tau}}{\lambda\tau}\right) + C\left(\frac{1 - e^{-\lambda\tau}}{\lambda\tau} - e^{\lambda\tau}\right). \tag{3.2.1}$$

Svensson includes a second curvature parameter (C') and an additional decay parameter (λ') for the the second curvature term. The yield curve has a variety of shapes through time, including upward, downward, humped and inverted humped. The Nelson-Siegel term structure can replicate all these shapes dependent upon the variation in (L, S, C, C') and the choice of decay parameters (λ, λ').

Due the parsimonious parameterization and the economic interpretability of the Nelson-Siegel model, it has been world-widely used by central banks and monetary policy maker in different markets. The most common way to fit the Nelson-Siegel term structure is to estimate the parameters L, S and C using yield data or zero-coupon bonds data provided by Famma-Bliss data. In practice, by fixing the shape parameter λ we can convert the non-linear problem to linear problem and estimate the remaining three parameters $\theta = (L, S, C)^T$ using ordinary least squares (OLS) to

minimize the sum of square errors

$$Q(\theta) = \left(X\theta - Y^{\text{obs}}\right)^T \left(X\theta - Y^{\text{obs}}\right), \tag{3.2.2}$$

where

$$\begin{aligned}
X &= \begin{pmatrix} 1 & \phi_1(\tau_1) & \phi_2(\tau_1) \\ \vdots & \vdots & \vdots \\ 1 & \phi_1(\tau_N) & \phi_2(\tau_N) \end{pmatrix}, \\
Y^{\text{obs}} &= (Y_1, \cdots, Y_N)^T, \\
\phi_1(\tau) &= \frac{1 - e^{-\lambda\tau}}{\lambda\tau}, \\
\phi_2(\tau) &= \frac{1 - e^{-\lambda\tau}}{\lambda\tau} - e^{\lambda\tau}.
\end{aligned}$$

Though fixing the decay parameter simplifies our model, the effect of the decay parameter still exists if one wants to fit sequential yield curves and this effect can only be revealed by non-linear estimation. Diebold and Li [37] studied the Nelson-Siegel model with time-varying decay parameter and found that the fitting and forecasting are not influenced by a varying decay parameter. On the other hand, Hurn, Lindsay, and Pavlov [73] and De Pooter [35] point out that the Nelson-Siegel model is very sensitive to the choice of the decay parameter and the remaining parameter estimates may take extreme values under different decay parameters. However, Annaert, Claes, De Ceuster, and Zhang [2] found that ridge regression can reduce the multi-collinearity problem caused by fixed decay parameter in time series and also reduce the sensitivity problem. Diebold and Li [37] show that the Nelson-Siegel model performs well in forecasting yields and the fixed decay parameter does not impact the out-of-sample forecasting. The effect of decay parameter can be viewed from the the forward rate model

$$f(t) = L + Se^{-\lambda t} + C\lambda t e^{-\lambda t}. \tag{3.2.3}$$

which is in accordance with Nelson-Siegel term structure. If the value of λ is small, then the forward curve (3.2.3) decays slowly and fits better to the observations on long time intervals. On the contrary, if we choose a large value for λ, then the forward curve decays fast and fit better on short time intervals.

Theoretically, the Nelson-Siegel model does not naturally preclude the arbitrage opportunities as shown by Björk and Christensen [6]. However, there are different opinions on the arbitrage-freeness of the Nelson-Siegel model. Coroneo, Nyholm, and Vidova-Koleva [26] find that Nelson-Siegel is compatible with the arbitrage-freeness on the US market in a statistical sense. Christensen et al. [21] try to remove the arbitrage from the Nelson-Siegel model and also obtain good results. The most common way to investigate arbitrage opportunities in the Nelson-Siegel model is to consider the forward rate curve by an affine term-structure model which simplifies fitting procedure and improves forecasting performance. Ang and Piazzesi [1] presents the class of arbitrage-free

Nelson-Siegel model by

$$y(t,\tau) = a_\tau + b_\tau X_t,$$

where b_τ is the loading parameter given by

$$b_\tau = \left(1, \frac{1-e^{-\lambda\tau}}{\lambda\tau}, \frac{1-e^{-\lambda\tau}}{\lambda\tau} - e^{\lambda\tau}\right),$$

and $X_t = (L_t, S_t, C_t)$ is the time varying parameters assumed to follow a Gaussian vector autoregression process

$$X_t = \mu + \Phi X_{t-1} + u_t,$$

with error term $u_t \sim N(0, \Sigma\Sigma^T)$ as a 3×1 vector, μ as a 3×1 vector, and Φ as a $K\times K$ autoregressive matrix. The arbitrage-free restrictions are given by

$$A_{\tau+1} = A_\tau + B_\tau^T(\mu - \Sigma\lambda_0) + \frac{1}{2}B_\tau^T\Sigma\Sigma^T B_\tau - A_1, \tag{3.2.4}$$

$$B_{\tau+1} = (\Phi - \Sigma\lambda_1)^T B_\tau - B_1, \tag{3.2.5}$$

with

$$A_\tau = -a_\tau\tau,$$
$$B_\tau = -b_\tau\tau.$$

Arbitrage is precluded form the recursive equations (3.2.4) for some parameters λ_0 (3×1 matrix) and λ_1 (3×3 matrix) governing the market price of risks

$$\Lambda_t = \lambda_0 + \lambda_1 X_t.$$

Another approach to the arbitrage-free Nelson-Siegel model follows the arbitrage pricing theorem. For example, Christensen et al. [21] introduce a theoretically rigorous yield curve model that simultaneously displays empirical tractability, well fitness, and superior forecasting performance. They conclude that imposing the arbitrage-free restrictions in the yield curve model downgrades the performance of forecasting. Another approach by Kratsios and Hyndman [86] implement the arbitrage restrictions in deep-forward neural networks and also find the same conclusion. However, the classical approaches used by the above authors can only obtain models statistically arbitrage-free for the in-sample-data. It is not know whether the models still keep arbitrage-free for the out-of-sample data. Therefore, we will consider the arbitrage-free Nelson-Siegel model with deep dynamic parameters and implement different filtering methods to update the parameters.

3.3 Arbitrage-free pricing framework

The no-arbitrage term-structure literature builds upon the theoretical structure introduced by Heath et al. [66]. Ang and Piazzesi [1] studied affine no-arbitrage term structure models which preclude arbitrage opportunities between the dynamic evolution of the yield curve factors and the yields at different maturity segments. The interest rates forecasting introduced by Diebold and Li [37] shows good out-of-sample forecasting performance using the no-arbitrage approach. Christensen et al. [21] demonstrates that the no-arbitrage approach downgrades the performance when the model is restricted to preclude the arbitrage opportunity.

3.3.1 Arbitrage-free forward rate model

The Heath-Jarrow-Morton (HJM) model [66] provides a powerful framework in modeling the instantaneous forward and fixed income assets in an arbitrage-free setting. The theoretical form of the HJM model allows infinite-dimensional combinations of risk factors. Given that the affine structure is widely applied in dynamic models, we consider the realization of HJM in finite-dimensional affine structure and the arbitrage-free condition under the risk-neutral measure $\mathbb{Q}$

$$df(t,\tau) = \mu(t,\tau)\,dt + \sum_{i=1}^{d} \eta_i(t,\tau)\,dW_i(t), \tag{3.3.1}$$

where τ is the tenor from time t to maturity T, $W_i(t)$ for $i = 1,2,\ldots,d$ are independent standard Brownian motions, $\mu \in \mathbb{R}$ is the drift term and $\eta_i \in \mathbb{R}$ for $i = 1,2,\ldots,d$ are risk factors. We assume that (3.3.1) is separable in t and τ and has a finite-dimensional representation by the following affine structure

$$f(t,\tau) = \beta_\tau X_t, \tag{3.3.2}$$

for a deterministic loading parameter $\beta_\tau \in \mathbb{R}^{1\times d}$ and a dynamic process $X_t \in \mathbb{R}^{d\times 1}$ containing the risk factors. We assume the loading parameter is chosen such that the corresponding yield curves are in the class of Nelson-Siegel term structure and the risk is only from the time varying process X_t.

Next, we determine the realization of the forward rate process in finite space and the specification of the volatility term. The finite-dimensional realization of the forward rate process requires the drift and volatility located in the tangent space of the manifold where the forward rate evolves to avoid the projection error, see Björk and Svensson [7]. The different choice of volatility will reduce the HJM forward rate curve to simpler finite-dimensional models such as the Ho-Lee model with constant volatility ot the Hull White model with exponentially decaying volatility. The most common specification of volatility in bond markets is a multiple factor interpretation using Principle Component Analysis (PCA). As documented by Litterman and Scheinkman [89], the three-factor approach explains no less than 94% of the total variance in the U.S yields crossing different term of maturities. The first factor as a 'parallel shift' accounts for 80%˘90% of the term structure variation. The second factor as a 'steepness' where the short and long rates move in opposite directions accounts for on average 81% of the remaining variation. The third factor as a 'curvature' accounts for 0%˘5% of the total variation. Therefore, we will consider a three-factor model for X_t with

cross-variable interaction instead of independent variables.

Another requirement for the calibration of the forward rate model is that the initial forward curve requires empirically observed forward rates. We implement the calibration under a machine learning framework where the observations will be sequentially batched into many subsets. Thus, we apply a 'fake' initials to all subsets, which is obtained from the training set. In the following section, we introduce the loading parameter β_τ in exponential space and specify the risk variable X_t as a mean-reverting process which we will be tested in later section. We define X_t as extended Vašíček process

$$dX_t = \kappa_t \left(\theta_t - X_t\right) dt + \sigma_t dW_t, \tag{3.3.3}$$

where κ_t, θ_t and σ_t are functions which depend on X_t. Equation (3.3.3) is the factor model and the risk factor X_t is the state variable. The dynamics of the forward rate model f defined in (3.3.2) with state variable X_t defined in (3.3.3) is also mean-reverting process

$$\begin{aligned}
df(t,\tau) =& -\frac{d\beta_\tau}{d\tau} X_t dt + \beta_\tau dX_t \\
=& -\frac{d\beta_\tau}{d\tau} X_t dt + \beta_\tau \kappa_t \left(\theta_t - X_t\right) dt + \beta_\tau \sigma_t dW_t \\
=& \left(\beta_\tau \kappa_t \theta_t - \left(\beta_\tau \kappa_t + \frac{d\beta_\tau}{d\tau}\right) X_t\right) dt + \beta_\tau \sigma_t dW_t \\
=& \left(\beta_\tau \kappa_t + \frac{d\beta_\tau}{d\tau}\right) \left(\left(\beta_\tau \kappa_t + \frac{d\beta_\tau}{d\tau}\right)^{-1} \beta_\tau \kappa_t \theta_t - X_t\right) dt + \beta_\tau \sigma_t dW_t \\
=& \bar{\kappa}(t,\tau) \left(\bar{\theta}(t,\tau) - X_t\right) dt + \beta_\tau \sigma_t dW_t,
\end{aligned}$$

where

$$\bar{\kappa}(t,\tau) = \left(\beta_\tau \kappa_t + \frac{d\beta_\tau}{d\tau}\right), \tag{3.3.4}$$

$$\bar{\theta}(t,\tau) = \left(\beta_\tau \kappa_t + \frac{d\beta_\tau}{d\tau}\right)^{-1} \beta_\tau \kappa_t \theta_t. \tag{3.3.5}$$

From the affine forward rate (3.3.2), we obtain the short rate

$$r(t) = \beta_0 X_t, \tag{3.3.6}$$

and the value of zero-coupon bond $PV(t,\tau)$ which pays unit dollar at time $T = t + \tau$

$$PV(t,\tau) = \exp\left(-\int_0^\tau f(t,s) ds\right) = \exp\left(-B_\tau X_t\right), \tag{3.3.7}$$

where $B_\tau = \int_0^\tau \beta_u du$.

Following the arbitrage-free methodology introduced by Heath et al. [66], we define an accumulation factor $R(t)$ corresponding to the accumulated value of a dollar invested in the money

market account over the time period $[0,t]$ by

$$R(t) = \exp\left(\int_0^t r(s)ds\right). \tag{3.3.8}$$

The relative bond price $Z(t,\tau) = \frac{PV(t,\tau)}{R(t)}$ representing the bond's excess value over the risk-free investment follows the dynamics

$$\frac{dZ(t,\tau)}{Z(t,\tau)} = \Lambda(t,\tau)\,dt - B_\tau \sigma_t dW_t, \tag{3.3.9}$$

where

$$\Lambda(t,\tau) = \frac{1}{2}B_\tau \Sigma_t B_\tau^T - B_\tau \kappa_t(\theta_t - X_t) + (\beta_\tau - \beta_0)X_t, \tag{3.3.10}$$

and

$$\Sigma_t = \sigma_t \sigma^T.$$

Note that $\Lambda(t,\tau)$ defines the instantaneous excess return on the bond above the risk free rate and Heath et al. [66] proves that there exists a unique market price of risk such that the forward rate model is arbitrage-free. Therefore, the condition $\Lambda(t,\tau) = 0$ determines risk neutral pricing measure and precludes arbitrage opportunities. We summarize these facts in the following theorem.

Theorem 3.1. *Suppose the forward rate model has an affine structure give by (3.3.2)*

$$f(t,\tau) = \beta_\tau X_t,$$

and a mean-reverting state variable defined by (3.3.3)

$$dX_t = \kappa_t(\theta_t - X_t)\,dt + \sigma_t dW_t,$$

where $\beta_\tau \in \mathbb{R}^{1\times d}$, $X_t \in \mathbb{R}^{d\times 1}$, and

$$\kappa_t(X_t) : \mathbb{R}^{d\times 1} \to \mathbb{R}^{d\times d},$$
$$\theta_t(X_t) : \mathbb{R}^{d\times 1} \to \mathbb{R}^{d\times 1},$$
$$\sigma_t(X_t) : \mathbb{R}^{d\times 1} \to \mathbb{R}^{d\times d}.$$

If the following condition is satisfied for all $t \geq 0$ and $\tau \geq 0$.

$$\frac{1}{2}B_\tau \Sigma_t B_\tau^T - B_\tau \kappa_t(\theta_t - X_t) + (\beta_\tau - \beta_0)X_t = 0, \tag{3.3.11}$$

then $f(t,\tau)$ is an arbitrage-free forward rate model under risk-neutral measure $\mathbb{Q}$.

Proposition 3.2. *Suppose X_t evolves as mean-reverting process with time-dependent parameter*

given by equation (3.3.3). Then (3.3.3) with initial condition X_0 has a unique solution X_t given by

$$X_t = e^{-\int_0^t \kappa_u du} X_0 + \int_0^t e^{-\int_u^t \kappa_v dv} \kappa_u \theta_u du + \int_0^t e^{-\int_u^t \kappa_v dv} \sigma_u dW_u, \tag{3.3.12}$$

where the mean and variance of X_t are given by

$$\mathbb{E}[X_T|\mathcal{F}_t] = e^{-\int_t^T \kappa_u du} X_t + \int_t^T e^{-\int_u^T \kappa_v dv} \kappa_u \theta_u du, \tag{3.3.13}$$

$$Var[X_T|\mathcal{F}_t] = \int_t^T e^{-\int_u^T \kappa_v dv} \Sigma_u e^{-\int_u^T \kappa_v^T dv} du. \tag{3.3.14}$$

Proof: see Appendix 5.12.

3.3.2 Dynamic Nelson-Siegel term structure

Choosing different loading parameters β_τ, we can generate forward rate curves by (3.3.2) that give different shapes of the term structure. Inspired by the prediction framework introduced by Diebold, Rudebusch, and Aruoba [38] and Diebold, Li, and Yue [39] where they introduced the dynamic Nelson-Siegel term structure and modeled the factors using auto-regressive processes, we will apply dynamic Nelson-Siegel term structure within the framework of the arbitrage-free forward rate model. We define the loading parameter β_τ as a three-dimensional vector basis for some $\lambda \in \mathbb{R}^+$

$$\beta_\tau = \left(1,\ e^{-\lambda\tau},\ \lambda\tau e^{-\lambda\tau}\right), \tag{3.3.15}$$

with each component

$$\begin{aligned}
\beta_1(\tau) &= 1, \\
\beta_2(\tau) &= e^{-\lambda\tau}, \\
\beta_3(\tau) &= \lambda\tau e^{-\lambda\tau}.
\end{aligned}$$

The Nelson-Siegel term structure space $\mathcal{NS}(\tau)$ is spanned by the exponential polynomial basis β_τ with one decay parameters λ

$$\mathcal{NS}(\tau) = \text{Span}\left\{ \left(1,\ e^{-\lambda\tau},\ \lambda\tau e^{-\lambda\tau}\right) \middle| \text{for some } \lambda \in \mathbb{R}^+ \right\}. \tag{3.3.16}$$

As shown by Björk and Svensson [7], as long as the drift and volatility of the forward rate process lie in $\mathcal{NS}(\tau)$ whose tangent space is itself then the forward rate process will evolve in $\mathcal{NS}(\tau)$. For some three-dimensional state vector $X_t = (X_1(t),\ X_2(t),\ X_3(t))^T \in \mathbb{R}^{3\times 1}$, the forward rate model $f(t,\tau) \in \mathcal{NS}(\tau)$

$$f(t,\tau) = \beta_\tau X_t = X_1(t) + e^{-\lambda\tau} X_2(t) + \lambda\tau e^{-\lambda\tau} X_3(t), \tag{3.3.17}$$

defines the dynamic Nelson-Siegel yield model

$$\begin{aligned} y(t,\tau) =& -\frac{\log \mathrm{PV}(t,\tau)}{\tau} \\ =& \frac{B_\tau}{\tau} X_t \\ =& X_1(t) + X_2(t)\left(\frac{1-e^{-\lambda\tau}}{\lambda\tau}\right) + X_3(t)\left(\frac{1-e^{-\lambda\tau}}{\lambda\tau} - e^{\lambda\tau}\right), \end{aligned} \tag{3.3.18}$$

where

$$B_\tau = \int_0^\tau \beta_u du = \left(\tau, \frac{1-e^{-\lambda\tau}}{\lambda}, \frac{1-e^{-\lambda\tau}}{\lambda} - \tau e^{\lambda\tau}\right). \tag{3.3.19}$$

In time-series of yields using the loading parameters $B_2 = \frac{1-e^{-\lambda\tau}}{\lambda\tau}$ and $B_3 = \frac{1-e^{-\lambda\tau}}{\lambda\tau} - e^{\lambda\tau}$ as suggested by Diebold and Li [37] avoids the multicollinearity from similar loading parameters using the original setup given by Nelson and Siegel [101]. Reviewing the limiting behavior of the loading parameters β_1, β_2 and β_3 and on $[0,+\infty)$, we interpret X_1 as the long-term risk factor (level), X_2 as the short-term risk factor (slope), and X_3 as mid-term risk factor (curvature). The term structure space $\mathfrak{B}$ can be expand to include additional loading term and different decay parameter so that we can also interpret the forward rate process as Svensson [113] term structure model with four state variable.

$$\mathcal{SV}(\tau) = \mathrm{Span}\left\{ \left(1,\ e^{-\lambda_1\tau},\ \lambda_1\tau e^{-\lambda_1\tau},\ \lambda_2\tau e^{-\lambda_2\tau}\right) \middle| \text{ for some } \lambda_1,\lambda_2 \in \mathbb{R}^+ \right\}. \tag{3.3.20}$$

By Theorem (3.1), the state vector X_t and loading parameters must satisfy the following condition to preclude the arbitrage opportunity from the dynamic Nelson-Siegel yield model (3.3.18)

$$\Lambda(t,\tau) = \frac{1}{2} B_\tau \Sigma_t B_\tau^T - B_\tau \kappa_t (\theta_t - X_t) - \beta_0 X_t = 0. \tag{3.3.21}$$

The value of τ is the maturity as seen from t and we can easily make it analogous to the maturities of bonds. It is feasible to measure the excess return at the maturities of bonds, however, it is complicated minimizing it in practice when the maturities of bonds vary from day to day. Thus, we choose some fixed values between 3 months and 30 years as T_j and define the accumulated excess return (AER) introduced by Kratsios and Hyndman [86] as the penalty term

$$\Lambda^{(p)} = \frac{1}{n}\sum_{i=1}^{n} \left\| \Lambda(t)(t_i,T_j) \right\|_p = \frac{1}{n}\sum_{i=1}^{n} \sqrt[p]{\frac{1}{m}\sum_{j=1}^{m} \left|\Lambda(t)(t_i,T_j)\right|^p}, \tag{3.3.22}$$

The accumulated excess return gives the mean square root term when $p=2$ and at time t_i its value quantifies the average distance of the objectives (yield or price) to the arbitrage-free values over the selected maturities T_j for $j = 1,\cdots,m$.

Credit risk can be added as additional term ξ_t in the forward rate model (see Ejsing, Grothe,

and Grothe [51])

$$f(t,\tau) = \xi_t + \beta_\tau X_t,$$

the price of corporate bond (3.3.7) is given by

$$PV(t,\tau) = \exp\left(-\xi_t \tau - B_\tau X_t\right),$$

and the yield curve model is given by

$$y(t,\tau) = \xi_t + \frac{B_\tau}{\tau} X_t.$$

However, our interest is to study the arbitrage-free pricing and forecasting problem, we simply assume the d market risks in state vector X_t include credit risk when we apply the model to corporate data instead of modeling it separately.

Next, we consider the application of the affine term structure in pricing coupon bonds. Assume the coupon bond periodically pays c_i at time τ_i up to m total payments and has value $Y(t,\tau)$ given by the arbitrage-free Nelson-Siegel model (3.3.18)

$$\hat{Y}(t,\tau) = \sum_{i=1}^{m} c_i e^{-\tau_i y(\tau_i)} = \sum_{i=1}^{m} c_i e^{-B_{\tau_i} X_t}. \tag{3.3.23}$$

From equation (3.3.23), we can extract the yield curve and the state variables from observations. The observations that we used are the daily closed bond data. We choose the coupon bonds whose tenors are greater than 3 months and less than 30 years. The state variable X_t can be extracted by minimizing the mean square error (MSE) between the observation Y and the model value $\hat{Y}$

$$X_t = \underset{X_t \in \mathbb{R}^d}{\arg\min} \frac{1}{n} \sum_{i=1}^{n} \left| Y(t,\tau_i) - \hat{Y}(t,\tau_i) \right|^2, \tag{3.3.24}$$

using classical methods such as linear estimator with smoothing penalties.

3.3.3 Data and estimation result

Our data set is composed of coupon bonds from both the corporate bond market (TRACE) and U.S.Treasures (Overbond) from 2017 to 2019, includes the daily closing prices (clean price), yield-to-maturity, coupon rate, coupon frequency, instrument type, indicator for convertible bonds, indicator for callable bonds, issue date and maturity date. The total data was pre-processed to retain bond prices according to the following principles:

i. Fixed coupon bond

ii. Non-callable bond

iii. Nonconvertible bond

iv. Unsecured and Senior Unsecured note and bond

v. Yield-to-maturity $\leq$ 700 basis points

vi. The difference between yields-to-maturity and coupon rate $\leq$ 500 basis points

vii. Remaining time to the maturity $\geq$ 3 months and $\leq$ 30 years from the trade date

After the pre-processing, we index the bonds by trading dates and keep four basic features for each bond: price, coupon rate, coupon frequency, and the remaining time to maturity (tenor). We run two separate estimations determining in each we determine the optimal decay parameter and daily optimal state variables.

For the first estimation, we select a common data consisting of a fixed number of daily observations from total data and split the bonds into three terms of maturity. We consider the short-term maturities is less than 2 years where the yield curves are rapidly increasing or decreasing until the top or the bottom of the hump, the mid-term maturities is from 2 years to 10 years where the yield curves may change the direction, and long-term maturities from 10 years to 30 years where the yield curves are almost flat. The common data are selected such that the bonds are almost traded everyday and the number of bonds in each term of maturity are represented of the total proportion in total data. For example, if the total data has 20% bonds in short-term maturities, 67% bonds in mid-term maturities, and 13% bonds in long-term maturities, then the common data with daily 68 number of bonds could consist of almost 14 bonds in short-term, 45 bonds in mid-term, and 9 bond in long-term. We may drop some trading dates with too few observations that occupy approximately 1% to 3% in total data. The common data is used with the Nelson-Siegel model (3.3.18) with trainable variable X_T as a $3 \times T$ matrix including all the three state variables and trainable variable λ controls the decay parameter. The model is trained to minimize the mean squares root error (3.3.24) and to determine the optimal decay parameter λ. The optimal value of decay parameter is $\lambda = 0.4488779759$ obtained from Treasury data. We also use this value for corporate data instead of estimating different decay parameters for each corporate since we mentioned before that a fixed decay parameter does not impact the out-of-sample forecasting.

In the second estimation, we fix the decay parameter as $\lambda = 0.4488779759$ and fit the Nelson-Siegel model with daily observations from total data by a sequential regression. We run the sequential regression using the optimal state variable X_{t-1} trained from previous data set as the initial state variable to fit the next data set and obtain the optimal state variable X_t. We choose the tenors in proportion to the number of bonds in each term of maturities and obtain yield data at those tenors shown in Table 3.1 with yield curves shown in Figure 3.1. The yield data is used as the input for the linear model and the common data is used as the input for the non-linear model which will be introduced in the next section.

Table 3.1: U.S. Treasury yields (in %)

date	3M	6M	9M	12M	15M	18M	...	120M	180M	240M	300M	360M
1/9/2017	0.735	0.822	0.906	0.987	1.066	1.143	...	2.532	2.798	2.938	3.024	3.081
1/10/2017	0.648	0.745	0.839	0.929	1.016	1.100	...	2.541	2.806	2.946	3.031	3.088
1/11/2017	0.672	0.768	0.861	0.950	1.035	1.117	...	2.535	2.794	2.932	3.015	3.071
1/12/2017	0.695	0.785	0.873	0.958	1.039	1.118	...	2.531	2.797	2.939	3.024	3.082
1/13/2017	0.702	0.791	0.879	0.963	1.045	1.124	...	2.547	2.817	2.960	3.047	3.105
...												

Figure 3.1: Treasury yield curves from 2017 to 2019

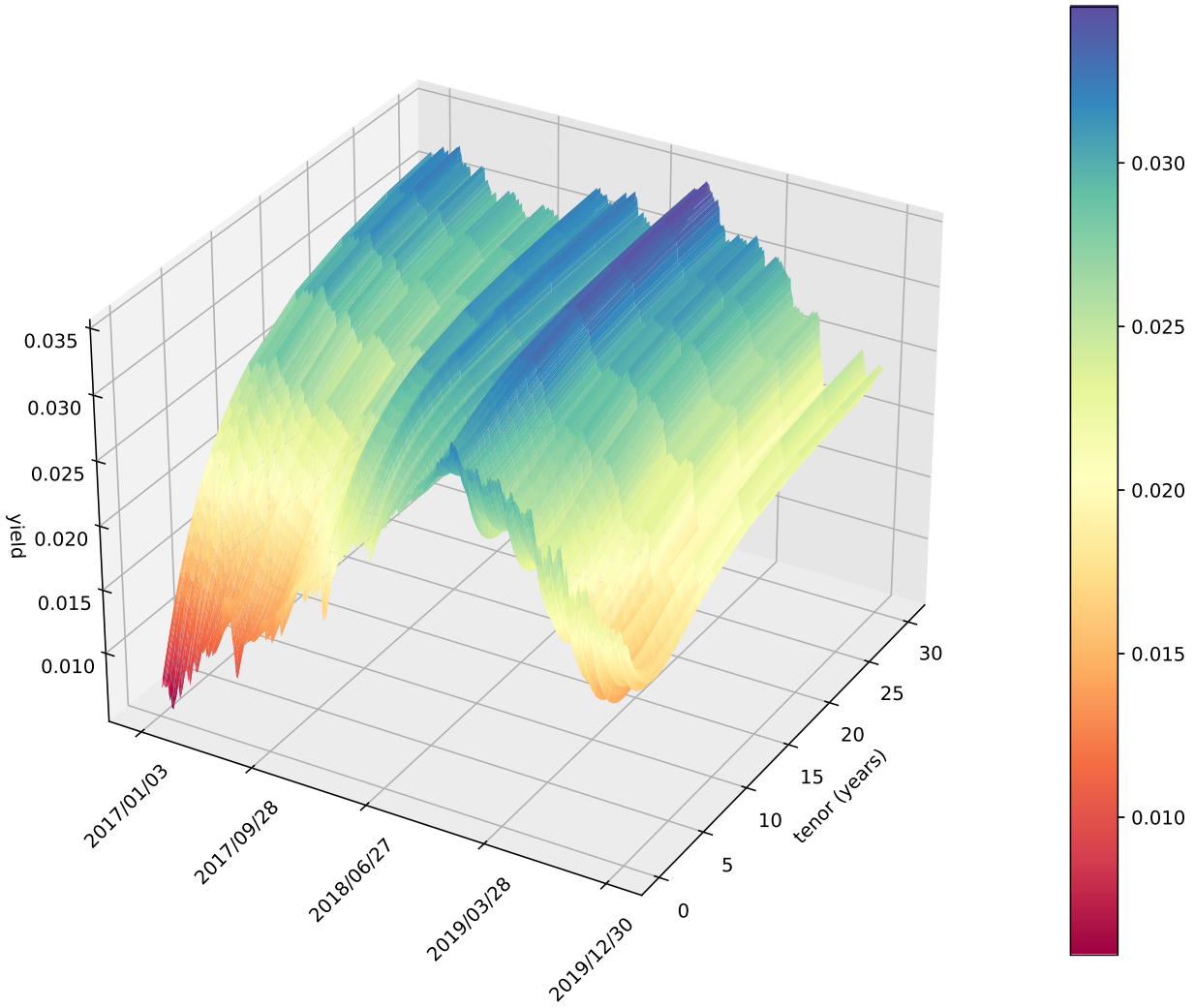

Figure 3.2: State variables of Treasury from 2017 to 2019

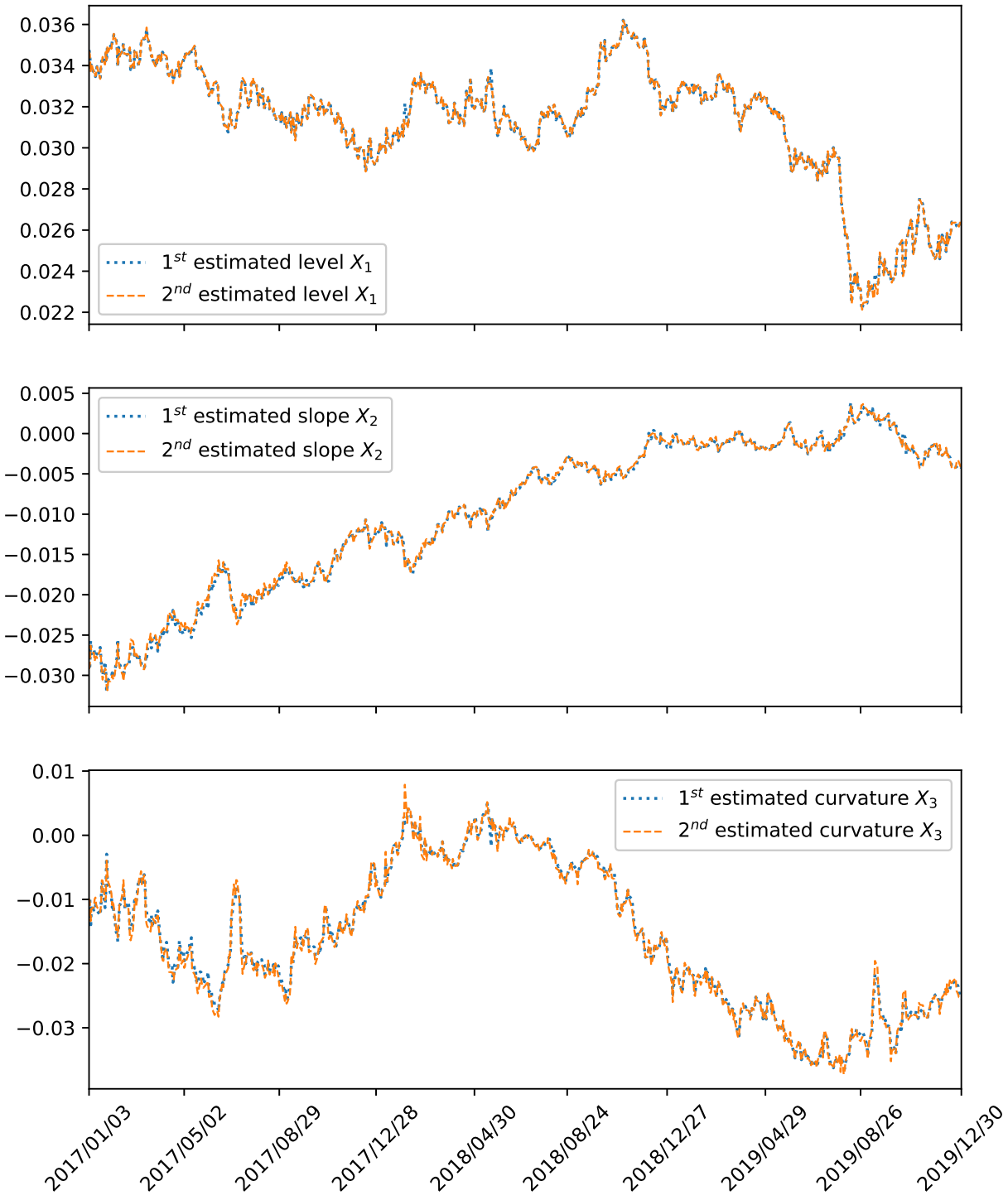

In Figure 3.2, we present the extraction optimal state variables obtained from second estimation. The dotted line shows the results of first estimation and the dashed line shows the results of second estimation.

In Table 3.2, we check the validity of the mean reversion assumption by Augmented Dickey-Fuller (ADF). The null-hypothesis of ADF test is that there exists a unit root (non-stationary) in the time series. The more negative the ADF statistics, the stronger the rejection of the null-hypothesis. The ADF test statistics of X_1, X_2 and X_3 are -1.601, -2.345 and -1.321 shown in Table 3.2 and are greater than the critical value -2.569 at 10%. This means we cannot reject the null-hypothesis and conclude that the series X_1, X_2 and X_3 are not stationary.

Table 3.2: Statistic of state variables

Factor	Mean	Std	Min.	Max.		Correlation		ADF	P-value	CV(10%)
$X_1(t)$	0.03120	0.0030	0.0221	0.0362	1	-0.541	0.430	-1.601	0.483	-2.569
$X_2(t)$	-0.0098	0.0093	-0.0310	0.0041	-	1	-0.353	-2.345	0.157	-
$X_3(t)$	-0.0163	0.0111	-0.0366	0.0049	-	-	1	-1.321	0.619	-

In the next section, we will introduce the filter-based method to calibrate the arbitrage-free model. The common data will be used as the input for the non-linear model and the yields will be used as the input for the linear model.

3.4 Forecasting framework

In this section, we introduce three filter-based sequential methods to estimate bond yields and bond prices given the parameters $(\kappa_t, \theta_t, \sigma_t)$. We then we introduce the estimation of parameters $(\kappa_t, \theta_t, \sigma_t)$ by deep neural networks. The Kalman filter and the extended Kalman filter have similar structure but one deals with yields prediction and the other deals with bond price prediction. We begin by introducing the Kalman filter in detail then extend the prior and post information updating method to the extended Kalman filter and the particle filter.

3.4.1 Yields prediction by Kalman filter

Consider the yields $y_t = (y_1, \cdots, y_m)$ at time t observed for fixed tenors $\tau_1, \cdots, \tau_m$. We assume that the noise between the observations and the state model (3.3.18) is Gaussian with mean zero and variance U_t

$$y(t,\tau) = \frac{B_\tau}{\tau} X_t + \varepsilon_t, \tag{3.4.1}$$

where $\mathbb{E}[\varepsilon_t] = 0$ and $\mathrm{Var}[\varepsilon_t] = U_t$. It is difficult to calculate the expectation and variance of X_t directly using Proposition 3.2 if the state variable is non-scalar and the parameters κ_t, θ_t and σ_t are matrices. So we seek a simplification by considering that the time increment $\Delta t_k = t_{k+1} - t_k$ are the same for the discretization $[t_0, t_1, \ldots, t_k, t_{k+1}, \ldots]$ and κ_t, θ_t, and σ_t are invariant on each time interval $t \in [t_k, t_{k+1})$. Then by Proposition 3.2, we obtain the following estimations

$$\mathbb{E}[X_{k+1}|\mathcal{F}_k] = e^{-\kappa_k \Delta t} X_k + \left(I - e^{-\kappa_k \Delta t}\right) \theta_k, \tag{3.4.2}$$

$$\mathrm{Var}[X_{k+1}|\mathcal{F}_k] = \int_0^{\Delta t} e^{-\kappa_k t} \Sigma_k e^{-\kappa_k^T t} dt. \tag{3.4.3}$$

We denote (3.4.3) as $Q_t = \mathrm{Var}[X_{k+1}|\mathcal{F}_k]$ and the computation of Q_t can be simplified using the diagonalization of the matrix κ_k

$$\kappa_k = EVE^{-1},$$

where E is the eigenvectors matrix of κ_k, and V is the diagonal matrix consisting of the eigenvalues ζ of κ_k. The integral in (3.4.3) can be simplified to

$$Q_k = E\left(\int_0^{\Delta t} e^{-Vt}\Omega e^{-V^T t}dt\right)E^T, \tag{3.4.4}$$

where $\Omega = E^{-1}\Sigma_k E^{-T} = \left(\omega_{i,j}\right)_{i,j}$. The integral in (3.4.4) can be simplified to

$$\begin{aligned}
&\int_0^{\Delta t}\left(e^{-Vt}\Omega e^{-V^T t}\right)_{i,j}dt \\
=&\int_0^{\Delta t} e^{-\zeta_i t}\omega_{i,j}e^{-\zeta_j t}dt \\
=&\frac{\omega_{i,j}}{\zeta_i+\zeta_j}\left(1-e^{-(\zeta_i+\zeta_j)\Delta t}\right).
\end{aligned}$$

Therefore, the estimation of Q_k is given by

$$Q_k = E\left(\frac{\omega_{i,j}}{\zeta_i+\zeta_j}\left(1-e^{-(\zeta_i+\zeta_j)\Delta t}\right)\right)_{i,j}E^T. \tag{3.4.5}$$

Equations (3.4.1) and (3.4.2) give us the state and observation equations

$$X_{k+1} = g(t_k, X_k) + w_k, \tag{3.4.6}$$
$$y_{k+1} = y(t_{k+1}, X_{k+1}) + \varepsilon_k, \tag{3.4.7}$$

where

$$\begin{aligned}
g(t,x) =& A_t x_t + D_t, \\
y(t,x) =& Mx_t, \\
A_t =& e^{-\kappa_t \Delta t}, \\
D_t =& \left(I - e^{-\kappa_t \Delta t}\right)\theta_t, \\
M =& \begin{bmatrix} \frac{B_1(\tau_1)}{\tau_1}, & \frac{B_2(\tau_1)}{\tau_1}, & \frac{B_3(\tau_1)}{\tau_1} \\ \vdots & \vdots & \vdots \\ \frac{B_1(\tau_m)}{\tau_m}, & \frac{B_2(\tau_m)}{\tau_m}, & \frac{B_3(\tau_m)}{\tau_m} \end{bmatrix}.
\end{aligned}$$

and τ_m is the maximum tenor among all the observations. The noise terms w_k and ε_k are assumed

to be Gaussian noise with mean zero and covariance Q_k and U_k

$$\begin{pmatrix} w_k \\ \varepsilon_k \end{pmatrix} \sim \mathrm{N}\left(\begin{pmatrix} 0 \\ 0 \end{pmatrix}, \begin{pmatrix} Q_k & 0 \\ 0 & U_k \end{pmatrix} \right).$$

Following Date and Ponomareva [34], the prediction step of the Kalman filter is given by

$$\begin{aligned} \hat{X}_{k|k-1} &= A_{k-1}\hat{X}_{k-1|k-1} + D_{k-1}, \\ \hat{P}_{k|k-1} &= A_{k-1}\hat{P}_{k-1|k-1}A_{k-1}^T + Q_{k-1}, \\ \hat{y}_k &= M\hat{X}_{k|k-1}, \end{aligned}$$

and measurement step of the Kalman filter is given by

$$\begin{aligned} \hat{X}_{k|k} &= \hat{X}_{k|k-1} + K_k v_k, \\ \hat{P}_{k|k} &= \hat{P}_{k|k-1} - K_k M \hat{P}_{k|k-1}, \\ v_k &= y_k - \hat{y}_k, \\ F_k &= M\hat{P}_{k|k-1}M^T + U_{k-1}, \\ K_k &= \hat{P}_{k|k-1}M^T F_k^{-1}. \end{aligned}$$

3.4.2 Price prediction by the extended Kalman filter

If, instead of considering predicted yields, we wish to consider price prediction directly, then we need to change the linear observation model to a non-linear model. In this case the extended Kalman filter will be considered. The observations $Y_k = \left(PV_k^{(1)}, \ldots, PV_k^{(n)}\right)$ contain n prices of coupon bonds and each observation is defined from (3.3.23) as

$$\hat{Y}(X_t, t) = \sum_j^m c_{\tau_j} e^{-B_{\tau_j} X_t} = C_\tau \exp\left(-B_\tau X_t\right), \tag{3.4.8}$$

where

$$\begin{aligned} C_\tau &= (c_{\tau_1}, c_{\tau_2}, \cdots, c_{\tau_m}) \in \mathbb{R}^{1\times m}, \\ B_\tau &= (B_{\tau_1}, B_{\tau_2}, \cdots, B_{\tau_m})^T \in \mathbb{R}^{m\times 3}. \end{aligned}$$

The extended Kalman filter (see Christensen et al. [21]) by the following system

$$\begin{aligned} \hat{X}_{k|k-1} &= A_k\hat{X}_{k-1|k-1} + D_k, \\ \hat{P}_{k|k-1} &= A_k\hat{P}_{k-1|k-1}A_k^T + Q_k, \end{aligned} \tag{3.4.9}$$

and measurement process

$$\begin{aligned} \hat{X}_{k|k} &= \hat{X}_{k|k-1} + K_k v_k, \\ \hat{P}_{k|k} &= \hat{P}_{k|k-1} - K_k M_k \hat{P}_{k|k-1}, \end{aligned}$$

$$
\begin{aligned}
v_k &= Y_k - \hat{Y}(\hat{X}_{k|k-1}, t_k), \\
F_k &= M_k \hat{P}_{k|k-1} M_k^T + U_k, \\
K_k &= \hat{P}_{k|k-1} M_k^T F_k^{-1},
\end{aligned} \tag{3.4.10}
$$

where the Hessian matrix M_k is calculated by

$$
M_k = \frac{\partial \hat{Y}(X,t)}{\partial X}\bigg|_{(X,t)=(\hat{X}_k,t_k)} \tag{3.4.11}
$$

Instead of using log-likelihood, which seeks to estimate parameters from statistical perspective, we directly minimize the the prediction error

$$
L(t) = \frac{1}{n} v_k^T v_k.
$$

In addition to the prediction error, we add the arbitrage penalty (3.3.22) in to the regularization so that our loss function is given by

$$
L(t) = \frac{1}{n} v_k^T v_k + \lambda \times \Lambda^{(p)}, \tag{3.4.12}
$$

with an arbitrage regularization term λ.

3.4.3 Price prediction by the particle filter

Compared to the extended Kalman filter, the particle filter has the advantage of not requiring any functional approximation and there is no need to calculate the Hessian matrix. However, these advantages are offset by increased computational requirements: the particle filter is a broad class of recursive Monte Carlo algorithms thus large samples are inevitable. Similar work can be found by Christoffersen, Dorion, Jacobs, and Karoui [22] predicting yield curves using the extended Kalman filter and the particle filter as well with LIBOR, Swap rates and Caps prices.

First, we introduce the general sequential Monte Carlo method then we add importance sampling from the measurement equations of the extended Kalman filter into the particle filter. Suppose the marginal densities of observations Y_t given the states X_t can be measured by some distribution $\mathcal{M}$

$$
Y_t \,|X_t \sim \mathcal{M}(Y_t \,\big|\hat{Y}\,(X_t,t)\,). \tag{3.4.13}
$$

In applications, we assume that the prediction error of prediction follows a Multivariate Generalized Gaussian Distribution (MGGD). Following the definition given by Pascal, Bombrun, Tourneret, and Berthoumieu [106], we define the pdf of n-dimensional MGGD for any $x \in \mathbb{R}^n$ as

$$
q(x\,|\bar{x}\,) = |U|^{-\frac{1}{2}} C_{p,n} \exp\left(-\frac{\left[(x-\bar{x})^T U^{-1} (x-\bar{x}) \right]^p}{2m^p} \right), \tag{3.4.14}
$$

where p is the shape parameter and m is the scale parameter, $U \in \mathbb{R}^{n\times n}$ is the variance matrix and $C_{p,n}$ is a normalization coefficient such that the integral of the distribution is 1

$$C_{p,n} = p\left(2^{\frac{1}{p}}\pi m\right)^{-\frac{n}{2}}\Gamma\left(\frac{n}{2}\right)\Big/\Gamma\left(\frac{n}{2p}\right)$$

In particular, if p = 0.5, (3.4.14) gives multivariate Laplace distribution, and p = 1 gives a multivariate Gaussian distribution. In our model, we set the scale parameter m equal to the number of x.

The conditional expected value of X_t from the previous state X_{t-1} given observations $Y_{1:t-1} = y_{1:t-1}$ is denoted as the posterior distribution

$$p_t(X) = \mathbb{I}\left(X_t \in X \,|Y_{1:t-1}\right).$$

The calculation of the expectation is estimated by Monte Carlo sampling

$$\mathbb{E}^{\mathbb{I}}\left[f(X)\right] = \frac{f(X_1)+f(X_2)+\cdots+f(X_N)}{N},$$

In practice, it is hard to sample from the posterior distribution $p(X_k\,|Y_{1:k})$. Assume we can sample from some prior distribution $q(X_k\,|Y_{1:k})$ called the importance distribution, then we can estimate the conditional expectation through the following steps

$$\begin{aligned}
\mathbb{E}^{\mathbb{I}}\left[f(X_t)\,|Y_{1:t}\right] &= \int f(X_t)p(X_t|Y_{1:t})dX_t \\
&= \int f(X_t)\frac{p(X_t|Y_{1:t})}{q(X_t|Y_{1:t})}q(X_t|Y_{1:t})dX_t \\
&= \frac{1}{p(Y_{1:t})}\int f(X_t)\frac{p(Y_{1:t}|X_t)p(X_t)}{q(X_t|Y_{1:t})}q(X_t|Y_{1:t})dX_t \\
&= \frac{\int f(X_t)w_t(X_t)q(X_t|Y_{1:t})dX_t}{\int w_t(X_t)q(X_t|Y_{1:t})dX_t} \\
&= \frac{\mathbb{E}^q\left[w_t(X_t)f(X_t)|Y_{1:t}\right]}{\mathbb{E}^q\left[w_t(X_t)|Y_{1:t}\right]},
\end{aligned} \tag{3.4.15}$$

where

$$w_t(X_t) = \frac{p(Y_{1:t}|X_t)p(X_t)}{q(X_t|Y_{1:t})}.$$

The calculation of (3.4.15) can be estimated by sampling $\{X_t^{(i)}\} \sim q(X_t|Y_{1:t})$ for $i = 1,\cdots,N$. That is,

$$\begin{aligned}
\mathbb{E}^{\mathbb{Q}}\left[f(X_t)\,|Y_{1:t}\right] &= \frac{\mathbb{E}^q\left[w_t(X_t)f(X_t)\,|Y_{1:t}\right]}{\mathbb{E}^q\left[w_t(X_t)\,|Y_{1:t}\right]} \\
&= \frac{\frac{1}{N}\sum_{i=1}^N w_t(X_t^{(i)})f(X_t^{(i)})}{\frac{1}{N}\sum_{i=1}^N w_t(X_t^{(i)})}
\end{aligned}$$

$$= \sum_{i=1}^{N} \hat{w}_t(X_t^{(i)}) f(X_t^{(i)}),$$

where $\hat{w}_t$ are normalized weights

$$\hat{w}_t(X_t^{(i)}) = \frac{w_t(X_t^{(i)})}{\sum_{i=1}^{N} w_t(X_t^{(i)})}.$$

Suppose the prior distribution $q(\cdot)$ satisfies the Markov property, then we can rewrite w_k as a recursive identity

$$w_t^{(i)} = w_{t-1}^{(i)} \frac{p\left(Y_t \middle| X_t^{(i)}\right) p\left(X_t^{(i)} \middle| X_{t-1}^{(i)}\right)}{q\left(X_t^{(i)} \middle| X_{t-1}^{(i)}, Y_{1:t}\right)}. \tag{3.4.16}$$

If we choose the prior distribution $q\left(X_t \middle| X_{t-1}, Y_{1:t}\right) = p\left(X_t \middle| X_{t-1}\right)$ which is also widely used, we obtain the simple recursion

$$w_t^{(i)} = w_{t-1}^{(i)} p\left(Y_t \middle| X_t^{(i)}\right).$$

This choice of prior distribution does not incorporate the most recent observations Y_t, so it is inefficient. Javaheri et al. [76] propose using the extended Kalman filter to obtain the posterior information from the observations. The following distribution with prior mean $\hat{X}_{k-1|k-1}$ and posterior covariance P_{k-1} from the extended Kalman filter

$$q\left(X_k \middle| X_{k-1}, Y_{1:k}\right) = \mathcal{N}\left(X_k \middle| g(\hat{X}_{k-1|k-1}), P_{k-1}\right)$$

gives one way to implement the importance sampling in particle filter.

Standard importance sampling suffers the variance explosion problem since some particles may have increasingly large weights and others have very small weights. The variance of weights increases exponentially with respect the number of particles. This degeneration problem decreases the effectiveness of particles and increases variance of the weights. To address this problem, a resampling step is introduced into the recursive procedure. The resampling is equivalent to resample each particle in such a way that their offspring $o_t = \left(o_t^{[1]}, \cdots, o_t^{[N]}\right)$ follows a multinomial distribution with parameter vector $(N, \hat{w}_t)$ and each particle is distributed with equally probability of $1/N$. The resampled distribution is an unbiased estimation of the original particle distribution. As a consequence, resampling carries the computational efforts to retain the particles in dense probability mass by precluding the particles of low weights with high probability. The most widely-used resampling method is systematic resampling introduced by Kitagawa [84] which we will introduce in the algorithm.

On the other hand, resampling also has disadvantages. There could be the situation that a particle having a low weight could have a high weight at the next time and if this happens then resampling could be wasteful. Another immediate effect of resampling is some extra noise being introduced. One way we need resampling to control variance of weights and one way we do

not want introduce additional variance. However, a controlled variance of weights benefits more from the additional variance noise after resampling. In practice, it is more sensible to resample only when the variance of the normalized weights reaches some threshold. The commonly used threshold (see Liu [90]) is the Effective Sample Size (ESS)

$$\text{ESS} = \left(\sum_{i=1}^{N} \left(\hat{w}_t^{(i)} \right)^2 \right)^{-1}.$$

The ESS takes values between 1 and N and resampling is usually done when ESS is below $N/2$. This method is called adaptive resampling. In our application we do not apply the adaptive method but we will examine the efficiency of our model by investigating the ESS after the training.

Sequential importance resampling (SIR) particle filter

At time $k = 0$

- Sample initial $X_0^{(i)}$ from the initial states

  $$X_0^{(i)} = \hat{X}_0 + \hat{P}_0 W^{(i)},$$

  where $P_0 = \hat{P}_0 \hat{P}_0^T$ is the prior covariance matrix and $W^{(i)}$ is standard Gaussian random number.

- Update weights by initial observations and resampling to obtain equally distributed particles $\{X_0^{(i)}, w_0^{(i)} = 1/N\}$

From time $k \geq 1$

- Importance sampling:

  From the measurement and updating equations given by (3.4.9) and (3.4.10) in EKF, we obtain the posterior particles along with the posterior covariance

  $$\begin{aligned} \hat{X}_{k-1|k-1}^{(i)} &= X_{k-1}^{(i)} + K_{k-1} v_{k-1}^{(i)}, \\ P_{k-1|k-1}^{(i)} &= P_{k-1}^{(i)} - K_{k-1} M_{k-1} P_{k-1}^{(i)}, \end{aligned}$$

  then we sample particles from the posterior space

  $$X_k^{(i)} = A_{k-1} \hat{X}_{k-1|k-1}^{(i)} + D_{k-1} + \sqrt{P_k^{(i)}} W^{(i)},$$

where

$$
\begin{aligned}
P_k^{(i)} &= A_{k-1}^T P_{k-1|k-1}^{(i)} A_{k-1} + Q_{k-1}, \\
v_{k-1}^i &= Y_{k-1} - \hat{Y}(t_{k-1},\, X_{k-1}^{(i)}), \\
F_{k-1} &= M_{k-1} P_{k|k-1}^{(i)} M_{k-1}^T + U_{k-1}, \\
K_{k-1} &= P_{k-1}^{(i)} M_{k-1}^T F_{k-1}^{-1}, \\
M_{k-1} &= \left.\frac{\partial \hat{Y}}{\partial X}\right|_{X=X_{k-1}^{(i)}}.
\end{aligned}
$$

- Update weights:

$$
w_k^{(i)} = w_{k-1}^{(i)} \frac{p\left(Y_k \middle| X_k^{(i)}\right) p\left(X_k^{(i)} \middle| X_{k-1}^{(i)}\right)}{q\left(X_k^{(i)} \middle| x_{k-1}^{(i)}, Y_{1:k}\right)},
$$

where

$$
\begin{aligned}
p\left(Y_k \middle| X_k^{(i)}\right) &= \mathcal{M}\left(Y_k \middle| \hat{Y}(X_k^{(i)}), U_k\right), \\
p\left(X_k^{(i)} \middle| X_{k-1}^{(i)}\right) &= \mathcal{N}\left(X_k^{(i)} \middle| g(X_{k-1}^{(i)}), Q_{k-1}\right), \\
q\left(X_k^{(i)} \middle| X_{k-1}^{(i)}, Y_{1:k}\right) &= \mathcal{N}\left(X_k^{(i)} \middle| g(X_{k-1|k-1}^{(i)}), P_k^{(i)}\right).
\end{aligned}
$$

Calculate normalized weights

$$
\bar{w}_k^{(i)} = \frac{w_k^{(i)}}{\sum_{i=1}^N w_k^{(i)}}.
$$

- Systematic Resampling from $\left\{\bar{w}_k^{(i)}, X_k^{(i)}, P_k^{(i)}\right\}$ to obtain equally weighted particle sample $\left\{\frac{1}{N}, X_k^{(i)}, P_k^{(i)}\right\}$
  - Set $s_k^{(i)} = \frac{i-1+\tilde{s}_k}{N}$ with $\tilde{s}_k \sim \mathcal{U}[0,1]$ for $i = 1, \cdots, N$.
  - Then set the number of particles equal to the offspring

$$
o_k^{(i)} = \left| \left\{ s_k^{(j)} : \sum_{n=1}^{i-1} \bar{w}_k^{(n)} \le s_k^{(j)} \le \sum_{n=1}^{i} \bar{w}_k^{(n)} \right\} \right|,
$$

  which is the number of $s_k^{(j)}$ that locates in $\left[\sum_{n=1}^{i-1} \bar{w}_k^{(n)}, \sum_{n=1}^{i} \bar{w}_k^{(n)}\right]$.

3.5 Dynamic parameterization by Recurrent Neural Networks

The minimal neuron in neural networks is called dense which consists of a linear transform and an activation. In what follows, we denote a dense layer by D

$$y = D(x) := a(\mathfrak{W}x + \mathfrak{b}), \tag{3.5.1}$$

where x are the inputs, $\mathfrak{W}$ are the weights, $\mathfrak{b}$ is the bias, and the operation between the weights $\mathfrak{W}$ and the input x is usually a matrix product or a tensor product. The function a is called a activation function. The main reason why we use activation functions in neural networks is because we want some neurons to be activated or not activated. The activation functions can be basically divided into 2 types: linear function and non-linear functions. The non-linear activation functions are the most used activation functions.

In our model, we feed the data through sequential modules that repeatedly connect as a RNN and each module has four layers. Each layer is composed by several neurons and serves different purpose. The four layers are: the input layer, the residual layer, the state layer and the filter layer. The filter layer is also an output cell where we implement the filters, update the forward rate model, and output the predicted values. The filter layer uses the state variables $(\kappa_t, \theta_t, \sigma_t)$ which are generated from the state layer using weights, bias and the outputs from the input layer. In this section, we introduce the architecture of the input layer, the residual layer, and the state layer.

3.5.1 Input layer

Since the data are different for the linear model (yield model) and the non-linear model (price model), we will have different input layers. The linear model is trained with the yield data in a 3-dimensional tensor with a total size of $S \times T \times F$ and the input data for each time step is a $1 \times F$ vector. The input data for the linear model is in a 3-dimensional tensor with a size of $S \times T \times F$ where S is the total number of sample, T is the sequential length, and F is the feature size. In the yield model, we use the extracted yields as inputs and predict the yields as the model output. We choose the yields at the $F = 23$ fixed tenors 3, 6, 9, 12, 15, 18, 21, 24, 30, 36, 42, 48, 54, 60, 72, 84, 96, 108, 120, 180, 240, 300 and 360 months to match the proportion of traded bonds in each terms.

The input layer of the linear model consists of a stack of two connected cells of long short-term memory (LSTM). The LSTM is proposed by Hochreiter and Schmidhuber [68] in solving the vanishing gradient problem and is popular in supervised learning under RNN structure, especially training on a set of sequential data. In LSTM, except the data inputs x it requires two variables as the state inputs (c,h) including the output c and hidden state h from precious LSTM and generate two outputs with updated value of c and h correspondingly. We denote the LSTM cell by L in short

$$(c_t, h_t) = L(x, (c_{t-1}, h_{t-1})). \tag{3.5.2}$$

The compact forms of equations of the LSTM are composed by the following four dense layers

each serving different purpose

$$
\begin{aligned}
f_t =& a_g\left(\mathcal{W}_f x + \mathcal{W}'_f h_{t-1} + \mathcal{b}_f\right),\\
i_t =& a_g\left(\mathcal{W}_i x + \mathcal{W}'_i h_{t-1} + \mathcal{b}_i\right),\\
o_t =& a_g\left(\mathcal{W}_o x + \mathcal{W}'_o h_{t-1} + \mathcal{b}_o\right),\\
\tilde{c}_t =& a_c\left(\mathcal{W}_c x + \mathcal{W}'_c h_{t-1} + \mathcal{b}_c\right),\\
c_t =& f_t \circ c_{t-1} + i_t \circ \tilde{c}_t,\\
h_t =& o_t \circ a_h\left(c_t\right),
\end{aligned}
\tag{3.5.3}
$$

where the operator $\circ$ denotes the Hadamard product (element-wise product). In each LSTM cell, we have four gates (or layers): f_t is the 'forget' gate that serves to drop some weights, i_t is the input layer that receive the input, h_t is the hidden layer that passes the hidden states, and c_t is the output layer that combing the precious output c_{t-1} and current output $\tilde{c}_t$. initial values are with initials $c_0 = \bar{0}$ and $h_0 = \bar{0}$. The outputs of the LSTM include the hidden states h_t and the outputs c_t. For the input $X_t \in \mathbb{R}^N$ with feature size N and the predefined hidden units H, the model weights and bias are predefined by

$$
\mathcal{W}, \mathcal{W}' \in \mathbb{R}^{H\times N}, \text{ and } \mathcal{b} \in \mathbb{R}^H.
$$

The activation functions are suggested by

$$
\begin{aligned}
a_g(x) =& \frac{1}{1+e^{-x}},\\
a_c(x) =& \tanh(x),\\
a_h(x) =& \tanh(x).
\end{aligned}
$$

The sigmoid function a_g exists between 0 to 1 and is mainly used between layers in the neuron or especially to predict the probability as an output. The tanh function is like the sigmoid but ranges from -1 to 1 and is mainly used in the output layers or to classify between two classes. The input layer of the linear model with two connected LSTM L_1 and L_2 at time step t with input Y_t can be written as

$$
\begin{aligned}
\left(c_t^{I_1}, h_t^{I_1}\right) =& L_1\left(Y_t, \left(c_{t-1}^{I_1}, h_{t-1}^{I_1}\right)\right),\\
\left(c_t^{I_2}, h_t^{I_2}\right) =& L_2\left(c_t^{I_1}, \left(c_{t-1}^{I_2}, h_{t-1}^{I_2}\right)\right),\\
c_t^I =& c_t^{I_2},
\end{aligned}
\tag{3.5.4}
$$

where c_t^I is the output from input layer.

The non-linear model is trained with the price data in a 4-dimensional tensor with a size of $S \times T \times N \times F$ where N is the number of bonds and $F = 4$ is the feature size. The input data at each time step is then a $N \times F$ matrix that can not be fed into a standard LSTM. Hence, we apply a convolution LSTM (CLSTM) to decrease the input dimension from $N \times F$ to $1 \times H$ for some integer hyper-parameter H. Then we could connect it to the standard LSTM. The CLSTM is usually applied for image processing but we can consider our input as an image of single channel

$N \times F \times 1$ and use the convolution operation to obtain a vector output of any size H. The compact forms of equations of the CLSTM are similar to the standard LSTM (3.5.3) but using convolution instead of matrix product

$$\begin{aligned} f_t =& a_g\left(\mathcal{W}_f * x + \mathcal{W}'_f * h_{t-1} + b_f\right), \\ i_t =& a_g\left(\mathcal{W}_i * x + \mathcal{W}'_i * h_{t-1} + b_i\right), \\ o_t =& a_g\left(\mathcal{W}_o * x + \mathcal{W}'_o * h_{t-1} + b_o\right), \\ \tilde{c}_t =& a_c\left(\mathcal{W}_c * x + \mathcal{W}'_c * h_{t-1} + b_c\right), \\ c_t =& f_t \circ c_{t-1} + i_t \circ \tilde{c}_t, \\ h_t =& o_t \circ a_h\left(c_t\right), \end{aligned} \tag{3.5.5}$$

where the operator $*$ denotes the convolution operation. The kernel of the convolutional LSTM is defined by

$$\mathcal{W}, \mathcal{W}' \in \mathbb{R}^{K_W \times K_H \times K_D},$$

with K_W as width, K_H as height and K_D as depth. The convolution of $\mathcal{W} \in \mathbb{R}^{K_W \times K_H \times K_D}$ and $x \in \mathbb{R}^{N \times F \times 1}$ is a tensor satisfying the following dimension calculation

$$\dim\left(\mathcal{W} * x\right) = \left(\left\lfloor \frac{N + 2p - K_W}{s_W} + 1 \right\rfloor, \left\lfloor \frac{F + 2p - K_H}{s_H} + 1 \right\rfloor, K_D\right),$$

where p is the size of padding usually taking value of 0, (s_W, s_H) is the size of stride, and the operator $\lfloor \cdot \rfloor$ takes the integer part. To reduce the dimension of the input and obtain H-dimensional vector output, we set stride size $(s_W, s_H) = (1,1)$ and kernel size $(K_W, K_H, K_D) = \left(\lfloor \frac{N}{H} \rfloor, F, 1\right)$ for some hyper-parameters $H < N$, and eventually obtain an output with a size of $(H,1,1)$ which can be compressed to $1 \times H$. Then we could connect it to a standard LSTM. The input layer for the non-linear model consisting of a CLSTM L_c and a standard LSTM L is given by

$$\begin{aligned} Y_t \in \mathbb{R}^{N \times F} :\to Y'_t \in \mathbb{R}^{N \times F \times 1}, \\ \left(c_t^{I_c}, h_t^{I_c}\right) =& L_c\left(Y'_t, \left(c_{t-1}^{I_c}, h_{t-1}^{I_c}\right)\right), \\ c_t^{I_c} \in \mathbb{R}^{H \times 1 \times 1} :\to c'_t \in \mathbb{R}^{1 \times H}, \\ \left(c_t^I, h_t^I\right) =& L\left(c'_t, \left(c_{t-1}^I, h_{t-1}^I\right)\right). \end{aligned} \tag{3.5.6}$$

After some transformation, we obtain the final output from the input layer as a vector $c_t^I \in \mathbb{R}^{1 \times H}$ and pass it to the state layer.

3.5.2 State layer and Residual layer

Suppose we have an output $c_t^I \in \mathbb{R}^{1 \times H}$ from the input layer and consider it as the input for the state layer. We simply connect it to three dense layers κ, θ and σ in the state layer

$$\kappa(c_t^I) : [0,T] \times \mathbb{R}^{1 \times H} \to \mathbb{R}^{d \times d},$$

$$\theta(c_t^I) : [0,T] \times \mathbb{R}^{1\times H} \to \mathbb{R}^d,$$
$$\sigma(c_t^I) : [0,T] \times \mathbb{R}^{1\times H} \to \mathbb{R}^{d\times d}.$$

The equations of the state layer are given by

$$\begin{aligned}\kappa =& a_\kappa\left(\mathcal{W}_\kappa \cdot c_t^I + \mathfrak{b}_\kappa\right),\\ \theta =& a_\theta\left(\mathcal{W}_\theta \cdot c_t^I + \mathfrak{b}_\theta\right),\\ \sigma =& a_\sigma\left(\mathcal{W}_\sigma \cdot c_t^I + \mathfrak{b}_\sigma\right),\end{aligned} \tag{3.5.7}$$

where $\cdot$ is the tensor product, the kernels and bias are

$$\mathcal{W}_\kappa \in \mathbb{R}^{H\times d\times d}, \mathcal{W}_\theta \in \mathbb{R}^{H\times d}, \mathcal{W}_\sigma \in \mathbb{R}^{H\times d\times d},$$

and the bias are

$$\mathfrak{b}_\kappa \in \mathbb{R}^{d\times d}, \mathfrak{b}_\theta \in \mathbb{R}^d, \mathfrak{b}_\sigma \in \mathbb{R}^{d\times d}.$$

The activation functions in the state layer are chosen as

$$\begin{aligned}a_\kappa(x) =& x,\\ a_\theta(x) =& \tanh(x),\\ a_\sigma(x) =& \tanh(x).\end{aligned}$$

Each time we obtain predicted values $\hat{Y}_t$ and observed values Y_t, we could analyze the residual values and estimated the covariance matrix. In our model, we do these in the residual layer. We firstly batch normalize (BN) (see Ioffe and Szegedy [75]) the residual values $e_t = |Y_t - \hat{Y}_t|$ and then feed the normalized residual $\bar{e}_t = \mathrm{BN}(e_t)$ into a LSTM L_R and obtain a noise matrix u_t by connecting a dense layer D_R to it. The equations in the residual layer are given by

$$\begin{aligned}e_t =& |Y_t - \hat{Y}_t|,\\ \bar{e}_t =& \mathrm{BN}(e_t),\\ (c_t^R, h_t^R) =& L_R\left(\bar{e}_t, \left(c_{t-1}^R, h_{t-1}^R\right)\right),\\ u_t =& D_R\left(c_t^R\right).\end{aligned} \tag{3.5.8}$$

Once the parameters $(\kappa_t, \theta_t, \sigma_t, u_t)$, the state variables X_t, the predicted values $\hat{Y}_t$ and the observed values Y_t are obtained, we implement the filters in the filter layer and output state variables X_{t+1} and predicted values $\hat{Y}_{t+1}$. We obtain the final prediction $\hat{Y}_T$ after feeding the whole sequential data through the fully connected RNN networks and calculate the values of the arbitrage-free penalties $\Lambda^{(p)}$ using the sequential states $(X_t, \kappa_t, \theta_t, \sigma_t)$. The model weights including all the weights $\mathfrak{W}$ and bias $\mathfrak{b}$ in each layers will be trained to minimize the a measurement of the prediction error $|\hat{Y}_T - Y_T|$ and the penalty $\Lambda^{(p)}$ at the same time.

The basic module of RNN is formed from a fully linked four cells and the RNN is a stack of basic modules whose. Figure 3.3 shows the structure of basic module and the RNN.

Figure 3.3: Recurrent Neural Networks

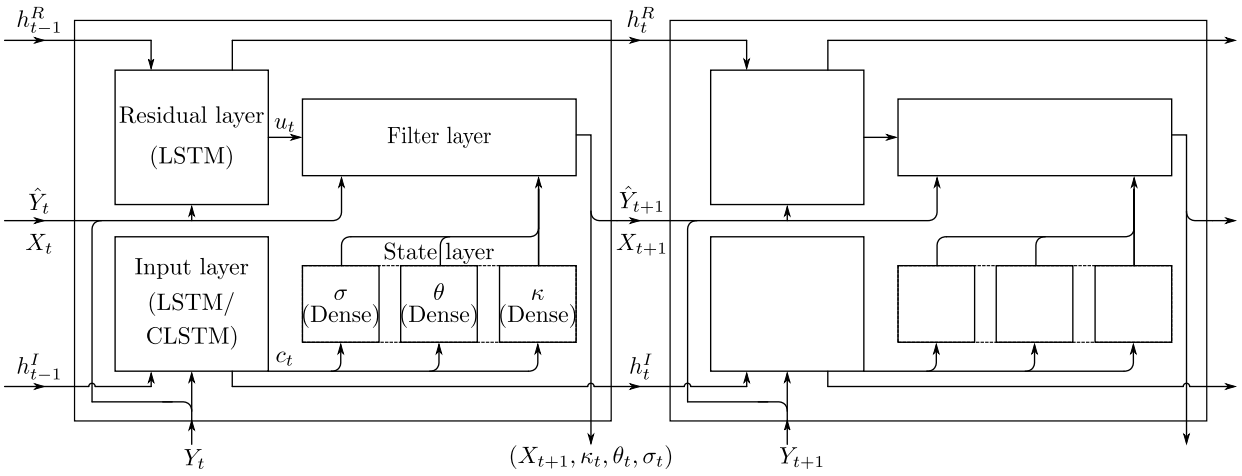

3.5.3 Loss function and optimizer

The loss function is summation of the MSE of the prediction errors and the arbitrage-free regularization

$$L(\vartheta) = \frac{1}{n}\sum_{i=1}^{n}\left|Y_i - \hat{Y}_i\right|^2 + \lambda\Lambda^{(p)}, \tag{3.5.9}$$

where ϑ denotes the model weights. The learning objective is to search the optimal parameters $\hat{\vartheta}$ on the manifold of ϑ that minimizes the loss function

$$\hat{\vartheta} = \arg\min_{\vartheta} L(\vartheta),$$

by the following gradient descend learning step with a learning rate $\alpha_k \in (0,1)$

$$\vartheta_k = \vartheta_{k-1} - \alpha_k \nabla_{\vartheta} L(\vartheta_{k-1}), \tag{3.5.10}$$

and the learning rate α_k is a step function of the loss value.

The training process is an optimization procedure in which an optimizer implements gradient computation by back-propagation through time and gradient descent in order to change model weights in proportion to the derivative of the error with respect to corresponding weights. The optimizer is an algorithm that defines how the gradient is decreased. The optimizer plays a key role in optimization process and a good optimizer brings fast training and good results. The most popular optimizers are Stochastic Gradient Descent (SGD) with momentum, RMSprop (root mean square), Adam (adaptive momentum estimation) and so on.

The Adam algorithms is introduced by Kingma and Ba [83] and is widely used in many kinds of training tasks. We briefly introduce the updating rules of the Adam optimizer which depends on the first-order gradient and the estimations of lower-order moments. At each time step t, the Adam optimizer updates the biased first moment m_t and biased second moment v_t according to the

gradient of the loss function $g_t = \nabla_\vartheta L(\vartheta_t)$, with initial $m_0 = 0$ and $v_0 = 0$

$$m_t = \beta_1 m_{t-1} + (1-\beta_1) g_t,$$
$$v_t = \beta_2 v_{t-1} + (1-\beta_2) g_t^2,$$

then we apply bias-correction since the value of m_t and v_t will decline to their initial zeros if no adjustment is applied

$$\hat{m}_t = \frac{m_t}{1-\beta_1^t},$$
$$\hat{v}_t = \frac{v_t}{1-\beta_2^t},$$

where β_1^t and β_2^t denote β_1 and β_2 to the power t. The learning step is then given by

$$\vartheta_t = \vartheta_{t-1} - \alpha_t \frac{\hat{m}_t}{\sqrt{\hat{v}_t} + \varepsilon}, \tag{3.5.11}$$

where the parameters settings are $\beta_1 = 0.9$, $\beta_2 = 0.999$ and $\varepsilon = 10^{-8}$. We reduce the learning rate α_t by a factor of 10^{-1} once the value of loss function stagnates

$$\alpha_t = \left(1 - 0.91_{\left|\frac{L(\vartheta_t)-L(\vartheta_{t-1})}{L(\vartheta_{t-1})}\right|<0.001}\right) * \alpha_{t-1},$$

with

$$1_{\left|\frac{L(\vartheta_t)-L(\vartheta_{t-1})}{L(\vartheta_{t-1})}\right|<0.001} = \begin{cases} 1, & \text{if } \left|\frac{L(\vartheta_t)-L(\vartheta_{t-1})}{L(\vartheta_{t-1})}\right| < 0.001, \\ 0, & \text{otherwise.} \end{cases}$$

The adaptive optimizer means the learning rate α_k will be automatically adjusted by the optimizer according to the current gradient and the momentum. The advantage is obviously: firstly it reduces the risk of over training, secondly, it reduces the time to reach optimal solution, thirdly, we do not need to manually adjust the learning rate too frequently.

3.6 Applications

In this section, we apply the arbitrage-free prediction models on daily U.S. Treasury coupon bonds with minimum 60 daily bonds and 12 corporate bond issuers with around 10 to 30 daily bonds from 2017/01/03 to 2019/12/30. Our data contains four attributes: bond price, tenor, coupon frequency and coupon rates for each observation. This is a small feature size compared to Ganguli and Dunnmon [61] where they use 61 features including extensive trading information. We keep 80% of the data as training set (in-sample data) and the remaining 20% as test set (out-of-sample data). We feed the data in monthly sequence each contains $T = 20$ daily observations and generate h-day-ahead predictions. The results are presented as the mean absolute prediction error (MAPE) and root mean square prediction error (RMSPE). In addition to the forecasting error, we present

the forecasting accuracy as the hit rate measured from the absolute forecasting error and bid-ask spreads which we consider three spread level: 0.1, 0.25 and 0.5 in dollars

$$\text{Hit rate (spread)} = \frac{1}{NT}\sum_{i}^{T}\sum_{j}^{N}\mathbf{1}_{\left\{\left|Y(t_i,\tau_j)-\hat{Y}(t_i,\tau_j)\right|\leq\frac{1}{2}\text{spread}\right\}}. \tag{3.6.1}$$

Generally in finance, if the price predictions are within bid-ask spreads we would consider them as good predictions. To compare the hit rate, we include a benchmark where we apply the observed yield curve to forecast the price of coupon bond in h days.

We consider 1-day-ahead and 5-day-ahead forecasting. The data used for h-day-ahead forecasting is batched from daily observations by every 5 days. By this method, we batch our data into h non-overlapping sequences and we can assume the h sequences as the observations on every Monday, Tuesday, Wednesday, Thursday and Friday. Restricted by the amount of data, we mixed the five distinct sequences as one training set instead of training them separately. To compare the forecasting results, we present the forecasting of yields in different terms of maturity: 3, 12, 36, 60, 120, 240, 360 months and group the forecasting of bond prices by maturities: $0\sim 2$, $2\sim 10$, $10\sim 30$ year.

We train three models: Kalman filter (KF), extended Kalman filter (EK) and particle filter (PF) with two arbitrage schemes $\lambda = 0$ and $\lambda = 1$ (arbitrage-regularized). The results from the Kalman filter contains only yield forecasts, hence we transform the predicted yields into prices of coupon bonds to examine the performance of our model. The extended Kalman filter provides both yields and prices forecasting. The particle filter predicts only prices and we apply an additional step to extract forecasted yields from the forecasted prices. Here, we briefly mention the forecasting results given by Ganguli and Dunnmon [61] where they calculated the forecasting error by a weighted error in prediction per sample (WEPS). However, it is difficult to exactly compare our results to Ganguli and Dunnmon [61] and we will estimate a forecasting benchmark where we use the observed yield curve to forecast h-day-ahead bond prices.

In our training, we run our models on Google Colab around 30$\sim$50 epochs which shows the optimal result without significant bias. The running times for the three filters are very different: the Kalman filter runs with the fastest speed in a couple of minutes, the extended Kalman filter takes at most 15 seconds to finish 1 epoch depending on the amount of daily observations and the training time of the particle filter increases exponentially as the number of particles increase which can take a few hours with 300 particles.

3.6.1 Results of U.S. Treasury

In Figure 3.4 and 3.5, we present the h-day-ahead forecasting of state variables $X = (X_1, X_2, X_3)$ comparing to the observed state variables on a daily basis as short-term, mid-term and long-term levels. In Figure 3.4 showing the 1-day-ahead forecasting, the difference between the forecasted result and observed results are undiscernible. However, in Figure 3.5 showing the 5-day-ahead forecasting, we see that the forecasted result with arbitrage regularization (AR) is closer to the observed results. The forecasted path of state variables of extended Kalman filter shows more oscillation than that of particle filter.

Figure 3.4: Result of U.S. Treasury: path of state variables in 1-day-ahead forecasting

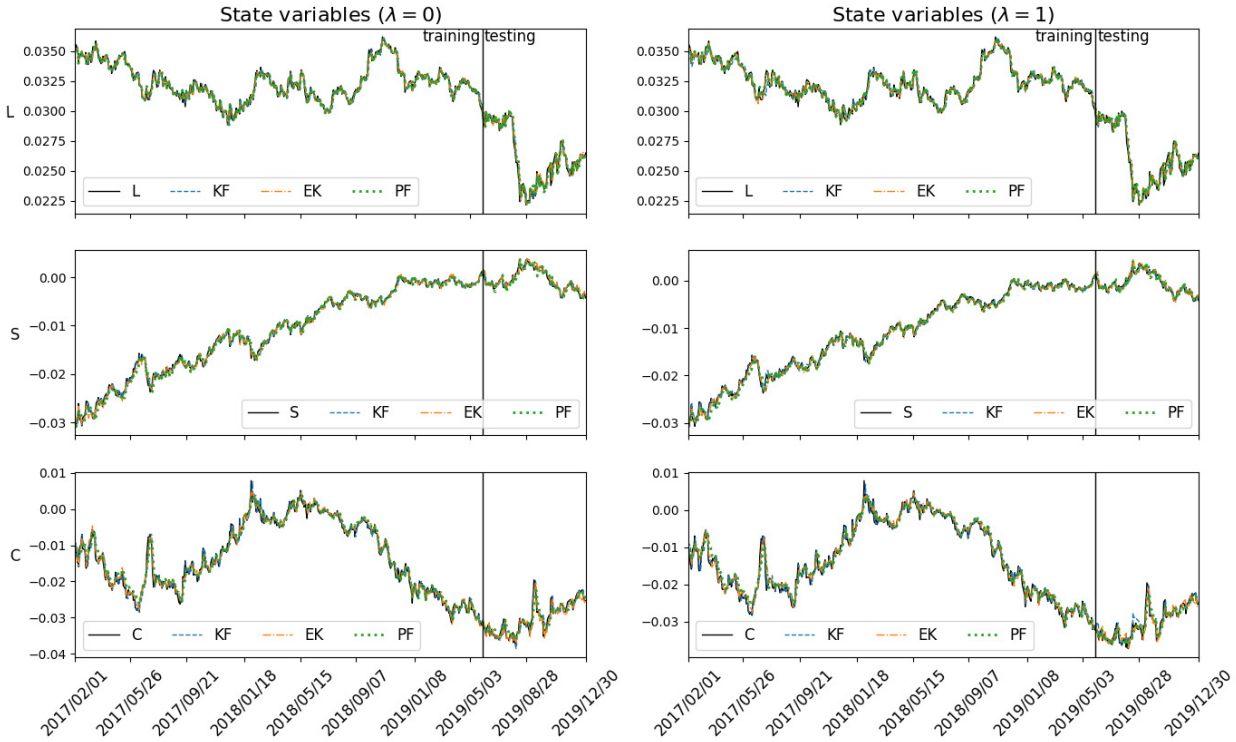

Figure 3.5: Result of U.S. Treasury: path of state variables in 5-day-ahead forecasting

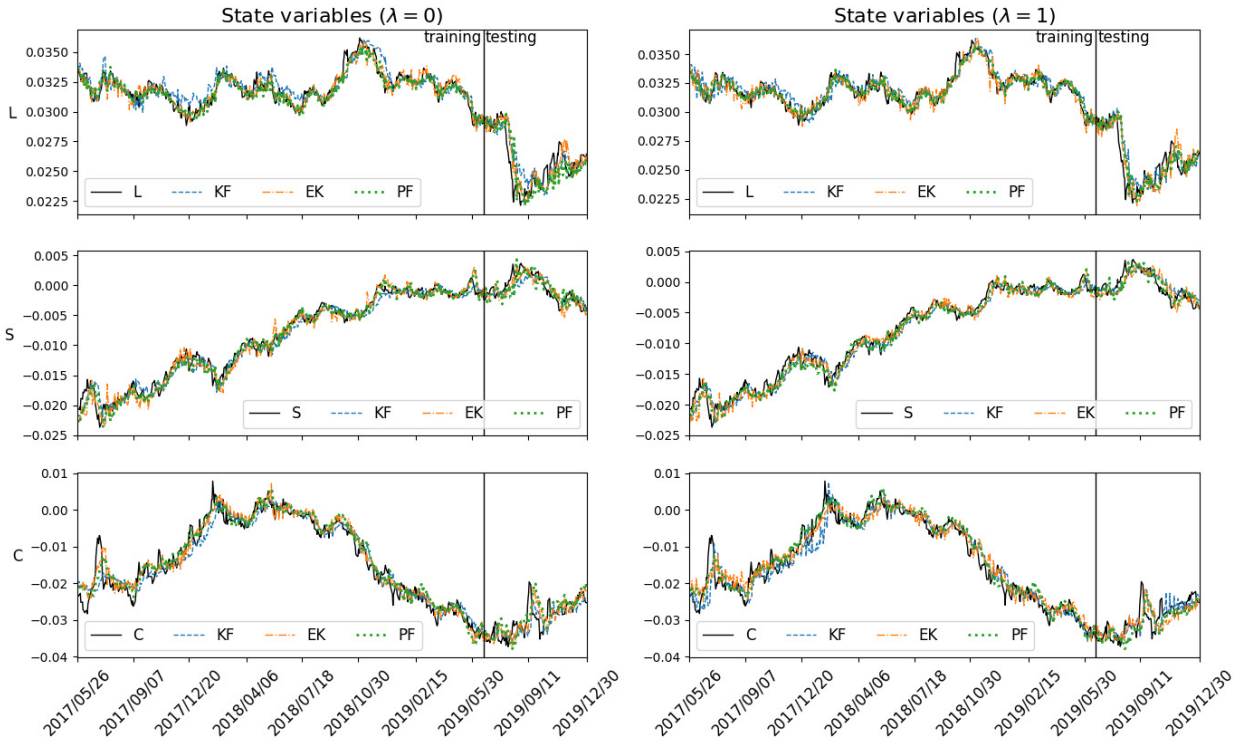

Figure 3.6: Result of U.S. Treasury: yield curves of 1-day-ahead forecasting

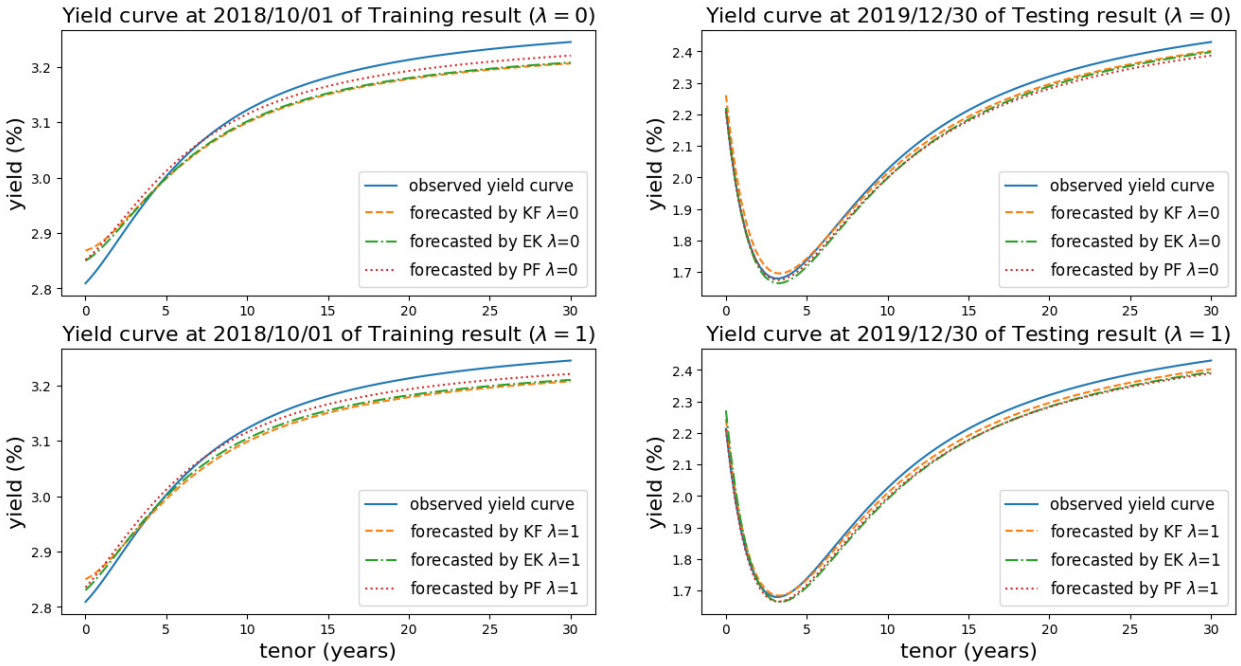

Figure 3.7: Result of U.S. Treasury: yield curves of 5-day-ahead forecasting

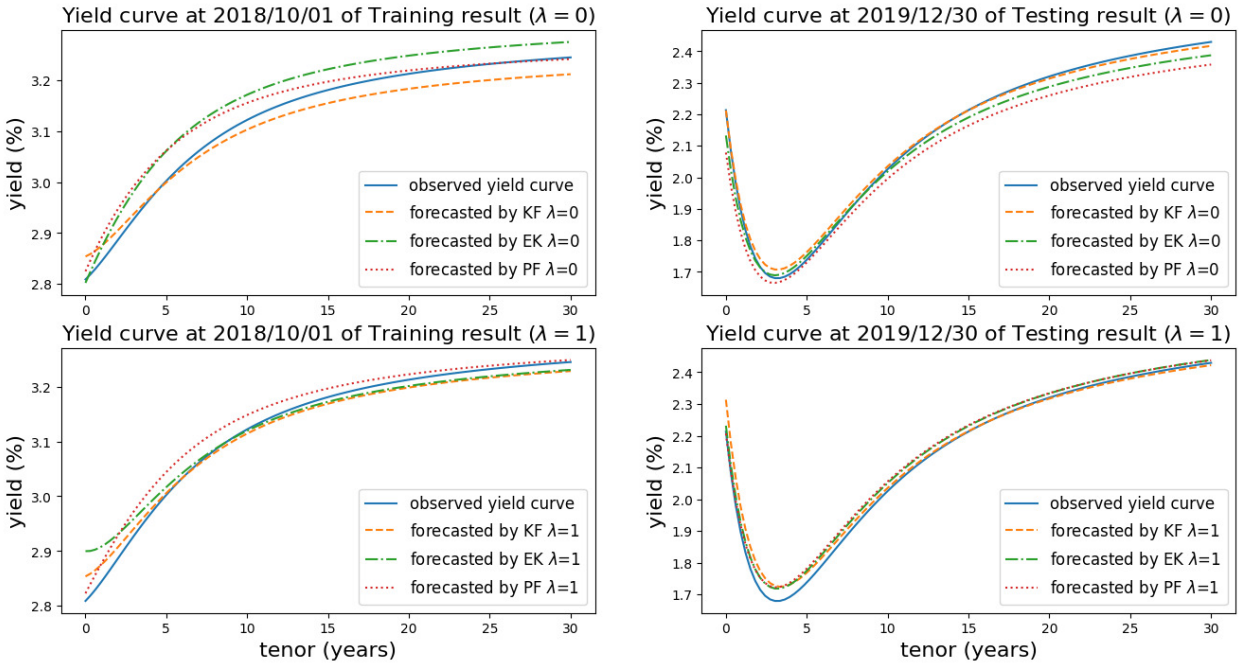

We present two examples of predicted yield curves in Figure 3.6 and Figure 3.7: one is an increasing yield curve from the training set and the other one is an inverted humped yield curve from the testing set. The effect of arbitrage-free regularization is more obvious in 5-day-ahead forecasting as we can see that it heavily controls the convergence of the tail part of the yield curve in most cases and affects the yield points at mid-term level of maturity. In Tables (3.3) and (3.6), we see that the Kalman Filter performs better in out-of-sample data and in different time horizons than other two filters. We interpret the reason as the yield points contains more substantial information to forecast the evolution of the yield curve than using the coupon bonds.

In Tables 3.3, 3.4, 3.5, 3.6, 3.7 and 3.8 we present the mean absolute prediction error (MAPE) and root mean square prediction error (RMSPE) to compare the yield error and price error. In these tables, we can see that the yield forecasting using the dynamic Nelson-Siegel model shows small variation in prediction errors from the short-term maturities to long-term maturities. The Kalman filter performs better in bias-variance trade-off and in long time forecasting than the other two filters which have high variance between the training results and testing results. The best results are given by the Kalman filter where the prediction errors of Treasury yields are around 2.8 bps to 4.9 bps in 1-day-ahead forecasting and 4.5 bps to 8 bps in 5-day-ahead forecasting. Arbitrage regularization improves the forecasting error of yields with short-term (3 months to 1 year) and long-term (10 years to 30 years) maturities but downgrades the performance of predicted yields in mid-term (3 years to 5 years) maturities. Comparing the MPE between our models and the benchmark, we find that our models has almost the same performance in 1-day-ahead forecasting but the Kalman filter without arbitrage-penalty out performs the benchmark in 5-day-ahead forecasting and in all terms of maturities.

Tables 3.3, 3.4 and 3.5 show the results of the 1-day-ahead forecasting error. The three filters have similar performance of 1-day-ahead forecasting forecasting. The Kalman filter performs better in bias-variance trade-off and in long time forecasting than the other two filters which have high variance between the training results and testing results. By looking into the testing MAPE, we find that the arbitrage-penalty slightly improves the fornicating performance of the Kalman filter in short and mid-term maturities, and improves that of the particle filter in mid and long-term maturities. However, the extended Kalman filter seems not affected too much from the arbitrage regularization. In Tables 3.6, 3.7 and 3.8 we present the results of 5-day-ahead forecasting error. We find that the arbitrage-regularization downgrades the forecasting performance in most level of maturities.

Therefore, we conclude that: firstly, the yield forecasting model without arbitrage penalty has better forecasting performance in long time horizons than the benchmark; secondly, the arbitrage-restriction has better forecasting performance in short time horizons and downgrades the forecasting performance as the time horizons increase which is consistent to the finding of Christensen et al. [21]; thirdly, the Kalman filter has better forecasting performance in short and mid maturities and the particle filter has better forecasting performance in long maturities.

Table 3.3: U.S. Treasury: yield prediction error (in bps) of 1-day-ahead forecasting

Tenor	MAPE		RMSPE		STD		MAPE		RMSPE		STD	
	Train	Test	Train	Test	Train	Test	Train	Test	Train	Test	Train	Test
	KF(λ=0)						KF(λ=1)					
3M	3.01	2.90	4.13	3.83	4.12	3.78	3.02	2.86	4.17	3.88	4.17	3.81
1Y	2.14	2.85	2.87	3.78	2.87	3.74	2.13	2.78	2.90	3.61	2.89	3.57
3Y	2.40	3.66	3.15	4.90	3.15	4.89	2.39	3.51	3.16	4.52	3.15	4.51
5Y	2.75	3.95	3.52	5.21	3.52	5.21	2.75	3.73	3.54	4.83	3.53	4.83
10Y	2.64	3.92	3.40	4.99	3.40	4.99	2.73	3.72	3.49	4.74	3.49	4.73
20Y	2.56	3.81	3.35	4.89	3.35	4.88	2.74	3.82	3.58	4.78	3.58	4.77
30Y	2.62	3.83	3.44	4.97	3.44	4.95	2.82	3.89	3.72	4.91	3.72	4.89
	EK(λ=0)						EK(λ=1)					
3M	3.42	3.69	4.47	4.92	4.35	4.72	3.85	3.64	5.06	4.69	5.01	4.68
1Y	2.30	3.40	2.97	4.57	2.87	4.48	2.63	3.27	3.38	4.37	3.34	4.37
3Y	1.61	3.96	2.08	5.24	2.06	5.24	1.80	3.89	2.30	5.19	2.29	5.18
5Y	1.71	4.18	2.20	5.43	2.19	5.43	1.88	4.15	2.38	5.46	2.37	5.45
10Y	1.57	4.03	2.06	5.11	2.06	5.11	1.70	4.10	2.17	5.24	2.16	5.23
20Y	1.54	3.91	2.04	4.99	2.04	4.98	1.64	4.08	2.11	5.16	2.10	5.16
30Y	1.60	3.94	2.12	5.07	2.12	5.05	1.69	4.11	2.20	5.25	2.19	5.24
	PF(λ=0)						PF(λ=1)					
3M	4.72	4.83	6.46	6.24	6.24	6.21	6.74	5.89	9.31	8.10	9.30	8.10
1Y	3.07	4.01	4.12	5.07	3.95	5.05	4.32	4.38	5.84	5.90	5.84	5.89
3Y	1.75	3.97	2.17	5.15	2.12	5.15	2.25	3.67	2.89	4.84	2.89	4.83
5Y	1.84	4.15	2.27	5.34	2.26	5.34	2.52	3.87	3.20	5.00	3.19	4.98
10Y	1.64	4.01	2.10	5.05	2.09	5.05	2.49	3.80	3.18	4.80	3.18	4.79
20Y	1.49	3.93	1.99	5.01	1.97	5.00	2.35	3.77	3.07	4.79	3.06	4.79
30Y	1.57	4.01	2.08	5.13	2.06	5.12	2.40	3.85	3.16	4.92	3.15	4.92

Table 3.4: U.S. Treasury: price prediction error (in dollars) of 1-day-ahead forecasting

Model	Yield MAPE		Yield RMSPE		Yield STD		Price MAPE		Price RMSPE		Price STD	
	Train	Test	Train	Test	Train	Test	Train	Test	Train	Test	Train	Test
KF(λ=0)	2.49	3.55	2.51	3.57	0.28	0.44	0.15	0.17	0.25	0.32	0.25	0.32
EK(λ=0)	1.87	3.86	1.93	3.87	0.48	0.27	0.11	0.18	0.16	0.35	0.16	0.35
PF(λ=0)	2.19	4.06	2.35	4.07	0.85	0.22	0.11	0.18	0.16	0.34	0.16	0.34
KF(λ=1)	2.53	3.42	2.55	3.45	0.32	0.41	0.16	0.17	0.26	0.31	0.26	0.31
EK(λ=1)	2.08	3.85	2.16	3.86	0.57	0.33	0.12	0.18	0.17	0.35	0.17	0.35
PF(λ=1)	3.09	4.03	3.32	4.06	1.20	0.54	0.15	0.17	0.23	0.33	0.23	0.33

Table 3.5: U.S. Treasury: hit rate and percentage error of 1-day-ahead forecasting

Spread	≤ 0.1		≤ 0.25		≤ 0.5		MPE		MPE		MPE	
Tenor(y)	$0 \sim 2$		$2 \sim 10$		$10 \sim 30$		$0 \sim 2$		$2 \sim 10$		$10 \sim 30$	
Model	Train	Test	Train	Test	Train	Test	Train	Test	Train	Test	Train	Test
Benchmark	84%	79%	87%	80%	65%	42%	0.059	0.065	0.131	0.157	0.427	0.683
KF(λ=0)	83%	77%	87%	80%	65%	45%	0.060	0.067	0.133	0.159	0.440	0.672
EK(λ=0)	87%	78%	94%	76%	86%	38%	0.058	0.066	0.103	0.168	0.265	0.725
PF(λ=0)	85%	79%	94%	77%	85%	37%	0.059	0.065	0.105	0.167	0.260	0.722
KF(λ=1)	84%	77%	86%	81%	61%	42%	0.061	0.066	0.133	0.152	0.475	0.681
EK(λ=1)	84%	80%	93%	77%	83%	38%	0.059	0.065	0.107	0.168	0.284	0.741
PF(λ=1)	81%	77%	88%	79%	68%	42%	0.062	0.067	0.128	0.157	0.400	0.693

Table 3.6: Result of U.S. Treasury: yield prediction error (in bps) of 5-day-ahead forecasting

Tenor	MAPE		RMSPE		STD		MAPE		RMSPE		STD	
	Train	Test	Train	Test	Train	Test	Train	Test	Train	Test	Train	Test
	KF(λ=0)						KF(λ=1)					
3M	5.92	4.55	8.36	6.00	8.35	5.76	6.26	9.21	8.87	11.2	8.86	6.68
1Y	4.34	4.70	5.82	6.25	5.81	6.23	4.56	5.70	6.34	7.51	6.32	6.66
3Y	5.16	7.06	6.84	9.29	6.83	9.20	5.25	7.14	7.25	9.35	7.21	9.06
5Y	6.12	7.99	7.85	10.3	7.80	10.1	6.08	7.91	8.10	10.1	8.00	9.85
10Y	6.25	8.01	7.98	10.2	7.80	9.93	6.24	7.80	8.54	9.99	8.25	9.83
20Y	6.22	7.60	8.16	9.80	7.84	9.48	6.84	9.23	9.72	12.0	9.24	10.0
30Y	6.37	7.51	8.41	9.75	8.04	9.43	7.32	10.3	10.4	13.3	9.90	10.3
	EK(λ=0)						EK(λ=1)					
3M	7.59	6.66	10.1	8.19	9.76	8.14	7.68	6.95	10.3	8.66	10.0	8.65
1Y	5.11	6.53	6.78	8.27	6.52	8.27	5.16	6.88	6.90	8.31	6.74	8.23
3Y	3.41	8.45	4.40	11.0	4.38	11.0	3.93	9.81	5.01	12.5	5.01	12.3
5Y	3.49	9.25	4.48	11.9	4.48	11.8	4.14	10.7	5.25	13.8	5.24	13.6
10Y	3.15	8.91	4.06	11.4	4.06	11.3	3.69	10.2	4.67	12.9	4.67	12.8
20Y	3.05	8.36	3.98	11.0	3.98	10.9	3.34	9.40	4.28	11.9	4.28	11.8
30Y	3.21	8.29	4.18	11.0	4.17	10.9	3.38	9.21	4.38	11.7	4.38	11.6
	PF(λ=0)						PF(λ=1)					
3M	6.92	8.33	9.36	10.1	8.81	9.81	8.03	10.4	11.3	13.4	11.3	10.0
1Y	4.87	7.66	6.38	9.89	6.00	9.78	5.61	8.56	7.70	11.3	7.68	9.44
3Y	3.62	9.23	4.67	12.0	4.58	12.0	4.40	9.19	5.73	11.8	5.71	11.6
5Y	3.71	9.57	4.77	12.5	4.74	12.5	4.74	9.66	6.10	12.4	6.08	12.3
10Y	3.27	9.16	4.26	11.8	4.22	11.8	4.43	9.23	5.85	11.9	5.83	11.9
20Y	3.10	9.07	4.09	11.8	3.98	11.8	4.24	8.69	5.72	11.8	5.69	11.8
30Y	3.23	9.30	4.25	12.2	4.12	12.1	4.34	8.64	5.87	12.0	5.83	12.0

Table 3.7: Result of U.S. Treasury: price prediction error (in dollars) of 5-day-ahead forecasting

Model	Yield MAPE		Yield RMSE		Yield STD		Price MAPE		Price RMSPE		Price STD	
	Train	Test	Train	Test	Train	Test	Train	Test	Train	Test	Train	Test
KF(λ=0)	5.51	6.75	5.57	6.89	0.83	1.37	0.29	0.30	0.55	0.62	0.54	0.61
EK(λ=0)	3.96	8.11	4.13	8.17	1.18	1.01	0.18	0.35	0.28	0.74	0.28	0.73
PF(λ=0)	3.98	8.85	4.10	8.88	0.95	0.64	0.18	0.37	0.29	0.78	0.28	0.78
KF(λ=1)	5.71	7.50	5.78	7.62	0.88	1.35	0.30	0.34	0.63	0.79	0.62	0.79
EK(λ=1)	4.32	9.13	4.45	9.24	1.05	1.45	0.20	0.40	0.31	0.79	0.31	0.79
PF(λ=1)	4.93	9.11	5.01	9.13	0.93	0.52	0.23	0.37	0.39	0.79	0.39	0.78

Table 3.8: Result of U.S. Treasury: hit rate and percentage error of 5-day-ahead forecasting

Spread	≤ 0.1		≤ 0.25		≤ 0.5		MPE		MPE		MPE	
Tenor(y)	$0 \sim 2$		$2 \sim 10$		$10 \sim 30$		$0 \sim 2$		$2 \sim 10$		$10 \sim 30$	
Model	Train	Test	Train	Test	Train	Test	Train	Test	Train	Test	Train	Test
Benchmark	71%	68%	66%	55%	36%	25%	0.078	0.085	0.234	0.320	0.897	1.439
KF(λ=0)	72%	69%	63%	58%	30%	19%	0.077	0.081	0.249	0.286	1.071	1.301
EK(λ=0)	73%	66%	81%	50%	57%	22%	0.075	0.087	0.157	0.343	0.515	1.533
PF(λ=0)	73%	65%	80%	49%	58%	15%	0.074	0.091	0.164	0.362	0.516	1.614
KF(λ=1)	70%	67%	65%	57%	30%	22%	0.081	0.086	0.240	0.284	1.161	1.706
EK(λ=1)	72%	65%	76%	44%	52%	19%	0.077	0.090	0.178	0.399	0.557	1.673
PF(λ=1)	66%	64%	72%	49%	47%	25%	0.087	0.096	0.202	0.365	0.717	1.580

In Figure 3.8, we present the convergence of our model with the training and testing results. The loss of the Kalman filter is the MSE of yield prediction and the loss of the particle filter is the MSE of the bond price prediction. Figures 3.9, 3.10, 3.11 and 3.12 show the variation of the state parameters: κ_t, θ_t and σ_t obtained from the yield prediction and bond price prediction models using the Kalman filter and the particle filter, respectively, with and without arbitrage-free regularization. We graph the path of each component of the state parameters. Figure 3.9 shows the state parameters for the yield prediction model using the Kalman filter without regularization and we observe that there appears to be regime-switching in κ_t, θ_t and σ_t. Figure 3.10 shows the result of the yield prediction model using the Kalman filter with arbitrage-free regularization and we observe that the state parameters become stabilized. Figures 3.11 and 3.12 show the result of the bond price prediction model using the particle filter and we observe that the state parameters estimated with and without arbitrage-free regularization are both stable. These results deserve further investigation.

Figure 3.8: Result of U.S. Treasury: Model loss

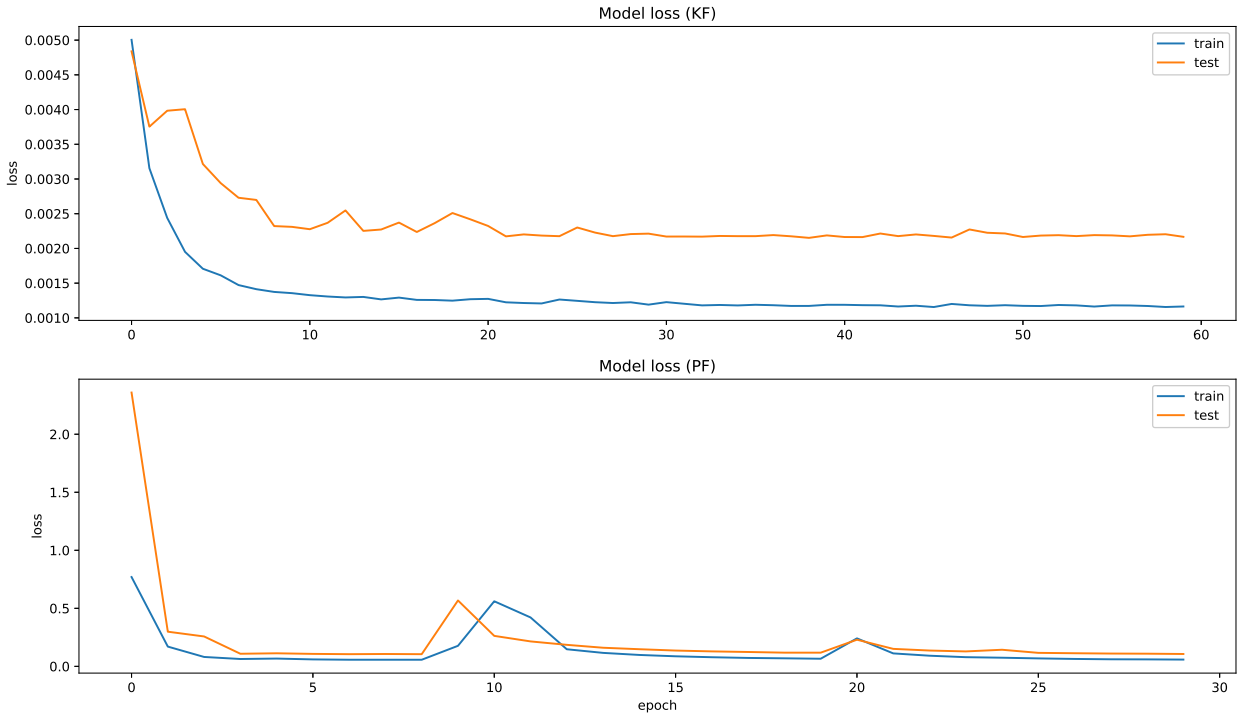

Figure 3.9: Result of U.S. Treasury: State parameters (Kalman filter)

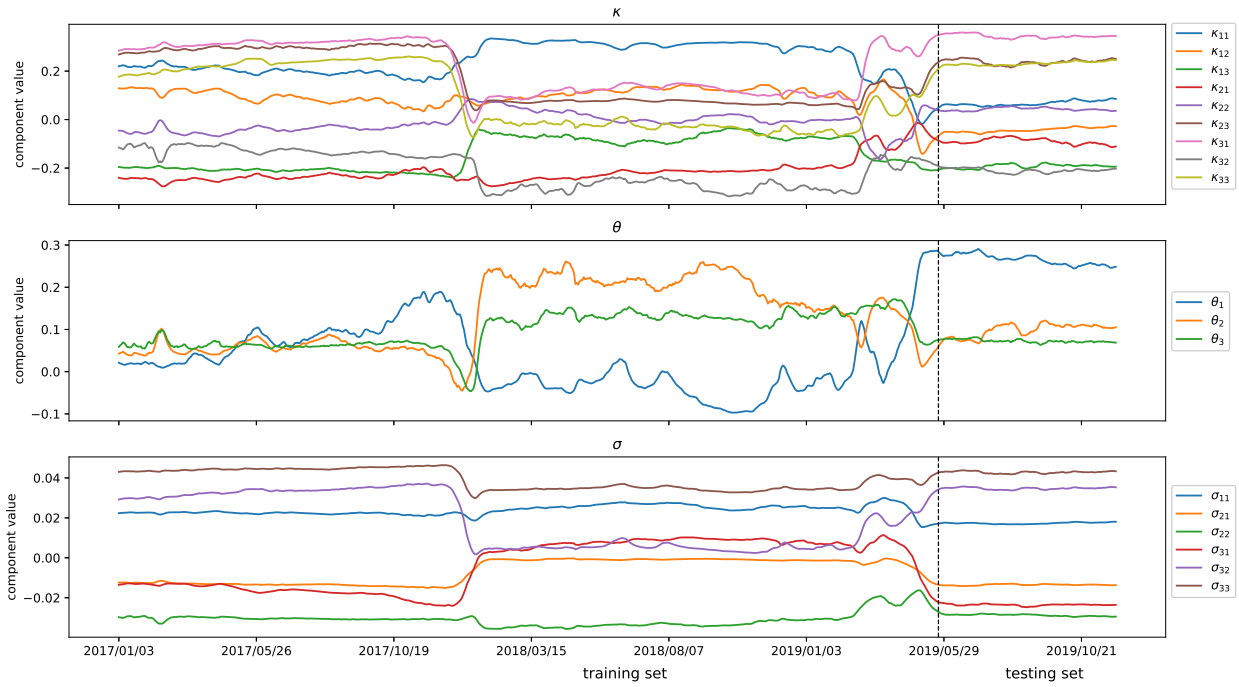

Figure 3.10: Result of U.S. Treasury: State parameters (Kalman filter + arbitrage regularization)

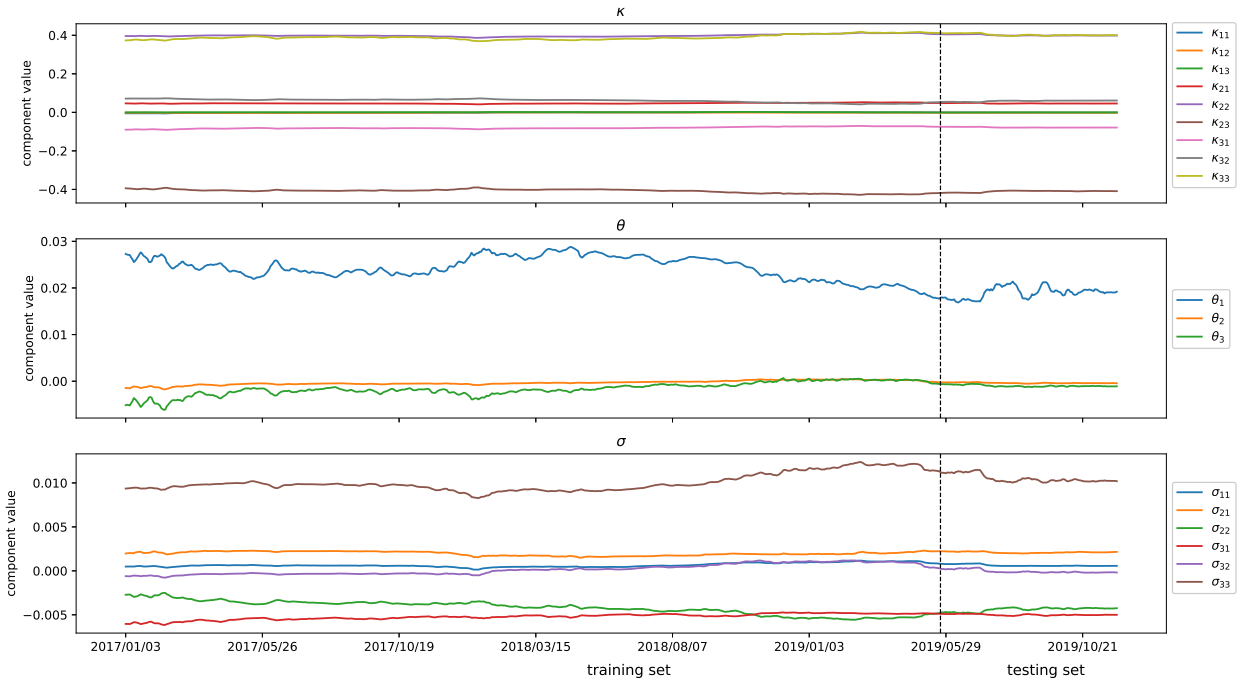

Figure 3.11: Result of U.S. Treasury: State parameters (Particle filter)

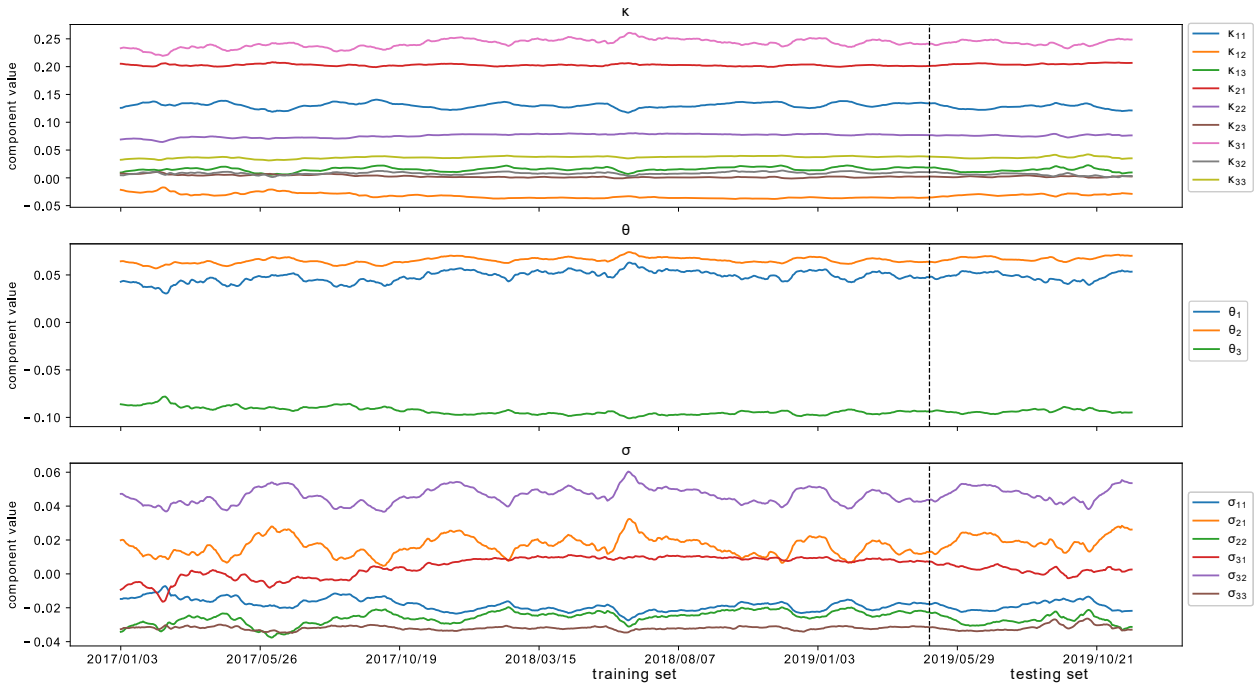

Figure 3.12: Result of U.S. Treasury: State parameters (Particle filter + arbitrage regularization)

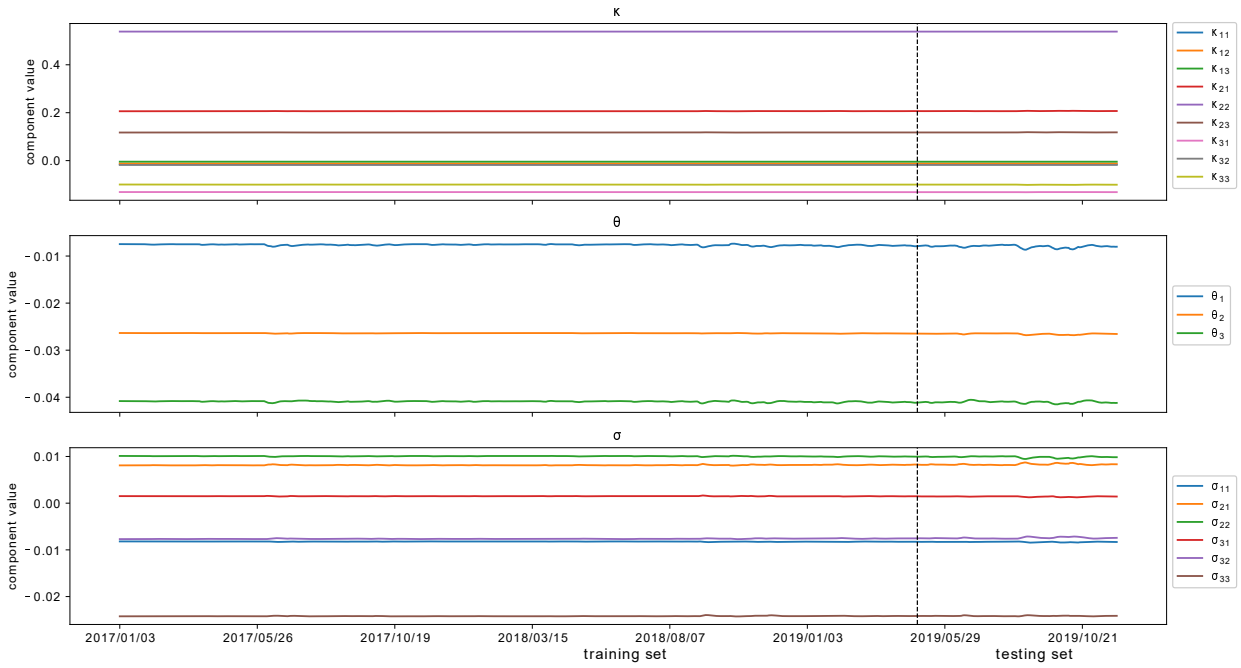

In Figure 3.13, we present the average excess return (AER) obtained from the evolution of forward rate curves that indicates the excess rate of the bond prices over the risk-free prices. The AER theoretically improves the soundness of the model and minimizes arbitrage opportunity in the dynamics of forward curves. The value of AER shown in Figure 3.13 is obtained from the trained model with arbitrage-free regularization, in contrast, which is very high in the model without arbitrage-free regularization. Among the three filters, the prediction result of the Kalman filter has the least arbitrage opportunity than the other two filters. The prediction result of the extended Kalman filter has the highest arbitrage opportunity at long-term maturities and that of the particle filter is in the short-term maturities. From the perspective of models, the consistency and the minimum value of AER provided by the Kalman filter across the training result and the testing result indicates that the yield forecasting with arbitrage-free regularization is more robust than the bond price model.

Figure 3.13: Result of U.S. Treasury: Average excess return of 1-day-ahead forecasting

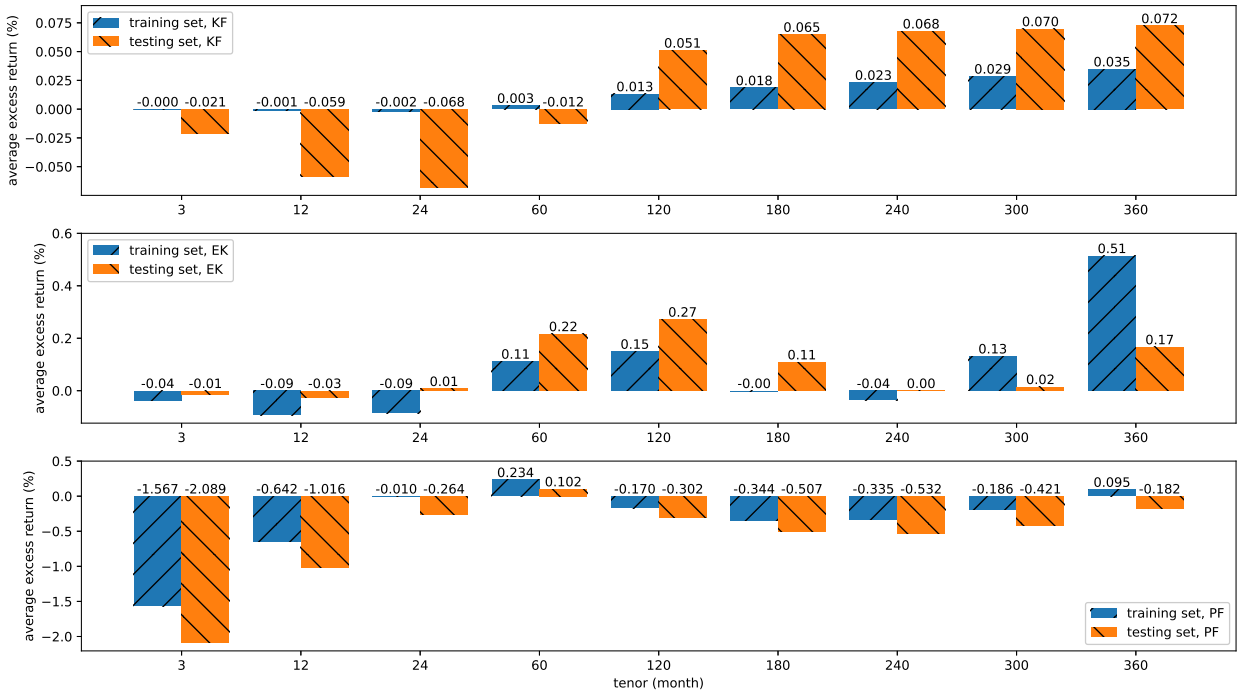

The effective sample size (ESS) shown in Figure 3.14 and 3.15 presents the variance of the particles over the maximum number of particles (300). The value of ESS is between 0 and 100% and the threshold in adaptive resampling is usually at 50%. In other words, if the ESS is less than half of the total number of particles then the particle filter is considered inefficient and resampling is necessary. In our application, we run systematic resampling at every time step instead of an adaptive method and examine the efficiency of the particle filter using the ESS. In Figure 3.14, we vary the regularization and compare the ESS at degree $p = 1.5$. The small initial value of ESS in the first step is due to the inexact initial particles which are sampled from the sample means of the estimated state variables and are not exactly the accurate initials for the forward rate curve. The result in Figure 3.14 shows the ESS of the particles stays above 85% in the training set and decays to 60% in the testing set over time, which also indicates that the particle filter does not suffer from serious degeneracy. In Figure 3.15, we vary p, the degree of the distribution, and compare the ESS with regularization $\lambda = 1$. We observe that the MGGD with $p = 0.62$ has much higher ESS in the later time steps and the ESS is not decaying in the testing set. Later, we will show that the optimal value of p is around 0.62 in the error distribution of the predicted bond prices. Therefore, we conclude that the particle filter with multivariate generalized Gaussian distribution is very efficient and stable for bond prices forecasting in both training and testing data.

Figure 3.14: Result of U.S. Treasury: Effective sample size with different regularization

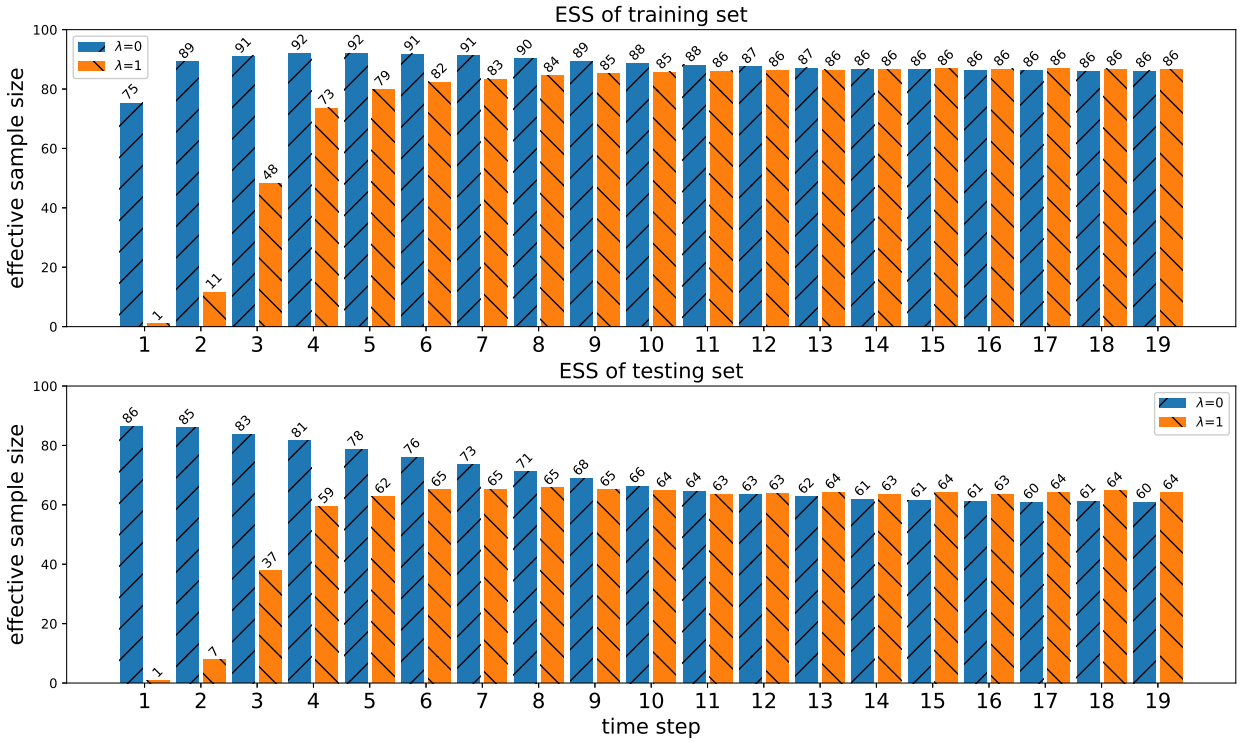

Figure 3.15: Result of U.S. Treasury: Effective sample size with different degree

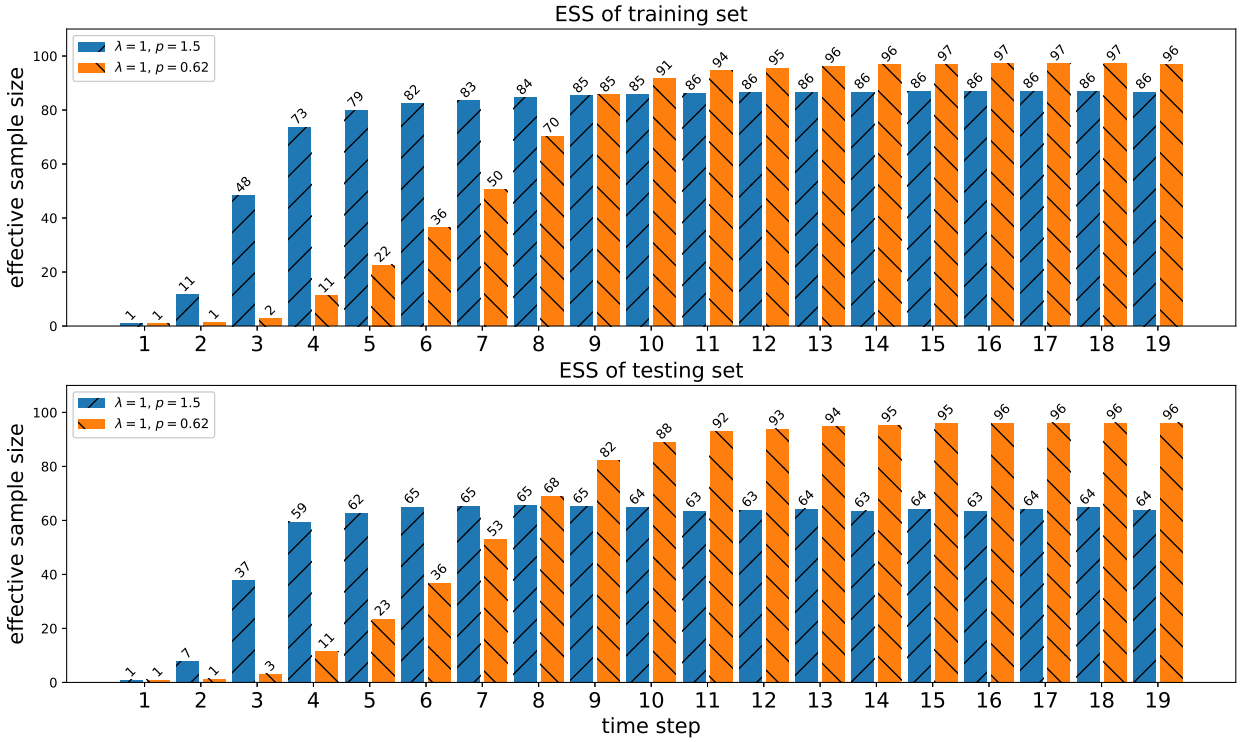

Figure 3.16: Result of U.S. Treasury: Price error distribution of 1-day-ahead forecasting

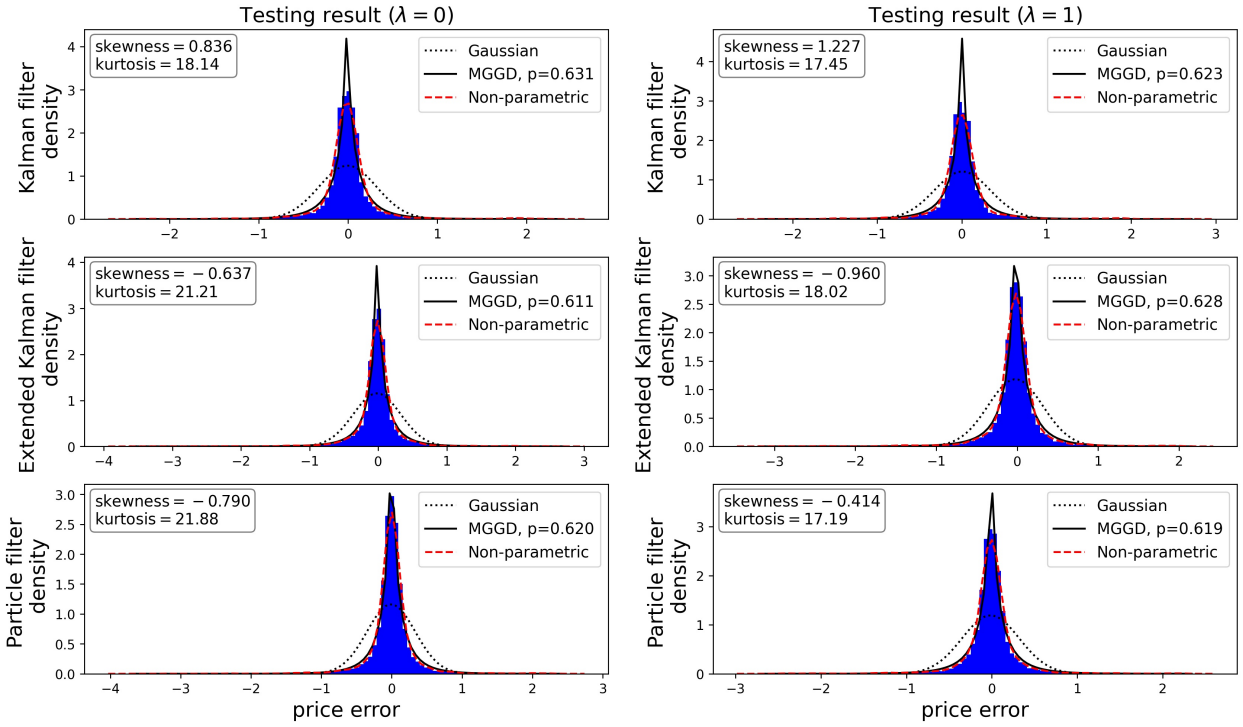

Figure 3.17: Result of U.S. Treasury: QQ-plot (price error) of 1-day-ahead forecasting

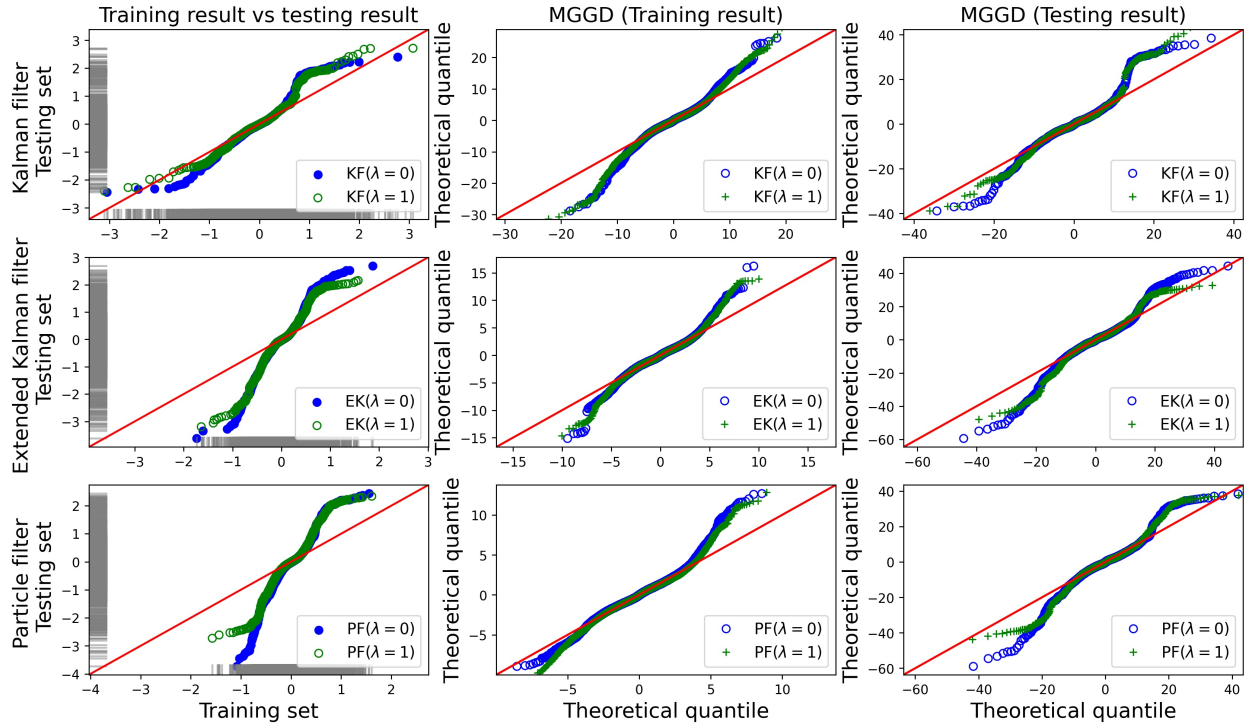

Figure 3.18: Result of U.S. Treasury: Yield error distribution of 1-day-ahead forecasting

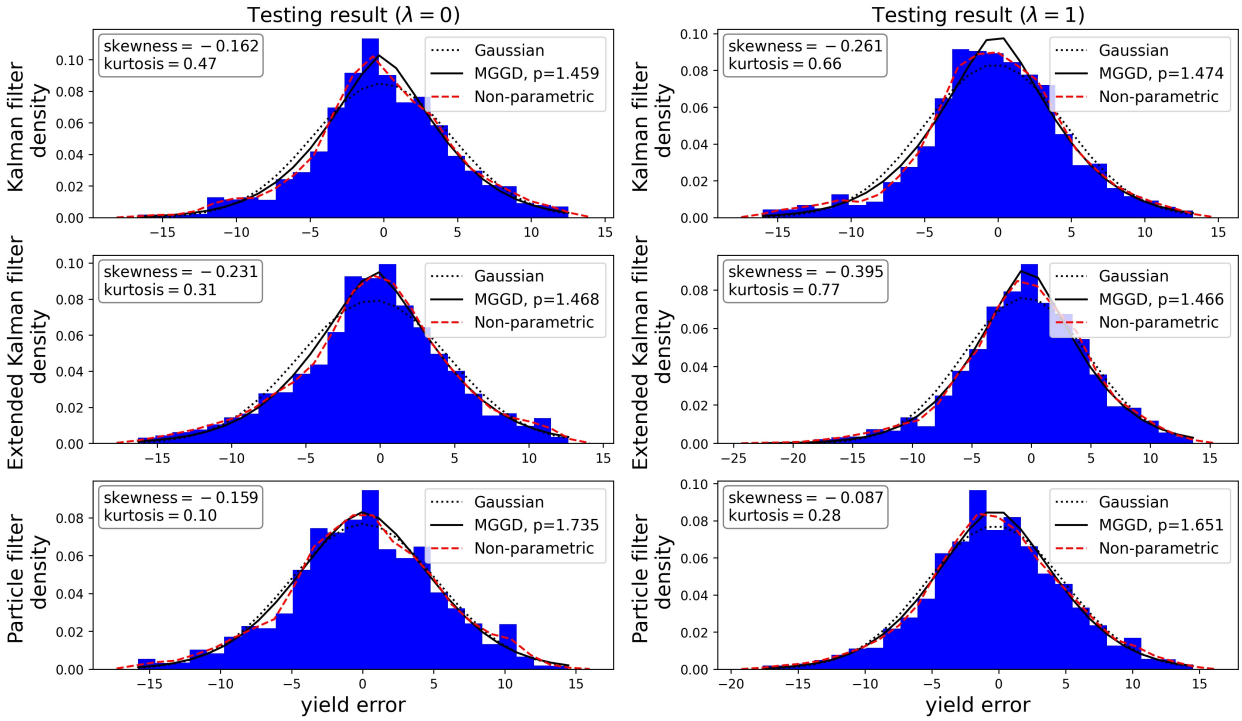

Figure 3.19: Result of U.S. Treasury: QQ-plot (yield error) of 1-day-ahead forecasting

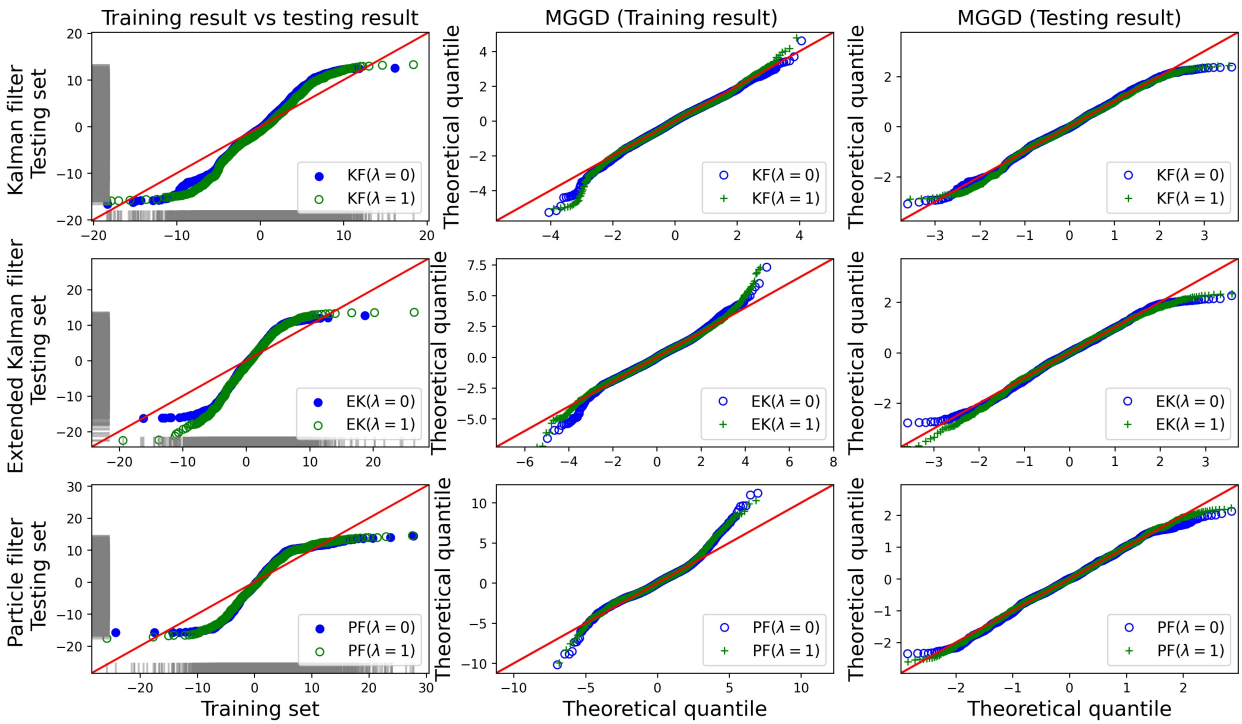

In Figures 3.16, 3.17, 3.18 and 3.19, we fit the 1-day-ahead prediction error of Treasury yields and bond proces with three distributions and make an analysis from the qq plot. Figure 3.16 shows the prediction error distribution of bond prices and there exists excess kurtosis problem which could be decreased by arbitrage-penalty. Figures 3.17 shows qq plot of the price error fitting with MGGD and we find that the fat tail problem is very severe for the non-linear model. Figure 3.18 shows the prediction error distribution of yields and the kurtosis below than 1 and find that the prediction error of yields has a low kurtosis problem which could be increased by the arbitrage-penalty. Comparing the the result of the paricle filter shown in Figure 3.16 and 3.18, we find the MGGD could fit in both of the excess kurtosis and low kurtosis situations and the main problem of the prediction error is the fat tail problem. For the problem of excess kurtosis in the particle filter, it could be improved by considering a non-parametric distribution for the observation instead of the MGGD. For the fat tail problem, we refer to Brigo, Dalessandro, Neugebauer, and Triki [16] who suggest adding a jump term in the mean-reverting dynamics to solve the fat tail problems which we will discuss later as a future direction.

From Tables 3.9 to 3.16, we present the h-day-ahead forecasting results on data from twelve corporate bond issuers with the predicted corporate spread calculated by subtracting the the predicted Treasury yield from the predicted corporate yield and comparing to the observed value. For the forecasting results of corporate data, we present the predicted spread error (predicted corporate yield - predicted Treasury yield) ranging between 2.8 bps to 11 bps in 1-day-ahead forecasting and between 5.2 bps to 14 bps in 5-day-ahead forecasting. Since credit risk factors are not included and the corporate data contains only around 10 to 30 daily bonds which is too few, the forecasting performance of corporate data is not comparable to that of Treasury data. From the corporate results, we find that the Kalman filter significant outperforms the extended Kalman filter and the particle filter. Therefore, we recommend to using yield points for forecasting both corporate yields and coupon coupon bonds when the daily number of bonds is not sufficiently large.

Other models with credit risk factors such as Duffie [46] show that the forecasting has a prediction error around 100 basis points on short-term corporate bond yields and around 9 basis points on long-term. Duffee [43] investigates 161 firm's bonds on monthly basis and shows the RMSE forecasting yield error in 34.56 bps for 6 months maturity and 7.77 bps for 30 years maturities, using the Kalman filter and a CIR model as interest rate in 1-month-ahead forecasting. However, Duffee [43] does not provide the out-of-sample tests.

Available corporate coupon bonds contain only 10 to 30 bonds on average which are much fewer than Treasury bonds traded on a daily basis. The overall forecasting performance for the corporate is not comparable to the Treasury result, since our model isn't including the credit risk and the corporate data is deficient on both daily observation and features. As comparison we found in Ganguli and Dunnmon [61]'s work, they have 61 features including information from second market and from both trading sides and present training/testing results of different models and running times: (0.8043 / 0.8455) by OLS in 23 seconds, (0.0055 / 2.4369) by regression trees with 83 hours, (0.6668 / 0.7012) by neural networks (two-layer 30 neurons) in 2 hours. As noted in Diebold and Li [37], there is a persistent discrepancy between actual bond prices and the prices estimated from term structure models for the Treasury bonds. We do not smooth the observed prices so the discrepancy in the corporate bonds would be much larger than the Treasury bonds due to credit risk and/or liquidity problem.

3.6.2 Results of corporate data

Table 3.9: Summary of 1-day-ahead forecasting: predicted spread error (in bps) and price error (in dollars), part 1

Ticker	Spread MAPE		Spread RMSPE		Spread STD		Price MAE		Price RMSPE		Price STD	
Model	Train	Test	Train	Test	Train	Test	Train	Test	Train	Test	Train	Test
AAPL												
KF(λ=0)	3.05	2.81	3.27	2.96	1.16	0.93	0.161	0.156	0.267	0.224	0.267	0.223
EK(λ=0)	4.04	4.86	4.49	5.33	1.96	2.20	0.161	0.185	0.263	0.310	0.263	0.309
PF(λ=0)	4.08	6.45	4.60	7.55	2.13	3.93	0.154	0.187	0.240	0.291	0.240	0.290
KF(λ=1)	3.06	2.65	3.29	2.83	1.19	1.00	0.159	0.153	0.267	0.219	0.267	0.219
EK(λ=1)	3.91	5.89	4.37	6.63	1.95	3.04	0.154	0.188	0.243	0.293	0.243	0.292
PF(λ=1)	4.02	6.04	4.58	7.02	2.19	3.58	0.152	0.180	0.239	0.285	0.239	0.284
BAC												
KF(λ=0)	9.07	11.16	9.36	11.47	2.34	2.63	0.384	0.408	0.618	0.664	0.616	0.658
EK(λ=0)	9.22	8.56	9.83	9.46	3.40	4.03	0.365	0.343	0.557	0.514	0.557	0.514
PF(λ=0)	10.07	9.65	10.69	10.16	3.58	3.17	0.362	0.449	0.555	0.716	0.555	0.691
KF(λ=1)	8.73	11.87	9.01	12.15	2.22	2.59	0.367	0.454	0.592	0.728	0.590	0.727
EK(λ=1)	9.95	9.09	10.48	9.39	3.29	2.32	0.369	0.401	0.567	0.620	0.567	0.613
PF(λ=1)	10.10	8.85	10.65	9.33	3.38	2.96	0.373	0.396	0.583	0.633	0.583	0.630
C												
KF(λ=0)	6.03	6.36	6.32	6.57	1.91	1.65	0.264	0.344	0.419	0.545	0.419	0.545
EK(λ=0)	6.75	7.29	7.10	7.64	2.22	2.29	0.257	0.366	0.408	0.557	0.408	0.557
PF(λ=0)	6.71	8.40	7.13	9.18	2.39	3.70	0.241	0.369	0.362	0.573	0.362	0.573
KF(λ=1)	6.09	6.56	6.38	6.83	1.90	1.89	0.263	0.361	0.414	0.577	0.414	0.575
EK(λ=1)	6.76	8.05	7.15	8.53	2.33	2.80	0.249	0.374	0.384	0.576	0.384	0.576
PF(λ=1)	6.67	8.39	7.06	8.80	2.30	2.63	0.246	0.398	0.380	0.606	0.380	0.606
DIS												
KF(λ=0)	4.44	4.91	4.71	5.19	1.56	1.67	0.193	0.264	0.317	0.572	0.317	0.572
EK(λ=0)	5.45	6.23	5.98	6.68	2.47	2.41	0.188	0.261	0.291	0.447	0.291	0.447
PF(λ=0)	6.18	8.16	6.95	9.28	3.18	4.43	0.185	0.264	0.268	0.430	0.268	0.430
KF(λ=1)	4.53	8.24	4.80	8.72	1.58	2.86	0.195	0.323	0.325	0.694	0.325	0.684
EK(λ=1)	5.67	7.13	6.26	7.81	2.65	3.18	0.185	0.268	0.269	0.484	0.269	0.483
PF(λ=1)	5.85	9.09	6.56	10.60	2.98	5.45	0.183	0.274	0.268	0.487	0.268	0.484
GS												
KF(λ=0)	5.69	6.16	5.96	6.36	1.77	1.58	0.293	0.339	0.453	0.493	0.452	0.491
EK(λ=0)	6.54	6.86	7.16	7.12	2.91	1.93	0.282	0.341	0.419	0.513	0.418	0.511
PF(λ=0)	6.30	7.31	6.84	7.54	2.68	1.87	0.262	0.358	0.376	0.553	0.375	0.553
KF(λ=1)	5.64	6.41	5.91	6.55	1.77	1.36	0.288	0.359	0.441	0.537	0.441	0.534
EK(λ=1)	6.44	8.52	7.13	9.05	3.06	3.06	0.268	0.373	0.389	0.565	0.388	0.564
PF(λ=1)	6.22	7.44	6.83	7.82	2.84	2.41	0.257	0.361	0.372	0.547	0.372	0.546
JNJ												
KF(λ=0)	5.15	5.33	5.51	5.81	1.98	2.30	0.269	0.296	0.427	0.440	0.427	0.439
EK(λ=0)	5.99	6.44	6.64	7.00	2.85	2.74	0.270	0.329	0.414	0.551	0.414	0.550
PF(λ=0)	6.29	6.57	6.96	7.25	2.96	3.06	0.267	0.323	0.398	0.524	0.398	0.523
KF(λ=1)	5.22	5.35	5.62	5.83	2.07	2.30	0.267	0.294	0.416	0.438	0.416	0.438
EK(λ=1)	6.34	7.16	7.18	7.88	3.37	3.31	0.267	0.322	0.409	0.497	0.409	0.496
PF(λ=1)	6.50	6.98	7.41	7.85	3.57	3.60	0.266	0.301	0.407	0.477	0.406	0.476

Table 3.10: Summary of 1-day-ahead forecasting: predicted spread error (in bps) and price error (in dollars), part 2

Ticker	Spread MAPE		Spread RMSPE		Spread STD		Price MAE		Price RMSPE		Price STD	
Model	Train	Test	Train	Test	Train	Test	Train	Test	Train	Test	Train	Test
JPM												
KF(λ=0)	4.73	5.11	4.96	5.48	1.49	1.97	0.289	0.441	0.557	1.060	0.557	1.030
EK(λ=0)	5.78	8.56	6.34	9.55	2.61	4.22	0.220	0.312	0.335	0.566	0.335	0.563
PF(λ=0)	6.03	9.57	6.66	10.75	2.84	4.90	0.217	0.305	0.329	0.511	0.329	0.510
KF(λ=1)	4.74	5.56	4.98	5.98	1.51	2.21	0.286	0.448	0.538	1.062	0.536	1.027
EK(λ=1)	6.37	10.87	7.05	11.92	3.01	4.89	0.232	0.338	0.354	0.550	0.354	0.550
PF(λ=1)	5.79	9.48	6.45	10.45	2.85	4.38	0.214	0.326	0.326	0.572	0.326	0.570
MS												
KF(λ=0)	6.60	6.62	6.90	6.81	2.00	1.60	0.248	0.268	0.379	0.432	0.377	0.432
EK(λ=0)	6.90	7.06	7.39	7.34	2.66	2.01	0.239	0.272	0.370	0.429	0.369	0.427
PF(λ=0)	6.89	8.64	7.53	9.38	3.03	3.66	0.221	0.283	0.330	0.439	0.330	0.438
KF(λ=1)	6.46	6.51	6.83	6.74	2.19	1.75	0.240	0.259	0.376	0.421	0.376	0.421
EK(λ=1)	6.72	7.84	7.20	8.19	2.60	2.36	0.227	0.282	0.342	0.455	0.342	0.455
PF(λ=1)	7.06	8.54	7.66	9.22	2.97	3.46	0.232	0.276	0.361	0.441	0.361	0.441
MSFT												
KF(λ=0)	3.49	3.27	3.82	3.45	1.56	1.10	0.215	0.244	0.333	0.332	0.333	0.331
EK(λ=0)	4.18	5.31	4.81	6.02	2.38	2.84	0.201	0.250	0.296	0.362	0.296	0.361
PF(λ=0)	4.69	5.95	5.53	6.71	2.93	3.12	0.192	0.246	0.271	0.356	0.271	0.355
KF(λ=1)	3.56	3.22	3.92	3.47	1.65	1.29	0.215	0.242	0.331	0.327	0.331	0.326
EK(λ=1)	4.54	5.90	5.26	6.41	2.66	2.52	0.196	0.263	0.283	0.384	0.283	0.381
PF(λ=1)	4.33	6.22	5.01	7.25	2.51	3.73	0.194	0.253	0.279	0.374	0.279	0.371
T												
KF(λ=0)	5.69	5.25	6.18	5.53	2.42	1.73	0.264	0.278	0.418	0.585	0.418	0.585
EK(λ=0)	6.38	7.47	7.06	8.25	3.03	3.49	0.258	0.310	0.396	0.576	0.396	0.576
PF(λ=0)	6.51	7.53	7.38	8.29	3.46	3.46	0.242	0.304	0.362	0.579	0.362	0.579
KF(λ=1)	5.79	6.31	6.30	6.97	2.47	2.95	0.264	0.301	0.421	0.582	0.420	0.581
EK(λ=1)	6.43	8.08	7.28	8.93	3.41	3.80	0.246	0.316	0.372	0.563	0.372	0.562
PF(λ=1)	6.61	8.77	7.60	10.20	3.76	5.21	0.239	0.302	0.356	0.527	0.356	0.527
UNH												
KF(λ=0)	4.36	4.86	4.73	5.31	1.81	2.13	0.213	0.220	0.343	0.377	0.342	0.377
EK(λ=0)	5.45	5.87	6.13	6.43	2.81	2.63	0.209	0.228	0.324	0.368	0.324	0.368
PF(λ=0)	5.89	6.59	6.78	7.40	3.36	3.37	0.203	0.228	0.295	0.392	0.295	0.392
KF(λ=1)	4.45	5.93	4.82	6.48	1.86	2.60	0.213	0.256	0.344	0.465	0.343	0.464
EK(λ=1)	5.85	6.56	6.63	7.09	3.11	2.69	0.208	0.236	0.315	0.397	0.314	0.397
PF(λ=1)	5.53	6.67	6.30	7.46	3.03	3.36	0.205	0.230	0.316	0.371	0.316	0.368
WFC												
KF(λ=0)	5.56	5.43	5.79	5.64	1.61	1.53	0.271	0.288	0.511	0.585	0.510	0.585
EK(λ=0)	6.70	8.06	7.29	8.25	2.88	1.78	0.260	0.344	0.465	0.626	0.465	0.625
PF(λ=0)	6.40	8.36	6.84	8.60	2.42	2.02	0.243	0.353	0.419	0.641	0.419	0.639
KF(λ=1)	5.58	5.53	5.81	5.70	1.61	1.37	0.267	0.278	0.508	0.536	0.507	0.536
EK(λ=1)	6.53	8.22	7.03	8.40	2.63	1.74	0.248	0.369	0.438	0.729	0.438	0.728
PF(λ=1)	6.69	10.02	7.30	10.49	2.90	3.13	0.245	0.394	0.428	0.783	0.428	0.783

Table 3.11: Summary of 1-day-ahead forecasting: hit rate and percentage error, part 1

Spread	≤ 0.1		≤ 0.25		≤ 0.5		MPE		MPE		MPE	
Tenor(y)	$0 \sim 2$		$2 \sim 10$		$10 \sim 30$		$0 \sim 2$		$2 \sim 10$		$10 \sim 30$	
Ticker	Train	Test	Train	Test	Train	Test	Train	Test	Train	Test	Train	Test
AAPL												
KF(λ=0)	67%	64%	80%	75%	53%	54%	0.082	0.085	0.157	0.174	0.639	0.604
EK(λ=0)	66%	58%	80%	70%	58%	37%	0.083	0.096	0.160	0.194	0.578	0.900
PF(λ=0)	65%	62%	80%	76%	55%	38%	0.087	0.089	0.160	0.177	0.597	0.800
KF(λ=1)	67%	63%	81%	78%	52%	46%	0.082	0.086	0.154	0.170	0.643	0.572
EK(λ=1)	66%	53%	82%	68%	59%	33%	0.084	0.108	0.154	0.198	0.543	0.776
PF(λ=1)	67%	58%	81%	72%	60%	40%	0.082	0.101	0.153	0.189	0.525	0.784
BAC												
KF(λ=0)	41%	40%	50%	51%	31%	30%	0.161	0.153	0.331	0.287	0.957	0.911
EK(λ=0)	38%	35%	50%	56%	42%	50%	0.170	0.181	0.320	0.277	0.763	0.602
PF(λ=0)	38%	41%	50%	41%	39%	24%	0.176	0.158	0.335	0.363	0.801	0.994
KF(λ=1)	40%	38%	50%	48%	34%	29%	0.161	0.155	0.337	0.321	0.935	0.904
EK(λ=1)	39%	40%	48%	39%	36%	38%	0.173	0.168	0.339	0.365	0.844	0.786
PF(λ=1)	40%	42%	49%	42%	35%	39%	0.171	0.151	0.339	0.344	0.870	0.820
C												
KF(λ=0)	44%	33%	58%	47%	33%	27%	0.136	0.166	0.267	0.303	0.767	0.913
EK(λ=0)	45%	33%	60%	46%	37%	26%	0.134	0.185	0.265	0.332	0.740	0.924
PF(λ=0)	44%	31%	61%	47%	45%	25%	0.138	0.193	0.254	0.327	0.611	0.961
KF(λ=1)	44%	34%	59%	48%	36%	31%	0.136	0.165	0.267	0.297	0.765	0.924
EK(λ=1)	43%	28%	60%	43%	42%	27%	0.139	0.194	0.257	0.334	0.679	0.953
PF(λ=1)	45%	32%	61%	40%	40%	24%	0.135	0.186	0.256	0.365	0.673	1.027
DIS												
KF(λ=0)	47%	43%	73%	59%	33%	29%	0.122	0.140	0.195	0.256	0.853	1.832
EK(λ=0)	48%	44%	73%	58%	41%	30%	0.121	0.145	0.198	0.265	0.760	0.996
PF(λ=0)	47%	43%	72%	56%	48%	23%	0.126	0.146	0.197	0.280	0.592	0.914
KF(λ=1)	49%	44%	72%	58%	33%	24%	0.122	0.138	0.199	0.262	0.868	1.860
EK(λ=1)	47%	41%	73%	57%	45%	27%	0.123	0.149	0.199	0.268	0.589	1.060
PF(λ=1)	48%	39%	73%	58%	42%	30%	0.124	0.161	0.194	0.273	0.631	1.040
GS												
KF(λ=0)	40%	33%	64%	62%	46%	42%	0.141	0.171	0.223	0.210	0.644	0.602
EK(λ=0)	40%	40%	64%	56%	49%	44%	0.150	0.150	0.223	0.242	0.593	0.623
PF(λ=0)	39%	40%	64%	58%	57%	43%	0.152	0.156	0.218	0.250	0.501	0.661
KF(λ=1)	42%	34%	64%	59%	49%	42%	0.142	0.175	0.221	0.223	0.623	0.637
EK(λ=1)	39%	40%	64%	52%	55%	42%	0.149	0.158	0.218	0.263	0.531	0.686
PF(λ=1)	41%	40%	65%	58%	57%	40%	0.148	0.151	0.210	0.248	0.505	0.676
JNJ												
KF(λ=0)	44%	42%	67%	64%	48%	47%	0.137	0.150	0.215	0.217	0.614	0.533
EK(λ=0)	44%	39%	64%	61%	51%	44%	0.142	0.154	0.224	0.227	0.593	0.699
PF(λ=0)	44%	42%	65%	61%	51%	42%	0.143	0.154	0.226	0.227	0.558	0.672
KF(λ=1)	45%	42%	68%	62%	48%	49%	0.138	0.151	0.213	0.218	0.607	0.520
EK(λ=1)	42%	39%	67%	61%	50%	45%	0.148	0.165	0.220	0.242	0.575	0.619
PF(λ=1)	43%	37%	67%	64%	51%	52%	0.147	0.161	0.219	0.227	0.574	0.570

Table 3.12: Summary of 1-day-ahead forecasting: hit rate and percentage error, part 2

Spread	≤ 0.1		≤ 0.25		≤ 0.5		MPE		MPE		MPE	
Tenor(y)	$0 \sim 2$		$2 \sim 10$		$10 \sim 30$		$0 \sim 2$		$2 \sim 10$		$10 \sim 30$	
Ticker	Train	Test	Train	Test	Train	Test	Train	Test	Train	Test	Train	Test
JPM												
KF(λ=0)	41%	41%	70%	64%	30%	14%	0.143	0.148	0.200	0.211	0.991	1.930
EK(λ=0)	41%	41%	72%	60%	52%	27%	0.139	0.152	0.186	0.248	0.520	0.921
PF(λ=0)	42%	41%	68%	63%	44%	31%	0.145	0.147	0.210	0.225	0.636	0.755
KF(λ=1)	41%	41%	69%	65%	29%	14%	0.143	0.150	0.203	0.206	0.961	1.790
EK(λ=1)	43%	39%	69%	49%	50%	27%	0.137	0.162	0.202	0.311	0.539	0.845
PF(λ=1)	42%	46%	67%	65%	43%	35%	0.142	0.134	0.210	0.210	0.651	0.640
MS												
KF(λ=0)	45%	51%	59%	56%	44%	39%	0.139	0.131	0.269	0.269	0.638	0.706
EK(λ=0)	48%	42%	60%	57%	49%	36%	0.132	0.154	0.260	0.275	0.615	0.713
PF(λ=0)	48%	40%	63%	56%	54%	38%	0.132	0.167	0.238	0.289	0.530	0.671
KF(λ=1)	44%	49%	62%	59%	44%	36%	0.138	0.131	0.254	0.257	0.661	0.683
EK(λ=1)	48%	43%	63%	55%	46%	38%	0.132	0.154	0.243	0.287	0.576	0.767
PF(λ=1)	48%	42%	63%	56%	47%	38%	0.133	0.158	0.249	0.278	0.610	0.730
MSFT												
KF(λ=0)	47%	33%	71%	58%	46%	28%	0.128	0.163	0.196	0.237	0.653	0.723
EK(λ=0)	48%	37%	72%	63%	56%	46%	0.125	0.164	0.191	0.224	0.550	0.645
PF(λ=0)	49%	40%	73%	61%	60%	53%	0.124	0.155	0.186	0.231	0.478	0.568
KF(λ=1)	46%	34%	71%	57%	46%	36%	0.129	0.165	0.194	0.238	0.660	0.669
EK(λ=1)	48%	35%	73%	61%	60%	43%	0.128	0.168	0.186	0.239	0.510	0.654
PF(λ=1)	51%	39%	73%	62%	59%	48%	0.121	0.164	0.187	0.231	0.499	0.615
T												
KF(λ=0)	35%	34%	67%	69%	39%	30%	0.165	0.172	0.209	0.200	0.803	0.966
EK(λ=0)	37%	41%	67%	64%	38%	29%	0.161	0.165	0.210	0.218	0.786	0.988
PF(λ=0)	35%	39%	68%	67%	48%	30%	0.164	0.168	0.204	0.215	0.667	0.956
KF(λ=1)	36%	34%	67%	70%	38%	27%	0.165	0.168	0.210	0.193	0.809	0.995
EK(λ=1)	36%	36%	69%	65%	43%	24%	0.167	0.179	0.201	0.223	0.714	0.987
PF(λ=1)	37%	38%	69%	66%	47%	31%	0.163	0.179	0.200	0.216	0.655	0.915
UNH												
KF(λ=0)	48%	47%	72%	70%	36%	34%	0.124	0.133	0.194	0.194	0.804	0.878
EK(λ=0)	48%	41%	71%	66%	48%	30%	0.125	0.144	0.197	0.211	0.673	0.936
PF(λ=0)	47%	44%	71%	65%	52%	28%	0.130	0.142	0.195	0.211	0.565	0.954
KF(λ=1)	49%	45%	72%	63%	36%	26%	0.122	0.149	0.196	0.216	0.798	1.158
EK(λ=1)	47%	45%	71%	65%	48%	36%	0.131	0.139	0.197	0.218	0.628	1.036
PF(λ=1)	49%	47%	72%	65%	46%	26%	0.125	0.141	0.192	0.214	0.656	0.964
WFC												
KF(λ=0)	50%	63%	72%	61%	31%	30%	0.118	0.094	0.218	0.275	0.970	1.028
EK(λ=0)	50%	49%	72%	50%	31%	26%	0.121	0.124	0.210	0.351	0.915	1.062
EK(λ=0)	50%	49%	72%	50%	31%	26%	0.121	0.124	0.210	0.351	0.915	1.062
PF(λ=0)	53%	50%	70%	47%	31%	26%	0.118	0.128	0.219	0.396	1.077	1.281
EK(λ=1)	52%	51%	73%	53%	37%	22%	0.118	0.119	0.205	0.360	0.836	1.256
PF(λ=1)	51%	47%	73%	50%	33%	25%	0.120	0.126	0.201	0.383	0.827	1.345

Table 3.13: Summary of 5-day-ahead forecasting: predicted spread error (in bps) and price error (in dollars), part 1

Ticker	Spread MAPE		Spread RMSPE		Spread STD		Price MAE		Price RMSPE		Price STD	
Model	Train	Test	Train	Test	Train	Test	Train	Test	Train	Test	Train	Test
AAPL												
KF(λ=0)	5.30	5.27	5.71	5.85	2.13	2.54	0.265	0.241	0.457	0.355	0.456	0.353
EK(λ=0)	5.98	11.47	6.55	12.54	2.66	5.08	0.223	0.397	0.349	0.636	0.349	0.635
PF(λ=0)	6.66	10.40	7.23	10.95	2.81	3.44	0.261	0.259	0.437	0.393	0.437	0.386
KF(λ=1)	5.88	6.70	6.18	7.35	1.91	3.02	0.249	0.246	0.421	0.359	0.421	0.359
EK(λ=1)	6.62	10.52	7.28	11.09	3.02	3.51	0.240	0.355	0.390	0.524	0.389	0.523
PF(λ=1)	6.15	9.44	6.70	9.79	2.66	2.58	0.230	0.351	0.369	0.534	0.369	0.533
BAC												
KF(λ=0)	12.71	14.74	13.25	15.79	3.75	5.65	0.521	0.568	0.844	0.931	0.842	0.910
EK(λ=0)	12.47	11.77	13.30	12.01	4.63	2.42	0.436	0.527	0.655	0.857	0.655	0.853
PF(λ=0)	12.35	11.45	13.36	11.86	5.10	3.06	0.430	0.499	0.640	0.799	0.639	0.796
KF(λ=1)	12.92	14.64	13.44	15.77	3.71	5.86	0.502	0.534	0.802	0.874	0.802	0.867
EK(λ=1)	12.82	11.56	13.65	11.81	4.68	2.40	0.442	0.508	0.677	0.813	0.676	0.789
PF(λ=1)	12.32	12.38	13.12	12.83	4.51	3.37	0.429	0.630	0.645	1.018	0.645	0.946
C												
KF(λ=0)	9.02	9.93	9.46	10.35	2.83	2.92	0.359	0.447	0.602	0.722	0.602	0.713
EK(λ=0)	8.48	10.66	8.82	11.16	2.44	3.27	0.310	0.454	0.494	0.728	0.494	0.726
PF(λ=0)	8.20	11.05	8.50	11.32	2.24	2.44	0.303	0.490	0.464	0.847	0.464	0.816
KF(λ=1)	8.41	9.34	8.70	9.53	2.22	1.92	0.326	0.449	0.538	0.709	0.538	0.704
EK(λ=1)	8.85	13.00	9.32	13.95	2.93	5.06	0.302	0.491	0.467	0.793	0.466	0.793
PF(λ=1)	8.65	14.03	8.99	15.44	2.46	6.45	0.310	0.534	0.486	0.899	0.486	0.898
DIS												
KF(λ=0)	7.15	7.83	7.70	8.56	2.85	3.46	0.279	0.365	0.484	0.849	0.483	0.847
EK(λ=0)	7.90	11.24	8.61	12.23	3.43	4.81	0.251	0.372	0.387	0.673	0.386	0.670
PF(λ=0)	8.56	11.33	9.51	12.17	4.16	4.44	0.251	0.383	0.382	0.724	0.382	0.721
KF(λ=1)	7.27	11.76	7.69	12.26	2.52	3.48	0.258	0.369	0.424	0.594	0.424	0.587
EK(λ=1)	8.18	11.02	8.97	11.70	3.68	3.94	0.248	0.394	0.386	0.761	0.385	0.757
PF(λ=1)	7.80	9.61	8.49	10.23	3.35	3.52	0.249	0.382	0.375	0.812	0.375	0.812
GS												
KF(λ=0)	8.32	8.75	8.70	9.21	2.55	2.89	0.376	0.426	0.587	0.622	0.587	0.615
EK(λ=0)	7.78	9.16	8.37	9.37	3.10	1.96	0.318	0.437	0.469	0.666	0.469	0.649
PF(λ=0)	7.77	10.24	8.47	10.69	3.37	3.06	0.295	0.433	0.423	0.655	0.423	0.653
KF(λ=1)	7.84	8.66	8.11	8.82	2.06	1.71	0.347	0.428	0.531	0.605	0.531	0.604
EK(λ=1)	7.98	10.81	8.74	11.15	3.57	2.72	0.299	0.434	0.430	0.663	0.429	0.658
PF(λ=1)	8.05	11.03	8.62	11.42	3.08	2.94	0.303	0.475	0.436	0.733	0.436	0.727
JNJ												
KF(λ=0)	7.54	7.38	8.20	8.29	3.21	3.78	0.410	0.454	0.668	0.709	0.668	0.706
EK(λ=0)	8.59	10.61	9.67	12.25	4.45	6.13	0.366	0.540	0.566	0.880	0.566	0.879
PF(λ=0)	8.43	9.96	9.51	10.74	4.39	4.01	0.349	0.578	0.519	0.960	0.517	0.937
KF(λ=1)	7.15	8.06	7.63	8.77	2.67	3.46	0.371	0.429	0.596	0.651	0.596	0.645
EK(λ=1)	8.77	10.21	9.89	10.82	4.57	3.58	0.344	0.541	0.519	0.884	0.518	0.882
PF(λ=1)	8.00	11.01	8.84	11.68	3.77	3.90	0.347	0.607	0.522	1.042	0.522	1.012

Table 3.14: Summary of 5-day-ahead forecasting: predicted spread error (in bps) and price error (in dollars), part 2

Ticker	Spread MAPE		Spread RMSPE		Spread STD		Price MAE		Price RMSPE		Price STD	
Model	Train	Test	Train	Test	Train	Test	Train	Test	Train	Test	Train	Test
JPM												
KF(λ=0)	5.97	6.46	6.12	6.70	1.39	1.77	0.346	0.346	0.585	0.617	0.585	0.616
EK(λ=0)	7.55	10.07	8.12	10.82	3.01	3.95	0.310	0.473	0.493	0.909	0.492	0.909
PF(λ=0)	7.67	10.62	8.25	11.21	3.05	3.58	0.299	0.491	0.464	0.917	0.461	0.914
KF(λ=1)	7.34	8.49	7.70	9.43	2.32	4.12	0.365	0.450	0.661	0.926	0.661	0.914
EK(λ=1)	8.39	11.31	9.22	11.80	3.83	3.38	0.311	0.508	0.485	0.961	0.485	0.960
PF(λ=1)	7.91	12.63	8.59	13.57	3.35	4.97	0.303	0.482	0.471	0.929	0.471	0.926
MS												
KF(λ=0)	9.66	8.79	10.16	9.09	3.17	2.29	0.347	0.350	0.579	0.573	0.578	0.564
EK(λ=0)	9.27	12.14	9.95	12.57	3.60	3.27	0.294	0.399	0.461	0.610	0.460	0.608
PF(λ=0)	10.19	11.37	10.96	11.82	4.04	3.24	0.341	0.352	0.539	0.558	0.539	0.549
KF(λ=1)	9.14	9.72	9.56	10.49	2.79	3.95	0.308	0.322	0.508	0.505	0.508	0.505
EK(λ=1)	9.75	15.84	10.52	16.40	3.94	4.23	0.293	0.483	0.458	0.741	0.458	0.741
PF(λ=1)	9.68	14.24	10.51	15.23	4.08	5.40	0.295	0.414	0.456	0.675	0.456	0.675
MSFT												
KF(λ=0)	7.92	5.62	8.55	6.27	3.21	2.77	0.419	0.343	0.814	0.503	0.813	0.492
EK(λ=0)	6.95	10.56	7.67	11.09	3.26	3.37	0.284	0.441	0.455	0.681	0.454	0.653
PF(λ=0)	7.52	11.60	8.29	12.32	3.50	4.14	0.323	0.393	0.522	0.609	0.522	0.594
KF(λ=1)	6.60	8.34	7.06	9.71	2.50	4.96	0.322	0.448	0.542	0.825	0.542	0.807
EK(λ=1)	7.34	9.90	8.22	10.30	3.70	2.84	0.288	0.429	0.465	0.681	0.465	0.662
PF(λ=1)	6.80	10.84	7.53	11.42	3.23	3.60	0.282	0.433	0.440	0.684	0.439	0.670
T												
KF(λ=0)	9.33	9.41	10.07	10.96	3.79	5.62	0.411	0.450	0.717	1.024	0.716	1.022
EK(λ=0)	9.54	10.56	10.59	11.52	4.59	4.59	0.353	0.489	0.545	0.956	0.545	0.951
PF(λ=0)	11.13	12.81	12.67	13.87	6.05	5.31	0.406	0.389	0.668	0.772	0.668	0.750
KF(λ=1)	8.75	10.26	9.24	11.46	2.98	5.11	0.369	0.407	0.641	0.855	0.640	0.850
EK(λ=1)	9.89	14.14	11.05	15.00	4.94	5.00	0.342	0.611	0.535	1.120	0.534	1.057
PF(λ=1)	10.08	14.04	11.26	15.50	5.03	6.55	0.349	0.530	0.546	1.035	0.546	1.032
UNH												
KF(λ=0)	7.24	8.34	7.88	9.10	3.12	3.63	0.314	0.404	0.548	0.885	0.548	0.881
EK(λ=0)	7.73	9.23	8.62	10.13	3.80	4.18	0.281	0.364	0.450	0.588	0.450	0.588
PF(λ=0)	8.91	10.96	9.82	11.39	4.12	3.09	0.332	0.378	0.562	0.744	0.561	0.744
KF(λ=1)	7.39	10.15	7.89	11.39	2.76	5.18	0.281	0.433	0.471	0.923	0.470	0.909
EK(λ=1)	8.24	11.68	9.13	12.57	3.92	4.65	0.284	0.376	0.446	0.618	0.446	0.615
PF(λ=1)	8.12	10.34	9.11	11.05	4.13	3.89	0.280	0.371	0.442	0.605	0.442	0.602
WFC												
KF(λ=0)	9.07	7.03	9.49	7.57	2.80	2.82	0.418	0.368	0.810	0.785	0.809	0.778
EK(λ=0)	8.88	12.14	9.44	12.60	3.21	3.38	0.330	0.560	0.557	1.128	0.557	1.117
PF(λ=0)	9.37	12.77	10.05	13.20	3.65	3.34	0.339	0.538	0.588	1.042	0.586	1.029
KF(λ=1)	8.79	10.64	9.17	11.27	2.61	3.72	0.365	0.442	0.709	0.898	0.708	0.878
EK(λ=1)	9.11	13.25	9.64	13.54	3.15	2.80	0.330	0.562	0.553	1.182	0.553	1.166
PF(λ=1)	9.58	13.71	10.31	14.15	3.79	3.52	0.350	0.583	0.587	1.132	0.587	1.120

Table 3.15: Summary of 5-day-ahead forecasting: hit rate and percentage error, part 1

Spread	≤ 0.1		≤ 0.25		≤ 0.5		MPE		MPE		MPE	
Tenor(y)	$0 \sim 2$		$2 \sim 10$		$10 \sim 30$		$0 \sim 2$		$2 \sim 10$		$10 \sim 30$	
Ticker	Train	Test	Train	Test	Train	Test	Train	Test	Train	Test	Train	Test
AAPL												
KF(λ=0)	59%	60%	58%	57%	33%	18%	0.098	0.104	0.283	0.281	1.048	0.868
EK(λ=0)	55%	48%	64%	37%	47%	12%	0.107	0.133	0.237	0.463	0.732	1.739
PF(λ=0)	57%	57%	60%	54%	35%	18%	0.107	0.105	0.273	0.304	1.019	0.961
KF(λ=1)	60%	60%	60%	54%	38%	18%	0.097	0.106	0.267	0.290	0.942	0.735
EK(λ=1)	57%	40%	62%	42%	37%	17%	0.110	0.158	0.254	0.410	0.853	1.369
PF(λ=1)	59%	50%	64%	39%	42%	24%	0.102	0.127	0.244	0.420	0.799	1.179
BAC												
KF(λ=0)	34%	32%	39%	38%	23%	22%	0.204	0.198	0.465	0.381	1.283	1.292
EK(λ=0)	32%	38%	41%	30%	35%	29%	0.215	0.167	0.419	0.506	0.909	1.112
PF(λ=0)	30%	35%	42%	33%	35%	34%	0.221	0.172	0.399	0.471	0.919	1.033
KF(λ=1)	38%	37%	45%	40%	30%	26%	0.171	0.196	0.384	0.386	1.060	1.144
EK(λ=1)	33%	38%	42%	32%	35%	28%	0.216	0.166	0.416	0.462	0.955	1.090
PF(λ=1)	33%	38%	42%	28%	33%	14%	0.209	0.170	0.404	0.541	0.923	1.475
C												
KF(λ=0)	40%	28%	46%	38%	27%	24%	0.154	0.195	0.369	0.398	1.093	1.179
EK(λ=0)	42%	38%	49%	36%	32%	21%	0.145	0.185	0.331	0.410	0.881	1.245
PF(λ=0)	40%	34%	49%	38%	37%	35%	0.152	0.193	0.328	0.445	0.779	1.296
KF(λ=1)	42%	31%	49%	36%	31%	20%	0.147	0.177	0.338	0.402	0.943	1.223
EK(λ=1)	41%	29%	49%	36%	38%	19%	0.150	0.213	0.329	0.446	0.772	1.282
PF(λ=1)	40%	29%	49%	31%	33%	22%	0.155	0.221	0.330	0.485	0.834	1.413
DIS												
KF(λ=0)	45%	45%	56%	48%	27%	6%	0.141	0.155	0.300	0.367	1.206	3.345
EK(λ=0)	45%	35%	57%	40%	41%	21%	0.137	0.182	0.285	0.408	0.819	1.478
PF(λ=0)	43%	37%	57%	40%	42%	16%	0.142	0.173	0.285	0.416	0.778	1.662
KF(λ=1)	46%	38%	58%	39%	31%	25%	0.135	0.170	0.281	0.481	1.028	1.252
EK(λ=1)	46%	40%	58%	39%	39%	20%	0.138	0.167	0.277	0.433	0.865	1.758
PF(λ=1)	45%	35%	58%	44%	39%	20%	0.138	0.184	0.281	0.385	0.798	1.887
GS												
KF(λ=0)	38%	29%	52%	54%	37%	34%	0.157	0.204	0.303	0.267	0.823	0.751
EK(λ=0)	38%	40%	56%	48%	48%	33%	0.158	0.167	0.271	0.310	0.631	0.813
PF(λ=0)	38%	36%	57%	49%	54%	33%	0.161	0.174	0.259	0.313	0.547	0.779
KF(λ=1)	40%	24%	54%	50%	41%	37%	0.146	0.199	0.288	0.292	0.732	0.720
EK(λ=1)	37%	35%	57%	51%	51%	35%	0.165	0.179	0.257	0.301	0.570	0.799
PF(λ=1)	38%	40%	54%	44%	53%	37%	0.159	0.170	0.267	0.355	0.567	0.849
JNJ												
KF(λ=0)	38%	32%	52%	48%	31%	30%	0.161	0.181	0.322	0.318	0.985	0.908
EK(λ=0)	39%	27%	54%	41%	36%	29%	0.162	0.226	0.301	0.398	0.834	1.108
PF(λ=0)	37%	30%	50%	43%	35%	32%	0.172	0.201	0.334	0.365	0.946	0.892
KF(λ=1)	42%	24%	55%	51%	33%	30%	0.148	0.191	0.297	0.308	0.862	0.821
EK(λ=1)	38%	32%	56%	41%	42%	25%	0.166	0.195	0.292	0.400	0.727	1.135
PF(λ=1)	35%	31%	55%	42%	40%	24%	0.166	0.201	0.295	0.404	0.739	1.390

Table 3.16: Summary of 5-day-ahead forecasting: hit rate and percentage error, part 2

Spread	≤ 0.1		≤ 0.25		≤ 0.5		MPE		MPE		MPE	
Tenor(y)	$0 \sim 2$		$2 \sim 10$		$10 \sim 30$		$0 \sim 2$		$2 \sim 10$		$10 \sim 30$	
Ticker	Train	Test	Train	Test	Train	Test	Train	Test	Train	Test	Train	Test
JPM												
KF(λ=0)	38%	40%	54%	51%	33%	35%	0.159	0.155	0.296	0.322	0.923	0.851
EK(λ=0)	41%	39%	57%	43%	36%	16%	0.152	0.171	0.269	0.390	0.785	1.525
PF(λ=0)	37%	35%	55%	44%	31%	27%	0.165	0.176	0.282	0.387	0.833	0.883
KF(λ=1)	38%	36%	55%	49%	24%	13%	0.161	0.165	0.287	0.295	1.120	1.640
EK(λ=1)	39%	35%	56%	37%	34%	15%	0.160	0.181	0.269	0.435	0.784	1.567
PF(λ=1)	40%	35%	57%	41%	38%	19%	0.156	0.171	0.267	0.411	0.740	1.504
MS												
KF(λ=0)	44%	44%	46%	47%	27%	38%	0.164	0.157	0.378	0.358	1.111	0.900
EK(λ=0)	44%	30%	50%	43%	35%	24%	0.152	0.215	0.323	0.417	0.815	0.978
PF(λ=0)	38%	45%	45%	46%	31%	40%	0.177	0.164	0.369	0.374	1.000	0.737
KF(λ=1)	44%	41%	49%	51%	27%	36%	0.154	0.161	0.330	0.326	0.991	0.761
EK(λ=1)	43%	28%	50%	33%	40%	20%	0.158	0.252	0.322	0.503	0.785	1.263
PF(λ=1)	43%	35%	50%	41%	39%	33%	0.159	0.219	0.324	0.434	0.780	1.008
MSFT												
KF(λ=0)	44%	37%	46%	44%	23%	21%	0.145	0.165	0.366	0.355	1.725	1.030
EK(λ=0)	45%	35%	57%	39%	36%	24%	0.138	0.195	0.273	0.413	0.918	1.240
PF(λ=0)	42%	38%	53%	39%	30%	23%	0.154	0.175	0.299	0.416	1.052	1.329
KF(λ=1)	45%	38%	53%	44%	28%	18%	0.143	0.166	0.304	0.362	1.282	1.058
EK(λ=1)	43%	36%	57%	42%	36%	15%	0.145	0.181	0.270	0.385	0.952	1.364
PF(λ=1)	46%	37%	58%	41%	32%	27%	0.140	0.188	0.267	0.402	0.908	1.252
T												
KF(λ=0)	30%	38%	51%	56%	21%	13%	0.197	0.160	0.305	0.274	1.456	2.448
EK(λ=0)	33%	37%	52%	48%	25%	16%	0.186	0.191	0.285	0.321	1.125	1.850
PF(λ=0)	29%	38%	50%	56%	20%	14%	0.221	0.163	0.311	0.273	1.354	1.810
KF(λ=1)	32%	41%	55%	58%	24%	16%	0.177	0.157	0.278	0.269	1.277	2.022
EK(λ=1)	32%	35%	54%	33%	27%	19%	0.191	0.200	0.274	0.446	1.082	2.064
PF(λ=1)	30%	33%	51%	56%	23%	14%	0.214	0.174	0.303	0.266	1.335	1.971
UNH												
KF(λ=0)	44%	43%	55%	50%	20%	20%	0.145	0.179	0.287	0.331	1.303	2.258
EK(λ=0)	45%	36%	56%	47%	38%	18%	0.140	0.175	0.272	0.362	0.901	1.558
PF(λ=0)	40%	40%	51%	51%	24%	22%	0.166	0.161	0.311	0.319	1.253	1.969
KF(λ=1)	48%	37%	59%	49%	25%	14%	0.128	0.177	0.261	0.349	1.104	2.556
EK(λ=1)	42%	36%	57%	47%	33%	18%	0.149	0.189	0.269	0.374	0.944	1.580
PF(λ=1)	43%	36%	57%	47%	36%	36%	0.146	0.179	0.266	0.382	0.907	1.343
WFC												
KF(λ=0)	44%	57%	53%	54%	18%	15%	0.149	0.109	0.337	0.298	1.666	1.582
EK(λ=0)	44%	48%	57%	39%	23%	11%	0.143	0.145	0.288	0.511	1.123	2.054
PF(λ=0)	35%	42%	53%	42%	20%	16%	0.187	0.135	0.338	0.418	1.414	1.527
KF(λ=1)	47%	51%	59%	39%	20%	16%	0.134	0.122	0.296	0.425	1.430	1.650
EK(λ=1)	45%	43%	57%	42%	24%	14%	0.145	0.160	0.290	0.500	1.110	2.078
PF(λ=1)	33%	41%	53%	44%	19%	19%	0.184	0.145	0.342	0.399	1.504	1.543

3.7 Conclusion

We have implemented the Kalman filter, the extended Kalman filter and the particle filter in deep neural network using dynamic parameterization to calibrate the forward curves in sense of arbitrage-free evolution and examine the model performance from the forecasting results. We provide various in-sample and out-of-sample tests under non-arbitrage regularization and arbitrage-free regularization where we find that the arbitrage-free regularization does not always downgrade the performance as suggested by other authors. We find that the arbitrage-restriction downgrades the forecasting performance in long time horizons which is consistent Christensen et al. [21]. However, we also find that the arbitrage-restriction could improve the forecasting performance in short time horizons. We find that the yield forecasting model without arbitrage penalty has better forecasting performance in long time horizons than the benchmark that uses the observed yield curve to predict bond prices. The filters demonstrate different advantages in calibrating the forward rate curves: the Kalman filter is the most consistent and stable model where the variance between in-sample data and out-of-sample data is the less than extended Kalman filter and particle filter. From the practical purpose, the extended Kalman filter is the most flexible model that could handle the forecasting of yield curves and bond prices at the same time with the least computational cost. The particle filter is the very robust model in studying different error distributions since it's sophisticated in theoretical structure.

The arbitrage penalty that derived from the forward rate model is able to fit into different type of asset pricing models in fixed income market. The implementation of AR method in our model does not cost too much extra computational effort and the benefit of AR method is obvious in short time level of forecasting. As pointed out by Christensen et al. [21] and Diebold and Li [37], models in arbitrage-free tradition are only theoretically rigorous insofar as they enforce absence of arbitrage theoretically, they still admit arbitrage possibility and there are still ways to go for overcoming this problem. The periodic phenomenon occurred in AER through out different terms of maturity can be applied further to portfolio optimization and risk management. Further research can be conducted to quantify the AER so as to identify the coupon bonds whether they are over-valued or under-valued. The fat tail problem can be further viewed by interpreting the mean-reverting process with extra jump process. The flexibility of machine learning allows us to study the arbitrage-opportunities in more details and the dynamic parameterization provides us a wide directions to study the classic no-arbitrage theory in the future researches.

Chapter 4

Conclusion and Future work

In this chapter, we summarize the thesis and our contributions including new theoretical results and numerical results. we also present some future directions for the three projects: the optimal annuitization problem with labor income, the convolution method for option pricing, and the bond pricing and forecasting problems.

4.1 Optimization problem

We extend the traditional annuitization problem to include labor market income and study with Cobb-Douglas utility. We derive closed-form solutions using martingale approach to the stochastic control and optimal stopping formulations of the problem and provide the semi-closed solution to the critical point. We also provide rigorous proofs that show our solution is optimal for the post-retirement annuitization problem with extra labor income. Usually the explicit solution is difficult to obtain for most of the stochastic control problem and is more difficult to prove the optimality of the explicit solution, for example, Lim et al. [88] provide the explicit solution but lack a rigorous proof.

With the explicit solution, we could investigate more deep into the model and obtain more application results than Gerrard et al. [63] where they studied the annuitization problem with labor income and they only give a numerical approach to the critical wealth. Thus Gerrard et al. [63] provide the only analysis of the effect of labor income to the critical point. Our model and numerical results provide sufficient analysis including the effect of labor income, the wage rate, the Sharpe Ratio, the optimal stopping time and so on.

From our numerical application, we find many new facts. First, the Cobb-Douglas utility is concave in labor rate and convex in wage rate. Second, the optimal annuitization time is strongly linear with respect to the initial wealth in both cases with and without labor income. Adding

other disturbance such as extra labor could change the slope and the continuation region where the optimal annuitization time is decreasing to 0. Third, we also find that under different labor schemes, the pensioners could have similar strategies of consumption but different strategies of work and investment strategies. Such different strategies behave in the opposite way and lead to very different results in the final annuity and the annuitization time.

4.1.1 Future work on regime-switching problem

We can assume the wage rate in a regime-switching environment (see Yin, Krishnamurthy, and Ion [119]), for a Markov chain w_t to model the wage rate in a finite state space $\mathbb{M} = \{w_1, w_2, \cdots, w_m\}$

$$dX_t = (r(X_T - \pi_t) - c_t + w_t(1 - l_t))\,dt + \pi_t dS_t.$$

under transition probability matrix

$$P^{\Delta t} = I + \Delta t Q,$$

where I is an $m \times m$ identity matrix, and $Q = (q_{ij}) \in \mathbb{R}^{m \times m}$ is a generator of a continuous-time Markov chain. Therefore, including the effect of wage rate in the utility $U(w,l,c)$, we could study the labor income in the regime-switching problem.

4.2 The option pricing problem

We have studied the convolution method in the BSDEs framework following Hyndman and Oyono Ngou [74] and proposed new shifting scheme to improve the numerical performance reaching a stable and converging result. The main advantages of the convolution method are its flexibility and computational speed. Like other FFT-based methods, we achieve a complexity of $\mathcal{O}(N \log_2 N)$, where N is the number of grid points. We provide the error analysis of the convolution transform using DFT approach and provide solid proofs. From our analysis, we find that the truncation error is at least $\mathbb{O}\left(N^{-2}\right)$ order and the discretization error is at e^{-cN} method.

We provide a new scheme in formulating the characteristic function of Heston model. Our formula has no-discontinuity and is easy to take derivatives which gives us the flexibility to apply for calibration. We have studied the application of convolution method in direct approach and in BSDEs approach for pricing options. In the direct approach, we propose a new method to accurately estimate the probabilities in martingale measure and risk neutral measure. In the BSDEs approach, we have improved the performance with consistent damping parameter and exponential shifting function which shows huge decrease in boundary errors. Except the improvement, we also show that the convolution method in BSDEs framework has a error problem at in-the-money side which is accumulated from the boundary error during time iterations.

We introduced two convolution schemes for pricing options with Heston model. Scheme I is similar to the Black-Scholes model and is able to give the accurate result of the value of the probabilities. The error analysis shows that if Scheme I has bounded errors at boundaries then the errors are bounded everywhere. Scheme II is similar to the Fourier method of Carr and Madan [18] but our truncation region is on log-prices. From our numerical results, Scheme II is even faster than Fourier method of Carr and Madan [18] with the same grid points and is very accurate

compared to their method. In conclusion, our methods have advantages in wide range of accuracy, fast computation and stable boundaries, which is able to applied for calibration purpose in the future studies. And our approach shows improved accuracy of application in BSDE framework than Hyndman and Oyono Ngou [74].

We make comparison between the convolution method, Fourier method and the integration method on grid of log-strikes and log-prices. Our comparison shows that convolution method possess good convergence on the whole grid and very fast computational speed in which the Scheme II convolution method is even faster than the Fourier method. Our methods have advantages in wide range of accuracy, fast computation and stable boundaries control, which could be applied in calibration in the future studies. Future research will focus on reducing the accumulated boundary error in BSDEs approach and potential extension of the convolution method to high-dimensional applications.

4.2.1 Future work on high-dimensional BSDEs

Aiming to solve the high-dimensional pricing problem in the future direction, we introduce some recent approaches that applied to the high-dimensional BSDEs. One approach that combines BSDEs with machine learning is to convert the BSDEs problem to an optimal stopping problems and estimate the control term by feed-forward neural network. The objective function is calculated from the boundary condition of the BSDEs. The learning process are performed on sample-based batch from the forward SDE. For example, in (2.2.15) and (2.2.16), if we regard the initial value of Y_t and Z_t as controls which in turns to minimize the loss function $|Y_T - g(X_T)|^2$, then we obtain a control problem. Such idea defines the first kind of the learning schemes. In Weinan, Han, and Jentzen [118], they applied this scheme and proposed the algorithms in such a way: the approximation of $u(t,X_t)$ starts from random variable $\mathcal{U}_0$, then at each time step, a multi-layer neural networks $\mathcal{Z}(X_t;\theta_t)$ is established as an approximation for Z_t, the whole process is defined as

$$\inf_{\mathcal{U}_0,\{\theta_t\}_{0\le t\le T}} \mathbb{E}\left[\left|g(X_T)-Y_T\right|^2\right], \tag{4.2.1}$$

$$\text{s.t. } Y_0 = \mathcal{U}_0, \tag{4.2.2}$$

$$Z_t = \mathcal{Z}(t,X_t;\theta_t), \tag{4.2.3}$$

$$Y_{t+1} = Y_t - f(t,X_t,Y_t,) + Z_t dW_t, \tag{4.2.4}$$

$$X_{t+1} = X_t + \mu(t,X_t)\,dt + \sigma(t,X_t)\,dW_t. \tag{4.2.5}$$

$$\tag{4.2.6}$$

The same approach is applied in solving fully coupled FBSDEs in Ji, Peng, Peng, and Zhang [77], the problem is defined as below

$$X_{t_{i+1}} = X_{t_i} + \mu(t_i,X_{t_i},Y_{t_i})\,dt + \sigma(t_i,X_{t_i},Y_{t_i})\,dW_{t_i}, \tag{4.2.7}$$

$$Y_{t_{i+1}} = Y_{t_i} - f(t_i,Y_{t_i},Z_{t_i})\,dt + Z_{t_i} dW_{t_i}, \tag{4.2.8}$$

$$\tag{4.2.9}$$

where they define the loss function recursively by backward induction at each time step. If we regard both of Y_t and Z_t as controls, the optimal control problem can be defined in the following

variational form

$$\begin{aligned}
&\inf_{\{\mathcal{U}_t,\mathcal{Z}_t\}_{0\le t\le T}} \mathbb{E}\left[|g(X_T)-Y_T|^2+\sum_{i=1}^{T}|Y_{t_i}-\mathcal{U}_{t_i}|^2\,dt\right],\\
&\quad \text{s.t. } Y_{t_0}=\mathcal{U}_0,\\
&\qquad Z_t=\mathcal{Z}(t,\cdot;\theta_t),\\
&\qquad X_{t_{i+1}}=X_{t_i}+\mu\left(t_i,X_{t_i},\mathcal{U}_{t_i}\right)dt+\sigma\left(t_i,X_{t_i},\mathcal{U}_{t_i}\right)dW_{t_i},\\
&\qquad Y_{t_{i+1}}=Y_{t_i}-f\left(t_i,Y_{t_i},Z_{t_i}\right)dt+Z_{t_i}dW_{t_i}.
\end{aligned}$$

The first approach (4.2.1) is a scheme defined on the forward dynamic relation, while another scheme defined on the backward dynamic relation see Huré, Pham, and Warin [72], where they propose the algorithms

$$\begin{aligned}
&\inf_{\theta_t^{(1)},\theta_t^{(2)}} \mathbb{E}\left[|Y_{t+1}-Y_t+f\left(t,X_t,Y_t,Z_t\right)-Z_t dW_t|^2\right],\\
&\text{s.t. } \mathcal{U}_T=g\left(X_T\right),\\
&\qquad Y_t=\mathcal{U}(t,\cdot;\theta_t^{(1)}),\\
&\qquad Z_t=\sigma^T\nabla_x\mathcal{U}_t,\text{ or },\mathcal{Z}(t,\cdot,\theta_t^{(2)}),\\
&\qquad X_{t+1}=X_t+\mu\left(t,X_t\right)dt+\sigma\left(t,X_t\right)dW_t.
\end{aligned}$$

A possible topic for future research is to apply the machine learning with convolutional neural networks and the recurrent neural networks to solve the high-dimensional problem in BSDE framework. Considering the relationship that $Y_t=u(t,X_t)$ and $Z_t=\sigma^T\nabla_x u(t,X_t)$ from equation (2.2.18), we only need to build a deep neural network for Y_t and its first order derivatives which gives the approximation to Z_t. We use only one control u_t to approximate the target function Y_t. The learning problem can be defined in the following variational form

$$\begin{aligned}
&\inf_{Y_0,\{Z_t\}_{0\le t\le T}} \mathbb{E}\left[|g(X_T)-Y_T|^2\right],\\
&\quad \text{s.t. } Y_0=u(\cdot;\theta),\\
&\qquad Z_{t_i}=\sigma^T\nabla_x Y_t,\text{ or },\phi(\cdot;\theta)\\
&\qquad X_{t+1}=X_t+\mu\left(t,X_t\right)dt+\sigma\left(t,X_t\right)dW_i,\\
&\qquad Y_{t+1}=Y_t-f\left(t,Y_t,Z_t\right)dt+Z_t dW_t.
\end{aligned}$$

Applying the feed forward neural network for every $\theta_m\in\mathbb{R}^p$ and every $n\in\{0,1,...,N-1\}$ we may estimate $(X_{t_i},Y_{t_i},Z_{t_i})$ using the discrete from

$$\begin{aligned}
&Y_0^{m,i}=h\left(X_0^{m,i}\right),\\
&Z_{t_i}^{m,i}=\sigma^T\partial Y_{t_i}/\partial X_{t_i},\\
&Y_{t_{n+1}}^{m,i}=Y_{t_n}^{m,i}-f\left(t_n,X_{t_n}^{m,i},Y_{t_n}^{m,i},Z_{t_n}^{m,i}\right)dt+Z_{t_i}^{m,i}\Delta W_{t_i}.
\end{aligned}\tag{4.2.10}$$

To estimate $\sigma^T \partial Y_{t_i}/\partial X_{t_i}$, firstly we look into the dynamics of $Y_t^{t,x}$ in a small interval of time $[t, t+\Delta t]$

$$Y_{t+\Delta t}^{t,x} = Y_t^{t,x} - \int_t^{t+\Delta t} f\left(s, Y_s^{t,x}, Z_s^{t,x}\right) ds + \int_t^{t+\Delta t} Z_s^{t,x} dW_s.$$

Applying derivatives with respect ot x which is the value of X_t at time t to the above equation, we obtain

$$\partial_x Y_{t+\Delta t}^{t,x} = \partial_x Y_t^{t,x} - \int_t^{t+\Delta t} f_y \partial_x Y_t^{t,x} + f_z \partial_x Z_t^{t,x} ds + \int_t^{t+\Delta t} \partial_x Z_s^{t,x} dW_s, \tag{4.2.11}$$

where $f_y = \partial_y f(t,y,z)$ and $f_z = \partial_z f(t,y,z)$. Between Y_t and Z_t we have the following relationship under Lipschitz conditions,

$$Z_s^{t,x} = \sigma^T \left(X_s^{t,x}\right) \partial_x Y_s^{t,x} \left(\partial_x X_s^{t,x}\right)^{-1}. \tag{4.2.12}$$

Using equation (4.2.12), we can simplify equation (4.2.11) as the following discrete form

$$\partial_x Y_{t+\Delta t}^{t,x} \approx \sigma_t^{-T} \left(I - \Delta t f_y\left(t, Y_t^{t,x}, Z_t^{t,x}\right)\right) Z_t^{t,x} + \left(\Delta W_t - \Delta t f_z\left(t, Y_t^{t,x}, Z_t^{t,x}\right)\right) \partial_x Z_t^{t,x}. \tag{4.2.13}$$

Equation (4.2.13) shows us that we only need to calculate one derivative of $\partial_x Z_t,^{t,x}$ so as to obtain an approximation of $\partial_x Y_{t+\Delta t}^{t,x}$.

Through equations (4.2.11) and (4.2.13), we obtain the following approaches: suppose we have an estimator $\dot{Y}$ which is to estimate the value of $Y_0^{0,x}$ and we build a deep neural network $\{\dot{Z}_{t_i}\}_{i=0}^n$ as estimators for Z_{t_i}, $i = 0, \ldots n$, then we can build the model to satisfy the following conditions from (4.2.12) and (4.2.13)

$$\begin{aligned}
\sigma(x)\, \partial_x \dot{Y}_0^{0,x} =& \dot{Z}_0^{0,x}, \\
\dot{Z}_{t+\Delta t}^{t,x} =& \sigma^T \left(X_{t+\Delta t}^{t,x}\right) \partial_x Y_{t+\Delta t}^{t,x} \left(\partial_x X_s^{t,x}\right)^{-1}, \\
\partial_x Y_{t+\Delta t}^{t,x} =& \sigma_t^{-T} \left(I - \Delta t f_y\left(t, Y_t^{t,x}, \dot{Z}_t^{t,x}\right)\right) \dot{Z}_t^{t,x} \\
&+ \left(\Delta W_t - \Delta t f_z\left(t, Y_t^{t,x}, \dot{Z}_t^{t,x}\right)\right) \partial_x \dot{Z}_t^{t,x}, \\
Y_T^{0,x} =& g\left(X_T^{0,x}\right),
\end{aligned}$$

for all $t \in \{1, 2, \ldots, n\}$.

The main difficulties of implementing machine learning schemes in high dimensional BSDEs is the accuracy. By decreasing the versatility of the algorithm, we will increase the computational complexity in each sample point, which in turn will give more accurate results. The advantage of the machine learning in high dimensional BSDEs is the versatility and small computation cost comparing to Monte-Carlo method. As the model can be reused and be applied to different sample region while the Monte-Carlo can not unless the sample region is contained inside the simulation. The recent researches we mentioned in this section, they focus on define a good updating scheme from the boundary ot the solution either by a forward method using the BSDE or a backward method using the PDE. In the future research, we plan to interpret the BSDE scheme in backward

method and also try to combine the fast Fourier transform inside the updating steps.

4.3 The yield curve and bond price problem

We combine the equilibrium model with no-arbitrage model together and introduced an feasible and easy implementable method to obtain rigorous arbitrage-free in both theoretical perspective and practical perspective. We provide the closed-form to the Vašíček model with fully dynamic parameters and provide the estimation method to the expectation and variance. We introduced an advanced and efficient framework using deep neural networks to dynamically parameterize model parameter and present stable performance in both in-sample test and out-of-sample test. The particle filter in the recurrent neural networks has overcome the degeneracy problem and shows good efficiency in long sequential process. From our forecasting result, we show that yield prediction is also stable enough for forecasting coupon bonds. As the forecasting model, the Kalman filter shows the best performance in yield forecasting and the particle filter is very robust in model setup. In the practical views, we studied the distribution of predicted price errors and yield errors. We show that both of these error are not Gaussian style and there exists fat tail problem in the forecasting errors. We also quantify and present the average excess return as a measurement to the arbitrage opportunity. We provide various in-sample and out-of-sample tests under non-arbitrage regularization and arbitrage-free regularization where we find that the arbitrage-free regularization could improve the forecasting performance in short time horizons and decrease that in long time horizons.

4.3.1 The fat tail problem and excess kurtosis

The fat tail and excess kurtosis is usually two characteristics in financial time series and we have seen these problems in our forecasting results. As the volatility of most financial factors evolves over time, modeling the dynamic behavior of the state variables, yield curves and bond prices based on Gaussian distribution or generalized Gaussian distribution may be insufficient.

An inference method using bootstrapping method has been studied by Ruiz and Pascual [110] to overcome the excess kurtosis problem in financial time series. However, in out study of bond prices and yields, the observations containing high-dimensional features at each time step form a multi-variate time series which is more complicated to apply the traditional bootstrapping method. Therefore, a future direction could be extending the bootstrapping method on multi-variate time series. Another future direction could be improve importance sampling with a non-parametric distribution instead of the MGGD or change the measurement of the observation with a non-parametric distribution in the particle filter.

The fat tail problem and credit risk factors can be addressed at the same time by including an extra term J_t in our factor model. Proposed by Brigo et al. [16], if J_t is a jump process in mean-reverting dynamic, the fat tail problem will be improved. Such J_t process has the following dynamic

$$dX_t = \kappa_t (\theta_t - X_t) dt + \sigma_t dW_t + dJ_t, \tag{4.3.1}$$

where the jumps J_t are defined as

$$J_t = \sum_{i=1}^{N_t} G_i, \;\; dJ_t = G_{N_t} dN_t, \tag{4.3.2}$$

with Poisson process N_t of tensity γ and i.i.d random variable G_i modeling the i^{th} jump size, see Brigo et al. [16]. The extra jump term has significant effect to reduce the fat-tail. In our model, the fat-tail problem comes from the residual error between the yields Y_t and the state variables X_t and such problem is amplified in price error. Considering another approach, the residual error shows auto-correlation in time series, therefore, we could add the jump term to the yield process in stead of the state process

$$y_t = -\frac{B_\tau}{\tau} X_t + J_t, \tag{4.3.3}$$

and the residual shows we consider the residual term We assume that the jump size is determined from the residual from previous time step

$$G_{N_t} \sim y(X_{t-1}, t-1) - \hat{y}(X_{t-1}, t-1). \tag{4.3.4}$$

Therefore, the extra jump term J_t could be used to model the credit risk and improve the fat tail problem at the same time.

Chapter 5

Appendix

5.1 Proof of Lemma 1.4

Proof. We define the following continuous process X_t and by Bayes's rule we have

$$\begin{aligned} X_t &= \frac{1}{H_t}\mathbb{E}_{\mathbb{P}}\left[\int_{t\wedge\tau}^{\tau} H_s\left(c_s+wl_s\right)ds + H_\tau\left(B+\frac{w}{r}\right)\middle|\mathcal{F}_t\right] - \frac{w}{r} \\ &= \mathbb{E}_{\mathbb{P}_0}\left[\int_{t\wedge\tau}^{\tau} e^{-r(s-t)}\left(c_s+wl_s\right)ds + e^{-r(\tau-t)}\left(B+\frac{w}{r}\right)\middle|\mathcal{F}_t\right] - \frac{w}{r}, \end{aligned}$$

Obviously we have $X_0 = x$ and $X_\tau = B$ *a.s.*

By Fatou's lemma, the process inside the expectation holds for all positive B and any stopping time τ

$$\int_t^{\tau} e^{-r(s-t)}\left(c_s+wl_s\right)ds + e^{-r(\tau-t)}\left(B+\frac{w}{r}\right) \geq 0,\ \forall t\in[0,T],$$

which gives

$$X_t \geq -\frac{w}{r}.$$

Similarly to Karatzas and Wang [80], we define the following process

$$M(t) = e^{-rt}\left(X(t) + \frac{w}{r}\right) + \int_0^t e^{-rs}\left(c(s) + wl(s)\right) ds. \tag{5.1.1}$$

Then $M(t)$ in (5.1.1) is a martingale under $\mathbb{P}_0$

$$\begin{aligned}
\mathbb{E}_{\mathbb{P}_0}\left[M(t)\middle|\mathcal{F}(s)\right] =& \mathbb{E}_{\mathbb{P}_0}\left[\int_0^\tau e^{-rt}\left(c(t) + wl(t)\right) dt + e^{-r\tau}\left(B + \frac{w}{r}\right)\middle|\mathcal{F}(s)\right] \\
=& e^{-rs}\mathbb{E}_{\mathbb{P}_0}\left[\int_s^\tau e^{-r(t-s)}\left(c(t) + wl(t)\right) dt + e^{-r(\tau-s)}\left(B + \frac{w}{r}\right)\middle|\mathcal{F}(s)\right] \\
&+ \int_0^s e^{-rt}\left(c(t) + wl(t)\right) dt \\
=& e^{-rs}\left(X(s) + \frac{w}{r}\right) + \int_0^s e^{-rt}\left(c(t) + wl(t)\right) dt \\
=& M(s).
\end{aligned}$$

By martingale representation theorem, there exists a progressively measurable process $\phi(t)$ such that $\int_0^T \|\phi_t\|^2 dt < \infty$ with probability one and $M(t)$ can be written as

$$M(t) = x + \frac{w}{r} + \int_0^t \phi_s d\bar{B}_s. \tag{5.1.2}$$

Let $\pi_t = e^{rt}\phi_t/\sigma$, then we can verify from (1.1.3), (5.1.1) and (5.1.2) that $X_t = X_t^{(\pi)}$ a.e. □

5.2 Proof of Lemma 1.5

Proof. The convexity of $\bar{U}_1$ and $\bar{U}_2$ gives

$$\bar{U}_i(x) - \bar{U}_i(y) \geq \bar{U}_i'(y)(x-y), \quad \forall x,\ y > 0,\ \text{for } i = 1,2.$$

By the definition of $\bar{U}_1$ and $\bar{U}_2$ we obtain

$$\begin{aligned}
\bar{U}_1'(y) &= I_c(y) + wI_l(y), \\
\bar{U}_2'(\rho y) &= I\left(\rho y\right),
\end{aligned}$$

For any real number h satisfying $|h| << y$, we have

$$\begin{aligned}
&\bar{V}(x, y+h) - \bar{V}(x,y) \\
\geq& h\mathbb{E}\left[\int_0^{\tau_y^*} H_t \bar{U}_1'(Y_t^y) + H_{\tau_y^*}\left(\bar{U}_2'\left(\rho Y_{\tau_y^*}^y\right) - \frac{w}{r}\right)\right] + h(x + \frac{w}{r}) \\
=& -h\mathbb{E}\left[\int_0^{\tau_y^*} H_t\left(I_c(Y_t^y) + wI_l(Y_t^y)\right) dt + H_{\tau_y^*}\left(I\left(\rho Y_{\tau_y^*}^y\right) + \frac{w}{r}\right)\right] + h(x + \frac{w}{r}) \\
=& h\left(x - \mathbb{X}_{\tau_y^*}(y)\right)
\end{aligned}$$

$=0,$

which leads to

$$\lim_{h\to 0^-}\frac{\bar{V}(x,y+h)-\bar{V}(x,y)}{h}\leq 0\leq \lim_{h\to 0^+}\frac{\bar{V}(x,y+h)-\bar{V}(x,y)}{h}.$$

If $\bar{V}(y)$ is differentiable at y, then we have

$$\frac{\partial \bar{V}}{\partial y}(x,y)=\lim_{h\to 0^-}\frac{\bar{V}(x,y+h)-\bar{V}(x,y)}{h}=\lim_{h\to 0^+}\frac{\bar{V}(x,y+h)-\bar{V}(x,y)}{h}=0.$$

□

5.3 Proof of Theorem 1.6

Proof. Consider $\tau_y^*=\inf\left\{t\,\middle|\,Y_t^y\leq y^*\right\}$,. For any $x>0$, we know that there exists a $y>0$ satisfying (1.2.30) that $x=\mathbb{X}_{\tau_y^*}(y)$. By lemma (1.4), we know that there exists a portfolio process $\bar{\pi}$ with $X_{\tau_y^*}^{x,c^*,l^*,\pi^*}=I\big(\mathbb{Y}_{\tau_y^*}(x)\big)$, where $c^*=I_c\big(\mathbb{Y}_{\tau_y^*}(x)\big)$ and $l^*=I_l\big(\mathbb{Y}_{\tau_y^*}(x)\big)$. we obtain

$$\begin{aligned}
V(x)\geq & J(x;\tau_y^*)\\
=&\mathbb{E}\left[\int_0^{\tau_y^*}e^{-\rho t}U_1(c_t,l_t)dt+\frac{e^{-\rho\tau_y^*}}{\rho}U_2(kX_\tau^{0,x})\right]\\
=&\mathbb{E}\left[\int_0^{\tau_y^*}e^{-\rho t}\bar{U}_1(Y_t^y)dt+\frac{e^{-\rho\tau_y^*}}{\rho}\left(\bar{U}_2(\rho Y_{\tau_y^*}^y)-\rho\frac{w}{r}Y_{\tau_y^*}^y\right)\right]\\
&+y\mathbb{E}\left[\int_0^{\tau_y^*}H_t\left(I_c(Y_t^y)+wI_l(Y_t^y)\right)dt+H_{\tau_y^*}\left(I(\rho Y_{\tau_y^*}^y)+\frac{w}{r}\right)\right]\\
=&\mathbb{E}\left[\int_0^{\tau_y^*}e^{-\rho t}\bar{U}_1(Y_t^y)dt+\frac{e^{-\rho\tau_y^*}}{\rho}\left(\bar{U}_2(\rho Y_{\tau_y^*}^y)-\rho\frac{w}{r}Y_{\tau_y^*}^y\right)\right]+y(x+\frac{w}{r})\\
=&\bar{V}(x,y)\\
\geq&\inf_{y>0}\bar{V}(x,y).
\end{aligned}\tag{5.3.1}$$

Combine (5.3.1) and (1.2.29) we have proved the equality of (1.2.34)

$$V(x)=\inf_{y>0}\bar{V}(x,y).$$

Conversely, if for some pair (x,y) that satisfies (1.2.34) then such pair (x,y) also satisfies (1.2.28)

$$V(x;\tau_y^*)=\bar{V}(x,y;\tau_y^*).$$

For the optimal stopping time $\bar{\tau}_y^*$, we say it is an optimal stopping time to $V(x)$ as well. We can see this from below

$$V(x) = \inf_{y>0} \bar{V}(x,y) \leq \bar{V}(x,y) = \bar{V}(x,y;\tau_y^*) = V(x;\tau_y^*),$$

on the other hand, we have

$$V(x) = \bar{V}(x,y) \geq \bar{V}(x,y;\tau_y^*) = V(x;\tau_y^*),$$

which concludes that

$$V(x) = V(x;\tau_y^*).$$

Therefore, τ_y^* is the optimal stopping time to $V(x)$. □

5.4 Proof of Theorem 1.8

Proof. Assume that $\bar{V}^*(y)$ is the solution to (1.2.38) and $\frac{\partial \bar{V}^*}{\partial y}$ is absolutely continuous. First, we show that $\bar{V}^*$ is the solution to the dual problem (1.2.25). We apply Ito's formula to $e^{-\rho t}\bar{V}^*(Y_t)$ for any $t \geq 0$

$$e^{-\rho t}\bar{V}^*(Y_t) = \bar{V}^*(y) + \int_0^t e^{-\rho s}\theta Y_s \frac{\partial \bar{V}^*}{\partial y}(Y_s)dB_s + \int_0^t e^{-\rho s}\left(-\rho \bar{V}^*(Y_s) + \mathcal{L}\bar{V}^*(Y_s)\right)ds. \quad (5.4.1)$$

Hence, we obtain the following definitive equation for all t

$$\bar{V}^*(y) = \mathbb{E}\left\{ e^{-\rho t}\bar{V}^*(Y_t) + \int_0^t e^{-\rho s}\left(\rho \bar{V}^*(Y_s) - \mathcal{L}\bar{V}^*(Y_s)\right)ds \right\}. \quad (5.4.2)$$

Equation (1.2.38) implies $\bar{V}^*(Y_t) \geq \frac{1}{\rho}\bar{U}_2(\rho Y_t) - \frac{w}{r}Y_t$ and $\rho \bar{V}^*(Y_t) - \mathcal{L}\bar{V}^*(Y_t) \geq \bar{U}_1(Y_t)$ for all Y_t. For all stopping time τ, we have

$$\bar{V}^*(y) \geq \mathbb{E}\left\{ e^{-\rho\tau}\left(\frac{1}{\rho}\bar{U}_2(\rho Y_\tau) - \frac{w}{r}Y_\tau\right) + \int_0^\tau e^{-\rho s}\bar{U}_1(Y_s^y)ds \right\}.$$

Therefore, we obtain

$$\bar{V}^*(y) \geq \bar{V}(y).$$

Let $t = \tau^* = \inf\{t \geq 0 : Y_t^y \leq y^*\}$ in (5.4.2) and notice that $\bar{V}^*(Y_{\tau^*}) = \frac{1}{\rho}\bar{U}_2(\rho Y_{\tau^*}) - \frac{w}{r}Y_{\tau^*}$ and $\left(\rho \bar{V}^*(Y_s) - \mathcal{L}\bar{V}^*(Y_s)\right) = \bar{U}_1(Y_s^y)$, hence we see that

$$\bar{V}^*(y) = \mathbb{E}\left\{ e^{-\rho\tau^*}\left(\frac{1}{\rho}\bar{U}_2(\rho Y_{\tau^*}) - \frac{w}{r}Y_{\tau^*}\right) + \int_0^{\tau^*} e^{-\rho s}\bar{U}_1(Y_s^y)ds \right\}$$

$$\leq \bar{V}(y).$$

Therefore, $\bar{V}(y) = \bar{V}^*(y)$ and τ^* is the optimal solution to dual problem (1.2.25).

Consider any $y > 0$ and any stopping time τ. If $P(\tau < \tau^*) > 0$, then we have $Y_\tau > y^*$ and

$$\begin{aligned}
&\mathbb{E}\left\{ e^{-\rho\tau}\left(\frac{1}{\rho}\bar{U}_2(\rho Y_\tau) - \frac{w}{r}Y_\tau\right) + \int_0^\tau e^{-\rho s}\bar{U}_1(Y_s^y)ds \right\} \\
<&\mathbb{E}\left\{ e^{-\rho\tau}\bar{V}(Y_\tau) + \int_0^\tau e^{-\rho s}\left(\rho\bar{V}(Y_s) - \mathcal{L}\bar{V}(Y_s)\right)ds \right\} \\
=&\bar{V}(y),
\end{aligned}$$

which implies τ is not optimal in problem (1.2.25). Assuming that $P(\tau > \tau^*) > 0$, for the process $\tilde{Y}_t = Y_{\tau^*+t} - Y_t$ and any $\varepsilon > 0$, we have $\inf_{t\in[0,\varepsilon]}\tilde{Y}_t < 0$ a.s.. It follows from (5.4.2) that $\bar{V}(Y_t) \geq \frac{1}{\rho}\bar{U}_2(Y_t) - \frac{w}{r}Y_t$ and $\rho\bar{V}(Y_t) - \mathcal{L}\bar{V}(Y_t) > \bar{U}_1(Y_t)$ a.s. on $(0,\infty)\setminus y^*$ indicating that τ is not optimal in (1.2.25). Therefore, τ^* is the unique optimal stopping time to (1.2.25). □

5.5 Proof of Lemma 1.9

Proof. We denote

$$\bar{U}(x) = \bar{U}_1(x) + \frac{n(p_2')}{\rho}\bar{U}_2(\rho x) + wx,$$

and

$$F(x) = \int_{+\infty}^{x} \frac{\bar{U}(z)}{z^{n_1+1}}(z)dz$$

If $0 < p_1' < p_2' < 1$, then there is a unique $y_0 \in (0,\infty)$ such that $\bar{U}(y_0) = 0$ and

$$\begin{cases} \bar{U}(y) > 0, & y_0 < y \\ \bar{U}(y) < 0, & 0 < y < y_0. \end{cases}$$

Since

$$\lim_{x\to 0^+}\frac{\bar{U}(x)}{x^{n_1+1}} = \lim_{x\to 0^+} x^{p_1'-(1+n_1)}\left(\tilde{A} - \frac{n(p_2')}{\rho p_2' k^{p_2'}}x^{p_2'-p_1'}\right) = -\infty,$$

and

$$\lim_{x\to+\infty}\frac{\bar{U}(x)}{x^{n_1+1}} = 0^+,$$

that implies

$$\lim_{x\to 0^+} F(x) = +\infty,$$

and

$$\lim_{x\to +\infty} F(x) = 0^-.$$

Thus, there exists a $y^* \in (0, y_0)$ such that $F(y^*) = 0$.

Suppose there exists another $y_* \in (0, y_0)$ such that $F(y_*) = 0$, then we get

$$\int_{y_*}^{y^*} \frac{\bar{U}(z)}{z^{n_1+1}} dz = 0,$$

since $\bar{U}$ is negative on $(0, y_0)$, we must have $y_* = y^*$. Therefore, the solution of y^* is unique and

$$\begin{cases} F(y) \geq 0, & y \leq y^* \\ F(y) \leq 0, & y \geq y^*. \end{cases}$$

□

5.6 Proof of Lemma 1.10

Proof. First, we show that the following ODE with the boundary has a unique solution

$$-\rho\phi(y) + (\rho - r)y\phi(y)' + \frac{1}{2}\theta^2 y^2 \phi(y)'' + \bar{U}_1(y) = 0. \tag{5.6.1}$$

We first consider the general solution to the following ODE

$$-\rho\phi(y) + (\rho - r)y\phi(y)' + \frac{1}{2}\theta^2 y^2 \phi''(y) = 0. \tag{5.6.2}$$

Solving (5.6.2), we obtain

$$\phi(y) = C_1 y^{n_1} + C_2 y^{n_2}, \tag{5.6.3}$$

where C_1 and C_2 are some constant that is determined from boundary value y^*, $n_1 > 1$ and $n_2 \leq -\frac{2(\rho-r)}{\theta^2} < 0$ are the two roots of function $n(x)$

$$n(x) = \frac{1}{2}\theta^2 x^2 + (\rho - r - \frac{1}{2}\theta^2)x - \rho. \tag{5.6.4}$$

A particular solution for (5.6.1) is given by

$$\phi(y) = \frac{2}{\theta^2(n_1 - n_2)} \left(y^{n_1} \int \frac{-\bar{U}_1(y)}{y^{n_1+1}} dy - y^{n_2} \int \frac{-\bar{U}_1(y)}{y^{n_2+1}} dy \right). \tag{5.6.5}$$

Combining (5.6.3) and (5.6.5), we have general solution to (5.6.1),

$$\phi(y) = C_1 y^{n_1} + C_2 y^{n_2} + \frac{2}{\theta^2(n_1-n_2)}\left(y^{n_1}\int_{y^*}^{y}\frac{-\bar{U}_1(z)}{z^{n_1+1}}dz - y^{n_2}\int_{y^*}^{y}\frac{-\bar{U}_1(z)}{z^{n_2+1}}dz\right). \tag{5.6.6}$$

For the boundary problem, We show that for some positive y^* the solution given in (5.6.6) satisfies the boundary condition $\phi(y) = \frac{1}{\rho}\bar{U}_2(\rho y) - \frac{w}{r}y$, for $0 < y \le y^*$. By investigating the convexity of $\bar{V}$

$$\begin{aligned}\phi'(y) = &\left(C_1 n_1 + \frac{2n_1}{\theta^2(n_1-n_2)}\int_{y^*}^{y}\frac{-\bar{U}_1(z)}{z^{n_1+1}}dz\right)y^{n_1-1}\\ &+\left(C_2 n_2 - \frac{2n_2}{\theta^2(n_1-n_2)}\int_{y^*}^{y}\frac{-\bar{U}_1(z)}{z^{n_2+1}}dz\right)y^{n_2-1},\end{aligned}$$

we find that $\phi(y)$ is strictly convex and decreasing. Thus the first term containing y^{n_1-1} in (5.6.6) must be zero as $y \to +\infty$

$$\lim_{y\to+\infty} C_1 n_1 + \frac{2n_1}{\theta^2(n_1-n_2)}\int_{y^*}^{y}\frac{-\bar{U}_1(z)}{z^{n_1+1}}dz = 0,$$

and we obtain

$$C_1 = \frac{2}{\theta^2(n_1-n_2)}\int_{+\infty}^{y^*}\frac{-\bar{U}_1(z)}{z^{n_1+1}}dz. \tag{5.6.7}$$

Use (5.6.7) and simplify (5.6.6) with some constant C.

$$\phi(y) = Cy^{n_2} + \frac{2y^{n_1}}{\theta^2(n_1-n_2)}\int_{+\infty}^{y}\frac{-\bar{U}_1(z)}{z^{n_1+1}}dz - \frac{2y^{n_2}}{\theta^2(n_1-n_2)}\int_{y^*}^{y}\frac{-\bar{U}_1(z)}{z^{n_2+1}}dz. \tag{5.6.8}$$

Applying the smooth connected conditions at y^*, we obtain

$$C = C(y^*) = \frac{y^{*-n_2}}{n_1-n_2}\left((n_1-p_2')\frac{1}{\rho}\bar{U}_2(\rho y^*) - (n_1-1)\frac{w}{r}y^*\right), \tag{5.6.9}$$

and

$$\frac{2y^{*n_1}}{\theta^2}\int_{+\infty}^{y^*}\frac{-\bar{U}_1(z)}{z^{n_1+1}}dz = y^*U_2'(\rho y^*) - \frac{n_2}{\rho}\bar{U}_2(\rho y^*) - (1-n_2)\frac{w}{r}y^*. \tag{5.6.10}$$

Since we can rewrite

$$y^*U_2'(\rho y^*) - \frac{n_2}{\rho}\bar{U}_2(\rho y^*) = \frac{p_2'-n_2}{\rho}\bar{U}_2(\rho y^*) = \frac{2y^{*n_1}}{\theta^2}\int_{+\infty}^{y^*}\frac{\frac{n(p_2')}{\rho}\bar{U}_2(\rho z)}{z^{n_1+1}}dz, \tag{5.6.11}$$

and

$$(1-n_2)\frac{w}{r}y^* = \frac{(1-n_2)(1-n_1)}{r}\frac{wy^*}{1-n_1} = \frac{2y^{*n_1}}{\theta^2}\int_{+\infty}^{y^*}\frac{n(1)\frac{w}{r}z}{z^{n_1+1}}dz = -\frac{2y^{*n_1}}{\theta^2}\int_{+\infty}^{y^*}\frac{wz}{z^{n_1+1}}dz. \quad (5.6.12)$$

We simplify (5.6.10) using (5.6.11) and (5.6.12)

$$\frac{2y^{*n_1}}{\theta^2}\int_{+\infty}^{y^*}\frac{\bar{U}_1(z)+\frac{n(p_2')}{\rho}\bar{U}_2(\rho z)+wz}{z^{n_1+1}}dz = 0. \quad (5.6.13)$$

By Lemma 1.9, there exists a unique $y^* > 0$ that solves equation (5.6.13). Therefore, $\phi(y)$ with C given in (5.6.9) and the value y^* determined by (5.6.13) satisfies the boundary condition.

Second, we show that $\phi(y)$ and y^* are the optimal solutions to the dual problem by showing that $\phi(y)$ and y^* solve the variational inequalities. We denote

$$\Phi(y) = \phi(y) - \left(\frac{1}{\rho}\bar{U}_2(\rho y) - \frac{w}{r}y\right).$$

For $0 < y < y^*$, we have

$$\begin{aligned}
-\rho\phi(y) + \mathcal{L}\phi(y) + \bar{U}_1(y) &= -\rho\left(\frac{1}{\rho}\bar{U}_2(\rho x) + \frac{w}{r}x\right) + \mathcal{L}\left(\frac{1}{\rho}\bar{U}_2(\rho x) + \frac{w}{r}x\right) + \bar{U}_1(y) \\
&= \bar{U}_1(y) + \frac{n(p_2')}{\rho}\bar{U}_2(\rho y) + wy \\
&= \bar{U}(y) \\
&\leq 0. \quad (5.6.14)
\end{aligned}$$

For $y^* \leq y$, we have

$$\begin{aligned}
-\rho\Phi(y) + \mathcal{L}\Phi(y) &= -\rho\left(\phi(y) - \frac{1}{\rho}\bar{U}_2(\rho y) + \frac{w}{r}y\right) + \mathcal{L}\left(\phi(y) - \frac{1}{\rho}\bar{U}_2(\rho y) + \frac{w}{r}y\right) \\
&= -\rho\phi(y) + \mathcal{L}\phi(y) - \left(\frac{n(p_2')}{\rho}\bar{U}_2(\rho y) + wy\right) \\
&= -\left(\bar{U}_1(y) + \frac{n(p_2')}{\rho}\bar{U}_2(\rho y) + wy\right) \\
&= -\bar{U}(y). \quad (5.6.15)
\end{aligned}$$

Since $\Phi(y^*) = 0$ and $\Phi'(y^*) = 0$, the (5.6.15) implies

$$\Phi(y) = \frac{2y^{n_1}}{\theta^2(n_1-n_2)}\int_{y^*}^{y}\frac{-\bar{U}(z)}{z^{n_1+1}}dz - \frac{2y^{n_2}}{\theta^2(n_1-n_2)}\int_{y^*}^{y}\frac{-\bar{U}(z)}{z^{n_2+1}}dz.$$

Denote

$$\psi(y) = y^{-n_2}\Phi(y) = \frac{2y^{n_1-n_2}}{\theta^2(n_1-n_2)}\int_{y^*}^{y}\frac{-\bar{U}(z)}{z^{n_1+1}}dz - \frac{2}{\theta^2(n_1-n_2)}\int_{y^*}^{y}\frac{-\bar{U}(z)}{z^{n_2+1}}dz. \quad (5.6.16)$$

Taking derivative to (5.6.16), we obtain

$$\begin{aligned}\psi'(y) =&\frac{2y^{n_1-n_2-1}}{\theta^2}\int_{y^*}^{y}\frac{-\bar{U}(z)}{z^{n_1+1}}dz-\frac{2y^{n_1-n_2}}{\theta^2(n_1-n_2)}\cdot\frac{\bar{U}(y)}{y^{n_1+1}}+\frac{2}{\theta^2(n_1-n_2)}\cdot\frac{\bar{U}(y)}{y^{n_2+1}}\\ =&\frac{2y^{n_1-n_2-1}}{\theta^2}\int_{y^*}^{y}\frac{-\bar{U}(z)}{z^{n_1+1}}dz\\ =&-\frac{2y^{n_1-n_2-1}}{\theta^2}F(y).\end{aligned}$$

Since $F(y)\leq 0$ for $y\geq y^*$, we have

$$\psi'(y)\geq 0,$$

which implies $\psi(y)$ is monotone increasing function on $[y^*,\infty]$.

$$\Phi(y)=y^{n_2}\psi(y)\geq y^{n_2}\psi(y^*)=0.$$

Therefore, we have $\phi(x)\geq\left(\frac{1}{\rho}\bar{U}_2(\rho x)-\frac{w}{r}x\right)$ for $y\in[y^*,\infty)$. □

5.7 Proof of Theorem 1.12

Proof. The optimal stopping time $\bar{\tau}$ is a straightforward result of Theorem 10.4.1 of Øksendal [102]. The optimal consumption and labor income are directly results from the dual problem. So we only need to show the optimal portfolio processes is generated by the optimal wealth processes (1.2.45). Applying Itô's formula to the optimal wealth process (1.2.45), we obtain

$$\begin{aligned}dX_t^* =&\left(-(\rho-r)Y_t\bar{V}''(Y_t)-\frac{1}{2}\theta^2Y_t^2\bar{V}'''(Y_t)\right)dt+\theta Y_t\bar{V}''(Y_t)dB_t\\ =&-\left(Cn_2\left((\rho-r)(n_2-1)+\frac{1}{2}\theta^2(n_2-1)(n_2-2)\right)Y_t^{n_2-1}\right.\\ &+\frac{2n_1Y_t^{n_1-1}}{\theta^2(n_1-n_2)}\left((\rho-r)(n_1-1)+\frac{1}{2}\theta^2(n_1-1)(n_1-2)\right)\int_{+\infty}^{Y_t}\frac{-\bar{U}_1(z)}{z^{n_1+1}}dz\\ &-\frac{2n_2Y_t^{n_2-1}}{\theta^2(n_1-n_2)}\left((\rho-r)(n_2-1)+\frac{1}{2}\theta^2(n_2-1)(n_2-2)\right)\int_{y^*}^{Y_t}\frac{-\bar{U}_1(z)}{z^{n_2+1}}dz\\ &\left.+\frac{2\bar{U}_1(Y_t)}{Y_t}-\bar{U}_1'(Y_t)\right)dt+\theta Y_t\bar{V}''dB_t\\ =&\left(rX\left(X_t^*+\frac{w}{r}\right)+\bar{U}_1'(Y_t)\right)dt+\theta Y_t\bar{V}''dB_t\\ &-\left(Cn_2\left((\rho-r)n_2-\rho+\frac{1}{2}\theta^2(n_2-1)(n_2-2)\right)Y_t^{n_2-1}\right.\end{aligned}$$

$$
\begin{aligned}
&+\frac{2n_1Y_t^{n_1-1}}{\theta^2(n_1-n_2)}\left((\rho-r)n_1-\rho+\frac{1}{2}\theta^2(n_1-1)(n_1-2)\right)\int_{+\infty}^{Y_t}\frac{-\bar{U}_1(z)}{z^{n_1+1}}dz\\
&-\frac{2n_2Y_t^{n_2-1}}{\theta^2(n_1-n_2)}\left((\rho-r)n_2-\rho+\frac{1}{2}\theta^2(n_2-1)(n_2-2)\right)\int_{y^*}^{Y_t}\frac{-\bar{U}_1(z)}{z^{n_2+1}}dz\\
&+\frac{2\bar{U}_1(Y_t)}{Y_t}\Bigg)dt\\
=&(rX_t^*+w+\bar{U}_1'(Y_t))dt+\theta Y_t\bar{V}''dB_t\\
&-\Bigg(Cn_2\left(-\frac{1}{2}\theta^2n_2(n_2-1)+\frac{1}{2}\theta^2(n_2-1)(n_2-2)\right)Y_t^{n_2-1}\\
&+\frac{2n_1Y_t^{n_1-1}}{\theta^2(n_1-n_2)}\left(-\frac{1}{2}\theta^2n_1(n_1-1)+\frac{1}{2}\theta^2(n_1-1)(n_1-2)\right)\int_{+\infty}^{Y_t}\frac{-\bar{U}_1(z)}{z^{n_1+1}}dz\\
&-\frac{2n_2Y_t^{n_2-1}}{\theta^2(n_1-n_2)}\left(-\frac{1}{2}\theta^2n_2(n_2-1)+\frac{1}{2}\theta^2(n_2-1)(n_2-2)\right)\int_{y^*}^{Y_t}\frac{-\bar{U}_1(z)}{z^{n_2+1}}dz\\
&+\frac{2\bar{U}_1(Y_t)}{Y_t}\Bigg)dt\\
=&(rX_t^*+w+\bar{U}_1'(Y_t))dt+\theta Y_t\bar{V}''dB_t\\
&+\theta^2Y_t\Bigg(Cn_2(n_2-1)Y_t^{n_2-2}-\frac{2\bar{U}_1(Y_t)}{\theta^2Y_t^2}\\
&+\frac{2n_1(n_1-1)Y_t^{n_1-2}}{\theta^2(n_1-n_2)}\int_{+\infty}^{Y_t}\frac{-\bar{U}_1(z)}{z^{n_1+1}}dz-\frac{2n_2(n_2-1)Y_t^{n_2-2}}{\theta^2(n_1-n_2)}\int_{y^*}^{Y_t}\frac{-\bar{U}_1(z)}{z^{n_2+1}}dz\Bigg)dt\\
=&\left(rX_t^*+(r-r)\frac{\theta}{\sigma}Y_t\bar{V}''+\bar{U}_1'(Y_t)+w\right)dt+\sigma\frac{\theta}{\sigma}Y_t\bar{V}''dB_t. \qquad (5.7.1)
\end{aligned}
$$

We replace the last term in (5.7.1) using that fact that

$$
\begin{aligned}
\pi_t^*=&\frac{\theta}{\sigma}Y_t\bar{V}''\\
=&\frac{\theta}{\sigma}\Bigg(Cn_2(n_2-1)Y_t^{n_2-1}-\frac{2\bar{U}_1(Y_t)}{\theta^2Y_t}\\
&+\frac{2n_1(n_1-1)Y_t^{n_1-1}}{\theta^2(n_1-n_2)}\int_{+\infty}^{Y_t}\frac{-\bar{U}_1(z)}{z^{n_1+1}}dz-\frac{2n_2(n_2-1)Y_t^{n_2-1}}{\theta^2(n_1-n_2)}\int_{y^*}^{Y_t}\frac{-\bar{U}_1(z)}{z^{n_2+1}}dz\Bigg),
\end{aligned}
$$

and

$$
\bar{U}_1(Y_t)'=-c_t^*-l_t^*w,
$$

then we have

$$dX_t^* = (rX_t^* + (r-r)\pi^* - c^* + (1-l^*)w)\,dt + \sigma\pi^* dB_t.$$

So the optimal wealth process and optimal controls are verified. □

5.8 Proof of Theorem 2.4

Proof. Firstly, we refer to the solution given by Drăgulescu and Yakovenko [42]. The time evolution of the probability density function $P_t(x,v|x_i,v_i)$ is governed by the following Fokker Planck equation,

$$\frac{\partial}{\partial t}P = \kappa\frac{\partial}{\partial v}((v-\theta)P) + \left(\frac{1}{2}\frac{\partial}{\partial x} + \rho\sigma\frac{\partial^2}{\partial x\partial v} + \frac{1}{2}\frac{\partial^2}{\partial x^2}\right)(vP) + \frac{\sigma^2}{2}\frac{\partial^2}{\partial v^2}(vP), \tag{5.8.1}$$

with initial given by a product of 2 delta functions

$$P_{t=t_i}(x,v|x_i,v_i) = \delta(x-x_i)\delta(v-v_i). \tag{5.8.2}$$

For simplicity, in the following proof, x is stand for $x-x_i$.

By introducing a parameter u with respect to Fourier transform on x

$$\bar{P}_t(u,v|v_i) = \int_{\mathbb{R}} e^{-2\pi \mathrm{i}ux}P_t(x,v|v_i)dx, \tag{5.8.3}$$

and a parameter s with respect to Laplace transform on v

$$\tilde{P}_t(u,s|v_i) = \int_0^{+\infty} e^{-sv}\bar{P}_t(u,v|v_i)dv), \tag{5.8.4}$$

we obtain the following Riccati type PDE with constant coefficient

$$\left[\frac{\partial}{\partial t} + \left(\frac{\sigma^2}{2}s^2 + \alpha s + \beta\right)\frac{\partial}{\partial s}\right]\tilde{P} = -\kappa\theta s\tilde{P}, \tag{5.8.5}$$

with initial

$$\tilde{P}_{t=t_i}(u,s|x_i,v_i) = e^{-2\pi \mathrm{i}ux_i - sv_i}, \tag{5.8.6}$$

where the parameter functions α and β are given by

$$\alpha = 2\pi \mathrm{i}\rho\sigma u + \kappa,$$
$$\beta = \mathrm{i}\pi u - 2\pi^2 u^2.$$

The solution to(5.8.5) is given by

$$\tilde{P}_t(u,s|v_i) = \exp\left(-\tilde{s}(t_i)v_i + \frac{\kappa\theta\,(\alpha-\lambda)\,\Delta t_i}{\sigma^2} - \frac{2\kappa\theta}{\sigma^2}\ln\frac{\gamma-e^{-\lambda t}}{\gamma-e^{-\lambda t_i}}\right), \tag{5.8.7}$$

where

$$\begin{aligned}
\Delta t_i &= t - t_i,\\
\lambda &= \sqrt{\alpha^2(u) - 2\sigma^2\beta},\\
\gamma &= 1 + \frac{2\lambda}{\sigma^2 s + \alpha - \lambda},\\
\tilde{s}(\tau) &= \frac{2\lambda}{\sigma^2}\frac{1}{Ce^{\lambda(t-\tau)}-1} - \frac{\alpha-\lambda}{\sigma^2},
\end{aligned}$$

and $\tilde{s}(\tau)$ is obtained from the following characteristic differential equation

$$\frac{\partial}{\partial\tau}\tilde{s}(\tau) = \frac{\sigma^2}{2}\tilde{s}^2(\tau) + \alpha\tilde{s}(\tau) + \beta, \tag{5.8.8}$$

with the boundary condition $\tilde{s}(t) = s$ at $\tau = t$.

Second, we consider the behavior of x_t and v_t in a short time interval $\Delta t_i = t - t_i$. Then equation (5.8.7) can be simplified to

$$\tilde{P}_t(u,s|v_i) = \exp\left(-\tilde{s}(t_i)v_i - \kappa\theta\Delta t_i s\right), \tag{5.8.9}$$

and equation (5.8.8) gives

$$\tilde{s}(t_i) = -\beta\Delta t_i - \frac{\sigma^2}{2}s^2\Delta t_i - (\alpha\Delta t_i - 1)\,s. \tag{5.8.10}$$

Substitute (5.8.10) into (5.8.9) and apply inverse Laplace transform on $\tilde{P}$ and retrieve $\bar{P}_t(u,v|x_i,v_i)$, we obtain

$$\begin{aligned}
\bar{P}_t(u,v|v_i) =& \mathcal{L}^{-1}\left[\tilde{P}_t(u,s|v_i)\right](v)\\
=& \frac{1}{2\pi\mathrm{i}}\int_{-\mathrm{i}\infty}^{+\mathrm{i}\infty} e^{sv}\exp\left(\frac{\sigma^2 v_i\Delta t_i}{2}s^2 + (\alpha v_i\Delta t_i - v_i - \kappa\theta\Delta t_i)s + \beta v_i\Delta t_i\right)ds\\
=& \frac{1}{2\pi}\int_{-\infty}^{+\infty}\exp\left(-\frac{\sigma^2 v_i\Delta t_i}{2}y^2 + \mathrm{i}(\alpha v_i\Delta t_i + v - v_i - \kappa\theta\Delta t_i)y + \beta v_i\Delta t_i\right)dy\\
=& \frac{1}{\sqrt{2\pi\sigma^2 v_i\Delta t_i}}\exp\left(-\frac{(\alpha v_i\Delta t_i + v - v_i - \kappa\theta\Delta t_i)^2}{2\sigma^2 v_i\Delta t_i} + \beta v_i\Delta t_i\right).
\end{aligned} \tag{5.8.11}$$

We apply inverse Fourier transform to (5.8.11) and retrieve $P_t(x,v|v_i)$, and to make it short, we

denote $\iota = v - v_i - \kappa(\theta - v_i)\Delta t_i$

$$
\begin{aligned}
P_t(x, v|v_i) =& \mathcal{F}^{-1}\left[\bar{P}_t(u, v|v_i)\right](x) \\
=& \frac{1}{\sqrt{2\pi\sigma^2 v_i \Delta t_i}} \int_{-\infty}^{+\infty} e^{2\pi \mathrm{i} u x} \exp\left(-\frac{\left(\alpha v_i \Delta t_i + v - v_i - \kappa\theta\Delta t_i\right)^2}{2\sigma^2 v_i \Delta t_i} + \beta v_i \Delta t_i \right) du \\
=& \frac{1}{\sqrt{2\pi\sigma^2 v_i \Delta t_i}} \int_{-\infty}^{+\infty} \exp\left(-\frac{\left(2\pi\mathrm{i}\sigma\rho v_i \Delta t_i u + \iota\right)^2}{2\sigma^2 v_i \Delta t_i} + \pi\mathrm{i}\left(2x + v_i\Delta t_i\right)u - 2\pi^2 v_i \Delta t_i u^2 \right) du \\
=& \frac{1}{\sqrt{2\pi\sigma^2 v_i \Delta t_i}} \int_{-\infty}^{+\infty} \exp\left(-\left(1-\rho^2\right) v_i \Delta t_i u^2 + \pi\mathrm{i}\left(2x + v_i\Delta t_i - \frac{2\rho}{\sigma}\iota\right)u \right. \\
& \qquad \left. - \frac{1}{2\sigma^2 v_i \Delta t_i}\iota^2 \right) du \\
=& \frac{1}{\sqrt{2\pi\sigma^2 v_i \Delta t_i}} \frac{1}{\sqrt{2\pi\left(1-\rho^2\right) v_i \Delta t_i}} \exp\left(-\frac{\left(x + \frac{1}{2}v_i\Delta t_i - \frac{\rho}{\sigma}\iota\right)^2 + \frac{1-\rho^2}{\sigma^2}\iota^2}{2\left(1-\rho^2\right) v_i \Delta t_i} \right) \\
=& \frac{1}{2\pi\sigma\sqrt{\left(1-\rho^2\right)} v_i \Delta t_i} \exp\left(-\frac{\sigma^2\left(x + \frac{1}{2}v_i\Delta t_i\right)^2 - 2\rho\sigma\iota\left(x + \frac{1}{2}v_i\Delta t_i\right) + \iota^2}{2\sigma^2\left(1-\rho^2\right) v_i \Delta t_i} \right) \\
=& \frac{|\Sigma(v_i)|^{-\frac{1}{2}}}{2\pi\Delta t_i} \exp\left(-\frac{\left(X - \eta(v_i)\Delta t_i\right)^T \Sigma^{-1}(v_i)\left(X - \eta(v_i)\Delta t_i\right)}{2\Delta t_i} \right),
\end{aligned}
$$

where $X = (x, v - v_i)^T$ and

$$
\begin{aligned}
X &= \begin{pmatrix} x \\ v - v_i \end{pmatrix}, \\
\eta(v) &= \begin{pmatrix} -\frac{1}{2}v, \\ \kappa(\theta - v) \end{pmatrix}, \\
\Sigma(v) &= \begin{pmatrix} v & \sigma\rho v \\ \sigma\rho v & \sigma^2 v \end{pmatrix}.
\end{aligned}
$$

Finally, we replace x by $x - x_i$, which gives $X = (x - x_i, v - v_i)$. The above result shows that, in short time Δt_i, the conditional probability density of the joint process X evolves in bi-variate Gaussian manner.

□

5.9 Proof of Theorem 2.6

Proof. We solve the PDE (2.4.39)

$$
\frac{\partial P_i}{\partial t} + (r + c_i v)\frac{\partial P_i}{\partial x} + (a - b_i v)\frac{\partial P_i}{\partial v} + \frac{1}{2}v\frac{\partial^2 P_i}{\partial x^2} + \frac{\sigma^2}{2}v\frac{\partial^2 P_i}{\partial v^2} + \rho\sigma v\frac{\partial^2 P_i}{\partial x \partial v}\psi = 0, \tag{5.9.1}
$$

with boundary condition where $U=(p,q)^T$ and $X=(x,v)^T$

$$P_i(T,U,X)=e^{\mathrm{i}U^TX}=e^{\mathrm{i}(px+qv)}. \tag{5.9.2}$$

According to the form of the initial condition and some experience with PDE function, we make an ansatz for $\psi(t,p,q,x,v)$ in the following form

$$P_i(t,p,q,x,y)=\exp\left(A_i(t)x+B_i(t)v+C_i(t)\right), \tag{5.9.3}$$

where functions $A(t)$, $B(t)$ and $C(t)$ depend only on t and satisfy boundary conditions $A(T)=\mathrm{i}p$, $B(T)=\mathrm{i}q$ and $C(T)=0$.

Applying the ansatz to the PDE, we simplify and obtain the following ODE

$$A_i'(t)x+\left(B_i'(t)+\frac{1}{2}A_i^2+c_iA_i-b_iB_i+\frac{1}{2}\sigma^2B_i^2+\rho\sigma A_iB_i\right)v+C_i'(t)+rA_i(t)+aB_i(t)=0. \tag{5.9.4}$$

If the ansatz ODE (5.9.4) hold for all $x\in\mathbb{R}$, $v\in(0,\infty)$ and $t\in[0,T]$, then we must have

$$A'(t)=0, \tag{5.9.5}$$

$$B'(t)+\frac{1}{2}A^2+c_iA-b_iB+\frac{\sigma^2}{2}B^2+\rho\sigma AB=0, \tag{5.9.6}$$

$$C'(t)+rA(t)+aB(t)=0, \tag{5.9.7}$$

so we obtain

$$A(t)=\mathrm{i}p. \tag{5.9.8}$$

Replace equation (5.9.8) in equation (5.9.6) and simplify

$$B'(t)+\frac{1}{2}\sigma^2B^2(t)-\left(b_i-\mathrm{i}\sigma\rho p\right)B(t)-\frac{p^2-2\mathrm{i}c_ip}{2}=0. \tag{5.9.9}$$

Equation (5.9.9) is Riccati equation with constant coefficients. Solve it with boundary $B(T)=\mathrm{i}q$, we obtain

$$B(t)=\frac{\mathrm{i}\gamma}{\sigma^2}\tan\left(\frac{\mathrm{i}\gamma}{2}(T-t)+\vartheta\right)+\frac{b_i-\mathrm{i}\sigma\rho p}{\sigma^2}, \tag{5.9.10}$$

where

$$\begin{aligned}
\vartheta&=\arctan\left(\frac{\mathrm{i}\lambda}{\gamma}\right),\\
\gamma&=\sqrt{\sigma^2\left(p^2-2\mathrm{i}c_ip\right)+\left(b_i-\mathrm{i}\sigma\rho p\right)^2},\\
\lambda&=b_i-\mathrm{i}\sigma\rho p-\mathrm{i}\sigma^2q.
\end{aligned}$$

Solve equation (5.9.7) with boundary $C(T)=0$ and simplify it with notation $\tau = T-t$, we obtain

$$\begin{aligned}
C(t) =& -\int_T^t (\mathrm{i}pr + aB(s))\,ds \\
=& \mathrm{i}pr(T-t) + \frac{a(b_i - \mathrm{i}p\rho\sigma)}{\sigma^2}(T-t) - \frac{2a}{\sigma^2}\ln\frac{\cos\left(\frac{\mathrm{i}\gamma}{2}(T-t)+\vartheta\right)}{\cos(\vartheta)} \\
=& \mathrm{i}pr\tau + \frac{a(b_i - \mathrm{i}p\rho\sigma)}{\sigma^2}\tau - \frac{2a}{\sigma^2}\ln\frac{\cos\left(\frac{\mathrm{i}\gamma\tau}{2}\right)\cos(\vartheta) - \sin\left(\frac{\mathrm{i}\gamma\tau}{2}\right)\sin(\vartheta)}{\cos(\vartheta)} \\
=& \mathrm{i}pr\tau + \frac{a(b_i - \mathrm{i}p\rho\sigma)}{\sigma^2}\tau - \frac{2a}{\sigma^2}\ln\left(\cos\left(\frac{\mathrm{i}\gamma\tau}{2}\right) - \sin\left(\frac{\mathrm{i}\gamma\tau}{2}\right)\tan(\vartheta)\right) \\
=& \mathrm{i}pr\tau + \frac{a(b_i - \mathrm{i}p\rho\sigma)}{\sigma^2}\tau - \frac{2a}{\sigma^2}\ln\left(\cosh\left(\frac{\gamma\tau}{2}\right) - \mathrm{i}\sinh\left(\frac{\gamma\tau}{2}\right)\frac{\mathrm{i}\lambda}{\gamma}\right) \\
=& \mathrm{i}pr\tau + \frac{a(b_i - \mathrm{i}p\rho\sigma)}{\sigma^2}\tau - \frac{2a}{\sigma^2}\ln\left(\frac{e^{\frac{\gamma\tau}{2}}+e^{-\frac{\gamma\tau}{2}}}{2} + \frac{\lambda}{\gamma}\cdot\frac{e^{\frac{\gamma\tau}{2}}-e^{-\frac{\gamma\tau}{2}}}{2}\right) \\
=& \mathrm{i}pr\tau + \frac{a(b_i - \mathrm{i}p\rho\sigma)}{\sigma^2}\tau - \frac{2a}{\sigma^2}\ln e^{-\frac{\gamma\tau}{2}}\frac{\gamma(e^{\gamma\tau}+1)+\lambda(e^{\gamma\tau}-1)}{2\gamma} \\
=& \mathrm{i}pr\tau + \frac{a(b_i - \mathrm{i}\sigma\rho p + \gamma)}{\sigma^2}\tau + \frac{2a}{\sigma^2}\ln\frac{2\gamma}{(\gamma+\lambda)e^{\gamma\tau}+\gamma-\lambda}.
\end{aligned} \tag{5.9.11}$$

We keep simplifying (5.9.10)

$$\begin{aligned}
B(t) =& \frac{\mathrm{i}\gamma}{\sigma^2}\tan\left(\frac{\mathrm{i}\gamma\tau}{2}+\vartheta\right) + \frac{b_i - \mathrm{i}\sigma\rho p}{\sigma^2} \\
=& \frac{\mathrm{i}\gamma}{\sigma^2}\left(\frac{\tan\left(\frac{\mathrm{i}\gamma\tau}{2}\right)+\tan(\vartheta)}{1-\tan\left(\frac{\mathrm{i}\gamma\tau}{2}\right)\tan(\vartheta)}\right) + \frac{b_i - \mathrm{i}\sigma\rho p}{\sigma^2} \\
=& \frac{\mathrm{i}\gamma}{\sigma^2}\left(\frac{\mathrm{i}\tanh\left(\frac{\gamma\tau}{2}\right)+\mathrm{i}\frac{\lambda}{\gamma}}{1-\mathrm{i}\frac{\lambda}{\gamma}\mathrm{i}\tanh\left(\frac{\gamma\tau}{2}\right)}\right) + \frac{b_i - \mathrm{i}\sigma\rho p}{\sigma^2} \\
=& \frac{\mathrm{i}\gamma}{\sigma^2}\left(\frac{\mathrm{i}\frac{e^{\frac{\gamma\tau}{2}}-e^{-\frac{\gamma\tau}{2}}}{e^{\frac{\gamma\tau}{2}}+e^{-\frac{\gamma\tau}{2}}}+\mathrm{i}\frac{\lambda}{\gamma}}{1+\frac{\lambda}{\gamma}\frac{e^{\frac{\gamma\tau}{2}}-e^{-\frac{\gamma\tau}{2}}}{e^{\frac{\gamma\tau}{2}}+e^{-\frac{\gamma\tau}{2}}}}\right) + \frac{b_i - \mathrm{i}\sigma\rho p}{\sigma^2} \\
=& -\frac{\gamma}{\sigma^2}\left(\frac{e^{\frac{\gamma\tau}{2}}-e^{-\frac{\gamma\tau}{2}}+\frac{\lambda}{\gamma}\left(e^{\frac{\gamma\tau}{2}}+e^{-\frac{\gamma\tau}{2}}\right)}{e^{\frac{\gamma\tau}{2}}+e^{-\frac{\gamma\tau}{2}}+\frac{\lambda}{\gamma}\left(e^{\frac{\gamma\tau}{2}}-e^{-\frac{\gamma\tau}{2}}\right)}\right) + \frac{b_i - \mathrm{i}\sigma\rho p}{\sigma^2} \\
=& -\frac{\gamma}{\sigma^2}\left(\frac{\gamma(e^{\gamma\tau}-1)+\lambda(e^{\gamma\tau}+1)}{\gamma(e^{\gamma\tau}+1)+\lambda(e^{\gamma\tau}-1)}\right) + \frac{b_i - \mathrm{i}\sigma\rho p}{\sigma^2} \\
=& -\frac{\gamma}{\sigma^2}\left(\frac{(\gamma+\lambda)e^{\gamma\tau}+\lambda-\gamma}{(\gamma+\lambda)e^{\gamma\tau}+\gamma-\lambda}\right) + \frac{b_i - \mathrm{i}\sigma\rho p}{\sigma^2}
\end{aligned}$$

$$
\begin{aligned}
&= -\frac{\gamma}{\sigma^2}\left(1+\frac{2(\lambda-\gamma)}{(\gamma+\lambda)e^{\gamma\tau}+\gamma-\lambda}\right)+\frac{b_i-\mathrm{i}\sigma\rho p}{\sigma^2}\\
&= \frac{2\gamma(\gamma-\lambda)}{\sigma^2\left((\gamma+\lambda)e^{\gamma\tau}+\gamma-\lambda\right)}+\frac{b_i-\mathrm{i}\sigma\rho p-\gamma}{\sigma^2}.
\end{aligned}
\tag{5.9.12}
$$

Finally, we finalize the characteristic, denoting $\tilde{\zeta}=\frac{2\gamma}{(\gamma+\lambda)e^{\gamma\tau}+\gamma-\lambda}$

$$
\begin{aligned}
\psi(p,q,x,y) &= \exp\left(A(t)x+B(t)v+C(t)\right)\\
&= \exp\left(\mathrm{i}px+\left(\frac{2\gamma(\gamma-\lambda)}{\sigma^2\left((\gamma+\lambda)e^{\gamma\tau}+\gamma-\lambda\right)}+\frac{b_i-\mathrm{i}\sigma\rho p-\gamma}{\sigma^2}\right)v\right.\\
&\qquad \left.\mathrm{i}pr\tau+\frac{a(b_i-\mathrm{i}\sigma\rho p+\gamma)}{\sigma^2}\tau+\frac{2a}{\sigma^2}\ln\frac{2\gamma}{(\gamma+\lambda)e^{\gamma\tau}+\gamma-\lambda}\right)\\
&= \exp\left(\mathrm{i}p(x+r\tau)+\left(\frac{(\gamma-\lambda)\tilde{\zeta}}{\sigma^2}+\frac{\lambda-\gamma}{\sigma^2}+\mathrm{i}q\right)v\right.\\
&\qquad \left.+\frac{\lambda+\gamma}{\sigma^2}a\tau+\mathrm{i}qa\tau+\frac{2a}{\sigma^2}\ln\tilde{\zeta}\right)\\
&= \exp\left(\mathrm{i}p(x+r\tau)+\mathrm{i}q(v+a\tau)+\frac{\gamma-\lambda}{\sigma^2}\left(\tilde{\zeta}-1\right)v+\frac{\gamma+\lambda}{\sigma^2}a\tau+\frac{2a}{\sigma^2}\ln\tilde{\zeta}\right).
\end{aligned}
$$

The logarithm term $\ln\tilde{\zeta}$ may still encounter discontinuity as p increases. We can see that for $p\to\infty$, we have

$$
\begin{aligned}
&\mathrm{Re}(\gamma)\to\infty,\\
&\mathrm{Im}(\gamma)\to\infty,
\end{aligned}
$$

and

$$
\tilde{\zeta}\to 0.
$$

Though the value of $\tilde{\zeta}$ is bounded, the value of logarithm of $\tilde{\zeta}$ will change very fast when $\tilde{\zeta}$ approaches 0 and shifts phase eventually. To avoid the value of the logarithm term approaching either zero or infinity, we do the following variable change

$$
\begin{aligned}
\zeta &= \frac{2\gamma}{\gamma+\lambda+(\gamma-\lambda)e^{-\gamma\tau}},\\
\tilde{\zeta} &= \zeta e^{-\gamma\tau},\\
\ln\tilde{\zeta} &= -\gamma\tau+\ln\zeta,\\
\frac{\gamma-\lambda}{\sigma^2}(\tilde{\zeta}-1) &= \frac{\gamma+\lambda}{\sigma^2}(1-\zeta),
\end{aligned}
$$

Therefore, we finalize our characteristic function as

$$\psi(p,q,x,v) = \exp\left(\mathrm{i}p(x+r\tau)+\mathrm{i}q(v+a\tau)+\frac{\gamma+\lambda}{\sigma^2}(1-\zeta)v-\frac{\gamma-\lambda}{\sigma^2}a\tau+\frac{2a}{\sigma^2}\ln\zeta\right). \quad (5.9.13)$$

□

5.10 Proof of Proposition 2.9

Proof. We investigate the limiting behavior of the characteristic function given by (2.4.45) and the parameters γ, λ and ζ defined from (2.4.42) to (2.4.44)

$$\lim_{u\to\infty}\frac{\gamma}{u} = \sigma\sqrt{1-\rho^2}\frac{|u|}{u}, \quad (5.10.1)$$

$$\lim_{u\to\infty}\frac{\lambda}{u} = -\sigma\rho\mathrm{i}, \quad (5.10.2)$$

$$\lim_{u\to\infty}\zeta = 2\sqrt{1-\rho^2}\left(\sqrt{1-\rho^2}+\frac{|u|}{u}\rho\mathrm{i}\right), \quad (5.10.3)$$

which leads to

$$\lim_{u\to\infty}\ln\zeta = \ln\left(2\sqrt{1-\rho^2}\right)+\ln\left(\sqrt{1-\rho^2}+\frac{|u|}{u}\rho\mathrm{i}\right), \quad (5.10.4)$$

and

$$\begin{aligned}\lim_{u\to\infty}\frac{1}{u}\frac{\gamma+\lambda}{\sigma^2}(1-\zeta)v &= \lim_{u\to\infty}\frac{\gamma+\lambda}{\sigma^2 u}\left(1-\frac{2\gamma}{\gamma+\lambda+(\gamma-\lambda)e^{-\gamma\tau}}\right)\\ &= \lim_{u\to\infty}\frac{\gamma+\lambda}{\sigma^2 u}\left(\frac{\lambda-\gamma+(\gamma-\lambda)e^{-\gamma\tau}}{\gamma+\lambda+(\gamma-\lambda)e^{-\gamma\tau}}\right)\\ &= \lim_{u\to\infty}\frac{\lambda-\gamma}{\sigma^2 u}\\ &= -\frac{|u|}{u}\frac{\sqrt{1-\rho^2}}{\sigma}v-\frac{\rho}{\sigma}v\mathrm{i}, \end{aligned} \quad (5.10.5)$$

as well as

$$\lim_{u\to\infty}\frac{1}{u}\frac{\gamma-\lambda}{\sigma^2}a\tau = \frac{|u|}{u}\frac{\sqrt{1-\rho^2}}{\sigma}a\tau-\frac{a\tau}{\sigma}\mathrm{i}. \quad (5.10.6)$$

Let $\vartheta = \arcsin\left(\frac{|u|}{u}\rho\right)$ and transform (5.10.4) as

$$\lim_{u\to\infty}\ln\zeta(u) = \ln\left(2\sqrt{1-\rho^2}\right)+\vartheta\mathrm{i}. \quad (5.10.7)$$

Combining (5.10.5), (5.10.6) and (5.10.7), we finalize the proof

$$\lim_{u\to\infty}\psi_i(u)\approx A_\infty e^{\mathrm{i}B_\infty}\exp\left(-\frac{\sqrt{1-\rho^2}}{\sigma}\left(v+a\tau\right)|u|\right). \tag{5.10.8}$$

where

$$\begin{aligned}A_\infty &= \left(4\left(1-\rho^2\right)\right)^{\frac{a}{\sigma^2}},\\ B_\infty &= \frac{2a}{\sigma^2}\arcsin\left(\frac{|u|}{u}\rho\right)-\frac{\rho}{\sigma}\left(v+\frac{|u|}{u}a\tau\right)u.\end{aligned}$$

□

5.11 Proof of Theorem 2.10

Proof. We see that

$$E_i(x)=\int_{\mathbb{R}} f(y)h_i(x-y)dy, \tag{5.11.1}$$

with $f(y)$ replaced by its Fourier expansion given in (2.4.71)

$$\begin{aligned}P_i(x) &= \int_{\mathbb{R}}\sum_{j=-\infty}^{\infty}F_j e^{-\mathrm{i}j\frac{2\pi y}{L}}h_i(x-y)dy\\ &= \sum_{j=-\infty}^{\infty}F_j e^{-\mathrm{i}j\frac{2\pi x}{L}}\int_{\mathbb{R}}e^{\mathrm{i}j\frac{2\pi(x-y)}{L}}h_i(x-y)dy\\ &= \sum_{j=-\infty}^{\infty}F_j e^{-\mathrm{i}j\frac{2\pi x}{L}}\int_{\mathbb{R}}e^{\mathrm{i}j\frac{2\pi y}{L}}\phi_i(y)dy.\end{aligned} \tag{5.11.2}$$

Replace the integral in equation (5.11.2) by the kernel function (2.4.61)

$$P_i(x)=\sum_{j=-\infty}^{\infty}F_j e^{-\mathrm{i}j\frac{2\pi x}{L}}\psi_i\left(\frac{2\pi j}{L}\right). \tag{5.11.3}$$

We truncate the infinite summation in equation (5.11.3) from $-\frac{N}{2}$ to $\frac{N}{2}-1$

$$\dot{P}_i(x)=\sum_{j=-\frac{N}{2}}^{\frac{N}{2}-1}F_j e^{-\mathrm{i}j\frac{2\pi x}{L}}\psi_i\left(\frac{2\pi j}{L}\right), \tag{5.11.4}$$

and denote the truncation error as $e_{i,1}$

$$|e_{i,1}|=\left|P_i(x)-\dot{P}_i(x)\right|$$

$$
\begin{aligned}
&= \left| \sum_{j=-\frac{N}{2}-1}^{-\infty} F_j e^{-\mathrm{i} j \frac{2\pi x}{L}} \psi_i\left(\frac{2\pi j}{L}\right) + \sum_{j=\frac{N}{2}}^{\infty} F_j e^{-\mathrm{i} j \frac{2\pi x}{L}} \psi_i\left(\frac{2\pi j}{L}\right) \right| \\
&\leq \sum_{|j|=\frac{N}{2}}^{\infty} \left|F_j\right| \left| \psi_i\left(\frac{2\pi j}{L}\right) \right|.
\end{aligned}
$$

By Proposition 2.9, there exists a positive constant $\varepsilon_{v,\tau}$ such that

$$
|\psi_i(u,v)| \leq \varepsilon_{v,\tau} A_\infty \exp\left(-\frac{\sqrt{1-\rho^2}}{\sigma} (v + a\tau) |u| \right), \text{ for all } u. \tag{5.11.5}
$$

Denote

$$
D = \frac{\sqrt{1-\rho^2}}{\sigma} (v + a\tau).
$$

Combining (5.11.5) and (2.4.73) yields

$$
\begin{aligned}
|e_{i,1}| \leq & 2\varepsilon_{v,\tau} \bar{f} A_\infty \sum_{j=\frac{N}{2}}^{\infty} \exp\left(-D \left| \frac{2\pi j}{L} \right| \right) \\
\leq & 2\varepsilon_{v,\tau} \bar{f} A_\infty \frac{L}{2\pi} \int_{\frac{\pi(N-2)}{L}}^{\infty} \exp(-Du)\, du \\
\leq & \frac{\varepsilon_{v,\tau} \bar{f} L A_\infty}{\pi} \exp\left(-D \frac{\pi(N-2)}{L} \right) \\
= & \varepsilon_1 e^{-\frac{\pi D}{L} N},
\end{aligned}
$$

where

$$
\varepsilon_1 = \frac{L A_\infty e^{\frac{2\pi D}{L}}}{\pi D} \varepsilon_{v,\tau} \bar{f}.
$$

Next, we consider the discretization error arising from the DFT (2.4.68) which is equivalent to the following calculation

$$
\tilde{P}_i(x) = \sum_{j=-\frac{N}{2}}^{\frac{N}{2}-1} \tilde{F}_j e^{-\mathrm{i} j \frac{2\pi x}{L}} \psi_i\left(\frac{2\pi j}{L}\right), \tag{5.11.6}
$$

by approximating the Fourier coefficients F_j in (5.11.4) with

$$
\tilde{F}_j = \frac{\Delta x}{L} \sum_{k=0}^{N-1} f(x_k) e^{\mathrm{i} j \frac{2\pi x_k}{L}}. \tag{5.11.7}
$$

We denote the discretization error as $e_{i,2}$

$$\begin{aligned}|e_{i,2}| &= \left|\dot{P}_i(x) - \tilde{P}_i(x)\right| \\ &\leq \sum_{j=-\frac{N}{2}}^{\frac{N}{2}-1} \left|F_j - \tilde{F}_j\right| \left|\psi_j\left(\frac{2\pi j}{L}\right)\right|. \end{aligned} \tag{5.11.8}$$

Assuming that the discretization error of $\left|F_j - \tilde{F}_j\right|$ is of $O\left(N^{-m}\right)$, we can bound it with a positive bounding constant ε_L depending only on L

$$\left|F_j - \tilde{F}_j\right| \leq \varepsilon_L N^{-m}. \tag{5.11.9}$$

It is easy to see that under the trapezoidal rule for w_n, we can apply $m \geq 2$ in (5.11.9). Using the fact that $u_j = \frac{2\pi j}{L}$ defined in (2.4.67) for $j = -\frac{N}{2}, \cdots, \frac{N}{2} - 1$, we finalize the approximation in (5.11.8)

$$\begin{aligned}|e_{i,2}| \leq & \sum_{j=-\frac{N}{2}}^{\frac{N}{2}-1} \left|F_j - \tilde{F}_j\right| \left|\psi_j\left(\frac{2\pi j}{L}\right)\right| \\ \leq & \varepsilon_L \varepsilon_{v,\tau} A_\infty N^{-m} \sum_{j=-\frac{N}{2}}^{\frac{N}{2}-1} \exp\left(-D\left|\frac{2\pi j}{L}\right|\right) \\ \leq & \varepsilon_L \varepsilon_{v,\tau} A_\infty N^{-m} \frac{L}{2\pi} \int_{-\frac{N\pi}{L}}^{\frac{N\pi}{L}} \exp\left(-D|u|\right) du, \\ \leq & \frac{\varepsilon_L \varepsilon_{v,\tau} L A_\infty N^{-m}}{\pi} \int_0^\infty \exp\left(-Du\right) du, \\ = & \frac{\varepsilon_L \varepsilon_{v,\tau} L A_\infty N^{-m}}{\pi D} \\ = & \varepsilon_2 N^{-m}, \end{aligned}$$

where

$$\varepsilon_2 = \frac{L A_\infty}{\pi D} \varepsilon_L \varepsilon_{v,\tau}.$$

Therefore, the error of the P_i can be summarized as

$$\begin{aligned}|e_i| &= \left|P_i(x) - \tilde{P}_i(x)\right| \\ &\leq \left|P_i(x) - \dot{P}_i(x)\right| + \left|\dot{P}_i(x) - \tilde{P}_i(x)\right| \\ &\leq |e_{i,1}| + |e_{i,2}| \\ &\leq \varepsilon_1 e^{-\frac{\pi D}{L} N} + \varepsilon_2 N^{-m}, \end{aligned}$$

where the first component gives the top bound of the truncation error and the second component gives the top bound of the discretization error. □

5.12 Proof of Proposition 3.2

Proof. We show that

$$X_t = e^{-\int_0^t \kappa_u du} X_0 + \int_0^t e^{-\int_u^t \kappa_s ds} \kappa_u \theta_u du + \int_0^t e^{-\int_u^t \kappa_s ds} \sigma_u dW_u, \tag{5.12.1}$$

with initial X_0 is the solution to

$$dX_t = \kappa_t (\theta_t - X_t) dt + \sigma_t dW_t.$$

Take differentiation to equation (5.12.1), we obtain

$$\begin{aligned}
dX_t =& - dt \kappa_t e^{-\int_0^t \kappa_u du} X_0 - dt \int_0^t \kappa_t e^{-\int_u^t \kappa_s ds} \kappa_u \theta_u du - dt \int_0^t \kappa_t e^{-\int_u^t \kappa_s ds} \sigma_u dW_u \\
&+ e^{-\int_t^t \kappa_s ds} \kappa_t \theta_t dt + e^{-\int_t^t \kappa_s ds} \sigma_t dW_t \\
=& - \kappa_t dt e^{-\int_0^t \kappa_u du} X_0 dt - \kappa_t dt \int_0^t e^{-\int_u^t \kappa_s ds} \kappa_u \theta_u du - \kappa_t dt \int_0^t e^{-\int_u^t \kappa_s ds} \sigma_u dW_u \\
&+ e^{\bar{0}} \kappa_t \theta_t dt + e^{\bar{0}} \sigma_t dW_t \\
=& - \kappa_t dt \left(e^{-\int_0^t \kappa_u du} X_0 + \int_0^t e^{-\int_u^t \kappa_s ds} \kappa_u \theta_u du + \int_0^t e^{-\int_u^t \kappa_s ds} \sigma_u dW_u \right) \\
&+ I \kappa_t \theta_t dt + I \sigma_t dW_t \\
=& - \kappa_t X_t dt + \kappa_t \theta_t dt + \sigma_t dW_t \\
=& \kappa_t (\theta_t - X_t) dt + \sigma_t dW_t.
\end{aligned}$$

Similarly, the process for X_T, $t \leq T$, is given by

$$X_T = e^{-\int_t^T \kappa_u du} X_t + \int_t^T e^{-\int_u^t \kappa_s ds} \kappa_u \theta_u du + \int_t^T e^{-\int_u^t \kappa_s ds} \sigma_u dW_u, \tag{5.12.2}$$

and the mean and variance are given by

$$\begin{aligned}
\mathbb{E}[X_T | \mathcal{F}_t] =& e^{-\int_t^T \kappa_u du} X_t + \int_t^T e^{-\int_u^t \kappa_s ds} \kappa_u \theta_u du, \\
\mathrm{Var}[X_T | \mathcal{F}_t] =& \int_t^T e^{-\int_u^T \kappa_v dv} \Sigma_u e^{-\int_u^T \kappa_v^T dv} du.
\end{aligned}$$

□

Bibliography

[1] Andrew Ang and Monika Piazzesi. A no-arbitrage vector autoregression of term structure dynamics with macroeconomic and latent variables. *Journal of Monetary economics*, 50(4): 745–787, 2003.

[2] Jan Annaert, Anouk GP Claes, Marc JK De Ceuster, and Hairui Zhang. Estimating the spot rate curve using the nelson–siegel model: A ridge regression approach. *International Review of Economics & Finance*, 27:482–496, 2013.

[3] Guy Barles, Rainer Buckdahn, and Etienne Pardoux. Backward stochastic differential equations and integral-partial differential equations. *Stochastics: An International Journal of Probability and Stochastic Processes*, 60(1-2):57–83, 1997.

[4] Emilio Barucci and Daniele Marazzina. Optimal investment, stochastic labor income and retirement. *Applied Mathematics and Computation*, 218(9):5588–5604, 2012.

[5] Daniele Bianchi, Matthias Büchner, and Andrea Tamoni. Bond risk premiums with machine learning. *The Review of Financial Studies*, 2020.

[6] Tomas Björk and Bent Jesper Christensen. Interest rate dynamics and consistent forward rate curves. *Mathematical Finance*, 9(4):323–348, 1999.

[7] Tomas Björk and Lars Svensson. On the existence of finite-dimensional realizations for nonlinear forward rate models. *Mathematical Finance*, 11(2):205–243, 2001.

[8] Fischer Black and Myron Scholes. The pricing of options and corporate liabilities. *Journal of political economy*, 81(3):637–654, 1973.

[9] Zvi Bodie, Robert C Merton, and William F Samuelson. Labor supply flexibility and portfolio choice in a life cycle model. *Journal of economic dynamics and control*, 16(3-4): 427–449, 1992.

[10] Zvi Bodie, Jérôme B Detemple, Susanne Otruba, and Stephan Walter. Optimal consumption–portfolio choices and retirement planning. *Journal of Economic Dynamics and Control*, 28(6):1115–1148, 2004.

[11] Bruno Bouchard and Nizar Touzi. Discrete-time approximation and monte-carlo simulation of backward stochastic differential equations. *Stochastic Processes and their applications*, 111(2):175–206, 2004.

[12] Bruno Bouchard, Romuald Elie, and Nizar Touzi. Discrete-time approximation of bsdes and probabilistic schemes for fully nonlinear pdes. *Advanced financial modelling*, 8:91–124, 2009.

[13] Phelim Boyle, Mark Broadie, and Paul Glasserman. Monte carlo methods for security pricing. *Journal of economic dynamics and control*, 21(8-9):1267–1321, 1997.

[14] Phelim P Boyle. Options: A monte carlo approach. *Journal of financial economics*, 4(3): 323–338, 1977.

[15] Michael J Brennan and Eduardo S Schwartz. An equilibrium model of bond pricing and a test of market efficiency. *Journal of Financial and quantitative analysis*, pages 301–329, 1982.

[16] Damiano Brigo, Antonio Dalessandro, Matthias Neugebauer, and Fares Triki. A stochastic processes toolkit for risk management. *Available at SSRN 1109160*, 2007.

[17] Andrew JG Cairns, David Blake, and Kevin Dowd. Stochastic lifestyling: Optimal dynamic asset allocation for defined contribution pension plans. *Journal of Economic Dynamics and Control*, 30(5):843–877, 2006.

[18] Peter Carr and Dilip Madan. Option valuation using the fast fourier transform. *Journal of computational finance*, 2(4):61–73, 1999.

[19] Andrea Carriero, Todd E Clark, and Massimiliano Marcellino. Bayesian vars: specification choices and forecast accuracy. *Journal of Applied Econometrics*, 30(1):46–73, 2015.

[20] Eunsuk Chong, Chulwoo Han, and Frank C Park. Deep learning networks for stock market analysis and prediction: Methodology, data representations, and case studies. *Expert Systems with Applications*, 83:187–205, 2017.

[21] Jens HE Christensen, Francis X Diebold, and Glenn D Rudebusch. The affine arbitrage-free class of nelson–siegel term structure models. *Journal of Econometrics*, 164(1):4–20, 2011.

[22] Peter Christoffersen, Christian Dorion, Kris Jacobs, and Lotfi Karoui. Nonlinear kalman filtering in affine term structure models. *Management Science*, 60(9):2248–2268, 2014.

[23] Charles W Cobb and Paul H Douglas. A theory of production. *The American Economic Review*, 18(1):139–165, 1928.

[24] Samuel N Cohen and Martin Tegnér. European option pricing with stochastic volatility models under parameter uncertainty. In *International symposium on bsdes*, pages 123–167. Springer, 2017.

[25] James W Cooley and John W Tukey. An algorithm for the machine calculation of complex fourier series. *Mathematics of computation*, 19(90):297–301, 1965.

[26] Laura Coroneo, Ken Nyholm, and Rositsa Vidova-Koleva. How arbitrage-free is the nelson–siegel model? *Journal of Empirical Finance*, 18(3):393–407, 2011.

[27] John C Cox and Chi-fu Huang. Optimal consumption and portfolio policies when asset prices follow a diffusion process. *Journal of economic theory*, 49(1):33–83, 1989.

[28] John C Cox and Stephen A Ross. The valuation of options for alternative stochastic processes. *Journal of financial economics*, 3(1-2):145–166, 1976.

[29] John C Cox, Stephen A Ross, and Mark Rubinstein. Option pricing: A simplified approach. *Journal of financial Economics*, 7(3):229–263, 1979.

[30] John C Cox, Jonathan E Ingersoll, and Stephen A Ross. A theory of the term structure of interest rates. *Econometrica*, 53(2):385–407, 1985.

[31] John C Cox, Jonathan E Ingersoll Jr, and Stephen A Ross. A theory of the term structure of interest rates. In *Theory of Valuation*, pages 129–164. World Scientific, 2005.

[32] Yiran Cui, Sebastian del Baño Rollin, and Guido Germano. Full and fast calibration of the heston stochastic volatility model. *European Journal of Operational Research*, 263(2): 625–638, 2017.

[33] George Cybenko. Approximation by superpositions of a sigmoidal function. *Mathematics of control, signals and systems*, 2(4):303–314, 1989.

[34] Paresh Date and Ksenia Ponomareva. Linear and non-linear filtering in mathematical finance: a review. *IMA Journal of Management Mathematics*, 22(3):195–211, 2011.

[35] Michiel De Pooter. Examining the nelson-siegel class of term structure models: In-sample fit versus out-of-sample forecasting performance. *Available at SSRN 992748*, 2007.

[36] Pierre Del Moral. Nonlinear filtering: Interacting particle resolution. *Comptes Rendus de l'Académie des Sciences-Series I-Mathematics*, 325(6):653–658, 1997.

[37] Francis X Diebold and Canlin Li. Forecasting the term structure of government bond yields. *Journal of econometrics*, 130(2):337–364, 2006.

[38] Francis X Diebold, Glenn D Rudebusch, and S Boragan Aruoba. The macroeconomy and the yield curve: a dynamic latent factor approach. *Journal of econometrics*, 131(1-2):309–338, 2006.

[39] Francis X Diebold, Canlin Li, and Vivian Z Yue. Global yield curve dynamics and interactions: a dynamic nelson–siegel approach. *Journal of Econometrics*, 146(2):351–363, 2008.

[40] Xiao Ding, Yue Zhang, Ting Liu, and Junwen Duan. Deep learning for event-driven stock prediction. In *Twenty-fourth international joint conference on artificial intelligence*, 2015.

[41] Arnaud Doucet and Adam M Johansen. A tutorial on particle filtering and smoothing: Fifteen years later. *Handbook of nonlinear filtering*, 12(656-704):3, 2009.

[42] Adrian A Drăgulescu and Victor M Yakovenko. Probability distribution of returns in the heston model with stochastic volatility. *Quantitative finance*, 2(6):443–453, 2002.

[43] Gregory R Duffee. Estimating the price of default risk. *The Review of financial studies*, 12 (1):197–226, 1999.

[44] Gregory R Duffee. Term premia and interest rate forecasts in affine models. *The Journal of Finance*, 57(1):405–443, 2002.

[45] Gregory R Duffee. Forecasting with the term structure: The role of no-arbitrage restrictions. Technical report, Working paper, 2011.

[46] Darrell Duffie. Credit risk modeling with affine processes. *Journal of Banking & Finance*, 29(11):2751–2802, 2005.

[47] Darrell Duffie. *Dynamic asset pricing theory*. Princeton University Press, 2010.

[48] Darrell Duffie and Larry G Epstein. Asset pricing with stochastic differential utility. *The Review of Financial Studies*, 5(3):411–436, 1992.

[49] Darrell Duffie and Rui Kan. A yield-factor model of interest rates. *Mathematical finance*, 6 (4):379–406, 1996.

[50] Daniel J Duffy. *Finite Difference methods in financial engineering: a Partial Differential Equation approach*. John Wiley & Sons, 2013.

[51] Jacob Ejsing, Magdalena Grothe, and Oliver Grothe. Liquidity and credit risk premia in government bond yields. 2012.

[52] Nicole El Karoui and Marie-Claire Quenez. Dynamic programming and pricing of contingent claims in an incomplete market. *SIAM journal on Control and Optimization*, 33(1): 29–66, 1995.

[53] Nicole El Karoui, Shige Peng, and Marie Claire Quenez. Backward stochastic differential equations in finance. *Mathematical finance*, 7(1):1–71, 1997.

[54] E. Fama and Robert Bliss. The information in long-maturity forward rates. *The American Economic Review*, 77:680–692, 1987.

[55] Emmanuel Farhi and Stavros Panageas. Saving and investing for early retirement: A theoretical analysis. *Journal of Financial Economics*, 83(1):87–121, 2007.

[56] William Feller. Two singular diffusion problems. *Annals of mathematics*, pages 173–182, 1951.

[57] Damir Filipovic et al. Exponential-polynomial families and the term structure of interest rates. *Bernoulli*, 6(6):1081–1107, 2000.

[58] Mark Fisher, Douglas W Nychka, and David Zervos. Fitting the term structure of interest rates with smoothing splines. 1995.

[59] Wendell H Fleming and Raymond W Rishel. *Deterministic and stochastic optimal control*, volume 1. Springer Science & Business Media, 2012.

[60] Jean-Pierre Fouque, George Papanicolaou, and K Ronnie Sircar. *Derivatives in financial markets with stochastic volatility*. Cambridge University Press, 2000.

[61] Swetava Ganguli and Jared Dunnmon. Machine learning for better models for predicting bond prices. *arXiv preprint arXiv:1705.01142*, 2017.

[62] Jianwei Gao. Stochastic optimal control of dc pension funds. *Insurance: Mathematics and Economics*, 42(3):1159–1164, 2008.

[63] Russell Gerrard, Bjarne Højgaard, and Elena Vigna. Choosing the optimal annuitization time post-retirement. *Quantitative Finance*, 12(7):1143–1159, 2012.

[64] Ian Goodfellow, Yoshua Bengio, and Aaron Courville. *Deep learning*. MIT press, 2016.

[65] Hua He and Henri F Pages. Labor income, borrowing constraints, and equilibrium asset prices. *Economic Theory*, 3(4):663–696, 1993.

[66] David Heath, Robert Jarrow, and Andrew Morton. Bond pricing and the term structure of interest rates: A new methodology for contingent claims valuation. *Econometrica: Journal of the Econometric Society*, pages 77–105, 1992.

[67] Steven L Heston. A closed-form solution for options with stochastic volatility with applications to bond and currency options. *The review of financial studies*, 6(2):327–343, 1993.

[68] Sepp Hochreiter and Jürgen Schmidhuber. Long short-term memory. *Neural computation*, 9(8):1735–1780, 1997.

[69] Kurt Hornik, Maxwell Stinchcombe, Halbert White, et al. Multilayer feedforward networks are universal approximators. *Neural networks*, 2(5):359–366, 1989.

[70] TP Huijskens, Maria J Ruijter, and Cornelis W Oosterlee. Efficient numerical fourier methods for coupled forward–backward sdes. *Journal of Computational and Applied Mathematics*, 296:593–612, 2016.

[71] John Hull and Alan White. Numerical procedures for implementing term structure models i: Single-factor models. *Journal of derivatives*, 2(1):7–16, 1994.

[72] Côme Huré, Huyên Pham, and Xavier Warin. Some machine learning schemes for high-dimensional nonlinear pdes. *arXiv preprint arXiv:1902.01599*, 2019.

[73] Aubrey Hurn, Kenneth Lindsay, and Vladimir Pavlov. Smooth estimation of yield curves by laguerre functions. In *MODSIM 05-International Congress On MOdelling And Simulation Advances And Applications For Management And Decision Making*, pages 1042–1048. The Modelling and Simulation Society of Australia and New Zealand, 2005.

[74] Cody B Hyndman and Polynice Oyono Ngou. A convolution method for numerical solution of backward stochastic differential equations. *Methodology and Computing in Applied Probability*, 19(1):1–29, 2017.

[75] Sergey Ioffe and Christian Szegedy. Batch normalization: Accelerating deep network training by reducing internal covariate shift. *arXiv preprint arXiv:1502.03167*, 2015.

[76] Alireza Javaheri, Delphine Lautier, and Alain Galli. Filtering in finance. *Wilmott*, 3:67–83, 2003.

[77] Shaolin Ji, Shige Peng, Ying Peng, and Xichuan Zhang. Three algorithms for solving high-dimensional fully-coupled fbsdes through deep learning. *arXiv preprint arXiv:1907.05327*, 2019.

[78] Kyoung Jin Choi and Gyoocheol Shim. Disutility, optimal retirement, and portfolio selection. *Mathematical Finance: An International Journal of Mathematics, Statistics and Financial Economics*, 16(2):443–467, 2006.

[79] Christian Kahl and Peter Jäckel. Not-so-complex logarithms in the heston model. *Wilmott magazine*, 19(9):94–103, 2005.

[80] Ioannis Karatzas and Hui Wang. Utility maximization with discretionary stopping. *SIAM Journal on Control and Optimization*, 39(1):306–329, 2000.

[81] Ioannis Karatzas, John P Lehoczky, and Steven E Shreve. Optimal portfolio and consumption decisions for a "small investor" on a finite horizon. *SIAM journal on control and optimization*, 25(6):1557–1586, 1987.

[82] Ioannis Karatzas, Steven E Shreve, I Karatzas, and Steven E Shreve. *Methods of mathematical finance*, volume 39. Springer, 1998.

[83] Diederik P Kingma and Jimmy Ba. Adam: A method for stochastic optimization. *arXiv preprint arXiv:1412.6980*, 2014.

[84] Genshiro Kitagawa. Monte carlo filter and smoother for non-gaussian nonlinear state space models. *Journal of computational and graphical statistics*, 5(1):1–25, 1996.

[85] Gary M Koop. Forecasting with medium and large bayesian vars. *Journal of Applied Econometrics*, 28(2):177–203, 2013.

[86] Anastasis Kratsios and Cody B Hyndman. Arbitrage-free regularization. *arXiv preprint arXiv:1710.05114*, 2017.

[87] Sergei Levendorskiĭ. Efficient pricing and reliable calibration in the heston model. *International Journal of Theoretical and Applied Finance*, 15(07):1250050, 2012.

[88] Byung Hwa Lim, Yong Hyun Shin, and U Jin Choi. Optimal investment, consumption and retirement choice problem with disutility and subsistence consumption constraints. *Journal of mathematical analysis and applications*, 345(1):109–122, 2008.

[89] Robert Litterman and Jose Scheinkman. Common factors affecting bond returns. *Journal of fixed income*, 1(1):54–61, 1991.

[90] Jun S Liu. *Monte Carlo strategies in scientific computing*. Springer Science & Business Media, 2008.

[91] Roger Lord and Christian Kahl. Optimal fourier inversion in semi-analytical option pricing. 2007.

[92] Roger Lord and Christian Kahl. Complex logarithms in heston-like models. *Mathematical Finance: An International Journal of Mathematics, Statistics and Financial Economics*, 20 (4):671–694, 2010.

[93] Roger Lord, Fang Fang, Frank Bervoets, and Cornelis W Oosterlee. A fast and accurate fft-based method for pricing early-exercise options under lévy processes. *SIAM Journal on Scientific Computing*, 30(4):1678–1705, 2008.

[94] Jin Ma, J-M Morel, and Jiongmin Yong. *Forward-backward stochastic differential equations and their applications*. Number 1702. Springer Science & Business Media, 1999.

[95] Harry Markowitz. Portfolio selection. *The Journal of Finance*, 7(1):77–91, 1952.

[96] Harry M Markowitz. Foundations of portfolio theory. *The Journal of Finance*, 46(2):469–477, 1991.

[97] J Huston McCulloch. Measuring the term structure of interest rates. *The Journal of Business*, 44(1):19–31, 1971.

[98] J Huston McCulloch. The tax-adjusted yield curve. *The Journal of Finance*, 30(3):811–830, 1975.

[99] Robert C Merton. Optimum consumption and portfolio rules in a continuous-time model. *Journal of Economic Theory*, 3(4):373–413, 1971.

[100] Howard Musoff and Paul Zarchan. *Fundamentals of Kalman filtering: a practical approach*. American Institute of Aeronautics and Astronautics, 2009.

[101] Charles R Nelson and Andrew F Siegel. Parsimonious modeling of yield curves. *Journal of business*, pages 473–489, 1987.

[102] Bernt Øksendal. Stochastic differential equations. In *Stochastic differential equations*, pages 65–84. Springer, 2003.

[103] Etienne Pardoux and Shige Peng. Adapted solution of a backward stochastic differential equation. *Systems & Control Letters*, 14(1):55–61, 1990.

[104] Etienne Pardoux and Shige Peng. Backward stochastic differential equations and quasilinear parabolic partial differential equations. In *Stochastic partial differential equations and their applications*, pages 200–217. Springer, 1992.

[105] Etienne Pardoux and Shanjian Tang. Forward-backward stochastic differential equations and quasilinear parabolic pdes. *Probability Theory and Related Fields*, 114(2):123–150, 1999.

[106] Frédéric Pascal, Lionel Bombrun, Jean-Yves Tourneret, and Yannick Berthoumieu. Parameter estimation for multivariate generalized gaussian distributions. *IEEE Transactions on Signal Processing*, 61(23):5960–5971, 2013.

[107] Huyên Pham. *Continuous-time stochastic control and optimization with financial applications*, volume 61. Springer Science & Business Media, 2009.

[108] Stanley R Pliska. A stochastic calculus model of continuous trading: optimal portfolios. *Mathematics of operations research*, 11(2):371–382, 1986.

[109] Hannes Risken. Fokker-planck equation. In *The Fokker-Planck Equation*, pages 63–95. Springer, 1996.

[110] Esther Ruiz and Lorenzo Pascual. Bootstrapping financial time series. *Journal of Economic Surveys*, 16(3):271–300, 2002.

[111] Sreelekshmy Selvin, R Vinayakumar, EA Gopalakrishnan, Vijay Krishna Menon, and KP Soman. Stock price prediction using lstm, rnn and cnn-sliding window model. In *2017 international conference on advances in computing, communications and informatics (icacci)*, pages 1643–1647. IEEE, 2017.

[112] William F Sharpe. Capital asset prices: A theory of market equilibrium under conditions of risk. *The journal of finance*, 19(3):425–442, 1964.

[113] Lars EO Svensson. Estimating and interpreting forward interest rates: Sweden 1992-1994. Technical report, National bureau of economic research, 1994.

[114] Oldrich Vasicek. An equilibrium characterization of the term structure. *Journal of financial economics*, 5(2):177–188, 1977.

[115] Oldrich A Vasicek and H Gifford Fong. Term structure modeling using exponential splines. *The Journal of Finance*, 37(2):339–348, 1982.

[116] Daniel F Waggoner. Spline methods for extracting interest rate curves from coupon bond prices. *Federal Reserve Bank of Atlanta Working Paper*, pages 97–10, 1997.

[117] Eric A Wan and Rudolph Van Der Merwe. The unscented kalman filter for nonlinear estimation. In *Proceedings of the IEEE 2000 Adaptive Systems for Signal Processing, Communications, and Control Symposium (Cat. No. 00EX373)*, pages 153–158. Ieee, 2000.

[118] E Weinan, Jiequn Han, and Arnulf Jentzen. Deep learning-based numerical methods for high-dimensional parabolic partial differential equations and backward stochastic differential equations. *Communications in Mathematics and Statistics*, 5(4):349–380, 2017.

[119] G Yin, Vikram Krishnamurthy, and Cristina Ion. Regime switching stochastic approximation algorithms with application to adaptive discrete stochastic optimization. *SIAM Journal on Optimization*, 14(4):1187–1215, 2004.

[120] Jianfeng Zhang. A numerical scheme for bsdes. *Annals of Applied Probability*, 14(1): 459–488, 2004.

[121] Robert Zvan, Kenneth R Vetzal, and Peter A Forsyth. Pde methods for pricing barrier options. *Journal of Economic Dynamics and Control*, 24(11-12):1563–1590, 2000.